Electron paramagnetic resonance spectroscopy of spin-labeled RNA: An emerging tool for the elucidation of RNA structure and dynamics

Thomas Eugene Edwards

A dissertation submitted in partial fulfillment of the
requirements for the degree of

Doctor of Philosophy

University of Washington

2003

Program Authorized to Offer Degree: Chemistry

ProQuest Information and Learning Company
300 North Zeeb Road
P.O. Box 1346
Ann Arbor, MI 48106-1346

In presenting this dissertation in partial fulfillment of the requirements for the Doctoral degree at the University of Washington, I agree that the Library shall make its copies freely available for inspection. I further agree that extensive copying of the dissertation is available only for scholarly purposes, consistent with "fair use" as described in the U.S. Copyright Law. Requests for copying or reproduction of this dissertation may be referred to ProQuest Information and Learning, 300 North Zeeb Road, Ann Arbor, MI 48106-1346, to whom the author has granted "the right to reproduce and sell (a) copies of the manuscript in microform and/or (b) printed copies of the manuscript made from microform."

Signature 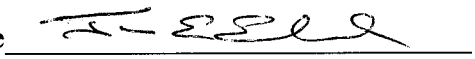

Date August 19, 2003

University of Washington
Graduate School

This is to certify that I have examined this copy of a doctoral dissertation by

Thomas Eugene Edwards

and have found that it is complete and satisfactory in all respects,
and that any and all revisions required by the final
examining committee have been made.

Chair of Supervisory Committee:

Snorri Thor Sigurdsson

Reading Committee:

Snorri Thor Sigurdsson

Bruce H. Robinson

Tomikazu Sasaki

Date: August 19, 2003

University of Washington

Abstract

Electron paramagnetic resonance spectroscopy of spin-labeled RNA: An emerging tool for the elucidation of RNA structure and dynamics

Thomas Eugene Edwards

Chair of the Supervisory Committee:

Research Associate Professor Snorri Thor Sigurdsson

Department of Chemistry

Electron paramagnetic resonance (EPR) spectroscopy was applied to the study of RNA structure and dynamics. A general and efficient method for the site-specific incorporation of nitroxide spin-labels into internal sites of RNA is described. The spin-labeling reagent 4-isocyanato TEMPO reacts with 2'-amino modified RNA in >90% conversion to produce spin-labeled RNA. Several spin-labeled RNAs were shown to exhibit structure-dependent dynamics.

The trans activation responsive (TAR) RNA of the human immunodeficiency virus (HIV) forms an essential interaction with the Tat protein during the HIV lifecycle. Four spin-labeled TAR RNAs were prepared, and their interactions with metal ions, derivatives of the Tat protein, and small molecules were studied by EPR spectroscopy. The spin-label was shown to have a minimal effect on RNA-peptide affinity. Argininamide and a mutant Tat peptide induced similar changes in TAR RNA internal dynamics upon binding. The wild-type Tat peptide was shown to have a dramatically different effect on the dynamics of U23 and U38 compared to the mutant peptide, despite similar binding affinities. Peptide sequence mutation and EPR spectroscopic analysis revealed that in addition to R52, modification at residues 53-57 affected TAR dynamics,

indicating their role in forming a specific TAR-Tat complex. Small molecules which were known to bind similarly induced similar changes in TAR RNA internal dynamics, correlating RNA structure to RNA dynamics. Dynamic signatures were used to provide evidence that guanidinoneomycin binds to the TAR RNA in a manner similar to that of argininamide rather than neomycin.

In addition to the ability to carry genetic information, RNA has been shown to catalyze chemical reactions. These "ribozymes" are important in many cellular processes and have implications for the origin of life. We studied the metal ion-dependent folding of the hammerhead ribozyme by EPR spectroscopy, specifically the two-step divalent metal ion-dependent pathway and the effect of high concentrations of monovalent metal ions. These results have implications for the role of metal ions in structure assembly of this well studied ribozyme.

TABLE OF CONTENTS

LIST OF FIGURES

LIST OF TABLES

Acknowledgements

The author wishes to express appreciation to many persons, especially the research supervisor, Snorri Thor Sigurdsson. I also appreciate the effort from the following collaborators on joint projects: Tamara M. Okonogi, Bruce H. Robinson, Thomas C. Leeper, Gabriele Varani, Axel Weber, Thomas F. Prisner, Olav Schieman, and Adrian Ferré D'Amaré. The following peers have also contributed to my graduate experience, and I would like to thank: Robert D. Nielsen, Eric A. Harwood, Frédéric Godde, Archna P. Massey, Emily J. Borda, Jeffrey D. Wellhausen, Nivrutti B. Barhate, and Panadda Chirakul.

The author acknowledges a training grant fellowship in molecular biophysics from the National Institutes of Health, provided through the Department of Biochemistry at the University of Washington.

I would also like to express my sincere appreciation to my family and my wife's family for their support and enthusiasm. Lastly I would like to thank my wife, Catherine J. Edwards for her love and support.

Dedication

To Hoa Thai Le

And

To my grandparents

Chapter 1

Introduction to RNA and EPR spectroscopy

Biological importance of RNA

Ribonucleic acids (RNA) perform a multitude of biological functions, including the transfer of genetic material, protein synthesis, intron splicing, regulation of gene expression, and catalysis of chemical reactions (Gesteland, Cech et al. 1999). The major categories of RNA include ribosomal RNA (rRNA), which is part of the machinery for protein synthesis and the most abundant cellular RNA by weight; messenger RNA (mRNA), the highly modified and dynamic RNA which is involved in the transfer of genetic material as well as encoding for proteins during protein synthesis; transfer RNA (tRNA), which are involved in the coding and addition of amino acids during protein synthesis; small nuclear RNA (snRNA) and small nucleolar (snoRNA), both involved in the maturation of the cellular nucleus; small interfering RNAs (siRNAs), 20-25 nucleotide long oligomers involved in the degradation of mRNA and gene silencing; and catalytic RNA (ribozymes), which catalyze the cleavage and formation of chemical bonds. Catalysis, molecular structure assembly, and molecular recognition are all central facets of RNA's ability to perform its multitude of functions.

During the early 1980s in the laboratories of Sidney Altman (Guerrier-Takada, Gardiner et al. 1983) and Thomas Cech (Kruger, Grabowski et al. 1982), it was discovered that RNA can catalyze the cleavage of phosphodiester bonds in the absence of proteins, increasing the list of known RNA cellular functions to include catalysis of chemical reactions. In addition to PNase P discovered by Altman, which is involved in the preparation of mature tRNAs, and the group I intron discovered by Cech, important for production of mature mRNAs, several other naturally occurring ribozymes have been discovered, including the hammerhead, hairpin, hepatitis delta virus, Neurospora VS, and group II intron (Sigurdsson, Thomson et al. 1998; DeRose 2002). Recently, a crystal

structure of the ribosome, which is the building machinery for protein synthesis, showed that no protein was present within 20 Å of the catalytic site, demonstrating that the RNA component was responsible for catalysis (Ban, Nissen et al. 2000). Indeed, the "ribosome is a ribozyme". Biochemical evidence points to the notion that the spliceosome is also a ribozyme (Valadkhan and Manley 2002). In addition to naturally occurring ribozymes, *in vitro* selection experiments, which start from randomized pools of RNA molecules and produce enriched pools of RNAs selected to contain certain physical properties (e.g. catalysis, molecule recognition), have increased the number of known catalytic RNAs as well as the molecular diversity of reactions that RNA can catalyze (Bittker, Phillips et al. 2002). Recently, the hammerhead ribozyme was discovered to have more than one catalytic center, providing the first example of sequential cleavage events as a possible regulatory mechanism in RNA (Markley, Godde et al. 2001; Borda, Markley et al. 2003). Many of these catalytic RNA molecules require metal ions for either structural support or direct participation in catalysis (DeRose 2002). In order for metal ions to bind and aid in catalysis and structure formation, the RNA must adopt an appropriate metal ion binding conformation.

Similarly to proteins, RNA can adopt a wide variety of three dimensional structures, enabling it to bind to highly variable cellular components including metal ions, proteins, DNA, RNA, membranes, sugars, and small molecules (Batey, Rambo et al. 1999). RNA molecules involved in molecular recognition have been identified from natural biological organisms or through *in vitro* selection experiments, termed sequential evolution of ligands by exponential enrichment (SELEX) (Gold, Polisky et al. 1995). RNA molecules identified by SELEX that bind to a target are named aptamers. Naturally occurring RNA molecules have been discovered which interact with small molecule metabilites in a mechanism which controls gene regulation (Lai 2003; Mandal, Boese et al. 2003). These molecules have been termed riboswitches. The multitude of RNA-protein (Varani 1997; Jones, A. et al. 2001) and RNA-small molecule complexes (Patel and Suri 2000) reveals a diverse nature of RNA-protein and RNA-small molecule recognition elements. Of current interest, biochemical and biophysical evidence exists

that many RNA molecules alter their structure in order to bind proteins and small molecules, prompting an "induced fit" theory of RNA-protein (Leulliot and Varani 2001) and RNA-small molecule binding (Hermann and Patel 2000). RNA can bind to proteins and small molecules with high affinity (e.g. HIV-1 RRE RNA-Rev peptide complex complex has a K_d = 4 nM; the Tobramycin-RNA aptamer complex has a K_d = 9 nM) (Hermann and Patel 2000). These complexes also display high selectivity. For example, the theophylline-binding RNA aptamer exhibits a 10,000-fold higher affinity for theophylline than for caffeine, a structural analog which differs only by the replacement of a hydrogen atom with a methyl group. In summary, RNA can fold into a wide diversity of structures to bind to various cellular components with a high degree of affinity and specificity.

In addition to its large diversity of molecule structure, catalysis, and recognition, many RNA molecules contain modifications which alter its binding properties. The spliceosome, tRNAs, and mRNAs are highly modified with methylated cytosine, adenosine, and guanosine residues as well as 4-thiouridine, pesudouridine, and other modified bases. These modifications are all important for molecular recognition with other cellular complements, most notably other RNA molecules, cellular proteins, and co-factors involved in protein synthesis.

Because RNA can carry genetic information, catalyze reactions, and bind to cellular co-factors (Sussman, Nix et al. 2000), an "RNA World" theory of evolution has been proposed (Gesteland, Cech et al. 1999). This theory provides an evolutionary pathway for the development of modern genetic material (DNA) and the wide variety of proteins inside single cell organisms through RNA catalysis and cellular machinery replication.

RNA and disease

Studies in epidemiology have shown that unmodified and modified RNAs play essential roles in the evolution and lifecycles of many infectious diseases. The structure

and therefore, mechanism of action, of many RNAs in not necessarily conserved between humans and bacteria. For example, the $tRNA^{tyr}$ and tyrosyl-$tRNA^{tyr}$ synthetase pair is orthogonal across three organisms, archea, bacteria, and eukariyots, a factor that has been exploited for incorporation of non-natural amino acids into proteins (Mehl, Anderson et al. 2003). In another example, erythromycin-resistant bacteria have a methylated adenosine residue in the ribosomal exit tunnel, which greatly decreases the binding affinity of the antibiotic drug. However, this modification does not affect the binding affinity of the next generation semi-synthetic antibiotic troleandomycin, a structural analog of erythromycin (Berusui, Schlaenzen et al. 2003).

While RNA is important in the lifecycle of infectious diseases, it may also be the key to therapeutic treatment of these diseases. Antisense oligos, RNA interference (RNAi), and ribozymes can be used in possible therapeutic treatments of disease. For example, small interfering RNAs (siRNAs) can silence gene expression in endogenous lamin A/C mRNA in human HeLa or mouse SW3T3 cells (Harborth, Elbashir et al. 2003). Natural RNAi pathways have also been observed. In one example, miscleaved mRNA genes copies induce gene silencing, resulting in low protein content rice (Kusaba, Miyahara et al. 2003; Surridge 2003). In addition, ribozymes engineered to cleave designated sequences can be used to control gene expression (Fritz, Lewin et al. 2002). For greater specificity *in vivo*, "allosteric ribozymes" can be engineered to be active only when bound to a specific small molecule, effectively turning on catalysis and off gene expression once the RNA has found the appropriate cellular target (e.g. DNA in tumor cells) (Wang, Lai et al. 2002; Silverman 2003).

The Human Immunodeficiency Virus (HIV)

The human immunodeficiency virus (HIV) has infected 42 million people world wide and is the precursor to acquired immunodeficiency syndrome (AIDS). Over three million people die each year as a result of long term HIV infection. In order to replicate its genetic information without hindrance, HIV depletes the host organism's immune

system, rendering the host more susceptible to infection by HIV and other foreign pathogens (e.g. pneumonia is the leading cause of AIDS-related deaths). The HIV lifecycle starts with the HIV particle recognizing CD4 receptors on the surface of host cells (Figure 1.1). After cell wall recognition, the HIV retrovirus particle fuses to the host cell wall and injects its RNA genome into the host cell. The virus then utilizes the host cell's transcriptional machinery to replicate itself, making HIV RNA genetic copies, which are reverse transcribed into DNA and incorporated into the host cell DNA by integrase enzymes. After the entire HIV genome is replicated and transcribed back into RNA, the fifteen proteins it encodes are over-expressed. These proteins and the HIV RNA genome are packaged into new HIV particles and released from the host cell to start the lifecycle over again (Frankel and Young 1998).

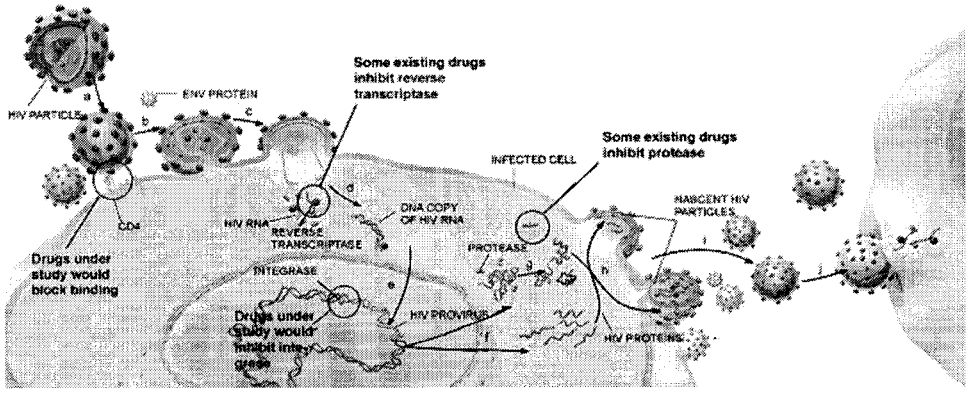

Figure 1.1. The HIV-1 lifecycle (Bartlett, and Moore 1998)

The TAR RNA of HIV

The first 59 nucleotides at the 5' end of nascent HIV mRNA transcripts, which is named the trans activation responsive region (TAR) RNA of HIV-1, interacts with the Tat (trans activator of transcription) protein during HIV transcription (Frankel 1992). In the absence of the TAR-Tat interaction, full length HIV genome production is inefficient (Jones and Peterlin 1994) due to a number of negative elongation factors (Yamaguchi, Wada et al. 1998). The TAR-Tat complex has been shown to sequentially bind to cyclin

T1 (CycT1) and cyclin dependent kinase 9 (CDK9) (Figure 1.2). This ribonucleoprotein complex has been named the positive transcription elongation factor (P-TEFb) complex because it counters the effect of the negative elongation factors, promoting efficient transcription of the full length HIV genome (Garber, Mayall et al. 2000). While the exact cellular mechanism is still unclear, CDK9 hyperphosphorylates RNA polymerase II (Garber, Mayall et al. 2000), which has been shown to correlate with additional complex stabilization and the observed enhanced elongation. Therefore, the TAR RNA activates P-TEFb complex formation to promote efficient production of viral transcripts. Because of its important role in HIV genome replication, the TAR RNA is an important target for therapeutic intervention of HIV replication (Froeyen and Herdewijn 2002). To better understand the function of the TAR RNA, its molecular and structural recognition of the Tat protein and small molecules drugs must be understood.

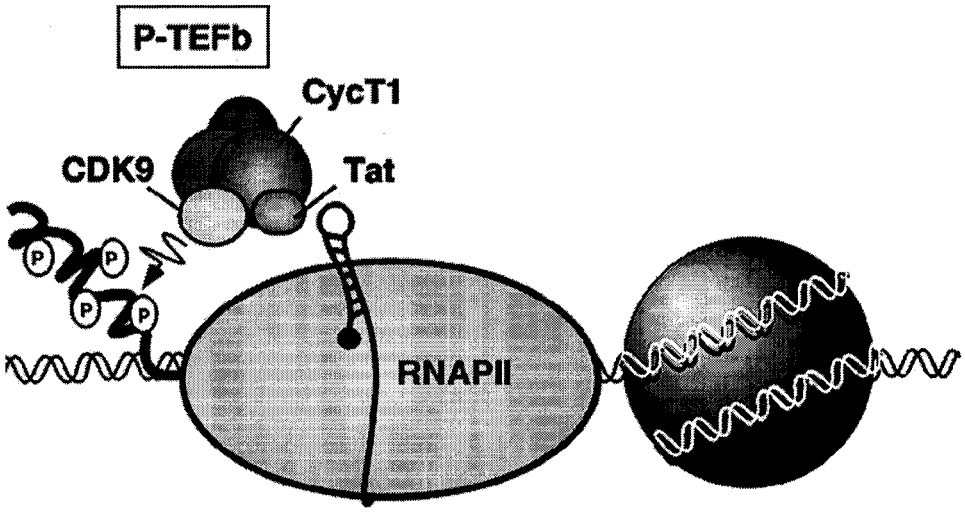

Figure 1.2. The HIV-1 P-TEFb complex, which consists of the TAR RNA, Tat, CycT1, and CDK9 proteins, attached to RNA polymerase II and the HIV genome template (Tutter and Jones 1998).

The toolbox of molecular structure elucidation

Atomic structure governs the function of biological molecules and biomolecular complexes (Pauling 1946). Therefore, the key to understanding molecular function is structural knowledge. While several simple and highly accurate techniques exist for determining the primary and secondary structure of biological compounds, there are few techniques for determining the tertiary structure (Kjems and Egenbjerg 1998). The tertiary structure is the architecture or three-dimensional spatial arrangement of atoms within a molecule. X-ray crystallography is the premier method for determining the three-dimensional structure of molecules at atomic resolution. While there are over a thousand X-ray crystallographic structures of proteins, the number of X-ray structures of multi-domain RNAs remains less than a dozen. Structures currently exist for several tRNAs (e.g. $tRNA_f^{met}$) (Woo, Roe et al. 1980), the P4-P6 domain of the *Tetrahymena* group I intron (Cate, Gooding et al. 1996), the hammerhead ribozyme (Pley, Flaherty et al. 1994; Scott, Finch et al. 1995; Murray, Szoke et al. 2000), the hepatitis delta virus ribozyme (Ferré-D'Amaré, Zhou et al. 1998), the hairpin ribozyme (Rupert and Ferré-D'Amaré 2001; Rupert, Massey et al. 2002), and the small and large subunits of the ribosome (Ban, Nissen et al. 2000; Clemons, Brodersen et al. 2001). The reason for the low number of RNA crystal structures is the difficulty in obtaining highly homologous crystals which defract well enough to give high resolution information.

One of the drawbacks of using crystallography to study biological function is that low energy conformations crystallize significantly better than high energy conformations, often resulting in the solution of static ground state structures incapable of performing the molecule's biological function. Thus solution methods, which can be used to determine molecular structure in an active environment, are essential complements to crystallography. Solution-state nuclear magnetic resonance (NMR) spectroscopy is the second most influential method for determining molecular structure. NMR spectroscopy has been particularly important for determining RNA-metal ion (Huppler, Nikstad et al. 2002) and RNA-small molecule complexes in solution (Hermann and Patel 2000).

However, the major drawbacks of NMR (tumbling of the molecule on the NMR time scale and resolution of atomic resonances, resulting in a molecular size limitation), typically limit NMR studies to single domains of multi-domain RNA molecules, RNA-metal ion, and RNA-small molecule complexes. Additionally, these samples must be isotopically labeled, an expensive and time consuming process.

Several biochemical methods exist that give low-resolution structural information. Transient electric birefringence (TEB) (Zacharias and Hagerman 1995) and non-denaturing comparative gel electrophoresis (Bassi, Mollegaard et al. 1995) can give information about global shape and conformational changes. Nucleotide analog interference mapping (NAIM) can allude to the importance of certain functional groups in the molecule's structure and function (Jones and Strobel 2003). Hydroxyl radical footprinting, and chemical nuclease footprinting can provide information about solvent accessibility, although one cannot distinguish between local steric protection effects and changes in global shape that produce steric protection effects. Chemical cross-linking can be used to determine the relative orientation of helical elements (Sigurdsson and Eckstein 1995; Sigurdsson, Tuschl et al. 1995). In addition, several biophysical techniques exist that can provide low-resolution structural information (Eriksson and Norden 2001). Circular dichroism (CD) and electric linear dichroism (ELD) spectroscopy can monitor global changes in molecular structure, but cannot identify local changes. For example, CD and ELD can provide information about disruption or formation of secondary structure, but cannot identify where the changes take place within the molecule. Fluorescence resonance energy transfer (FRET) can be used to measure distances of 35-85 Å, and thus provide information about global shape. This technique has been particularly important in the study of molecular folding pathways and is capable of detecting changes in single molecules (Zhuang, Kim et al. 2002).

Electron paramagnetic resonance (EPR) spectroscopy

Electron paramagnetic resonance (EPR) spectroscopy, also named electron spin resonance (ESR) spectroscopy, reports information about unpaired electrons and has been used extensively in the study of protein (Hubbell and Altenbach 1994; Hubbell, Gross et al. 1998; Hustedt and Beth 1999; Columbus and Hubbell 2002) and DNA (Robinson, Mailer et al. 1997; Keyes and Bobst 1998) structure, dynamics, and function. Three basic types of information about biomolecular structure and dynamics can be extracted using EPR spectroscopy. First, information about molecular dynamics on the picosecond to millisecond time scale can be measured using EPR (Berliner 1976). Dynamic information can be determined at the global (molecular) or local (amino acid or nucleotide) level. Second, the solvent accessibility at individual sites can be measured by monitoring the relative collision rates of the unpaired electron with paramagnetic relaxation reagents. This has been a particularly important biophysical tool for studying membrane bound proteins which are difficult to crystallize (Lin, Nielsen et al. 1998). Using these power saturation experiments, proteins can be studied directly in vesicle membranes. Third, intermediate range distances of 8-25 Å can be measured using a "spectroscopic ruler" developed for continuous wave (CW) EPR (Rabenstein and Shin 1995). More recently, pulsed electron-electron double resonance (PELDOR), which is also named double electron-electron resonance (DEER), has been developed and can measure significantly longer distances of 15-55 Å (Jeschke 2002; Jeschke 2002). In collaboration with Olav Schiemann at the J. W. Goethe-Universität in Germany, we have measured a 35 Å distance in a model RNA, the longest distance measured in an aqueous environment using an EPR technique (Schiemann, Weber et al. 2003). Of notable importance, CW and pulsed EPR techniques fill the distance measurement gap between nuclear Overhauser enhancement (NOE) NMR spectroscopy (0-6 Å) and FRET measurements (35-85 Å) in aqueous solution. Two advantages of using EPR spectroscopy are that only small amounts of material (typically a nmol) are required for EPR studies and that there is no upper bound on molecular size. By comparison, NMR requires three orders of magnitude

more material, and can only be used to study molecules up to ca. 20 kDa in size. The major drawback of using EPR is that because of the rarity of unpaired electrons in biological systems other than bound metal ions, external reporter groups must be incorporated into the biological molecule.

The work presented in this thesis focuses on the role of RNA structure and dynamics in molecular recognition as studied by EPR spectroscopy of spin-labeled RNA. First, a general and efficient method for the preparation of spin-labeled RNA will be presented. Several chapters will follow which describe the study of changes in HIV-1 TAR RNA internal dynamics upon binding to metal ions, derivatives of the Tat protein, and small molecules which inhibit TAR-Tat complex formation. After that a chapter will describe using EPR spectroscopy to monitor the metal ion-dependent folding pathway of the hammerhead ribozyme. The thesis will conclude with suggestions for future studies regarding the use of EPR spectroscopy of spin-labeled RNA to investigate RNA structure and dynamics.

Chapter 2

Preparation of spin-labeled RNA and structure-dependent dynamics of RNA by EPR spectroscopy

EPR spectroscopy

The use of EPR spectroscopy to study biomolecular structure and dynamics requires the site-specific incorporation of unpaired electrons. The binding affinity and local environment of paramagnetic metal ions in naturally occurring metal ion binding sites can be studied directly using EPR. For example, Mn^{2+} binding to the A9/G10.1 metal ion binding site of the hammerhead ribozyme has been studied by EPR spectroscopy and electron-nuclear double resonance (ENDOR), an EPR-NMR hybrid spectroscopic experiment (Horton, Clardy et al. 1998; Morrissey, Horton et al. 1999; Morrissey, Horton et al. 2000; Schiemann, Fritscher et al. 2003). Additionally, one can use electron spin-echo envelope modulation (ESEEM) EPR spectroscopy to determine the number of RNA-metal ion contacts for a paramagnetic metal ion in a single environment (Hoogstraten and Britt 2002; Hoogstraten, Grant et al. 2002).

In order to use EPR spectroscopy to study the structure and dynamics of biological molecules, rather than bound metal ions, stable free radicals must be site-specifically incorporated into the molecule of interest. Nitroxides are the most commonly used class of stable free radicals for molecular spin-labeling (Figure 2.1). The free electron in the nitroxide is exceptionally stable because it is shared by the nitrogen and the oxygen atoms, sterically protected from reaction with solvent and other molecules by the methyl groups, and electronically stabilized by the methyl groups which donate electron density to the heteroatoms. The molecular structure and the EPR first derivative spectrum of an example nitroxide are shown in Figure 2.1. Because ^{14}N has a nuclear

spin of 1, it couples with the electron to produce three energy states (-1, 0, +1) which are represented by the three lines in the EPR spectrum.

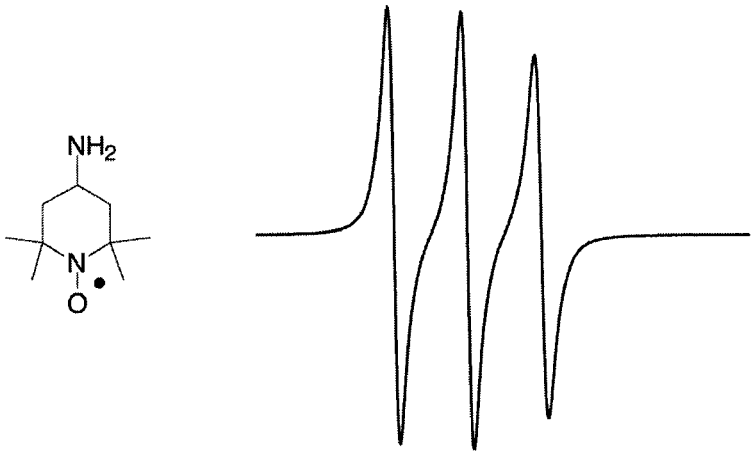

Figure 2.1. 4-amino-2,2,6,6-tetramethylpiperidyl-N-oxyl (4-amino TEMPO) and a typical fast motion EPR spectrum of a nitroxide

EPR spectroscopy has been used extensively in the study of protein and DNA structure and dynamics, but has only recently been applied to RNA, primarily due to the lack of a general and efficient method for preparing spin-labeled RNA. After a brief description of protein and DNA spin-labeling methods, a strategy for the preparation of spin-labeled RNA will be presented (Edwards, Okonogi et al. 2001). Verification of spin-label incorporation and the effect of the modification on RNA stability will be addressed. Finally, the spin-labeled RNA will be used to investigate structure-dependent dynamics in the TAR RNA.

Protein Spin-Labeling

The ease of preparation of nitroxide spin-labeled proteins and the universal applicability of the labeling methodology have been major contributing factors to the large body of literature reporting the study of protein structure and dynamics by EPR spectroscopy. Site-directed spin-labeling (SDSL), developed by Wayne Hubbell in the

1970s (Hubbell and Altenbach 1994), combines site-directed mutagenesis, a revolutionary technique which allows for incorporation of cysteine residues (or any natural amino acid) at desired positions of the protein sequence, and spin-labeling with a nitroxide methyl sulfonate spin-label (MTSSL) to produce spin-labeled proteins (R1) in high yield (Figure 2.2). Alternatively, the rigid backbone spin-label TOAC can be incorporated into short peptides via solid phase chemical synthesis (Monaco, Formaggio et al. 1999; McNulty, Silapie et al. 2000).

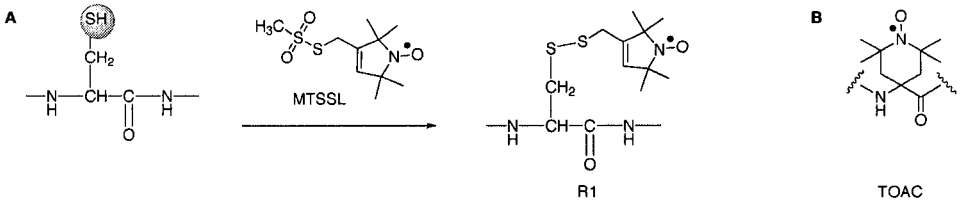

Figure 2.2. A) Spin-labeling of proteins at cysteine residues using MTSSL to produce the R1 site-directed spin-label. B) The rigid TOAC spin-label for peptide studies

DNA Spin-Labeling

Spin-labels have been site-specifically incorporated into deoxyribonucleic acids (DNA) through synthesis of modified nucleoside phosphoramidites and automated chemical oligonucleotide synthesis (Robinson, Mailer et al. 1997; Keyes and Bobst 1998). In addition, spin-labels have been incorporated into DNA via synthesis of modified nucleoside triphosphates and enzymatic oligonucleotide synthesis, although this method does not allow for site-specific incorporation (Kao and Bobst 1985; Keyes and Bobst 1998). Most commonly the nitroxide spin-label is attached to a pyrimidine nucleobase (Figure 2.3). This type of modification typically does not interfere with base-pairing and extends the spin-label into an open region of helical space.

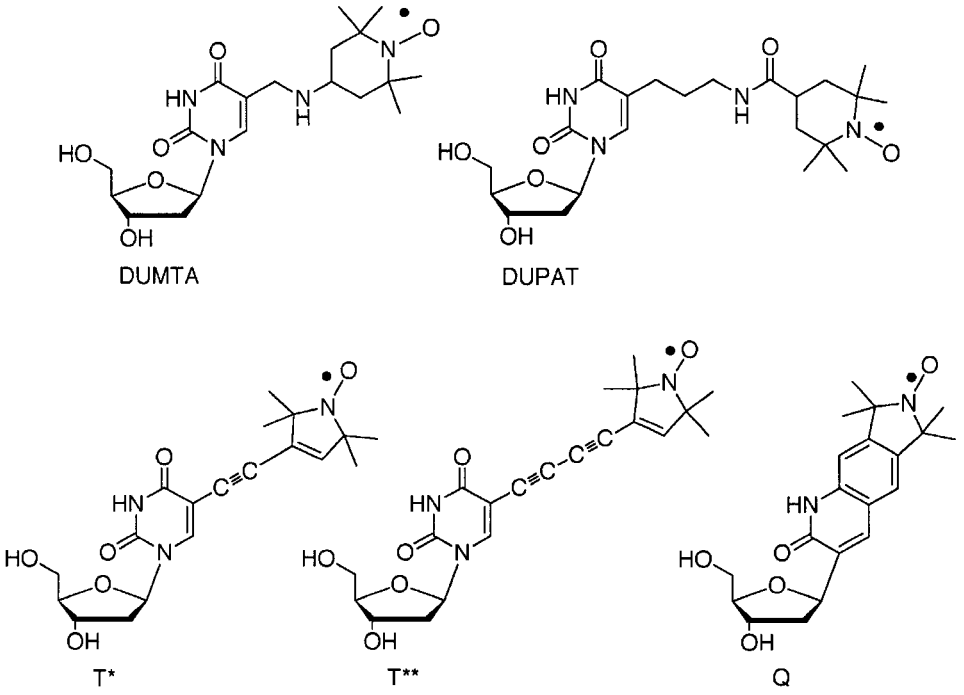

Figure 2.3. DUMTA, DUPAT, T*, T**, and Q spin-labeled nucleosides

All of these spin-labeled nucleosides require elaborate and labor-intensive multi-step syntheses. For example, T* is synthesized in 12 steps (Spaltenstein, Robinson et al. 1989), while Q is synthesized in 14 steps and requires incorporation of an additional non-natural nucleotide, 2-aminopurine (2AP), on the complement strand for appropriate base-pairing (Miller and Hopkins 1994; Miller, Alley et al. 1995).

Lessons from Protein and DNA Spin-Labeling

Several important lessons from the study of protein and DNA structure and dynamics by EPR spectroscopy are applicable to the study of RNA structure and dynamics. First, spin-labels should be linked to the biopolymer as rigidly as possible to facilitate correlation of spin-probe motions with the local dynamics of the biopolymer. For example, in DUMTA and DUPAT the nitroxide is conjugated to the nucleobase through a flexible tether, which allows for motion of the nitroxide independent of the

nucleic acid (Keyes and Bobst 1998). Therefore, the observed nitroxide motion is always faster than the actual motions of the nucleobase, which decreases the accuracy of the EPR measurements. For T* and the diacetylene analog T**, the nitroxide is connected to the nucleobase via a resonance conjugated linker, which should increase the correlation between the nitroxide motions and the nucleobase motions. However, T* and especially T** were shown to have significant rotation about the acetylene linkage (Kirchner, Hustedt et al. 1990; Hustedt, Kirchner et al. 1995). Nevertheless, incorporation of T* into several DNAs allowed for identification of nucleotides in different structural contexts (e.g. single nucleotide, single strand, hairpin loop, and base-paired duplex nucleotides (Spaltenstein, Robinson et al. 1989)), demonstrating that with the semi-rigid acetylene linker, T* largely reports the motions of the nucleotide to which it is attached. For the modified nucleoside Q (Miller and Hopkins 1994; Miller, Alley et al. 1995), the spin-label is rigidly attached to the nucleoside base, prohibiting movement of the nitroxide independent of the nucleic acid.

Second, ease of spin-labeled biopolymer preparation should be of high importance to facilitate rapid investigation of a wide variety of spin-labeled samples. While the spin-labeled DNAs were prepared by multi-step organic synthesis, the majority of protein spin-labeling is accomplished using a post-synthetic modification strategy. Each method (multi-step synthesis coupled with solid-phase biopolymer synthesis or post-biopolymer synthetic modification) has its advantages and disadvantages and must be balanced with linker flexibility. Finally, the method should be universally applicable, meaning that the spin-labels should be able to be attached to any position of the sequence, regardless of secondary structure. Specifically for RNA, the spin-labeling method should be applicable to all bases (A, G, C, U) and structural contexts (e.g. hairpin loops, duplex, triplex, and tertiary contact nucleotides).

RNA Spin-Labeling

The study of RNA structure and dynamics by EPR spectroscopy has been limited by the lack of a convenient, general, and efficient method for attachment of the spin-label to the nucleic acid (Dugas 1977). In the earliest examples of using EPR to study RNA structure and dynamics, spin-labels were attached to tRNAs, either by reaction of a bromoacetamido spin-label with a naturally occurring 4-thiouridine residue (Hara, Horiuchi et al. 1970) or by periodic cleavage of the 2'-3' diol at the 3' end of the RNA followed by reductive amination with 4-amino TEMPO to produce 3'-end morpholino spin-labeled RNA (Caron and Dugas 1976). Spin-labels have been incorporated into RNA by enzymatic synthesis (Kao and Bobst 1985), although this method does not allow for site-specific incorporation. Advances in solid phase RNA synthesis have allowed for the site-specific incorporation of 4-thiouridine residues, which can be spin-labeled with an iodoacetamide spin-label (Ramos and Varani 1998). This method was only applied to non-base-paired nucleotides, because the modification eliminates the hydrogen bonds of a traditional A·U base-pair. Spin-labels have be attached to the 5'-end of RNA by reaction of a sulfonate spin-label with a 5'-phosphorothioated RNA, prepared by enzymatic synthesis (Macosko, Pio et al. 1999). Circular permutation was employed to produce several different spin-labeled samples, although labeling was always restricted to the 5'-end. These methods are fairly limited and cannot be applied to base-pairing nucleotides.

We have reported a method for the incorporation of spin-labels into internal, base-pairing sites in RNA (Edwards, Okonogi et al. 2001), which will be described in the next section. Since publication of this strategy, other RNA spin-labeling methods have been reported. Spin-labels have been incorporated at the 5-position of uridine via Pd catalyst coupling to produce an RNA T* analog (Strube, Schiemann et al. 2001), at internal phosphorothioates (Qin, Butcher et al. 2001), and at 4-thiouridine residues using methane sulfonate spin-labeling reagents (Qin, Hideg et al. 2003).

A general and efficient method for the preparation of spin-labeled RNA

A variety of molecules have been conjugated to the 2'-position of nucleotides in single stranded and base-pairing regions of RNA (Eckstein 2002). Of particular interest, 2'-amino modified pyrimidine phosphoramidites are commercially available and protocols for the synthesis of the purine analogs have been reported. The multistep organic synthesis of the 2'-amino modified uridine phosphoramidite is detailed in Appendix 1. Aliphatic isocyanates have been shown to react selectively with 2'-amino groups to produce urea linked conjugated oligoribonucleotides (Sigurdsson and Eckstein 1996). Of additional imortance, a mild and simple procedure has been reported for the preparation of aliphatic isocyanates using trichloromethyl chloroformate and the corresponding aliphatic amine (Sigurdsson, Seeger et al. 1996). We prepared the spin-labeling reagent **1**, 4-isocyanato TEMPO, in one step in 87% yield using commercially available materials (Scheme 2.1) (Edwards, Okonogi et al. 2001). Subsequent reaction of **1** with 2'-amino modified RNA typically proceeded in >90% conversion to produce spin-labeled RNA (Edwards, Okonogi et al. 2001). Unbeknownst to us at the time of publication, another lab had reported a similar method to prepare **1**, although a different solvent and base were used (Dulog and Lutz 1991). We have since used this spin-labeling method on a wide variety of RNA lengths (8-38 nucleotides). Spin-labeling of the crude sample from solid phase synthesis allowed for a single purification step, and therefore high yields (Edwards, Okonogi et al. 2002). Depending on sequence length and the quality of the solid-phase synthesis, 400-700 nmol were routinely obtained for a 1.0 μmol syntheis of a short RNA sequence (12-15 nucleotides) and 200 nmols were obtained for long sequences (33-38 nucleotides). In addition to short oligoribonucleotide lengths prepared by solid phase synthesis (up to 40-50 nucleotides), long oligoribonucleotide samples can be made by ligation of short spin-labeled RNAs with longer sequences, prepared by in vitro transcription using a DNA template. While this process is not highly efficient, it is feasible, because EPR spectroscopy only requires small amounts of material (typically a nmol or less).

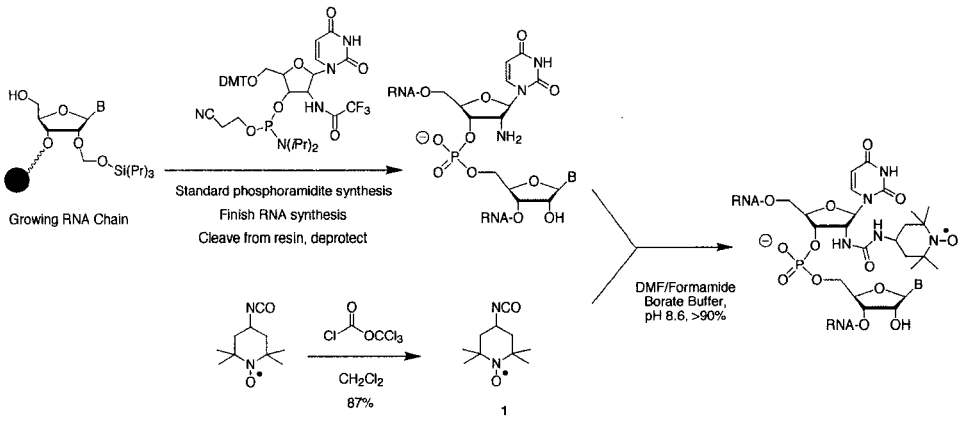

Scheme 2.1. Preparation of 2'-spin-labeled RNA by coupling 2'-amino modified RNA with the spin-labeling reagent 4-isocyanato TEMPO, **1**, prepared in one step using commercially available materials.

Verification of Spin-Label Incorporation

Reaction of **1** with 2'-amino modified RNA to produce 2'-urea-linked RNA was optically monitored at 260 nm using reverse phase high pressure liquid chromatography (RP-HPLC) (Figure 2.4). Before chemical modification, the 2'-amino oligoribonucleotide 5'-GC(2'-NH_2 U)CUCUGGCCC showed a single peak. After reaction with **1**, a new peak with a longer retention time was observed, leaving only a small peak corresponding to the starting oligomer. This analysis protocol allows for quantification of the conversion from 2'-amino to spin-labeled RNA. The spin-labeling reaction also was monitored by anion exchange HPLC, giving similar results (data not shown).

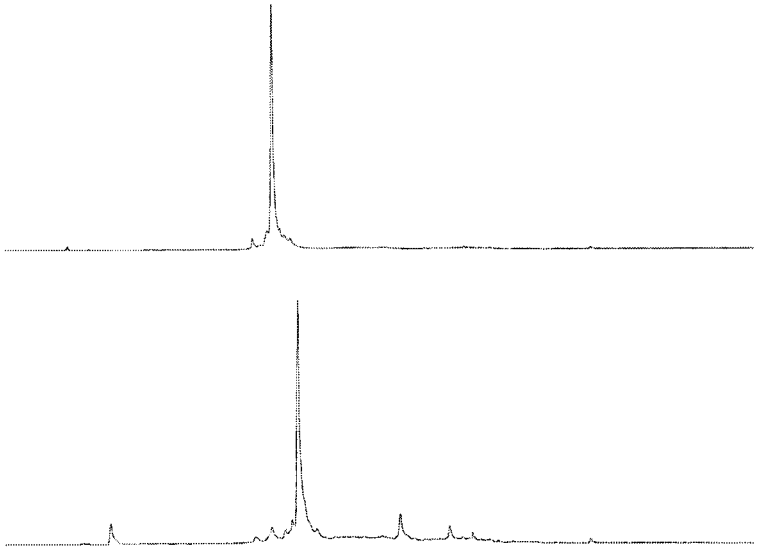

Figure 2.4. RP-HPLC analysis of the reaction of 5'-GC(2'-NH_2 U)CUCUGGCCC (top trace) with **1** (bottom trace), showing the appearance of a new peak, corresponding to the spin-labeled sequence.

Alternatively, RNA spin-labeling could be monitored by 20% denaturing polyacrylamide gel electroporesis (DPAGE), although this method is not quantitative (Figure 2.5). For example, after reaction of the 33 nucleotide sequence 5'-GGA AAG GUA CUG ACA GUA GUC AGU ACC UUU C(2'-NH_2 U)U with **1** (lane 2), the oligomer had reduced gel mobility, characteristic of a larger molecule, in comparison with the unreacted sequence (lane 1). A co-spot of the unlabeled and spin-label reaction mixtures (lane 3) confirmed the appearance of a new molecule. The spin-labeled samples were routinely purified by 20% DPAGE, rather than HPLC, because certain length spin-labeled RNA molecules would co-elute with a degradation product of **1**, resulting in free-spin contaminated samples.

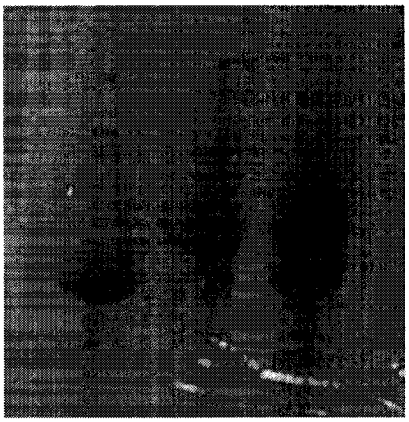

Figure 2.5. 20% DPAGE analysis of 5'-GGAAAGGUACUGACAGUAGUCAGUACCUUUC(2'-NH_2 U)U (lane 1), its spin-labeling with **1** (lane 2), and co-spot of lanes 1 and 2 (lane 3).

Electrospray ionization mass spectrometry (ESI-MS) verified incorporation of the nitroxide spin-label into the RNA. For example, 5'-GCUC(2'-NH_2 U)CUGGCCC (3723.20 observed deconvoluted mass, 3723.29 calculated mass) had a deconvoluted mass of 3920.50 (3920.55 calculated) after reaction with **1** (for actual observed mass peaks, see Table 2.1). Molecular ions were observed in the negative ion mode because the highly acidic phosphodiester backbone makes oligoribonucleotides negatively charged.

Table 2.1. ESI-MS of 5'-GCUC(2'-NH_2 U)CUGGCCC and the corresponding spin-labeled RNA.

Ion	2'-NH_2 RNA Observed (m/z)[a]	Calculated (m/z)	Spin-labeled RNA Observed (m/z)	Calculated (m/z)
$[M-4H]^{4-}$	929.81	929.82	978.68	979.14
$[M-5H]^{5-}$	743.54	743.66	782.96	783.11
$[M-6H]^{6-}$	619.57	619.55	652.44	652.43
$[M-7H]^{7-}$	530.98	530.90	559.11	559.08
$[M-8H]^{8-}$	464.48	464.41	489.17	489.07
Final M	3723.20	3723.29	3920.50	3920.55

[a] Error in molecular ion masses are estimated to be within 0.05 m/z.

Enzymatic digestion of the modified oligomer further verified incorporation of the spin-label. HPLC analysis of the enzymatic digestion of 5'-GCUC(2'-NH_2 U)CUGGCCC revealed 4 peaks, corresponding to C, 2'-NH_2 U, U, and G; there is no adenosine in this sequence (Figure 2.6). Digestion of the corresponding spin-labeled sequence revealed the

absence of the 2'-NH_2 U peak and the presence of a new, more strongly retained compound which was shown to co-elute with an authentic sample of the expected spin-labeled nucleoside, prepared by chemical synthesis (see Materials and Methods, Chapter 8).

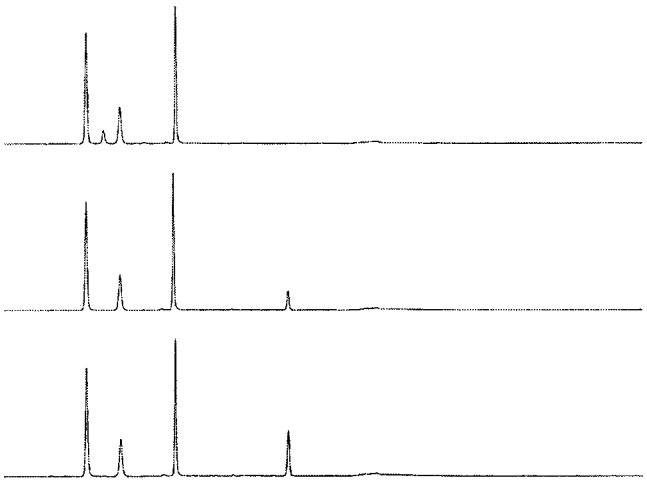

Figure 2.6. RP-HPLC chromatograms of oligoribonucleotides enzymatically digested with alkaline phosphatase and phosphodiesterase. a) enzymatic digestion of 5'-GCUC(2'-NH_2 U)CUGGCCC b) the corresponding spin-labeled RNA c) co-injection of the spin-labeled RNA digestion (trace b) and the expected spin-labeled nucleoside prepared by chemical synthesis.

Effect of Spin-Labeling on RNA Secondary Structure and Stability

To investigate the effect of spin-label modification on RNA secondary structure stability, four spin-labeled TAR RNA samples were prepared, each containing a single spin-label at U23, U25, U38, or U40 (Figure 2.7). UV-monitored thermal melting experiments were performed to investigate the effect of the spin-label on the thermodynamic parameters of duplex formation. The melting curves for unmodified and spin-labeled TAR RNA samples showed a cooperative melting transition, indicative of a two state unfolding pathway (Breslauer 1994). The melting temperatures for all modified RNA samples were within 3 °C of the unmodified RNA melting temperature, and the

difference in free energy ($-\Delta\Delta G_{37}$) between the spin-labeled and unmodified samples was < 1 kcal/mol (Table 2.2). Interestingly, spin-labels in the bulged region (U23 and U25) enhanced overall RNA duplex stability as evidenced by increases in $-\Delta G_{37}$ at both positions. These data indicate that the spin-label modifications do not appreciably perturb the RNA secondary structure stability.

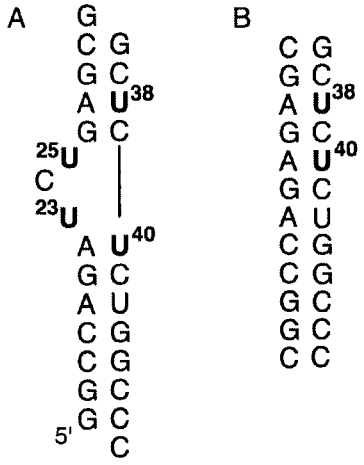

Figure 2.7. a) Sequence and secondary structure of the TAR RNA. b) Sequence and secondary structure of the TAR duplex lacking the trinucleotide bulge. Spin-labeling sites are shown in bold.

Table 2.2. Thermodynamic data for spin-labeled TAR RNA samples

Modification	T_m (°C)	$-\Delta G_{37}$ (kcal/mol)	$-\Delta H_{37}$ (kcal/mol)	$-\Delta S_{37}$ (cal/mol·K)
Unmodified	50.7 ± 1.1	2.45 ± 0.17	58.2 ± 5.2	180 ± 16
U23	51.6 ± 1.2	2.93 ± 0.24	66.4 ± 8.4	205 ± 26
U25	50.7 ± 0.8	3.12 ± 0.39	73.7 ± 1.8	227 ± 12
U38	47.8 ± 0.8	1.78 ± 0.07	53.5 ± 5.3	167 ± 17
U40	49.1 ± 1.2	2.19 ± 0.12	59.6 ± 2.8	185 ± 20

Structure-dependent dynamics of RNA by EPR spectroscopy

The spectral width ($2A_{zz}$) of an EPR spectrum, which spans the crest of the low field peak to the trough of the high field peak, is sensitive to the motions of the spin-probe (Freed 1976). For example, the small molecule 4-amino TEMPO displays rapid, isotropic motion in an aqueous medium, which is demonstrated by the near three line pattern of the EPR spectrum (Figure 2.8, top trace). Once attached to a uridine nucleoside

via a semi-rigid urea linker, the spin probe displays a wider spectral width, characteristic of reduced mobility, as expected due to the increase in size relative to the smaller molecule (Figure 2.8, middle trace). Upon incorporation into a short single stranded oligoribonucleotide, the spin probe shows an additional increase in spectral width, demonstrating further reduction in mobility (Figure 2.8, bottom trace). Combined these three spectra demonstrate how EPR spectroscopy is sensitive to the global motions of spin-labeled RNA.

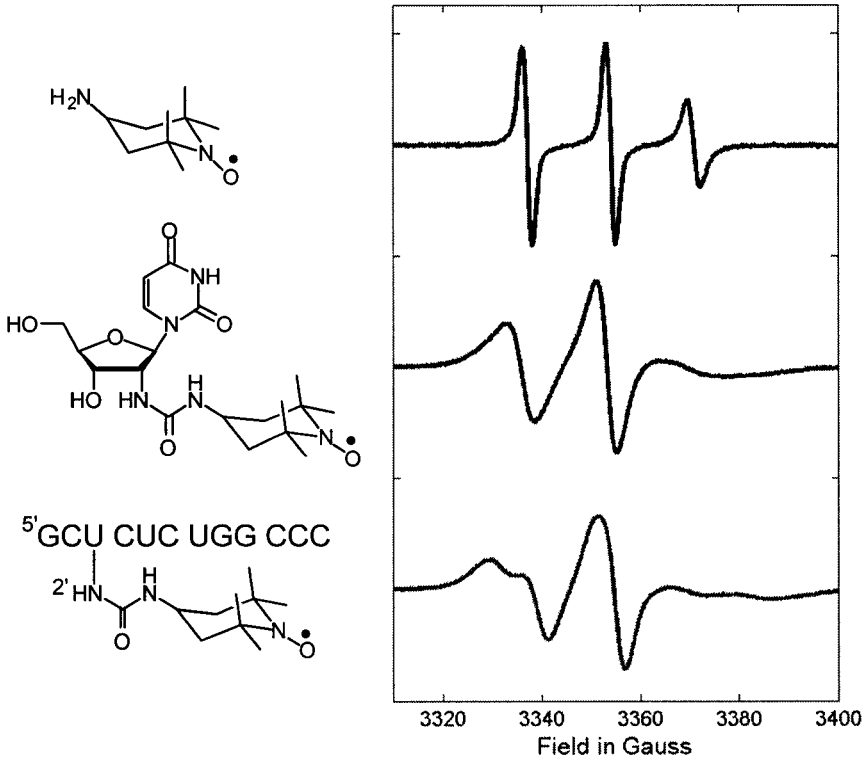

Figure 2.8. EPR spectra of 4-amino TEMPO (top), the spin-labeled nucleoside (middle) and U38 spin-labeled single strand (bottom) obtained in 50% sucrose/100 mM NaCl, 10 mM phosphate, 0.1 mM Na_2EDTA, pH 7.0.

To allow for EPR spectroscopic access to RNA internal dynamics, rather than global dynamics, spin-labeled samples were prepared in a viscous aqueous sucrose medium which effectively immobilizes the global tumbling of similar sized molecules on

the EPR time scale. EPR spectra were obtained of four TAR RNA samples, each containing a spin-label at a single position (Figure 2.9). As expected, nucleotides in the flexible bulge region (U23 and U25) have narrower EPR spectral widths than those in base-pairing regions (U38 and U40), demonstrating that these nucleotide are more mobile. Furthermore, the spectra for U23 and U25 show motions in the nanosecond range with a ca. 40-fold increase in mobility relative to the base-paired nucleotides U38 and U40. EPR spectroscopic simulations performed by our collaborators Tamara Okonogi and Bruce Robinson, showed that U40 single strand and U23 TAR displayed similar rotational correlation times (6 and 8 ns, respectively) and order parameters (0.63 and 0.67). Small rotational correlation times (nanosecond or less) are indicative of fast motions. Low order parameters (close to zero) are indicative of low degree or order, whereas order parameters close to 1 are indicative of a highly ordered state. On the other hand, U40 TAR showed significantly slower motions (τ_{perp} = 360 ns, τ_{para} = 190 ns) and a much higher order parameter (0.98). The fact that the motions in the TAR RNA bulge region are more mobile than those in the base-pairing region is an expected result and has been observed previously by ^{13}C NMR relaxation experiments (King, Harper et al. 1995).

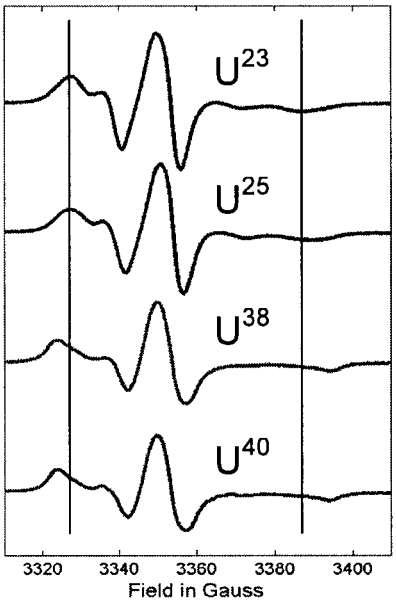

Figure 2.9. EPR spectra of spin-labeled TAR RNA samples. The position of the spin-label is incidated on each spectrum. The samples were prepared in 50% sucrose/100 mM NaCl, 10 mM sodium phosphate, 0.1 mM Na_2EDTA, pH 7.0. A line indicating the spectral width of U23 TAR RNA is extended through the other spectra, to allow for visual qualitative comparison of the EPR spectral widths.

These results provide evidence for structure-dependent dynamics of the spin-labeled RNA samples, indicating that there is little motion of the spin-probe independent of the nucleic acid. Therefore, the motions of the spin-probe are correlated with the motions of the nucleotide to which it is attached. In principle there can be rotation about two bonds in the linker which could have lead to significant mobility of the probe independent of the nucleic acid. This is an important result, which allows for further studies in RNA dynamics, and in particular enables the use of EPR spectroscopy and this spin-labeling strategy to investigate changes in RNA internal dynamics upon binding to RNA ligands such as metal ions, peptides, and small molecules.

Further applications of spin-labeled RNA

In addition to the study of RNA internal dynamics by EPR spectroscopy (described in Chapters 3-6), spin-labeled ribonucleic acids have other applications. Spin-

labeled RNAs are also useful tools for determining intermolecular contacts in RNA-protein and RNA-small molecules complexes using NMR spectroscopy. For example, 2D NMR experiments such as $^{1}H,^{15}N$ HSQC of isotopically amide labeled proteins and spin-labeled RNAs can be used to determine the relative spatial arrangement of amino acids with respect to a given nucleotide in a ribonucleoprotein (RNP) complex (Ramos and Varani 1998). Using the spin-labeling procedure presented below (Edwards, Okonogi et al. 2001) and that presented by Ramos and Varani (Ramos and Varani 1998), in collaboration with Gabriele Varani at the University of Washington, we were able to orient the RNT1p RNA tetraloop and protein into the RNP complex (unpublished results). In addition, using a 1D NMR $t_{1\rho}$ spin-lock experiment, the binding and orientation of small molecules to spin-labeled macromolecules can be monitored (Jahnke, Perez et al. 2000). For this experiment only small amounts of spin-labeled material are needed (10-20 nmol), making this technique feasible to use. We used this technique to provide preliminary results for TAR RNA-neomycin binding, although we observed that protons in different chemical environments, such as alkyl protons or protons attached to carbons connected to heteroatoms, relax at different rates, adding complexity to this type of analysis (unpublished results).

Chapter 3

EPR spectroscopic analysis of TAR RNA-metal ion interactions

RNA-metal ion interactions

Metal ions are important cofactors in the wide range of biological functions that RNA performs, facilitating RNA folding and structure assembly, tertiary structure stabilization, and catalysis (Pyle 1993; Pyle and Green 1995; DeRose 2002; Fedor 2002). Because RNA is a large polyanion, it needs the condensed positive charges offered by metal ions to balance the repulsive forces of the negatively charged phosphates toward one another. This allows the RNA to fold into the compact structures necessary for performing biological functions. There are three major categories of RNA-metal ion interactions (Pyle 1993; Pyle and Green 1995; Misra and Draper 1998). First, non-specific weak interactions are important for the global shape and fold of RNA and can be satisfied by monovalent and divalent ions alike. In this interaction, a delocalized cationic network of metal ions forms around the RNA molecule. Second, more-specific, higher affinity interactions are important for forming important local interactions in the RNA molecule. Typically, in this type of interaction, both the anionic phosphate and the cationic metal ion retain their full shell of solvation and the electrostatic interaction is stabilized through space. Therefore, the metal ion's ionic size, coordination geometry, and pK_a of its aqua complex are contributing factors to the metal ion specificity and affinity. Third, highly specific, high affinity interactions are important for direct and indirect participation in catalysis as well as for formation of highly specific local structure. In this type of interaction, the metal ion's sphere of hydration is often disrupted, allowing for intimate RNA-metal ion interactions.

Techniques for studying RNA-metal ion interactions

Several biochemical and biophysical techniques exist to directly probe the location and effect of specific RNA-metal ion contacts. Analysis of the effect of phosphorothioate and phosphonate mutations on the catalytic rate of ribozymes has been done routinely to probe specific phosphodiester-metal ion interactions (Piccirilli, Vyle et al. 1993; Sontheimer, Sun et al. 1997; Liao, Anjaneyulu et al. 2001; Shan, Kravchuck et al. 2001). Enzymatic activity can be rescued with thiophylic metal ions, such as Cd^{2+}. X-ray crystallography (Pley, Flaherty et al. 1994; Scott, Finch et al. 1995; Feig, Scott et al. 1998; Murray, Szoke et al. 2000; Egli, Minasov et al. 2002; Ennifar, Walter et al. 2003) and NMR spectroscopy (Schmitz and Tinoco 2000; Huppler, Nikstad et al. 2002) can identify RNA-metal ion interactions at the atomic level. Indirect methods for investigating important RNA-metal ion contacts include interference of lead(II)-induced cleavage (Brannvall, Mikkelsen et al. 2001; Olejniczak, Gdaniec et al. 2002), transient electric birefringence (Zacharias and Hagerman 1995), laser-induced lanthanide luminescence (Feig, Panek et al. 1999; Mundoma and Greenbaum 2002; Mundoma and Greenbaum 2003), fluorescence correlation spectroscopy (FCS) and fluorescence resonance energy transfer (FRET) measurements (Arzumanov, Godde et al. 2000; Kim, Nienhaus et al. 2002; Wilson and Lilley 2002), and phosphorous relaxation enhancement NMR spectroscopy (Summers, Shimko et al. 2002).

EPR spectroscopy (Horton, Clardy et al. 1998; Morrissey, Horton et al. 1999; Hoogstraten and Britt 2002; Hoogstraten, Grant et al. 2002) and ENDOR (Morrissey, Horton et al. 2000) can be used to directly study the binding affinity and sphere of hydration of free or bound paramagnetic metal ions. Alternatively, EPR spectroscopy of spin-labeled RNA molecules has been used to probe the importance of metal ions in RNA structure, folding, and RNA-RNA complex formation (Pscheidt and Wells 1986; Qin, Butcher et al. 2001).

Metal ions and the structure of the TAR RNA

Biochemical and biophysical evidence have shown that the bugle region of the TAR RNA binds metal ions, although the exact mechanism in solution is still cloudy. The X-ray crystal structure of the HIV-1 TAR RNA solved in the absence of the Tat protein (Ippolito and Steitz 1998) revealed a different structure than that previously obtained by solution NMR (Aboul-ela, Karn et al. 1996) (Figure 3.1). In the solution NMR structure, the trinucleotide bulge induced a ca. 50° bend between the upper and lower helices, similar to that calculated from transient electric birefringence (TEB) experiments (Zacharias and Hagerman 1995). Also in the TEB studies, the bend angle decreased significantly in the presence of 2 mM Mg^{2+}. However, this concentration of Mg^{2+} had an inhibitory effect on the TAR RNA-Tat complex formation, and higher Mg^{2+} concentrations were not investigated. Fluorescence studies provided further evidence that Mg^{2+} binds to TAR in an inhibitory manner, with an apparent $K_d \sim$ 1-3 mM, depending on the background K^+ concentration (Arzumanov, Godde et al. 2000). In contrast to the NMR solution structure solved in the presence of K^+, the X-ray structure displayed co-axial stacking of the upper and lower helices, while the bulge region was kinked away from the helical axis (Figure 3.1). The authors noted that their structure contained four specifically bound calcium ions, and they suggested that the calcium ions were responsible for the change in structure. Furthermore, because the crystals were grown in the presence of 50 mM Ca^{2+} and 1.25 mM Mg^{2+}, but only Ca^{2+} was found in the X-ray structure, the authors hypothesized that calcium might be important for the physiology of the RNA.

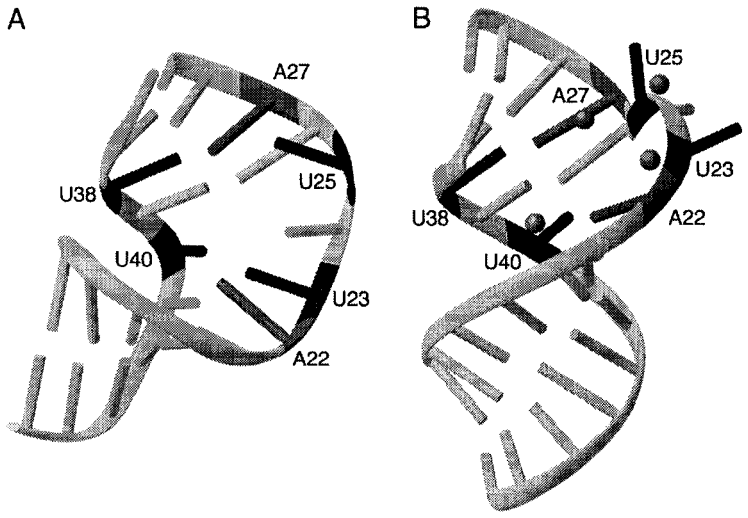

Figure 3.1. Structures of the TAR RNA in the absence of the Tat protein solved by NMR spectroscopy (left) (Aboul-ela, Karn et al. 1996) and X-ray crystallography (right) (Ippolito and Steitz 1998). The TAR RNA backbone is shown in cyan, spin-labeled nucleotides are shown in red (U23, U25, U38, and U40), and residues A22 and A27 which base-pair with U40 and U38, respectively, are shown in green. Calcium ions found in the crystal structure are shown in gold. This figure was created with the RIBBONS program,.

We decided to use EPR spectroscopy of spin-labeled TAR RNAs to determine whether or not the structural differences observed between the NMR structure and the X-ray structure could be detected in solution, and to determine whether or not the difference was specific for calcium ions (Edwards, Okonogi et al. 2002). Therefore, we first investigated metal ion binding to the TAR RNA under crystal structure-like metal ion concentrations in solution. Under these conditions we observed that sodium and calcium ions have a similar effect on the internal dynamics of the TAR RNA, although magnesium ions had a slightly different effect. Further investigation under significantly lower metal ion concentrations revealed three different categories of TAR RNA-metal ion dynamic signatures for the ten metal ions studied. These results demonstrate the utility of EPR spectroscopy for the detection of metal ion-induced changes in RNA internal dynamics and provide insight into the differences and similarities of a variety of TAR RNA-metal ion complexes.

Crystal structure-like metal ion concentrations in solution

To investigate the effect of crystal structure-like calcium concentrations on the internal dynamics of the TAR RNA in solution, conditions appropriate for studying the effects of high metal ion concentrations on RNA internal dynamics were used (Edwards, Okonogi et al. 2002). While previous EPR spectra were obtained in the presence of 50% (w/v) aqueous sucrose buffer (Edwards, Okonogi et al. 2001), we decided to acquire these spectra in the presence of only 20% sucrose (w/v) at 0 °C. At this viscosity (ca. 3.9 cP (1968)), most, but not all, of the global dynamics have been eliminated, and the relative mobility of the spin-probe falls into the highly sensitive portion of the slow motion region of spin-label dynamics (50-60 Gauss $2A_{zz}$). These conditions are considered more "biologically relevant," meaning that the lower percentage of sucrose is less likely to interfere with molecular recognition, and specifically RNA-metal ion complex formation. This concentration is similar to that employed in non-denaturing polyacrylamide gel electrophoresis, a routine biochemical analysis of molecular structure and recognition which typically contains 8-12% sucrose (at 4 °C). In the following discussions we will refer to changes at individual sites, and these changes in dynamics are largely due to changes in internal dynamics, although it is important to consider that large changes in global RNA conformation may lead to small differences in the observed RNA dynamics. The spectra were obtained in the presence of the commonly used EPR and NMR buffer PNE (100 mM NaCl, 10 mM sodium phosphate, 0.1 mM Na_2EDTA, pH 7.0) (Hustedt, Kirchner et al. 1995; Okonogi, Alley et al. 2002).

EPR spectra of spin-labeled TAR RNA samples each containing a single nitroxide spin-label at one of four sites (U23, U25, U38, and U40) were obtained in the absence and presence of crystal structure-like concentrations of $CaCl_2$ (50 mM) or similar ionic strength NaCl (150 mM) or $MgCl_2$ (50 mM) (Figure 3.2). The relationship between ionic charge, concentration, and strength is $I = 0.5\Sigma c_i z_i^2$, where I is the ionic strength, c_i is the ionic concentration, and z_i is the ionic charge. Changes in the EPR spectra indicating changes in RNA internal dynamics in the presence of metal ions were observed at each

position (Figure 3.2). This indicates that the metal ions affect the structure and dynamics of the TAR RNA through one (or more) of the three types of RNA-metal ion interactions. Because of the variability in change in dynamics at any given position, the observed dominant TAR RNA-metal ion interactions do not appear to be of the first type (non-specific, weak interactions indicative of a delocalized ionic network), but rather of the moderate to high affinity sites (second and third types). To further investigate this effect, we repeated this experiment with a duplex TAR RNA construct lacking the trinucleotide bulge. While we did observe subtle changes in dynamics at both U38 and U40 in the presence of both sodium and calcium, these changes were small in comparison with the changes observed at corresponding sites in the TAR RNA (data not shown), indicating that the trinucleotide bulge likely contained the specific, high affinity metal ion binding sites of the TAR RNA (type two and/or three RNA-metal ion interactions).

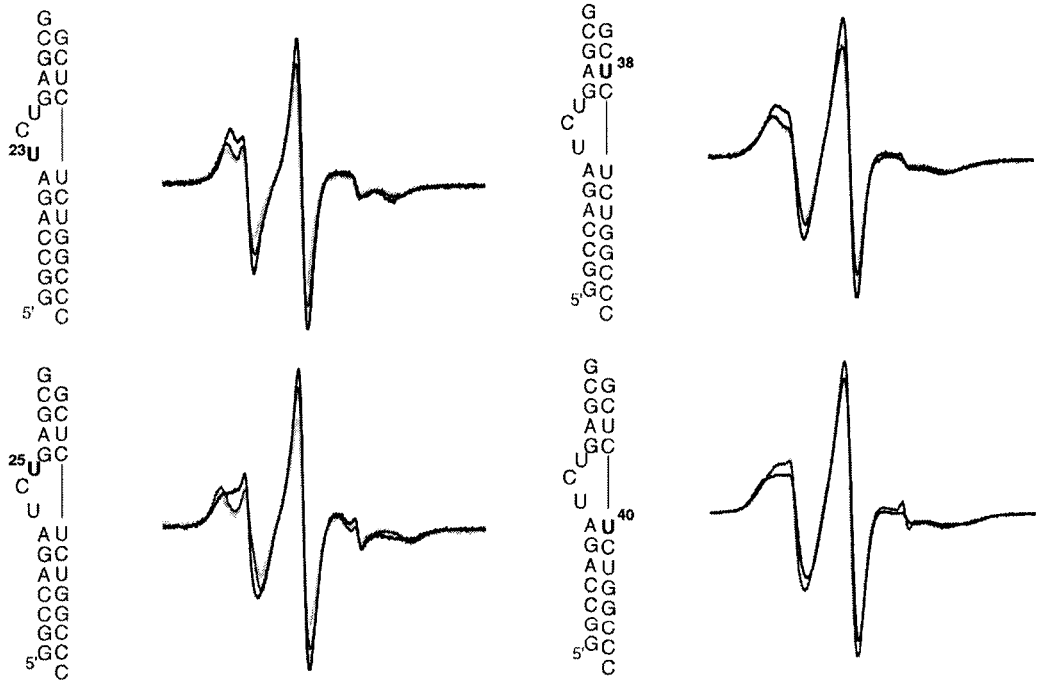

Figure 3.2. EPR spectra of the TAR RNA obtained in the absence (black spectra) and presence of similar ion strength Ca^{2+} (magenta spectra) and Na^{+} (cyan spectra). The position of the spin-label is indicated in bold on the secondary structure of the TAR RNA show to the left of each set of spectra.

The spectra obtained in the presence of similar ionic strength sodium and calcium ions are nearly identical at all positions. Plotting the change in spectral width ($\Delta 2A_{zz}$) as a function of position gives a quantitative representation of the changes in EPR spectral width. This gives us a "dynamic signature" for each set of conditions (Figure 3.3).

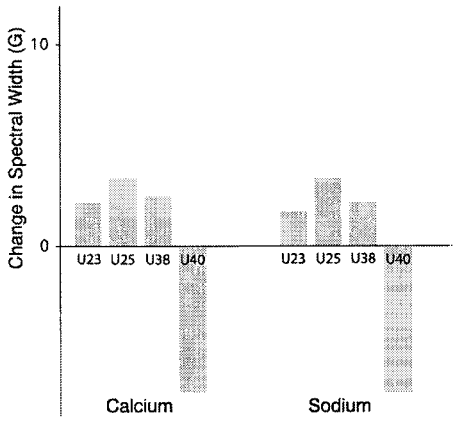

Figure 3.3. Quantitative representation of changes in RNA mobility upon binding to metal ions at crystal structure-like metal ion concentrations in solution. The change in EPR spectral width ($\Delta 2A_{zz}$) is plotted as a function of spin-labeled nucleotide position to give a dynamic signature for each set of conditions.

The dynamic signatures of calcium and sodium were nearly identical with increases in spectral width, indicative of a decrease in spin probe mobility, at positions U23, U25, and U38, and a decrease in spectral width, indicative of an increase in mobility at position U40. The high degree of similarity between the dynamics signatures of sodium and calcium argue against a calcium-specific TAR RNA structural change in solution. Therefore, it is unlikely that calcium ions play a specific role in the cellular function of the TAR RNA-Tat protein complex formation *in vivo*. The dynamic signatures of magnesium under similar conditions, gave similar results for U23, U38, and U40, although, interestingly, the spectral width of U25 decreased, indicating an increase in spin probe mobility (data not shown).

Lower metal ion concentrations in solution

High-resolution X-ray crystallography often requires metal ion concentrations much higher than physiological concentrations, and in order to study specific RNA-metal in contacts, techniques more sensitive to changes in RNA structure and dynamics under physiologically relevant conditions are required. ^{19}F NMR (Hammann, Norman et al. 2001; Olejniczak, Gdaniec et al. 2002), residual dipolar coupling (RDC) NMR (Al-Hashimi, Pitt et al. 2003), and EPR spectroscopy (Pscheidt and Wells 1986; Qin, Butcher et al. 2001) have been used to detect changes in RNA structure and dynamics induced by specific metal ions in solution. The work presented in this section describes the use of EPR spectroscopy to study metal ion-induced changes in TAR RNA structure and internal dynamics under biologically relevant metal ion concentrations. It parallels work done using ^{19}F NMR, RDC NMR, and EPR to study this and other systems under a variety of metal ion conditions. This method facilitates the rapid analysis of the similarities and differences in RNA-metal ion binding while providing information about RNA internal dynamics. Combined, these factors add to the novelty of using EPR spectroscopy to study specific RNA-metal ion interactions under biologically relevant metal ion concentrations.

While Na^+ and Ca^{2+} produced a similar effect on the TAR RNA internal dynamics under crystal structure-like conditions in solution, we wanted to know if this phenomenon occurred under more biologically relevant metal ion concentrations (Edwards and Sigurdsson 2003). Furthermore, because Mg^{2+} had a different effect at U25 than Ca^{2+} and Na^+, we decided to extend the study beyond sodium, calcium, and magnesium to include several metal ions commonly used in RNA structural investigations, in order to further pursue detection of similarities and difference in RNA-metal ion binding. This full list included Li^+, Na^+, Mg^{2+}, K^+, Ca^{2+}, Mn^{2+}, Co^{2+}, Ni^{2+}, Zn^{2+}, Sr^{2+}, Cd^{2+}, and Ba^{2+}. The buffer used in the previous study under crystal structure-like metal ion concentrations contained a high concentration of background Na^+ ions (92 mM), and thus new background metal ion conditions were selected (see the following section). Next, we

observed changes in dynamics at U40, which displayed the largest change under crystal structure-like ionic conditions in solution, upon titration with Mg^{2+} to determine the binding constant(s) of the high affinity metal ion binding site(s) and as a basis for comparison with other metal ions. Finally, we obtained a new set of dynamic signatures for the metal ions listed above under the new background conditions. These experiments produced similar results to those obtained under crystal structure-like ionic conditions in solution, and three categories of RNA-metal ion interactions were observed. Patterns in metal ion properties and a hypothesis for TAR RNA-metal ion binding are presented toward the end of this chapter.

Selection of background metal ion conditions

Background metal ions can potentially mask important contributions of a specific metal ion being studied, and thus, aqueous conditions void of background metal ions are optimal for the study of specific RNA-metal ion interactions. However, metal ions are required for RNA secondary structure formation, and therefore, conditions with a minimal amount of background metal ions that promote stable RNA duplex formation were selected. Potassium ions were chosen over sodium ions as the background monovalent metal ion due to its larger ionic size (1.33 Å), which makes it less likely to form specific interactions. Other RNA-metal ion studies have also used potassium for this reason (Pscheidt and Wells 1986). TAR RNA UV-monitored thermal denaturation experiments in the presence of 1.5 mM K^+ revealed a cooperative melting transition with a melting temperature of 47.3 °C, only 3.4 °C lower than that previous obtained in the presence of 58 mM Na^+ (Edwards, Okonogi et al. 2001) (see chapter 2). This data demonstrates that under these new conditions (1.0 mM potassium phosphate, pH 6.5), the TAR RNA forms a stable duplex. Furthermore, all four spin-labeled TAR RNA samples produced EPR spectra indicative of duplex formation in comparison with single stranded samples and previous results using the 20% aqueous sucrose/PNE buffer (Edwards, Okonogi et al. 2002). For example, the U40 TAR RNA sample had a significantly wider

spectral width ($2A_{zz}$) than that of the U40 single strand (Figure 3.4), the expected result for duplex formation in a larger molecule.

A minor percentage (estimated 10-20%) of the EPR spectra acquired throughout these and other EPR of RNA studies contain multiple spectral components. The EPR spectrum of U40 TAR RNA under these new ionic buffer conditions is a clear example of a multi-component EPR spectrum (Figure 3.4). For multi-component EPR spectra, the less mobile component, which has a wider spectral width, is without exception simpler and more accurate to measure. Therefore, we have chosen to always measure the slower component in referencing the changes in spectral width, because we can more safely and reasonably determine the change for this component. This issue will be further analyzed in Chapter 4 for one of the TAR RNA-Tat mutant peptide complexes.

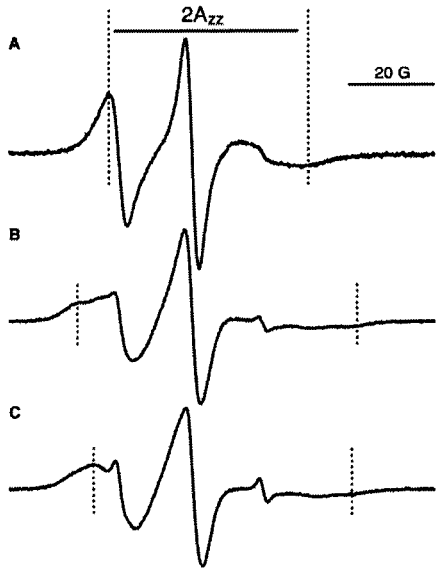

Figure 3.4. EPR spectra of spin-labeled U40 single strand (a) and U40 TAR RNA in the absence (b) and presence (c) of 10 mM $MgCl_2$. The outer hyperfine splitting, indicating the spectral width ($2A_{zz}$), are marked with dotted lines and the Gaussian scale is also indicated.

Monitoring the binding of Mg^{2+} to the TAR RNA by EPR spectroscopy

Magnesium is the most prolific RNA-binding metal ion (Misra and Draper 1998) and previously has been shown to bind to the TAR RNA, affecting its global structure (Zacharias and Hagerman 1995) and ability to bind to the Tat protein (Arzumanov, Godde et al. 2000). To investigate the concentration-dependence of TAR RNA-Mg^{2+} binding as a basis for comparison with other metal ions, the change in U40 TAR RNA EPR spectral width was monitored upon titration with increasing concentrations of Mg^{2+} (Figure 3.5). The EPR spectral width changed up to 2 mM Mg^{2+} with subtle changes in line shape up to 10 mM Mg^{2+}. No further change in either EPR spectral width or line shape was observed up to 50 mM Mg^{2+}. These results indicate a high affinity TAR RNA-Mg^{2+} complex formation with a binding constant of ~ 1 mM, which is similar to that measured by ^{19}F NMR (0.9 mM) (Olejniczak, Gdaniec et al. 2002) and consistent with the TAR-Tat half inhibitory concentration of Mg^{2+} which was observed at 1 mM under low K^+ concentrations (Arzumanov, Godde et al. 2000). Shortly after publication of this data (Edwards and Sigurdsson 2003), a study describing the use of residual dipolar coupling (RDC) NMR spectroscopy to study the TAR RNA-Mg^{2+} complex reported a similar binding constant (Al-Hashimi, Pitt et al. 2003). The subtle changes in spectral shape between 2-10 mM Mg^{2+} are likely due to the weak nonspecific RNA-metal ion interactions (type one) characteristic of a delocalized ionic network. To account for both changes in spectral width and line shape, 10 mM Mg^{2+} was chosen as the ionic strength reference point for the remainder of the report which focuses on the effect of a variety of metal ions on the TAR RNA internal dynamics. This concentration was also chosen because it is within the biologically relevant range which includes 2 mM in the blood plasma and 26 mM in the intercellular fluid. Furthermore, titration of U38 TAR RNA with Mg^{2+} revealed similar results in terms of change in EPR spectral width and line shape, reaffirming the binding constant measurement as well as choice of 10 mM Mg^{2+} as a reference point. In order to prepare samples under similar ionic strength, 10 mM

divalent and 30 mM monovalent metal ion concentrations were used (see equation in the section title "Crystal structure-like metal ion conditions in solution").

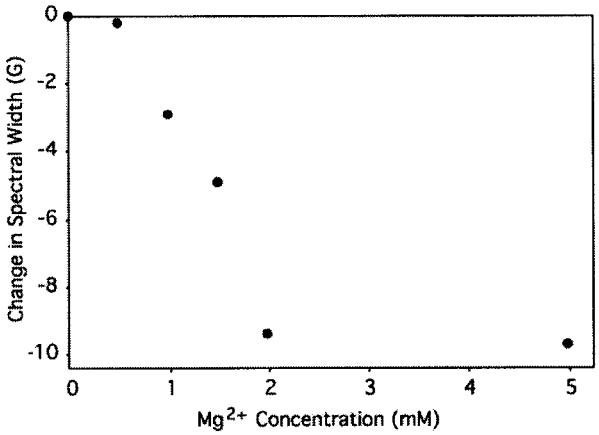

Figure 3.5. Measuring the Mg^{2+}-concentration dependence of U40 spin-labeled TAR RNA binding

Effect of a variety of metal ions on the dynamics of the TAR RNA

The changes in TAR RNA internal dynamics, as indicated by the changes in EPR spectral width, upon incubation with a variety of metal ions are shown in Figure 3.6. As described earlier, plotting the change in spectral width at a variety of positions (U23, U25, U38, and U40) gives a dynamic signature for each TAR RNA-metal ion complex. Three groups of dynamic signatures were observed under the biologically relevant metal ion concentrations presented here. The monovalent metal ions Li^+ and K^+ had only a small effect on TAR RNA internal dynamics. Na^+ and Ca^{2+} induced similar changes in TAR RNA internal dynamics, in agreement with earlier results obtained under crystal structure-like metal ion concentrations in solution. An increase in spectral width, indicative of a decrease in spin probe mobility, was observed at U23 and U38, little or no change was observed at U25, and a decrease in spectral width was observed at U40. In addition, Sr^{2+} gave a similar dynamic signature. It is interesting to note that Na^+ behaves differently than the other monovalent metal ions, which is an unexpected result. The binding of Na^+ could promote co-axial helical stacking as observed in the Mg^{2+}-bound RDC NMR structure (Al-Hashimi, Pitt et al. 2003) or as observed in the minor conformer

of the TAR RNA in solution in the presence of low background Na^+ concentrations (15 mM sodium cacodylate, pH 6.5) (Long and Crothers 1999). Nevertheless, the metal ions in this group have similar ionic radii (Na^+, 0.97 Å; Ca^{2+}, 0.99 Å; Sr^{2+}, 1.12 Å) and pK_as of their associated metal-aqua complexes (Na^+, 14.8; Ca^{2+}, 12.6, and Sr^{2+}, 13.2).

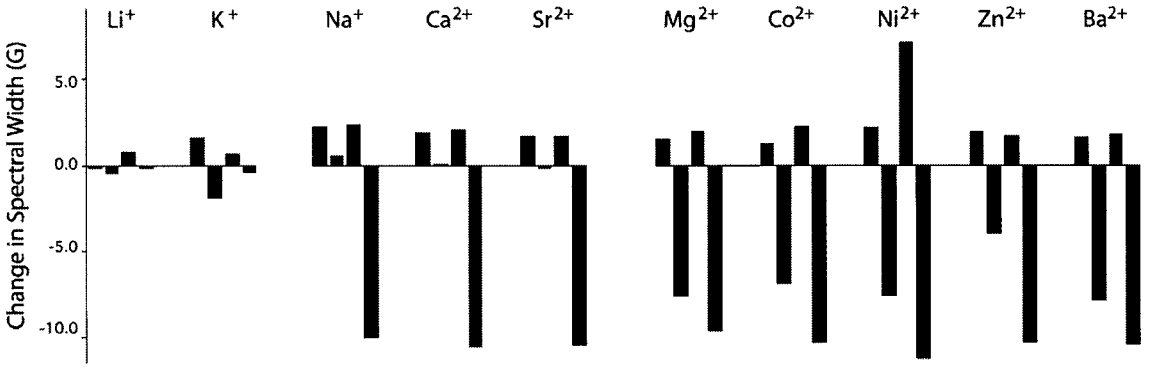

Figure 3.6. Changes in EPR spectral width are plotted as a function of spin-labeled position (U23, U25, U38, and U40) to give a TAR RNA dynamic signature for each metal ion.

In contrast to groups one and two, the metal ions in group three (Mg^{2+}, Co^{2+}, Ni^{2+}, Zn^{2+}, and Ba^{2+}) produced a strong decrease in EPR spectral width of U25, indicating an increase in spin probe mobility at this nucleotide in the RNA-metal ion complex. However, the metal ions in group three produced similar changes at U23, U38, and U40 in comparison with those in group two. With the exception of Ba^{2+} (1.34 Å and p*K*a 13.4) the metal ions in group three all have similar ionic radii (Mg^{2+}, 0.66 Å; Co^{2+}, 0.72 Å; Ni^{2+}, 0.69 Å; Zn^{2+}, 0.74 Å) and pK_as of their associated metal-aqua complexes (Mg^{2+}, 11.4; Co^{2+}, 9.6; Ni^{2+}, 10.6; Zn^{2+}, 9.0) that differ from those in groups one or two.

Ca^{2+} and Mg^{2+} showed different dynamic signatures, indicating that they bind differently to the TAR RNA. This result is in agreement with EPR results obtained under crystal structure-like metal ion concentrations in solution (Edwards, Okonogi et al. 2002) and ^{19}F NMR data which showed that Ca^{2+} and Mg^{2+} induced different changes in chemical shifts of 5-fluoro modified uridine residues at many of the same positions studied here (specifically, U23, U25, and U40) (Olejniczak, Gdaniec et al. 2002).

In addition, we attempted to obtain the dynamic signatures of Cd^{2+} and Mn^{2+} in complex with the TAR RNA. However, Cd^{2+} caused the RNA to precipitate, eliminating meaningful comparison of dynamics with other TAR-metal ion complexes because of the natural difference in dynamics between molecules in the solid state and molecules in the solution state. Mn^{2+} is paramagnetic and produces an EPR signal that overlaps with the nitroxide signal. At a similar concentration to that determined for Mg^{2+}-TAR binding (10 mM divalent metal ion), the spectra of the free Mn^{2+} must be subtracted from the spectra acquired containing the spin-labeled TAR RNA and 10 mM $MnCl_2$. The resulting nitroxide EPR spectra of spin-labeled TAR RNAs displayed a weak resonance at each position, much lower than that expected for 200 μM RNA (data not shown). Because of this result, accurate spectral widths for these spectra could not be measured, precluding the determination of the Mn^{2+} dynamic signature.

One explanation for the absence of a clear, definitive EPR nitroxide signal after spectral subtraction is that Mn^{2+} binds close to the bulge region of the TAR RNA (within 20 Å), diminishing the EPR nitroxide signal through electron-electron dipolar coupling of the nitroxide free electron with the unpaired electrons of the Mn^{2+}. This hypothesis is supported by results from the Ni^{2+}-TAR RNA complex EPR spectra. Ni^{2+} is often used as a paramagnetic relaxation reagent in power saturation experiments (Lin, Nielsen et al. 1998). Although Ni^{2+} spends much of its time in solution in the low spin diamagnetic state, it does spend some time in the high energy, high spin paramagnetic state. All spin-labeled TAR RNA samples in the presence of Ni^{2+} exhibited broadened nitroxide EPR spectra, characteristic of dipolar coupling between a bound nickel ion in the high spin state and the nitroxide within close proximity of one another (see Figure 8.12 of Chapter 8: Material and Methods). On the other hand, it is possible that enough Ni^{2+} is present that bulk collision of Ni^{2+} with the nitroxide spin-label results in the observed line broadening. This hypothesis could have been tested on an RNA known to not contain a high affinity metal ion binding site such as the construct of the TAR RNA lacking the trinucleotide bulge, but we no longer had any of this material readily available. Obtaining results in a frozen solution would eliminate collision effects as well, enabling

the differentiation between bound and collision effects. Nevertheless, nitroxide line broadening information obtained from the Mn^{2+} and Ni^{2+} experiments are not inconsistent with metal ions binding to the bugle region of the TAR RNA.

Another method to report results on RNA internal dynamics obtained by EPR spectroscopy is to calculate the rotational correlation time (τ_R) for each spin-labeled nucleotide. In the slow motion regime, the outer and inner hyperfine peaks are separated, which allows for accurate measurement of the spectral width ($2A_{zz}$). Under these conditions the EPR spectral width ($2A_{zz}$) relates to τ_R according to the following equation: $\tau_R = (5.4 \times 10^{-10})(1-(A_{zz}/A_{zz}^{max}))^{-1.36}$ (Freed 1976). τ_R was calculated for TAR RNA-metal ion samples and ranged from 2.3 to 6.4 ns (see Table 8.2 of Chapter 8: Materials and Methods). Plotting $\Delta\tau_R$ as a function of nucleotide position revealed a graph nearly identical to Figure 3.6 (data not shown). Simply plotting (τ_R) as a function of spin-labeled nucleotide position (Figure 3.7) reveals similar trends to that observed in Figure 3.6. In this plot, Ni^{2+} has a more pronounced difference in τ_R at U38 than the other metal ions in group three. Because of this difference, Ni^{2+} might bind in a slightly different manner than that observed for the other metal ions in group three.

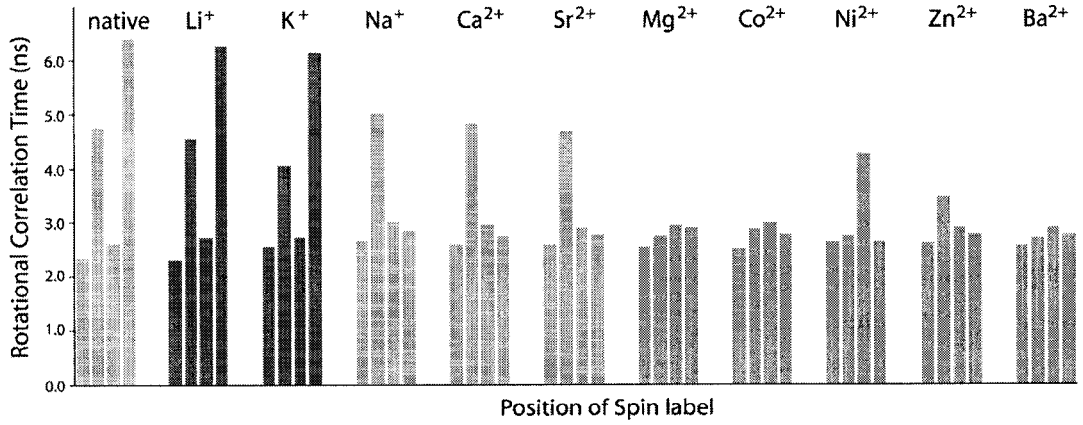

Figure 3.7. Rotational correlation times (τ_R) of the TAR RNA in the absence (far left) and presence of a variety of metal ions. Each set reports the correlation times of U23, U25, U38, and U40 as determined by EPR spectroscopy.

Due to the fact that the metal ions in group two and three induce similar change in RNA internal dynamics at U23, U38, and U40 and that the only major difference between these groups is at U25, it is likely that these metal ions bind in a largely similar manner to the TAR RNA bulge region. Differences in ionic radii and p*K*a of the corresponding metal ion-aqua complexes likely produce the difference in mobility observed at U25 between the two groups. However, Ba^{2+} (group three) does not follow the trend, because it has a size (1.34 Å) similar to that of K^{+} (group one) and a metal ion p*K*a (13.4) similar to that of Sr^{2+} (group two). Nevertheless, the general trend for ionic size and p*K*a of the metal-aqua complex and the moderate affinity binding constant ($K_d \sim 1$ mM) determined here (Edwards and Sigurdsson 2003) and elsewhere (Arzumanov, Godde et al. 2000; Olejniczak, Gdaniec et al. 2002) provide evidence that the metal ions bind to the TAR RNA through the type two RNA-metal ion interactions discussed in the section *RNA-metal ion interactions* at this beginning of this chapter; these interactions are characterized by metal ions binding with moderate specificity and affinity. In addition, because of the trends in p*K*a it is likely that the metal ions bind through outer sphere coordination and that the metal ion's sphere of hydration is not disrupted, although other solution based techniques such as ESEEM EPR (Hoogstraten and Britt 2002; Hoogstraten, Grant et al. 2002) or Eu^{3+} lanthanide luminescence spectroscopy (Mundoma and Greenbaum 2002; Mundoma and Greenbaum 2003) that can identify metal ion hydration content would be necessary to confirm this hypothesis.

Hypothesis for TAR RNA-metal ion binding

It is challenging to predict changes in mobility based on the transformation from one static structure (such as the NMR solution structure of TAR) to another (such as the Ca^{2+}-bound TAR RNA crystal structure). However, using simple chemical reasoning, some conclusions may be drawn from the available biochemical, structural, and dynamic information. With the exception of the X-ray structure, none of the studies have been able to identify the number of bound metal ions. In the X-ray structure, three Ca^{2+} ions were

clustered around the trinucleotide bulge region, while a fourth was located in the middle of the helix near the top of the lower stem (Figure 3.1). In addition, changes in fluorine chemical shift upon titration with metal ions revealed binding constants of $K_d = 0.9 \pm 0.6$ mM for Mg^{2+} and $K_d = 2.7 \pm 1.7$ mM for Ca^{2+}. However, this study did not identify the number of bound Mg^{2+} or Ca^{2+} ions. Because three metal ions were found in the bulge region of the TAR RNA X-ray structure, let us assume that there are three metal ion binding sites in this region. The differences in the dynamic signatures of groups two (the Ca^{2+}-containing group) and three (the Mg^{2+}-containing group) can be justified according to the following hypothesis. Two metal ions bind to the two higher affinity spots (presumably the ones close to nucleotides U23 and A27 in the crystal structure, Figure 3.1) with a combined $K_d^{apparent}$ of ~ 1 mM. This alters the RNA internal dynamics to give the dynamic signature observed in group three (the Mg^{2+}-containing group), in agreement with the measured binding constant for Mg^{2+}. In this state, the decrease in dynamics at U23 and U38 is consistent with the metal ions forming contacts with U23 and A27 (which base-pairs to U38). The observed increase in dynamics at U40 could be a result of helical stacking which eliminates the conformational restriction imposed on U40 in the bent, metal ion-absent conformation (i.e. in this structure U40 is the fulcrum and should experience significant conformational restriction resulting in reduced mobility compared to normal helical nucleotides). In the Mg^{2+}-bound state, the U40 τ_R increases to a value similar to that of the normal helical base-paired nucleotide U38 (ca. 2.9 ns; Figure 3.7), providing support for this hypothesis. Upon Mg^{2+} binding U25 may flip out, away from the helix, and become more mobile. These results are also in agreement with a recent RDC NMR structure of the TAR RNA in the presence of Mg^{2+} which demonstrated a bent helical conformation in the absence of Mg^{2+} (47°) and helical straightening in the presence of 3 mM Mg^{2+} (12°) and 4.5 mM Mg^{2+} (5°) (Al-Hashimi, Pitt et al. 2003). In addition, the largest changes in RNA chemical shifts in the Mg^{2+}-bound structure were observed at U23 and U40, consistent with the EPR observed changes in dynamics and the above analysis.

For the metal ions in group two, the size, coordination geometry, and p*K*a of the associated metal-aqua complex are appropriate for binding to the third metal ion binding site in the TAR RNA bulge, affording a final $K_d^{apparent}$ of ~ 3 mM for the Ca^{2+}-containing group, consistent with the value observed by ^{19}F NMR. This third metal ion binds close to U25, decreasing the dynamics of U25 relative to that observed in the Mg^{2+}-TAR RNA complex (group three).

In conclusion, a hypothesis presented here describes two sets of binding events which accounts for all of the known biochemical and biophysical data. Additional experiments such as RDC NMR of a TAR- Ca^{2+} structure showing the positioning of U25 or high field (Q-band or higher) ENDOR of a TAR-Mn^{2+} sample would be necessary to confirm this hypothesis.

Chapter 4

EPR spectroscopic analysis of RNA-peptide interactions: Elucidating the effect of Tat sequence mutation on TAR RNA internal dynamics

Structural requirements of TAR-Tat binding

RNA-protein complexes are critical components of many cellular processes. The binding of the trans activation responsive (TAR) RNA at the 5' end of HIV mRNA transcript to the Tat (trans activator of transcription) protein enhances transcription rates and elongation efficiency of HIV genome replication (Frankel 1992; Jones and Peterlin 1994; Frankel and Young 1998). The TAR RNA-Tat protein complex also binds to Cyclin T1 (CycT1) and cyclin dependent kinase 9 (CDK9) to form the positive transcription elongation factor (P-TEFb) complex, which appears to be responsible for activation of viral mRNA elongation by hyperphosphorylation of RNA polymerase II (Garber, Mayall et al. 2000; Kim and Sharp 2001) and countering the effect of negative elongation factors (Yamaguchi, Wada et al. 1998; Garber and Jones 1999). Understanding the structure and dynamics of the TAR RNA-Tat protein molecular assembly is essential to understanding the mechanism of HIV-1 transcription activation. Several biochemical experiments have identified the minimal binding elements for structural recognition in the TAR-Tat complex. First, the biochemical data investigating the RNA structural requirements will be described, followed by the biochemical data investigating the protein structural requirements.

Defining the RNA structural requirements. The trans activation responsive (TAR) region of HIV-1 is the first 59 nucleotides at the 5' end long term repeat in the nascent HIV-1 mRNA transcript (Frankel 1992; Jones and Peterlin 1994; Frankel and Young 1998). However, the full length TAR RNA is not necessary for recognition of the Tat protein. Mutations within the hexanucleotide loop lead to decreased levels of transcription (Feng and Holland 1988), but do not affect TAR-Tat binding, implying that

the loop forms contacts with other cellular cofactors (Cordingley, LaFemina et al. 1990; Roy, Delling et al. 1990; Calnan, Biancalana et al. 1991). More specifically, the TAR loop contacts the TRM arm of CycT1, which also forms contacts with the Tat protein through a Zn-finger bridge (Garber, Mayall et al. 2000). Mutational analysis has revealed the importance of the bulge in Tat binding, although only U23 is conserved in sequence, and the bulge can be between 2-5 residues in length and still retain activity (Cordingley, LaFemina et al. 1990; Roy, Delling et al. 1990; Sumner-Smith, Roy et al. 1991; Weeks and Crothers 1991; Churcher, Lamont et al. 1993; Hamy, Asseline et al. 1993). Mutation of N3 or O4 on uridine 23 severely decreases TAR-Tat binding affinity (Sumner-Smith, Roy et al. 1991). In addition to U23 of the bulge, the G26·C39 and A27·U38 base-pairs of the upper stem are also conserved (Weeks and Crothers 1991; Churcher, Lamont et al. 1993). Mutation of the two base-pairs separating the A27·U38 pair and the loop only moderately disrupts TAR-Tat binding (Cordingley, LaFemina et al. 1990). Contrary to this, a functional genomics approach has shown that the Tat protein forms some interaction with these base-pairs, based on interaction with CycT1 and transcription levels (Lund, Wahren et al. 2003). The sequence of the lower stem of the TAR is not conserved and can be truncated to just a few (as little as 3) base-pairs without disruption in Tat binding affinity (Sumner-Smith, Roy et al. 1991; Churcher, Lamont et al. 1993), although it must retain duplex structure (Roy, Delling et al. 1990). Phosphates 22 (5'of A22) and 23 (5' of U23) also appear to be important for Tat recognition (Calnan, Tidor et al. 1991; Weeks and Crothers 1991; Hamy, Asseline et al. 1993; Pritchard, Grasby et al. 1994; Rigl, Lloyd et al. 1997).

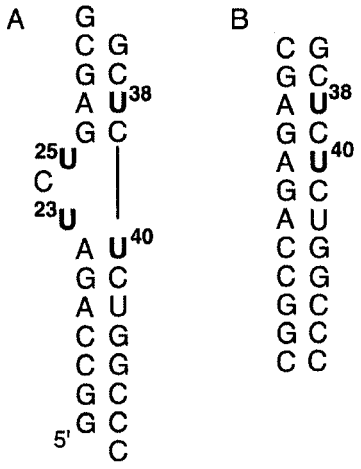

Figure 4.1. The sequence and secondary structure of the TAR construct (A) used in this study and TAR duplex lacking the trinucleotide bulge (B). Spin-labeled sites are labeled and shown in bold.

Defining the protein structural requirements. While the full length Tat peptide is ca. 86 residues long, the basic region of Tat appears to contain the TAR RNA binding domain (Frankel 1992; Jones and Peterlin 1994). Gel shift assays of the TAR RNA complexes with truncated versions of the Tat protein have shown that significant TAR-Tat binding is retained, provided that the basic region of Tat spanning residues Y47 to R58 is included (Cordingley, LaFemina et al. 1990; Roy, Delling et al. 1990; Calnan, Biancalana et al. 1991; Churcher, Lamont et al. 1993). The short peptide spanning this region YGRKKRRQRRR (Tat 47-58) bind to the TAR RNA with high affinity ($K_d \sim 200$ nM), only ca. 10-fold less than that observed in the native TAR RNA-Tat protein complex ($K_d \sim 15$ nM) (Roy, Delling et al. 1990; Hamy, Asseline et al. 1993). Mutational analysis indicates that only R52 is important for TAR-Tat binding transcriptional activation (Calnan, Tidor et al. 1991; Tao and Frankel 1992; Tao and Frankel 1993). Q54, R55K, and R56K do not appear to be essential for binding or activity (Calnan, Biancalana et al. 1991). The wild-type Tat-derived peptide YGRKKRRQRRR and the mutant Tat-derived peptide YKKKKRKKKKA had virtually the same binding affinity (Calnan, Tidor et al. 1991). The guanidine group of R52 is specifically important, and mutation of R52 to lysine (amino group), N^G-monomethyl-arginine or citrulline (urea group) severely decreased TAR-Tat binding (Tao and Frankel 1993). In agreement with this result, capillary electrophoresis mobility shift assays showed large decreases in TAR-Tat

peptide binding for R52 mutation to citrulline, ornithine (amino group, but shorter chain than lysine), N^G,N^G-dimethyl-arginine (assymetrical), and N^G-nitro-arginine (Mucha, Szyk et al. 2002). In addition, the TAR RNA has be purified from other RNAs using arginine affinity chromatography, further demonstrating the importance of an arginine residue in TAR-Tat binding (Tao and Frankel 1992).

Molecular structure of the TAR RNA-Tat protein complex

The three dimensional structure of the TAR RNA has been solved using solution NMR (Aboul-ela, Karn et al. 1996) and X-ray crystallography (Ippolito and Steitz 1998). As described in the previous chapter, these two structures are quite different due to the binding of metal ions to the bulge region (Olejniczak, Gdaniec et al. 2002; Al-Hashimi, Pitt et al. 2003; Edwards and Sigurdsson 2003). In addition, a residual dipolar coupling (RDC) NMR study described the global shape of the RNA in solution, confirming that previously studied by solution NMR (Al-Hashimi, Gosser et al. 2002). No high-resolution structure of the HIV-1 TAR RNA-Tat protein complex has been solved yet, although a low-resolution model exists (Seewald, Metzger et al. 1998). In the current model for TAR-Tat molecular recognition, R52 of the basic region of Tat binds to the bulge region of TAR, most likely forming contacts with phosphates P22 and P23, while inducing a U23·A27·U38 base-triple formation. During formation of the base-triple, the upper and lower helical stems stack co-axially. Base-triple formation has been observed in a C^+GC analog (Puglisi, Tan et al. 1992; Puglisi, L. et al. 1993; Tao, Chen et al. 1997), and recently in the native TAR RNA-Tat protein complex (Hennig and Williamson 2000). In support of this binding model, a high-resolution structure of the HIV-2 argininamide complex solved by solution NMR (Figure 4.2) , revealed contacts between the guanidine group of argininamide and U23, G26, and phosphate P23 (Brodsky and Williamson 1997). Significantly fewer intermolecular NOEs were observed in a HIV-1 TAR RNA-argininamide sample, due to increased flexibility of the RNA-small molecule interface. The HIV-2 construct contains a dinculeotide bulge, rather than the trinucleotide

bulge in HIV-1. NMR studies with the ADP-1 37-residue Tat-derived peptide (Aboul-ela, Karn et al. 1995) and Tfr24 Tat-derived peptide (Long and Crothers 1999) have illustrated some of the basic TAR-Tat recognition principles, although neither produced a high-resolution RNA-peptide structure or defined the position of particular amino acids within the complex. Recently, base flexibility in the HIV-2 TAR RNA-argininamide complex has been investigated by ^{15}N and ^{13}C NMR relaxation experiments (Dayie, Brodsky et al. 2002). A high resolution NMR structure of the bovine immunodeficiency virus (BIV) TAR RNA-Tat peptide complex has been solved, although this complex does not appear to be structurally similar to the human analog (Puglisi, Chen et al. 1995).

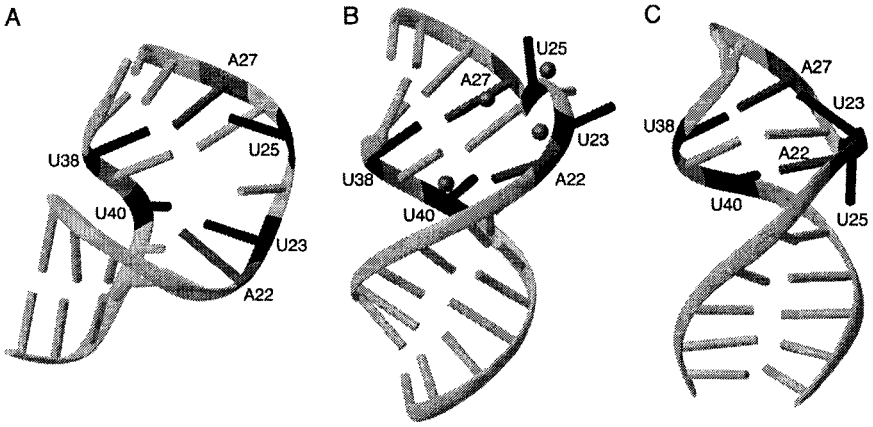

Figure 4.2. Structures of the TAR RNA. Nucleotides spin-labeled in this study are shown in red and labeled. (A) Solution NMR structure of the HIV-1 TAR RNA (Aboul-ela, Karn et al. 1996) (B) X-ray crystal structure of the HIV-1 TAR RNA in the presence of Ca^{2+} (Ippolito and Steitz 1998) (C) NMR solution structure of the HIV-2 TAR RNA-argininamide complex (Brodsky and Williamson 1997).

Low resolution biochemical and biophysical experiments have also provided valuable information about specific contacts or proximal residues within the TAR RNA-Tat protein complex. For example, photo-cross-linking experiments have shown that a 4-thiouridine residue incorporated at U31 in the hexanucleotide loop crosslinks with the Tat peptide (but not the RNA) upon irradiation, implying that U31 of the RNA is in close proximity to the peptide in the RNA-peptide complex (Wang, Huq et al. 1999). UV irradiation at 254 nm caused guanosine 26 of the TAR RNA to photo-cross-link to tyrosine 47 of the Tat protein (Liu, Wang et al. 1996). A 4-thiouridine modification at

U23 was shown to crosslink with R55 of the Tat peptide, inferring that these residues are in close proximity in the RNA-protein complex (Farrow, Aboul-ela et al. 1998). In addition, lysine 51 was shown to cross-link with U23 and U40 2'-functionalized TAR RNAs (Farrow, Aboul-ela et al. 1998). A chemical modification of phosphate 38 to a trisubstituted pyrophosphate was shown to cross-link to lysine 51, providing additional evidence that this residue is in close proximity to TAR in the TAR-Tat complex (Naryshkin, Farrow et al. 1997). Finally, Fe(II)-EDTA mediated RNA self-cleavage was used to investigate RNA-protein contacts, demonstrating that residue 24 of the RNA folds away from the rest of the RNA in the TAR-Tat complex (Huq, Tamilarasu et al. 1999). The low-resolution structural model for the TAR-Tat complex was largely based upon these cross-linking experiments in conjunction with the biophysical RNA structural data (Seewald, Metzger et al. 1998). TAR RNA-Tat protein complex formation was also investigated by molecular dynamics simulations (Nifosi, Reyes et al. 2000).

Investigating RNA-protein interactions by EPR spectroscopy

We are interested in applying electron paramagnetic resonance (EPR) spectroscopy to the investigation of biomolecular structure and function, specifically in the context of the TAR RNA-Tat protein complex. EPR spectroscopy has been used previously to study RNA-protein interactions, although most studies have used spin-labeled proteins (Gopalan, Kuhne et al. 1999; Biswas, Kuhne et al. 2001), rather than spin-labeled RNA (Macosko, Pio et al. 1999). In fact only a handful of papers have described the use of spin-labeled RNA to study RNA-protein structure and function (Plonka and Elas 2002). Because argininamide, the Tat mutant 1 peptide (YKKKKRKKKKA), and the Tat wild-type peptide (YGRKKRRQRRR) have all been proposed to bind to the TAR RNA in a similar manner, we decided to use EPR spectroscopy to observe changes in RNA dynamics upon binding to these Tat-derivaties and to determine if the observed changes were similar for all three compounds (Edwards, Okonogi et al. 2002). While these results do not provide direct structural information, the

EPR spectra yield a dynamic signature for the binding of each compound to the TAR RNA. As was the case with the metal ion study in the previous chapter, dynamic signatures were used to distinguish between different RNA binding modes. In summary, this chapter describes the use of EPR spectroscopy to identify changes in RNA dynamics upon binding to a series of Tat derived peptides and to provide evidence for the formation of specific contacts between Tat amino acids and the TAR RNA. These studies demonstrate the utility of EPR spectroscopy for investigating RNA-protein interactions

Effect of spin-labels on TAR-Tat complex formation

Four spin-labeled TAR RNA samples were prepared as described in Chapter 2, each containing a single nitroxide spin-label at one of four positions (U23, U25, U38, and U40) (Figure 4.1). Whenever an external reporter group is employed to investigate macromolecular structure and dynamics it is necessary to demonstrate whether or not the external reporter group interferes with the macromolecular structure and function being investigated. Otherwise the reporter group may "create the news, rather than report it." Before using these spin-labeled TAR RNAs to study the structure and dynamics of the TAR-Tat interaction, non-denaturing polyacrylamide gel electrophoresis (PAGE) was used to determine the effect of RNA spin-label modification on RNA-peptide binding for both the wild-type (YGRKKRRQRRR) and mutant 1 (YKKKKRKKKKA) Tat-derived peptides (Figure 4.3).

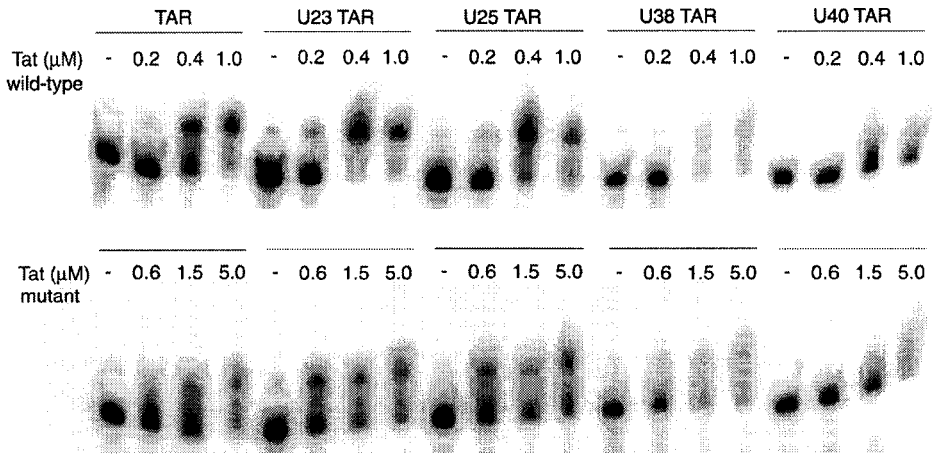

Figure 4.3. Non-denaturing PAGE analysis of RNA-peptide complex formation of unmodified and spin-labeled TAR RNAs with the wild-type Tat peptide (YGRKKRRQRRR) and the commonly used Tat mutant peptide (YKKKKRKKKKA).

The equilibrium dissociation complex was determined for each spin-labeled TAR RNA-Tat peptide complex and compared with that of the unmodified TAR RNA-Tat peptide complexes (Table 4.1). The unmodified TAR RNA bound to the Tat wild-type peptide with a $K_d \sim 0.4$ μM and to the Tat mutant 1 peptide with a $K_d \sim 1.5$ μM. Similar results were obtain for TAR RNAs containing a spin-label in the trinucleotide bulge (U23 or U25), whereas a 3-fold decrease in binding affinity was observed for the TAR RNA containing a spin-label at the base-paired residue U38. For the TAR RNA containing a spin-label modification at the base-paired nucleotide U40, the gel was highly smeared in the presence of either Tat-derived peptide, precluding the determination of K_d for these complexes. It is not clear why we were unable to obtain a K_d for TAR-Tat complexes containing a spin-label at U40, especially considering that the modification is located on the distal side of the RNA, relative to the Tat peptide binding site. In a chemical-cross-linking study, 2'-β-alanyl modification at U40 significantly decreased the TAR-Tat binding affinity, as determined by non-denaturing PAGE (Farrow, Aboul-ela et al. 1998). However, in the same study, filter binding assays revealed a mere 2-fold decrease in binding affinity of this same complex, prompting the authors to suggest that the results obtained for the U40 modification were due to a high rate of dissociation rather than low binding affinity. To test the binding affinity of the U40 spin-labeled TAR RNA-Tat wild-

type peptide complex, changes in the EPR spectrum of U40 were monitored upon titration of the RNA with the peptide. We observed changes in the EPR spectrum of U40 up to a concentration of 0.2 mM peptide (1 equivalent), after which no further change was observed up to a concentration of 0.7 mM peptide (data not shown). Similar results were obtained for the U38 TAR RNA-Tat wild-type peptide complex. These results demonstrate that the peptide binds specifically and stoichiometrically to the RNA, and that under the conditions employed for EPR spectroscopy the spin-label at U40 does not interfere with RNA-peptide complex formation. In conclusion, the spin-labels only appear to have a small affect on RNA-peptide complex formation, and that the peptides are fully bound under the conditions used for EPR spectroscopy.

Table 4.1. Equilibrium dissociation constants (K_d) for spin-labeled TAR RNA-Tat peptide complexes

Spin-labeled site	Tat (wt, μM)	Tat (m, μM)
Unmodified	0.4	1.5
U23	0.3	1.0
U25	0.4	2.0
U38	1.2	5.0
U40	nd	Nd

m: Tat mutant 1 peptide (YKKKKRKKKKA); nd: not determined; wt: wild-type Tat (YGRKKRRQRRR)

EPR spectroscopy: TAR-argininamide binding

Arginine affinity chromatographic purification of the TAR RNA (Tao and Frankel 1993) and a high-resolution NMR solution structure of argininamide bound to the HIV-2 TAR RNA (Brodsky and Williamson 1997) provide evidence for the specific binding of arginine 52 of the Tat protein to TAR RNA. To determine the binding constant of argininamide to the TAR RNA by EPR spectroscopy, the U38 TAR RNA was titrated with 0-10 mM argininamide. The EPR spectral width increased up to a concentration of 5 mM argininamide, demonstrating that the U38 TAR-argininamide complex has a $K_d \sim 2$-3 mM, similar to the value of 1.5 mM obtained by solution NMR (data not shown). EPR spectra of spin-labeled TAR RNAs in the presence of 5 mM argininamide displayed an increase in spectral width, indicative of a decrease in spin probe mobility, at U23, U38, and U40, and an decrease in spectral width at U25. To investigate if the observed changes

in nucleotide mobility were due to specific TAR-argininamide binding, the EPR spectra of a TAR duplex construct lacking the trinucleotide bulge (Figure 4.1) were acquired. Virtually no change was observed at either U38 or U40, indicating that the changes in nucleotide mobility in the TAR RNA samples are due to specific TAR-argininamide complex formation.

EPR spectroscopy: TAR-Tat(m1) and TAR-Tat(wt) binding

EPR spectroscopy was used to determine the changes in RNA internal dynamics upon binding to the Tat mutant 1 peptide (YKKKKRKKKKA) and the Tat wild-type peptide (YGRKKRRQRRR). To determine the concentration dependence for nonspecific RNA-peptide binding, the U38 TAR duplex lacking the trinucleotide bulge (Figure 4.1) was titrated with 0-2 mM mutant peptide. No detectable change in the EPR spectrum was observed up to a concentration of 0.5 mM peptide. At concentrations above 0.7 mM the EPR spectral features of U38 became broadened with the appearance of new, low intensity spectral features, indicating that nonspecific RNA-peptide interactions were being observed (data not shown). Nonspecific TAR RNA-Tat peptide interactions were also observed at this concentration by solution NMR (Long and Crothers 1999). Therefore, EPR samples of spin-labeled TAR RNA-Tat peptide complexes were obtained at 0.5 mM peptide and 0.2 mM RNA to ensure 1:1 specific complex formation (see previous section for analysis of U40 TAR RNA titration of 0-0.7 mM peptide concentrations). In the presence of the Tat mutant 1 peptide (YKKKKRKKKKA), small increases in EPR spectral width, indicating small increases in mobility, were obtained at U23 and U38, a moderate increase was obtained at U40, and a moderate decrease in EPR spectral width was obtained for U25 (Figure 4.4). Similar changes in RNA dynamics were observed at U25 and U40 in the presence of the wild-type Tat peptide. In contrast to the results obtained for the mutant peptide, significant decreases in spin-probe mobility were observed at U23 and U38 in the presence of the wild-type peptide.

Figure 4.4. EPR spectroscopy of spin-labeled TAR RNA samples in the presence of derivatives of the Tat protein. EPR spectra of the native TAR RNA (0.2 mM) are shown in black, and spectra of spin-labeled TAR RNA samples in the presence of 0.5 mM Tat-derivatives are shown in magenta. The position of the spin-label is shown to the left of each spectrum and the Tat-derivative is labeled above each spectral set.

As described earlier, plotting the change in EPR spectral width as a function of spin-labeled position yields a quantitative presentation of the EPR spectra called the dynamic signature for each set of experimental conditions. The dynamic signatures of the TAR-argininamide, TAR-Tat(m1), and TAR-Tat(wt) complexes obtained from the EPR spectra shown in Figure 4.4 are shown in Figure 4.5. The rotational correlation time (τ_R)

for each sample was calculated based on the EPR spectral width ($2A_{zz}$) and the following equation: $\tau_R = (5.4 \times 10^{-10})(1-(A_{zz}/A_{zz}^{max}))^{-1.36}$ (Freed 1976). Plotting $\Delta\tau_R$ as a function of spin-labeled nucleotide position yielded a plot almost identical to that shown in Figure 4.5 (data not shown; EPR spectra of spin-labeled TAR RNAs in the presence and absence of peptides are shown overlaid in Figure 4.4 or stacked in Figure 8.21-8.24 of Chapter 8).

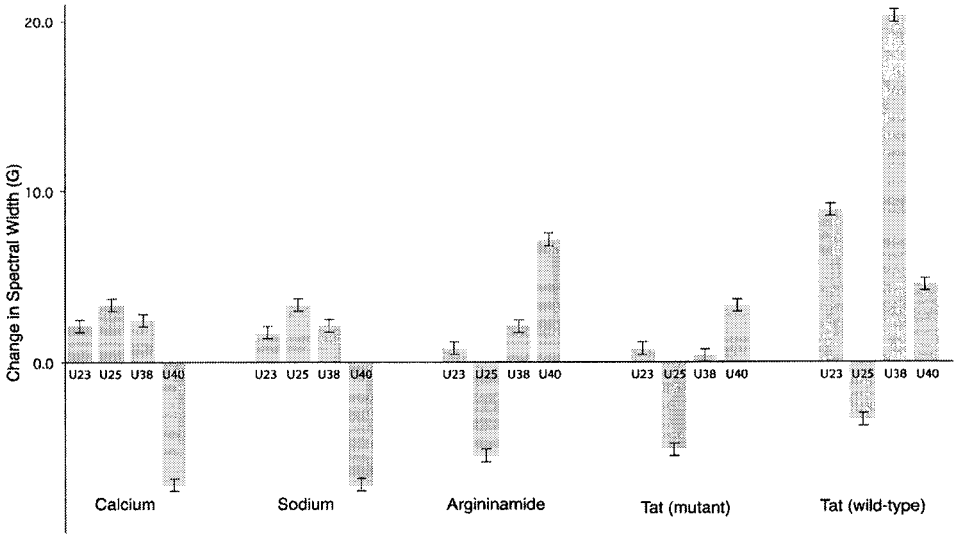

Figure 4.5. Dynamic signatures of TAR RNA-Tat derivative complexes

Discussion

Although a high-resolution structure of the TAR RNA-Tat protein or peptide complex has not been solved, solution NMR studies have indicated that argininamide and peptides derived from the Tat protein bind in a similar fashion (Puglisi, Tan et al. 1992; Puglisi, L. et al. 1993; Aboul-ela, Karn et al. 1995; Brodsky and Williamson 1997). Changes in the EPR spectra of spin-labeled TAR RNAs upon incubation with argininamide or the Tat peptides demonstrate that RNA-peptide complex formation affects the mobility of nucleotide within the RNA. For all Tat-derived samples, the mobility of U23, U38, and U40 decreased, while the mobility of U25 increased. Of note,

these dynamic signatures were different than those obtained in the presence of metal ions (see Chapter 3), implying that the metal ions and the Tat-derivatives interact with the RNA differently. The EPR-observed changes in nucleotide dynamics are consistent with the existing model for TAR-Tat complex formation. In this model, the trinucleotide bugle becomes inverted, with U25 flipping out, away from the helices, and U23 forming a Hoogsteen face base-triple with the A27·U38 base pair (Long and Crothers 1999). In forming the base-triple, the upper and lower helices stack co-axially (Figure 4.2). Therefore, the mobility of U25 should increase because its ribose ring is no longer in contact with the base of G26 and is positioned away from the RNA helix. The mobility of U23 and U38 decrease due to additional contacts formed in the base-triple. The decrease in U40 mobility upon binding the Tat-derivatives is not as easily justified using the current model for TAR-Tat binding. U40 is rather rigid in the unbound state ($2A_{zz}$ = 57.8 G; τ_R = 3.81 ns; M_s = 0.327) in comparison with the other base-paired spin-labeled nucleoside U38 ($2A_{zz}$ = 52.2 G; τ_R = 2.64 ns; M_s = 0.367; for M_s definition, see Chapter 6). This is likely due to the fact that U40 is the fulcrum between the upper and lower helices and is likely pinched by C39 of the upper helix and C41 of the lower helix. In the bound state, the guanidino group of R52 of the Tfr24 peptide (Long and Crothers 1999) or argininamide (Brodsky and Williamson 1997) stacks on top of A22, which could also produce a reduction in the dynamics of the A22 base-pair complement U40.

Concurrent to publication of our EPR data (Edwards, Okonogi et al. 2002), ^{15}N and ^{13}C NMR relaxation experiments were used to probe base dynamics in the HIV-2 TAR-argininamide complex (Dayie, Brodsky et al. 2002). These experiments showed the largest change (a decrease) in dynamics at U23 upon TAR-argininamide complex formation. U25 was highly flexible with a small increase in mobility (e.g. carbon $R_{1\rho}$ relaxation rate decreased upon binding). Detailed analysis of U38 and U40 dynamics were unsuccessful for a variety of reasons. First, the U40 imino proton was not observed above 5 °C, likely a result of fast solvent exchange as observed previously (Long and Crothers 1999). Due to resonance overlap of U38 and U40, no comparison of the carbon $R_{1\rho}$ relaxation rates in the unbound and argininamide bound samples were available.

However, A22 and A27 which base-pair with U40 and U38, respectively, showed decreases in mobility upon argininamide binding, and it is conceivable, therefore, that the mobility of U40 and U38 would also decrease. These experiments are in agreement with our EPR data at all positions (U23, U25, U38, and U40) and are a fine complementary technique because these experiments employ natural reporter groups (although ^{13}C and ^{15}N isotope enriched), and probe different types of motions (e.g. the ^{1}H-^{15}N and ^{1}H-^{13}C motional vectors) within the same molecule on a similar time scale (picoseconds to milliseconds). While the magnitude of data produced by NMR spectroscopy is much greater than that obtained by EPR spectroscopy, the NMR study is considerably more costly and time consuming, not all residues were well resolved (e.g. U38 and U40), and fewer bound state can be studied. On the other hand, EPR samples are rapidly and easily prepared, facilitating the study of individual nucleotide dynamics in a wide variety of bound studies. Therefore, the two techniques are highly complementary.

While argininamide and the Tat peptides produced related sets of TAR RNA internal dynamic signatures, the wild-type Tat peptide induced significantly larger decreases in dynamics at U23 and U38 (Figure 4.5). These results show that these compounds bind differently. This was an unexpected result because the mutant peptide contains the essential arginine (R52) and these two peptides bind the TAR RNA with similar affinity. The differences observed between peptide dynamic signatures demonstrate that amino acids present in the wild-type sequence that are not present in the Tat mutant 1 sequence are responsible for the additional decrease in mobility at these sites. This hypothesis and these results are supported by solution NMR data by Long & Crothers of the TAR RNA in the presence of a mutant peptide ("R52"; see Figure 4.6) for which "the markers for specific complex formation... were absent" (Long and Crothers 1999). More specifically, the solution NMR data showed a clean, well resolved U23 imino resonance in the presence of the wild-type peptide (Tfr24) that was absent in the presence of the mutant peptide (R52). Furthermore, the U38 imino resonance in the presence of the mutant peptide (R52) was much more similar to the unbound RNA than the wild-type complex. In a separate study by Long & Crothers, the single and double

arginine peptides, R52 and R52R53K54 were shown to exhibit biphasic dissociation curves as opposed to a monphasic dissociation curve observed for Tfr24 (Long and Crothers 1995). In addition, the single arginine peptide R52 only displayed a 4.3-fold higher affinity for TAR than for a construct of TAR lacking the trinucleotide bulge. These results are in agreement with our results, which indicate that the wild-type and single arginine mutant peptides bind to the TAR RNA differently.

Effect of Tat sequence mutation on TAR RNA internal dynamics

Because of the large differences in the mobility of U23 and U38 in the presence of the two Tat-derived peptides, we decided to further investigate which amino acids in the wild-type sequence were responsible for the additional decrease in mobility. A series of peptides were obtained, and their effects on TAR RNA internal dynamics were investigated by EPR spectroscopy. These peptides were designed to test the importance of G48, R49, R53, G54, R55, R56, and R57. The multiple sequence alignment of this series of peptides is shown in Figure 4.6.

```
HIV-1                      ...RKKRRQRRR...
HIV-2                      ...RKGRRRRTP...
SIV                     ...YEKSHRRRRTPKK
Tfr24                         RKKRRQRRRPPQGSQTHQVSLSKQ
R52                           RKKRKQKKKPPQGSQTHQVSLSKQ
R52R53K54                     RKKRRKKKKPPQGSQTHQVSLSKQ
Argininamide                     R
Tat(m1)                       YKKKKRKKKKA
Tat(wt)                       YGRKKRRQRRR
Arg-Arg-β-NA                       RR
Tat(m2)                       YGRKKRKQRRR
Tat(m3)                       YGRKKRRQ
Tat(m4)                         RKKRRQRRRY
Tat(m5)                       YGRKKRKKKKK
Tat(m6)                       YKKKKRRQRRR
Tat(m7)                       YGRKKRRQKRR
Tat(m8)                       YGRKKRRQRKR
Tat(m9)                       YGRKKRRQRRK
Tat(wt-36)     SFTTKALGISYGRKKRRQRRRPPQGSQTHQVSLSKQ
```

Figure 4.6. Multiple sequence alignment of wild-type HIV-1 and HIV-2 protein sequences; the Tat-derived peptides used by Long & Crothers, Tfr24, R52, and R52R53K54 (Long and Crothers 1999); and the Tat-derived peptides used in these EPR spectroscopic studies.

EPR spectroscopy: TAR-(arg-arg-β-naphthylamide) binding

Arginine 53 had previously been proposed to be important for the specific recognition of the TAR-Tat complex based on NMR data (Long and Crothers 1999). In addition, a version of the Tat protein containing R52K mutation (while retaining R53) produced only 2-3-fold lower levels of TAR-Tat activated transcription (Calnan, Tidor et al. 1991; Tao and Frankel 1993). We decided to investigate the binding of the arginine-arginine dipeptide unit to the TAR RNA to test the importance of R53. Due to the commercial unavailability of the single peptide arg-arg (custom peptide synthesis companies will not make it and no major chemical manufacturer sells it), the dipeptidase substrate arg-arg-β-naphthylamide (RR-β-na) was used instead. This small molecule displayed enhanced affinity for the TAR RNA relative to argininamide and was fully bound at a concentration of 0.5 mM small molecule (standard 0.2 mM spin-labeled RNA; data not shown). RR-β-na produced a similar dynamic signature to that obtained previously for argininamide, demonstrating that despite enhanced TAR affinity the

arginine-argninine unit is not sufficient for the wild-type binding observed previously by EPR (Figure 4.7). EPR spectra of spin-labeled TAR RNA-Tat mutant peptide complexes are shown in Figures 8.21-8.24 of Chapter 8.

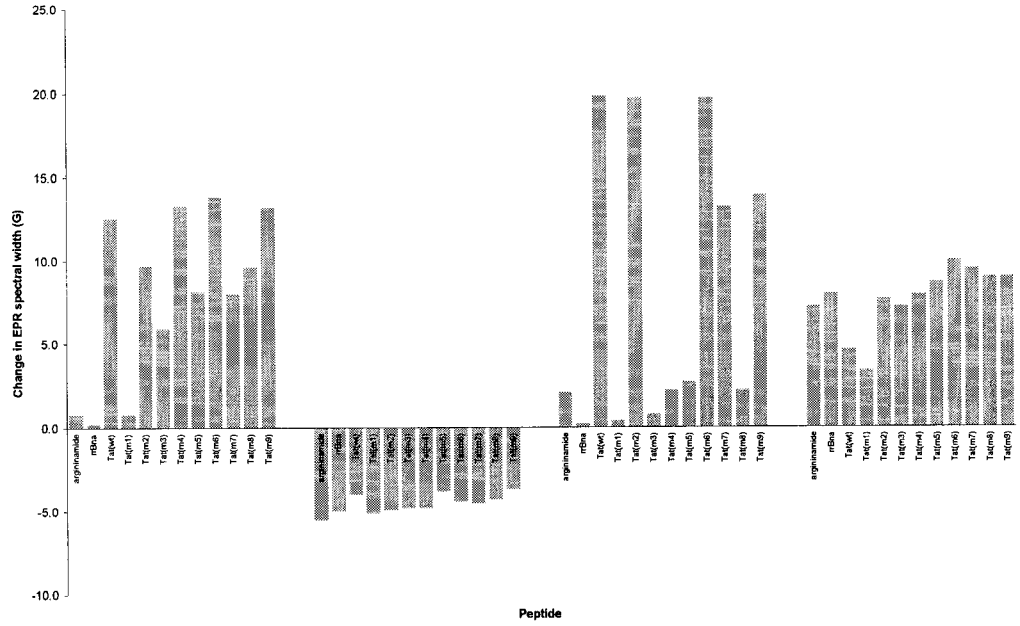

Figure 4.7. Dynamic signatures of TAR-Tat complexes. The changes in EPR spectral width ($\Delta 2A_{zz}$) is plotted as a function of spin-labeled nucleoside position (U23, U25, U38, and U40) to give a quantitative presentation (dynamic signature) for each RNA-peptide complex.

EPR spectroscopy: TAR-Tat mutant biding

In addition to RR-β-na, we studied the binding of a series of Tat-derived peptides to the TAR RNA by EPR spectroscopy in order to determine the impact of individual amino acids on the observed differences in TAR RNA internal dynamics in the presence of the wild-type and Tat mutant 1 peptides. The dynamic signatures of these RNA-peptide complexes are shown in Figure 4.7. To facilitate direct comparison between peptides, the changes in EPR spectral width for each peptide are grouped according the spin-labeled nucleotide (Figure 4.8 and Figure 4.10). First, the effects of peptide sequence mutation on U23 dynamics will be discussed, followed by analysis at U38.

U23 dynamics. The 11-mer Tat-derived peptide Tat(m2), which contained the wild-type sequence with the exception of an R53K single point mutation, was designed to test the importance of R53. This peptide produced a similar change in EPR dynamics at U23 as compared to the wild-type peptide, although the actual value for $\Delta 2A_{zz}$ was slightly less (9.7 rather than 12.5) (Figure 4.8). In conjunction with the dynamic signature for RR-β-na, this result demonstrates that R53 only has a minor effect on U23 dynamics in the TAR-Tat complex. Tat(m3) was designed to test the importance of the carboxyl terminal arginines (55-57), and the dynamic signature is shown in Figure 4.7. Tat(m3) showed a moderate reduction in U23 dynamics, but this reduction was roughly halfway between Tat(wt) and Tat(m1) dynamics at this position, demonstrating that either specific amino acids on the carboxy terminus are important for binding, or that their electrostatic interactions are important. To address the later case, Tat(m5) was synthesized. Some of the decrease in dynamics for the wild-type peptide are recovered in this peptide, but not all, perhaps due to the additional mutation at Q54. Arginine 55 might be involved in U23 wild-type binding, although it is not necessary given the EPR data for Tat(m3) and Tat(m5). Cross-linking studies showed that a 4-thiouridine U23 modified TAR forms a single cross-link with arginine 55, demonstrating that R55 is proximal to U23 in the TAR-Tat complex (Farrow, Aboul-ela et al. 1998). The Tat-derived peptides Tat(m7), Tat(m8), and Tat(m9) tested the importance of single arginine to lysine mutation for residues, 55, 56, and 57, respectively. The R55K and R56K mutations moderately diminished Tat wild-type-like dynamics, whereas the R57K mutation produced wild-type-like dynamics. Tat(m4), which was designed to test the importance of glycine 48, gave a U23 EPR spectrum similar to that obtained for Tat(wt), indicating that G48 is not involved for U23 wild-type dynamics. Furthermore, the Tat(m6) peptide, designed to test the importance of glycine 48 and arginine 49, gave a U23 EPR spectrum similar to that obtained for Tat(wt), demonstrating that these amino terminal residues are not necessary for U23 wild-type dynamics. EPR spectra of U23 TAR RNA in the presence of Tat mutants are shown in Figure 8.21 of Chapter 8.

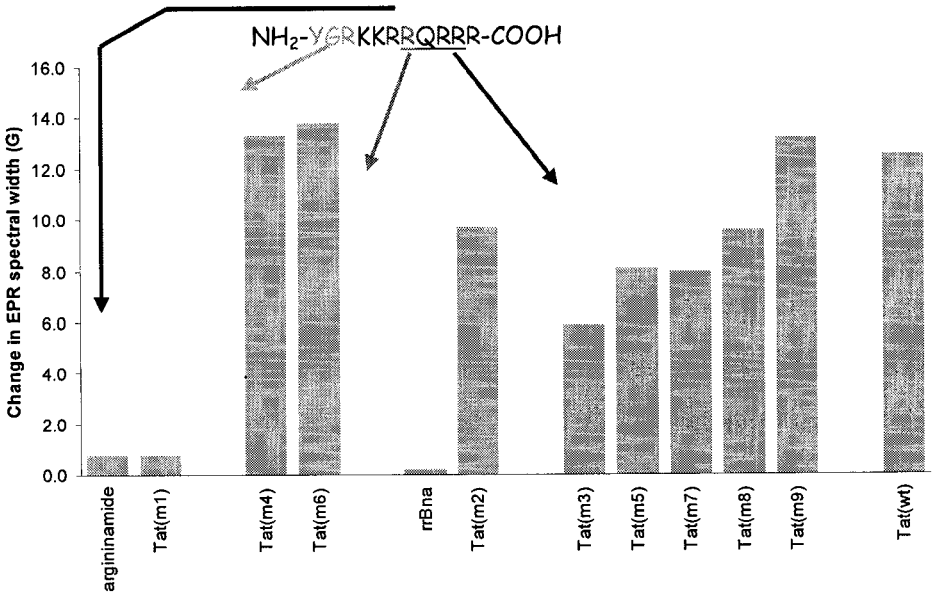

Figure 4.8. Changes in EPR spectral width ($\Delta 2A_{zz}$) at U23 in the presence of Tat-derived peptides.

U38 dynamics. As mentioned above, the arginine-arginine dipeptide was not sufficient for wild-type dynamics at U38, giving a pattern similar to that of arginine. Therefore, R53 is not sufficient for wild-type binding. Tat(m2) was designed to further probe the importance of R53. The EPR spectrum of U38 TAR RNA in the presence of Tat(m2) is more complicated and contains multiple spectral components (Figure 4.9). In multi-component spectra such as this, if only the slower component was reported, important macromolecular structural and dynamical information would be lost. The slower component has a spectral width of 71.9 G, virtually identical to that obtained for the wild-type Tat peptide at this position (Figure 4.10). However, the faster component has a spectral width of ca. 55 G, only slightly wider than that observed for either argininamide or the Tat mutant 1 peptide. Therefore, it is interesting, surprising, and noteworthy that this peptide induces both of these dynamic patterns. Furthermore, the central line width (H_o) of this sample is 5.73 G as opposed to 4.09 G for argininamide, 3.92 G for Tat(m1), and 7.58 G for Tat(wt). Solving the population of the two components using simple algebra based on the center line widths, gives a 0.55 population for the more mobile component and a 0.45 population for the more rigid component.

However, H_0 is naturally biased toward the more mobile component. A more accurate method for determining the population is to use normalized spin counts of the two spectral components (presumably the dynamics observed in the argininamide complex for the fast component, and those observed in the wild-type complex for the slow component) and solve by spectral addition. This type of analysis reveals a spin population of χ_f for the fast component and χ_s for the slow component. Because the EPR spectrum of U38 TAR in the presence of Tat(m2) peptide indicated that both wild-type and Tat(m1)-like dynamics were present, it is likely that R53 forms at least one important contact with the RNA that is only partially filled with a lysine mutation. It is possible that arginine 53 forms 2 contacts with the RNA, one of which leads to wild-type dynamics, the other to mutant dynamics. In the presence of the R53K mutation, the lysine makes both of these contacts, leading to a multi-component EPR spectrum.

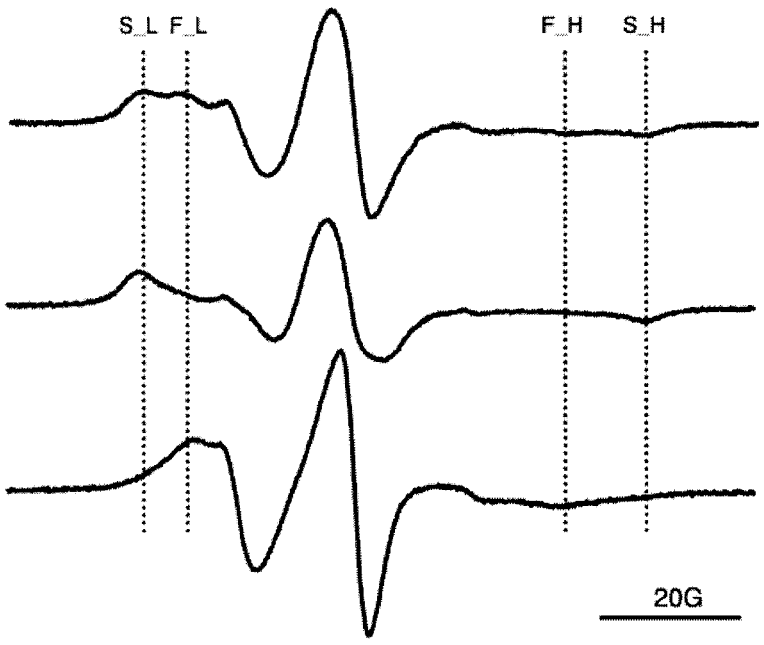

Figure 4.9. The EPR spectrum of U38 TAR RNA in the presence of Tat(m2) peptide (YGRKKRKQRRR) contains two spectral features (a). The slow component correspond to the Tat(wt) spectrum (b) and the fast component corresponds to the Tat(m1) EPR spectrum (c). The spectral features are as follows: S_L, slow component, low field peak; F_L, fast component, low field peak; F_H, fast component, high field peak; S_H, slow component, high field peak.

Tat(m3) was synthesized to test the importance of the carboxyl terminal arginines, and elimination of these residues leads to mutant-like dynamics (Figure 4.8). Tat(m5) was designed to test the specificity of the carboxyl terminal arginines, while retaining the favorable electrostatic interactions provided by lysine residues. This peptide also resulted in mutant U38 dynamics. Tat(m4) was synthesized to test the importance of glycine 48. For Tat(m4), a tyrosine was placed on the carboxy terminus to facilitate peptide quantification at 275 nm, and was rationalized as being a conservative mutation based on the fact that residue 58 in the wild-type protein is a proline which should be large enough to accommodate a tyrosine. We now believe this mutation to be disruptive of U38 binding. In agreement with this hypothesis, Tat(m6), which was designed to test the importance of glycine 48 and arginine 49, gave wild-type U38 dynamics. Therefore, it is likely that Tat(m4), which has a similar core as Tat(m6), disrupts wild-type binding at U38 because of the carboxyl terminal mutation. As described above, the peptides Tat(m7), Tat(m8), and Tat(m9) tested the single amino acid mutation of R55, R56, and R57, respectively. While the R55K and R57K mutations moderately affected U38 dynamics, the R56K mutation produced mutant 1-like dynamics. The EPR spectra of U38 spin-labeled TAR RNA in the presence of Tat-derived mutant peptides is shown in Figure 8.23 of Chapter 8.

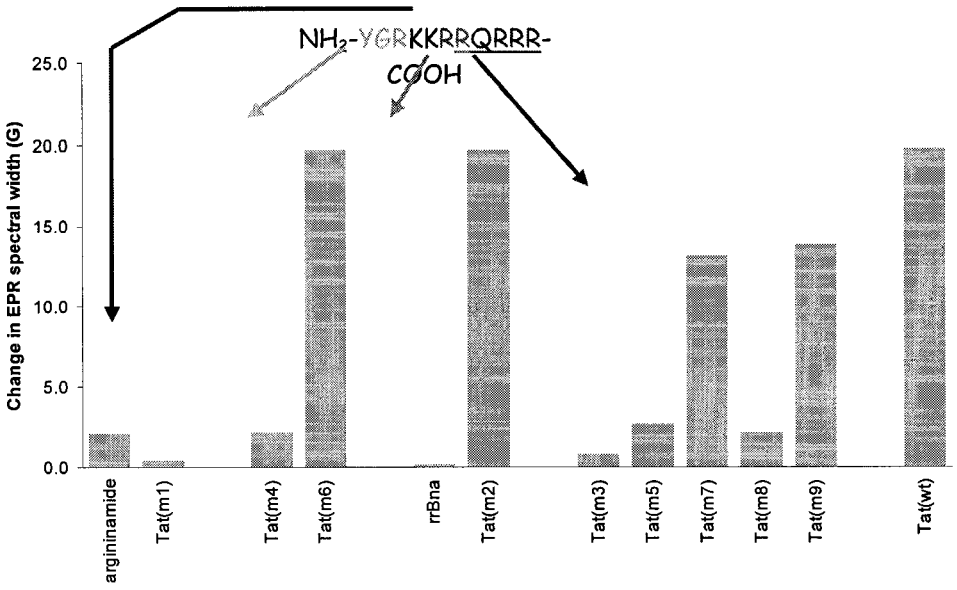

Figure 4.10. Changes in EPR spectral width ($\Delta 2A_{zz}$) at U38 in the presence of Tat-derived peptides.

In conclusion, mutations in the carboxyl terminus increase U23 dynamics away from Tat(wt) dynamics and toward the Tat(m1) dynamics, indicating that these residues form specific contacts with the TAR RNA. Only mutations in both the carboxyl and amino acid terminus of the basic core of Tat result in Tat(m1) dynamics. In contrast, U38 dynamics were much more sensitive to peptide mutation, especially at arginine residues 53, 55, 56, and 57.

Caveat of using external reporter groups

We have previously shown that the spin-labels used here detect structure-dependent dynamics in RNA (Edwards, Okonogi et al. 2001). However, some of the observed changes in spin-probe dynamics that we attribute to change in nucleotide dynamics are likely due to motion of the spin-probe independent of the nucleic acid. This independent motion may be due to either linker flexibility (bond rotation or TEMPO chair flip) or direct contact of the modification with either the RNA or the peptide. Despite this possibility, the data are representative of the expected changes in TAR RNA mobility upon binding to derivates of the Tat protein, based on the current model for

RNA-protein assembly (Seewald, Metzger et al. 1998) and TAR dynamics studied by NMR spectroscopy (Dayie, Brodsky et al. 2002). Therefore, we conclude that most of the observed changes in EPR spectra can be attributed to changes in nucleotide dynamics.

Adaptive recognition in RNA-protein binding

The EPR data presented in this chapter demonstrate that the HIV-1 TAR RNA internal dynamics change upon binding to derivatives of the Tat protein (Edwards, Okonogi et al. 2002). NMR data have also shown similar changes in HIV-2 TAR RNA dynamics upon binding to argininamide (Dayie, Brodsky et al. 2002) and other NMR experiments have shown the concomitant large change in RNA structure that accompanies the change in dynamics (Puglisi, Tan et al. 1992; Puglisi, L. et al. 1993; Aboul-ela, Karn et al. 1995; Long and Crothers 1999). Because of these large changes, the TAR-Tat interaction provides an example of the "induce fit" theory of RNA-protein binging (Williamson 2000; Leulliot and Varani 2001). The data presented here are in agreement with this theory rather than the "lock-and-key" theory of RNA-protein binding. Nucleotides that participate in intimate RNA-protein contacts, such as U23, exhibit significantly more mobility prior to peptide binding. Nucleotides that do not directly participate in RNA-protein binding are also affected. Furthermore, the specificity of the interactions, such as those observed in the Tat sequence mutation studies, are important for molecular recognition and adaptive binding.

Conclusion

In conclusion, EPR spectroscopy was used to investigate changes in RNA internal dynamics upon RNA-protein binding. 2'-urea-linked spin-labels are sensitive reporters of nucleotide dynamics and can be used to detect a wide range of RNA internal dynamics, including flexible bulge nucleotides that become even more flexible upon protein binding, flexible bulge nucleotides that become extremely rigid upon protein binding, or

conversely, relatively rigid nucleotides that become even more so upon protein binding. These dynamic signatures were used to evaluate the RNA structural changes that occur upon binding to small molecules and peptides that mimic RNA-protein binding. Specifically, U23 and U38 were shown to have significant decreases in mobility in the presence of the wild-type peptide relative to argininamide and the Tat mutant 1 peptide. Amino acids in the carboxyl terminus (R55, R56, R57) and to some extent R53 were determined to be responsible for these differences in RNA dynamics, providing evidence for specific RNA-protein contacts. These results illustrate that EPR spectroscopy is a powerful biophysical technique for the investigation of RNA internal dynamics in complexes with small molecules and peptides.

Chapter 5

EPR spectroscopic analysis of complexes of the TAR RNA with small molecules that inhibit HIV-1 TAR-Tat activated transcription

Targeting the HIV-1 and HIV-1 RNA with small molecule drugs

Most current anti-HIV treatments use several modified nucleosides that disrupt reverse transcription, such as azidothymidine (AZT), 2',3'-dideoxy inosine (ddI), and 2',3'-dideoxy cytosine (ddC). In addition, these drugs display high toxicity since they disrupt natural cellular transcription as well as viral transcription. Other antiviral strategies include inhibition of HIV protease activity and DNA integrase activity, which is amplified during HIV replication. Because of the rapid emergence of resistance to these strategies and their inherently high toxicity, other strategies need to be developed and validated.

The essential role of RNA in many cellular processes makes it a target for rational drug design (Chow and Bogdan 1997; Gesteland, Cech et al. 1999; Gallego and Varani 2001). Historically, the function and structure of RNA have not been well understood, and thus RNA has been relatively underused as a therapeutic target. Nevertheless, many specific RNA molecules and RNA-protein complexes present unique molecular assemblies that are attractive targets for therapeutic intervention. One such RNA target is the HIV-1 TAR RNA, which is involved in the production of full length viral transcripts. The cellular complements of the TAR RNA, such as the Tat protein, CycT1, CDK9, and RNA polymerase II, are all native to the host cell, and therefore not ideal targets for drug design because their inhibition interferes with natural cellular processes in the host cell. However, the TAR RNA is unique to HIV, and therefore small molecules which target the TAR RNA with high affinity should exhibit high antiviral selectivity. In fact, small molecules, such as hexaarginine neomycin (NeoR), that disrupt TAR activated transcription display antiviral activity in vitro (Litovchick, Evdokimov et al. 2000). To

facilitate the development of small molecules that inhibit TAR activated HIV-1 transcription, such as NeoR, it is necessary to utilize structural analysis methods to determine the important facets of TAR RNA-small molecule binding.

Techniques for determining the structure of RNA-small molecule complexes

Several methods exist for determining the structure and dynamics of RNA-small molecule complexes. While there are relatively few high-resolution RNA-small molecule crystal structures, there are a number of high-resolution NMR spectroscopic structures of RNA-small molecule complexes. These are both RNA aptamer-small molecule complexes and complexes of synthetic drugs with naturally occurring RNAs. Nevertheless, these structures are often difficult to solve due to the highly flexible nature of intermolecular RNA-small molecule assemblies, which can result in low numbers of intermolecular contacts (i.e. NOEs), and subsequently, low-resolution structural information. Because of the drawbacks and challenges of NMR and X-ray crystallography, the bulk of RNA-small molecule structural information has come from biochemical and biophysical experiments that give low-resolution structural information. For example, results demonstrating protection from chemical (e.g. uranyl and lead acetate) and enzymatic (e.g. RNase A, T, and V) cleavage in the presence of small molecules can be used to infer binding sites (Rosendahl and Douthwaite 1994; Recht, Fourmy et al. 1996; Dassonneville, Hamy et al. 1997; Gelus, Bailly et al. 1999; Gelus, Hamy et al. 1999; McPike, Goodisman et al. 2001). However, small molecule-induced RNA conformation changes can alter nuclease cleavage patterns, producing protective effects distal to the binding site in addition to local steric protection. Cirucular dichroism and electric linear dichroism can identify global differences in RNA structure, and thus the difference between intercalation and groove binding, but not individual binding sites (Eriksson and Norden 2001). Other methods for monitoring RNA-small molecule complex formation and for measuring binding constants include non-denaturing gel electrophoresis binding and competition (i.e. gel shift) assays (Mei, Galan et al. 1995;

Hamy, Brondani et al. 1998), mass spectrometry (Hofstadler and Griffey 2001), fluorescence anisotropy (Luedtke, Baker et al. 2000; Hamaski and Ueno 2001), and surface plasmon resonance (Davis and Wilson 2001). Techniques sensitive to changes in RNA internal structure and dynamics are complementary to those described above and are essential to the global knowledge of RNA-small molecule recognition.

Small molecules that target the HIV-1 TAR RNA

Several classes of compounds have been designed or found to inhibit TAR RNA activated HIV-1 transcription (Froeyen and Herdewijn 2002). Aminoglycoside antibiotics and their conjugates have been identified as TAR-Tat small molecule inhibitors (Walter, Vicens et al. 1999). For example, Mei and co-workers demonstrated that neomycin binds to the TAR RNA with moderate affinity (K_d = 0.9 μM), inhibiting TAR-Tat complex formation through an allosteric mechanism (Mei, Galan et al. 1995; Mei, Cui et al. 1998; Wang, Huber et al. 1998). Other aminoglycoside antibiotics bind to the TAR RNA, but with lower affinity (K_d ~ 10 μM) (Mei, Mack et al. 1997). The structure of free neomycin in aqueous solution was solved using NMR (Botto and Coxon 1984; Reid and Gajjar 1987).

Several aminoglycoside antibiotic conjugates have been synthesized to contain functional groups that mimic the binding of the essential arginine (52) of the Tat protein to the TAR RNA. For example, kanamycin and gentamicin conjugated with four arginine or γ-guanidino butyric acid moieties were shown to bind to the TAR RNA, inhibiting TAR-Tat binding (Litovchick, Evdokimov et al. 1999; Lapidot and Litovchick 2000; Litovchick, Evdokimov et al. 2000). Biochemical studies such as uranyl, lead acetate, and RNase A cleavage protection experiments provided evidence that the aminoglycoside-arginine conjugates bind to the bulge region, likely in the Tat binding site. Furthermore, antiviral activity was observed in ED cells. More recently, a hexaarginine-neomycin B conjugate (NeoR) was shown to have enhanced TAR RNA affinity (K_d ~ 50 nM by gel shift assay, 6 nM by fluorescence anisotropy competition experiments, and TAR-Tat

CD_{50} ~ 130 nM) and increased anti-HIV activity (Litovchick, Lapidot et al. 2001; Cabrera, Gutierrez et al. 2002). In addition to anti-TAR activity, NeoR is believed to be a Tat antagonist. HIV-1 Tat overexpression upregulates the production of cell wall receptors such as CXCR4 which allows HIV-1 particles to enter the host cell more readily. NeoR appears to counter this activity by binding to these receptors, effectively blocking HIV-1 particles from binding to host cells. Some of these aminoglycoside antibiotic-arginine conjugates also inhibit bacterial RNAse P activity (Eubank, Biswas et al. 2002).

Using a similar strategy, guanidine conjugates of neomycin B, kanamycin A & B, paromycin, and tobramycin have been synthesized and exhibit significantly higher anti-HIV-1 activity in HeLa cells relative to the natural aminoglycoside antibiotics (Baker, Luedtke et al. 2000; Luedtke, Baker et al. 2000). In addition, several pyrene-neamine conjugates were shown to disrupt TAR-Tat binding (Hamaski, C. et al. 2000; Hamaski and Ueno 2001).

Mutlicyclic dyes such as Hoechst 33258, DAPI, and berenil exhibit classic nucleic acid intercalation and groove binding activity (Tanious, Veal et al. 1992; Wilson, Ratmeyer et al. 1993; Pilch, Kirolos et al. 1995). Hoechst 33258 and ethidium are routinely used as gel staining reagents for visual identification of nucleic acids because of this binding ability. Several of these compounds have been shown to inhibit TAR-Tat complex formation, specifically by binding to the pocket of the TAR RNA created by the trinucleotide bulge (Bailly, Colson et al. 1996; Dassonneville, Hamy et al. 1997; Gelus, Bailly et al. 1999; Peytou, Condom et al. 1999).

The sperimine-acridine conjugate CGP 40336A, also named AD1, has shown the highest affinity for the TAR RNA of any drug to date (CD_{50} ~ 22 nM) (Hamy, Brondani et al. 1998). This molecule has been shown to selectively form contacts with the G26·C39 basepair in the upper stem of the TAR RNA, while stacking between nucleotides A22 and U23 (Gelus, Hamy et al. 1999). In addition to targeting the TAR-Tat interaction, CGP 40336A also disrupts U1A protein-RNA complex formation, although with significantly lower affinity (K_d ~ 1 μM) (Gayle and Baranger 2002). A structural analog

of CGP 40336A was identified from the Available Chemicals Database (ACD) by computational screening (Du, Lind et al. 2002). This compound, acetylpromazine, had strong affinity for TAR (K_d ~ 100 nM) and an NMR solution structure of the TAR RNA-acetylpromazine complex was solved. In this structure acetylpromazine formed close contacts with the G26·C39 basepair, while forming a highly stable complex with the bulge region, as evident by the 51 observed intermolecular NOEs, several of which were to U23 and U25.

Modified peptides or peptidomimetics have also been synthesized which inhibit TAR-Tat complex formation. For example, a Tat-derived oligourea peptide bound to the TAR RNA with a K_d = 110 nM (Tamilarasu, Huq et al. 1999). Several three amino acid long peptides also inhibited the TAR-Tat interaction, and the strongest tripeptide exhibited an IC_{50} ~ 50 nM (Hwang, Tamilarasu et al. 1999). Cyclic versions of the Tat peptide also inhibited native TAR-Tat complex formation (Friedler, Friedler et al. 2000), although this could simply be due to native Tat β-hairpin formation, similar to that observed in the BIV TAR-Tat complex (Puglisi, Chen et al. 1995), and simple comparative competition. In addition, a short peptoid oligomer of 9 residues was found to inhibit TAR-Tat interaction (Hamy, Felder et al. 1997). Not surprisingly, this peptoid has virtually the same sequence as the Tat peptide.

Several other types of compounds have been shown to bind to the TAR RNA and disrupt TAR-Tat transactivation of viral replication. Three Zn(II)-macrocyclic tetraamine compounds bound to a version of the TAR RNA containing a UUU trinucleotide bulge with affinities as high as 25 nM (Kikuta, Aoki et al. 2001). However, these compounds were also shown to bind to non-basepaired dTpdTpdT sequences extremely tightly (K_d ~ 0.8 nM). Structure-based computational screening methods have also identified TAR-Tat small molecule inhibitors (Filikov, Mohan et al. 2000; Lind, Du et al. 2002). Antisense 2'-O-methyl, 5-propyne, and G-clamp modified RNAs have been selected to form highly stable complexes with the TAR hexanucleotide loop (that interacts with Tat and CycT1) to inhibit TAR-Tat activated transcription (Mestre, Arzumanov et al. 1999; Hamma, Saleh et al. 2003; Holmes, Arzumanov et al. 2003). A small nucleolar RNA-DNA

chimera TAR decoy was shown to potently inhibit HIV-1 replication in human T lymphoblastoid CEM cells (Michienzi, Li et al. 2002). Rather than inhibiting TAR-Tat complex formation through a non-covalent interaction with the RNA, an anti-TAR hammerhead ribozyme was designed to cleave the TAR RNA, and thus inhibit TAR-Tat activated HIV transcription (Wyszko, Barciszewska et al. 2001). In addition, high concentrations of divalent metal ions have also had an inhibitory effect on TAR RNA-Tat protein complex formation, alluding to the importance of electrostatic interactions in the RNA-protein complex (Zacharias and Hagerman 1995; Arzumanov, Godde et al. 2000). The TAR-Tat interaction is also inhibited by the L-enantiomer of the Tat peptide (Garbesi, Hamy et al. 1998) as well as L-arginine, but not L-lysine (Tao and Frankel 1992).

We have determined EPR dynamic signatures for several compounds, which are known to inhibit TAR RNA-Tat peptide binding, in complex with the TAR RNA (Edwards and Sigurdsson 2002). Specifically, we studied the TAR RNA binding of the multicyclic dyes Hoechst 33258, DAPI, berenil, the spermine-acridine conjugate CGP 40336A, the aminoglycoside antibiotic neomycin, and the modified aminoglycoside antibiotic conjugate guanidinoneomycin (Figure 5.1). These compounds were specifically chosen because they target the TAR RNA through a wide variety of binding modes. Our previous results on RNA-metal ion (Edwards, Okonogi et al. 2002; Edwards and Sigurdsson 2003) and RNA-peptide (Edwards, Okonogi et al. 2002) binding provide evidence for a correlation between RNA structure and RNA dynamics, because metals ions bind differently than the Tat-derived peptides, and thus they produced different dynamic signatures. The goal of the current study is to investigate TAR RNA-small molecule binding as a basis for further investigation and confirmation of this correlation. In the current report, molecules which are known to bind similarly to the TAR RNA induced similar changes in TAR RNA internal dynamics, whereas molecules that are known to bind differently induced different changes in TAR RNA internal dynamics. Furthermore, EPR dynamic signatures were used to provide evidence for the mode of action of guanidinoneomycin in the absence of structural information. These results

provide an avenue into the dynamic aspects of RNA molecular recognition and demonstrate a strong correlation between RNA internal dynamics and RNA structure.

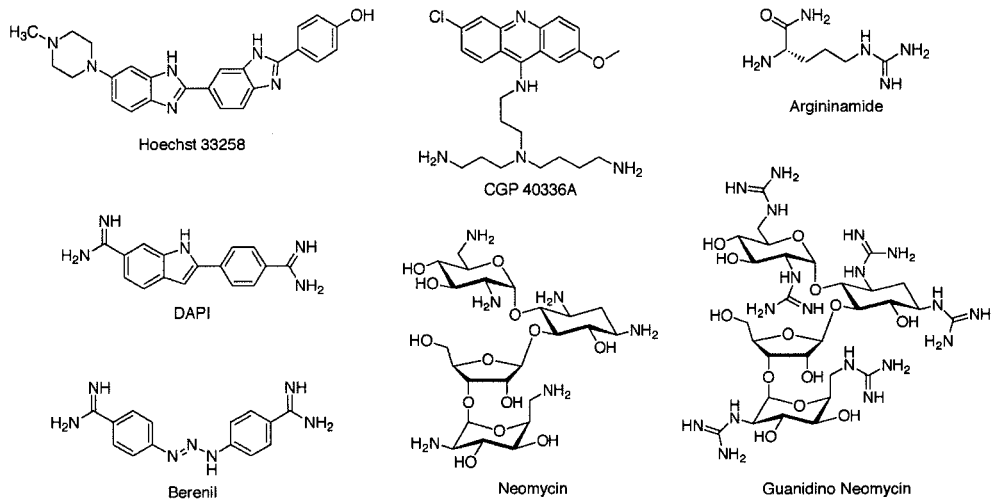

Figure 5.1. Structures of molecules used in this study that target the HIV-1 TAR RNA and inhibit TAR-Tat complex formation

EPR spectroscopy of TAR RNA-small molecule complexes

The multicyclic dyes. The concentration-dependent binding of the multicyclic dyes to the TAR RNA was investigated by monitoring the change in spin-labeled U23 TAR RNA (0.2 mM) EPR spectral width ($2A_{zz}$) upon incubation with variable concentrations of Hoechst 33258 (0-5 mM) (Figure 5.2).

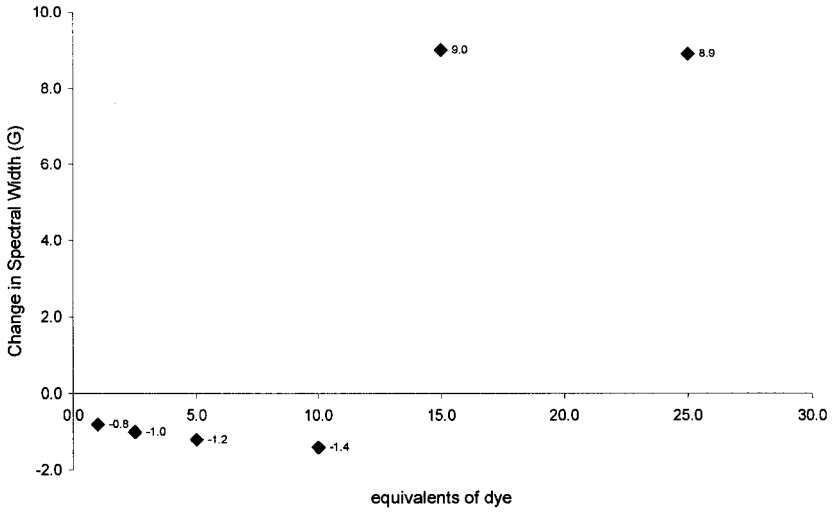

Figure 5.2. Titration of U23 TAR RNA (0.2 mM) with the multicyclic dye Hoechest 33258

Hoechst 33258 induced decreases in the EPR spectral width of U23, indicating an increase in mobility, up to a concentration of about 0.2 mM (1 equivalent) (Figure 5.2). Incubation with higher concentrations of the dye only moderately affected U23 dynamics until a drug concentration of 3.0 mM, where a large increase in spectral width was observed. No further change in RNA dynamics was observed above 3 mM drug concentrations. Similar results were obtained for the other multicyclic dyes, DAPI and berenil. To further illustrate the concentration dependence, EPR spectra of U25 TAR in the presence of 0, 0.5, and 5 mM Hoechst 33258 are shown in Figure 5.3.

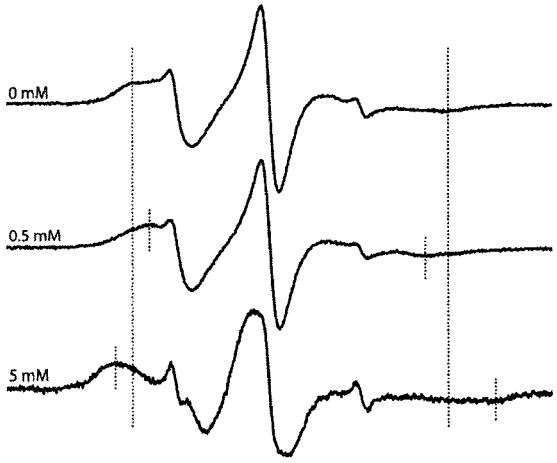

Figure 5.3. EPR spectra of U25 spin-labeled TAR RNA in the presence of 0, 0.5, and 5 mM Hoechst 33258. Dotted lines indicate spectral boundaries which define the spectral width ($2A_{zz}$). Samples were obtained in 20% aqueous sucose/100 mM NaCl, 10 mM sodium phosphate, 0.1 mM Na_2EDTA, pH 7.0.

Above 3 mM multicyclic dye concentration, large decreases in RNA mobility were observed at all positions (U23, U25, U38, and U40). A construct of the TAR RNA lacking the trinucleotide bulge showed virtually no change in EPR dynamics at U40 until 3.0 mM (data not shown). Combined, these results demonstrate that specific RNA-multicyclic drug interactions take place around 0.2-0.5 mM, whereas nonspecific RNA-multicyclic drug interactions occur above 3 mM. Therefore, the EPR dynamic signatures of specific TAR RNA-Hoechst 33258 complex formation was obtained at 0.5 mM drug concentration and nonspecific complex formation was obtained at 5 mM drug concentrations (Figure 5.4).

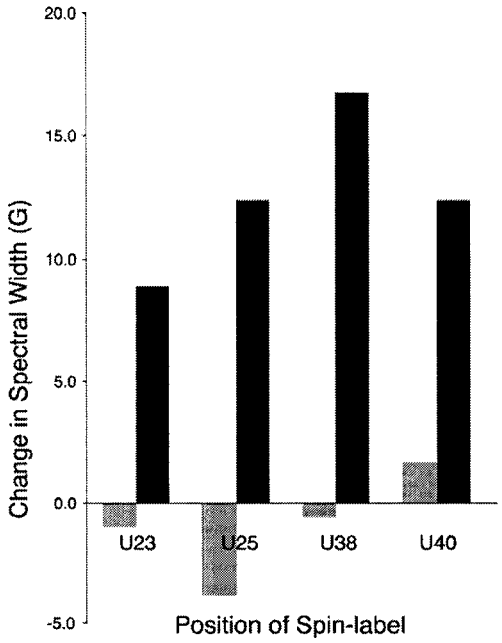

Figure 5.4. Dynamic signatures of TAR RNA-Hoechst 33258 at 0.5 (gray) and 5 mM (black) drug.

The EPR dynamic signatures of specific TAR RNA-DAPI and TAR RNA-berenil complex formation are shown in Figure 5.5.

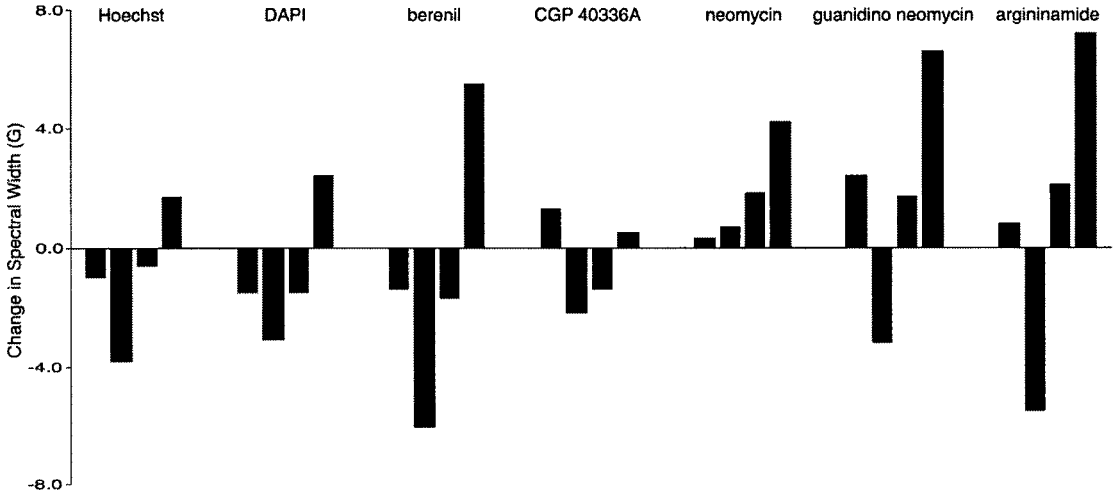

Figure 5.5. EPR dynamic signatures of spin-labeled TAR RNAs (U23, U25, U38, and U40) complexed with small molecules. Small molecules that bind in a similar manner give rise to similar changes in TAR RNA internal dynamics. Small molecules that bind in a different manner, give rise to different changes in TAR RNA internal dynamics.

The spermine-acridine conjugate CGP 40336A. Developed by Novartis, the spermine-acridine conjugate CGP 40336A is the highest affinity TAR RNA-Tat protein small molecule inhibitor. Because CGP 40336A is known to bind with 1:1 stoichiometry, no concentration-dependent complex formation EPR experiment was necessary, and thus TAR RNA-CGP 40336A specific complex formation was obtained in the presence of a small excess of drug (0.2 mM RNA, 0.5 mM drug). An increase in EPR spectral width, indicative of a decrease in mobility, was observed at U23 and U40, while a decrease in spectral width was observed at U25 and U40. The dynamic signature of this compound was therefore different from all of the other obtained (Figure 5.5).

Neomycin and guanidinoneomycin. Multiple aminoglycoside antibiotic-RNA binding has been observed previously by gel shift assay at high concentrations of neomycin (Mei, Mack et al. 1997), whereas at 0.4 mM neomycin and 0.2 mM RNA a 1:1 complex is predominantly formed (Faber, Sticht et al. 2000). Under these conditions, increases in mobility were observed at all positions studies (U23, U25, U38, and U40), resulting in a dynamic signature different than all of the other compounds studied (Figure 5.5). A further decrease in mobility was observed at U23 up to a concentration of about 2 mM (10 equivalents) neomycin, after which no further change in the EPR spectrum of U23 was observed (up to 10 mM, data not shown). EPR dynamic signature of the TAR RNA-neomycin complex under multiple drug binding conditions (5 mM neomycin) revealed moderate decreases in mobility at the bulge nucleotides (U23 and U25) and large decreases at the base-pairing nucleotides (U38 and U40; Figure 5.6). In comparison with the nonspecific binding of Hoechst 33258, where large decreases in dynamics were observed at all positions (Figure 5.4), the data for neomycin represent binding of multiple discrete molecules, rather than nonspecific binding, because the change in EPR dynamics is not uniform.

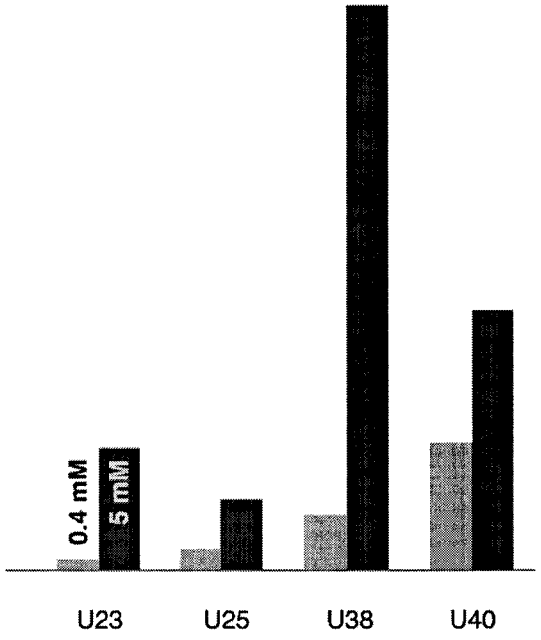

Figure 5.6. TAR RNA-neomycin binding under 1:1 RNA-drug complex formation (0.4 mM neomycin, 0.2 mM RNA, pink) and multi-drug binding concentrations (5 mM neomycin, maroon)

The aminoglycoside antibiotic conjugate guanidinoneomycin, in which the amino groups of neomycin have been replaced with guanidino groups (Figure 5.1), was designed to mimic the binding of the arginine-rich HIV peptides Rev and Tat to their RNA complements (RRE and TAR, respectively) while retaining the important pharmacological properties of the antibiotic neomycin. Although fluorescence experiments demonstrated that guanidinoneomycin binds to both the RRE and TAR RNAs with high affinity, no structural information describing its mode of binding currently exists (Baker, Luedtke et al. 2000; Luedtke, Baker et al. 2000). The EPR dynamic signature of guanidinoneomycin was similar to that previously obtained for argininamide and the Tat-derived peptide YKKKKRKKKKA, rather than that obtained for neomycin, with increases in spectral width at U23, U38, and U40, and a decrease in spectral width at U25 (Figure 5.5). This implies that guanidinoneomycin forms contacts with the TAR RNA similar to that of the essential guanidino group of R52 of the Tat protein.

Correlation of RNA dynamics with RNA structure

Previous studies on changes in TAR RNA dynamics upon binding to metal ions and derivatives of the Tat protein indicated that a correlation exists between RNA structure and RNA dynamics for an individual RNA or RNA-ligand complex. For example, the metal ions Ca^{2+} and Na^{+} produced one set of similar dynamic signatures, whereas the derivatives of the Tat protein produced a distinctively different set of dynamic signatures (Edwards, Okonogi et al. 2002). The central focus of the study presented in this chapter and reported in the literature (Edwards and Sigurdsson 2002) was to further investigate this correlation between RNA structure and RNA dynamics by monitoring the changes in TAR RNA internal dynamics upon binding to small molecules known to target different binding sites on the TAR RNA. Simply put, is this correlation a general theme? For each small molecule, conditions were selected or determined as necessary in which specific 1:1 RNA-drug complexes were formed. EPR spectra of spin-labeled TAR RNA-small molecule complexes were acquired, and the changes in EPR spectral width were plotted as a function of spin-labeled nucleotide position to give a dynamic signature for each compound (Figure 5.5). Figure 5.7 shows a simple model for the binding of several small molecule inhibitors studied here to the TAR RNA. The small molecules which are known to bind similarly (Figure 5.7) were shown to induce similar changes in RNA internal dynamics (Figure 5.5), whereas those that bound differently induced different changes in RNA internal dynamics. The strength of this approach lies in the selection of a sufficient number of spin-labeled sites to yield a unique EPR dynamic signature for each set of conditions studied. For example, if U25 was not included in the study, neomycin and the Tat-derived compounds would all appear to induce roughly similar changes in RNA internal dynamics, despite the known differences between these two classes of compounds. More specifically, neomycin has been shown to inhibit the TAR-Tat interaction through an allosteric mechanism.

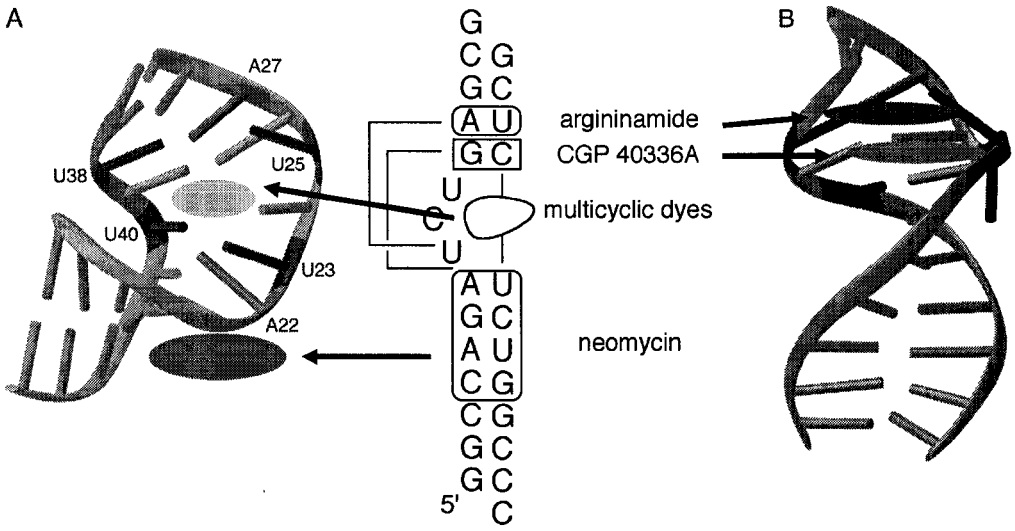

Figure 5.7. Schematic representation of the TAR RNA-small molecule binding interactions studied here. Neomycin binds to the minor groove of the lower stem (center, left). The multicyclic dyes Hoechst 33258, DAPI, and berenil bind to the TAR RNA pocket created by the trinucleotide bulge (center, left). The Novartis compound CGP 40336A binds to the G26·C39 base pair, while stacking between A22 and U23 (center, right). Argininamide, studied previously (Edwards, Okonogi et al. 2002), induces co-linear stacking of the upper and lower helices and U23·A27·U38 base-triple formation (center, right).

ELD, UV and CD spectroscopy, UV-monitored thermal denaturation, and nuclease footprinting experiments demonstrated that the structurally related multicyclic dyes, Hoechst 33258, DAPI, and berenil, bind to the major groove pocket of the TAR RNA created by the trinucleotide bulge (Bailly, Colson et al. 1996; Dassonneville, Hamy et al. 1997; Gelus, Bailly et al. 1999). The EPR dynamic signatures of the compounds were all similar (Figure 5.5) (Edwards and Sigurdsson 2002). Although the three molecules bind to the same site, ELD experiments suggested that berenil binds with a different geometry (Bailly, Colson et al. 1996). In agreement with that hypothesis, berenil has a slightly different EPR dynamic signature than the other two multicyclic dyes (Figure 5.5). Specifically, U40 is more rigid, while U25 is more mobile than that observed in the other TAR RNA-multicyclic dye complexes. This result further demonstrates the highly sensitive nature of EPR spectroscopy of spin-labeled RNA, previously observed in TAR RNA-Tat peptide mutant complexes.

Kinetic binding studies, enzymatic footprinting, and CD spectroscopy have provided evidence that the aminoglycoside antibiotic neomycin inhibits the TAR-Tat interaction through an allosteric mechanism. It is likely that neomycin binding to the minor groove of the lower stem induces a narrowing of the major groove Tat binding site, effectively blocking the Tat protein from binding to the RNA. A low resolution NMR solution structure provided further evidence that neomycin binds to the lower stem rather than to the Tat binding site located in the major groove at the bulge and surrounding nucleotides (Faber, Sticht et al. 2000). However, molecular dynamics simulations (Hermann and Westhof 1999) and comparative structure and sequence analysis of RNA-deoxystreptamine (the core rings I and II of neomycin) binding (Yoshizawa, Fourmy et al. 2002) suggested that neomycin binds to the major groove of the TAR RNA, downstream of the Tat binding site. Several of the same TAR-neomycin contacts were observed in the NMR solution structure and the molecular dynamic simulations, further clouding the model for RNA-antibiotic binding. Regardless of the actual position of neomycin binding, the allosteric mechanism of inhibition commands that neomycin binds to a site on the RNA other than the Tat binding site. In agreement with this, the EPR dynamic signature obtained for neomycin was different than that obtained for argininamide and the Tat-derived peptides.

Because the EPR dynamic signature of was similar to that obtained for argininamide rather than that obtained for neomycin (Figure 5.5), it is likely that a guanidino group of binds to the TAR RNA in a similar manner to that of the guanidino group of the essential R52 of the Tat protein. Furthermore, this EPR information provides evidence in the absence of structural and kinetic information that guanidinoneomycin likely inhibits the TAR-Tat interaction through a competitive mechanism rather than the non-competitive (allosteric) mechanism observed for neomycin. However, confirmation of this hypothesis would require kinetic inhibition biochemical experiments and a high-resolution structure of the TAR RNA- complex.

In conclusion, EPR spectroscopy was used to demonstrate that small molecules, which are known to inhibit the TAR-Tat interaction by binding to similar sites, induced

similar change in RNA internal dynamics. The converse, that molecules known to bind to different TAR RNA sites induce different changes in RNA internal dynamics was also true. Furthermore, EPR spectroscopy was used to provide evidence for the mode of binding of the small molecule guanidinoneomycin in the absence of structural and kinetic competition information. This study further demonstrates the utility of EPR spectroscopy of spin-labeled RNA for the investigation of RNA structure and RNA internal dynamics in RNA-small molecule complexes.

Chapter 6

Preliminary investigation of the metal ion-dependent folding pathway of the hammerhead ribozyme by EPR spectroscopy

The hammerhead ribozyme

The hammerhead ribozyme is the smallest known naturally occurring riboyzme, which catalyzes phosphodiester bond cleavage to produce a 5'-hydroxyl and a 2',3'-cyclic phosphate with a 10^6 rate enhancement over the uncatalyzed reaction (Figure 6.1) (Sigurdsson, Thomson et al. 1998; Gesteland, Cech et al. 1999; DeRose 2002).

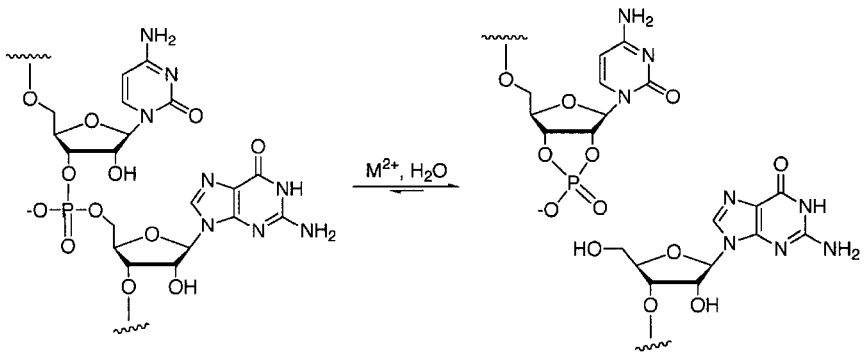

Figure 6.1. The phosphodiester bond cleavage reaction catalyzed by the hammerhead ribozyme

The structure and function of the hammerhead ribozyme have been extensively studied using numerous biochemical and biophysical experiments. Biochemical mutation and kinetic analysis studies revealed a highly conserved catalytic core flanked by three helical stems with little sequence conservation, providing the basis for a minimal catalytic unit. Although the naturally occurring hammerhead ribozyme catalyzes a self-cleavage reaction, the minimal catalytic unit can be modified to produce a multiple turnover catalyst. In this construct, the RNA is comprised of a catalytic strand (also called the ribozyme strand) and a substrate strand. The sequence and secondary structure of the hammerhead ribozyme, including the site of cleavage, are depicted in Figure 6.2.

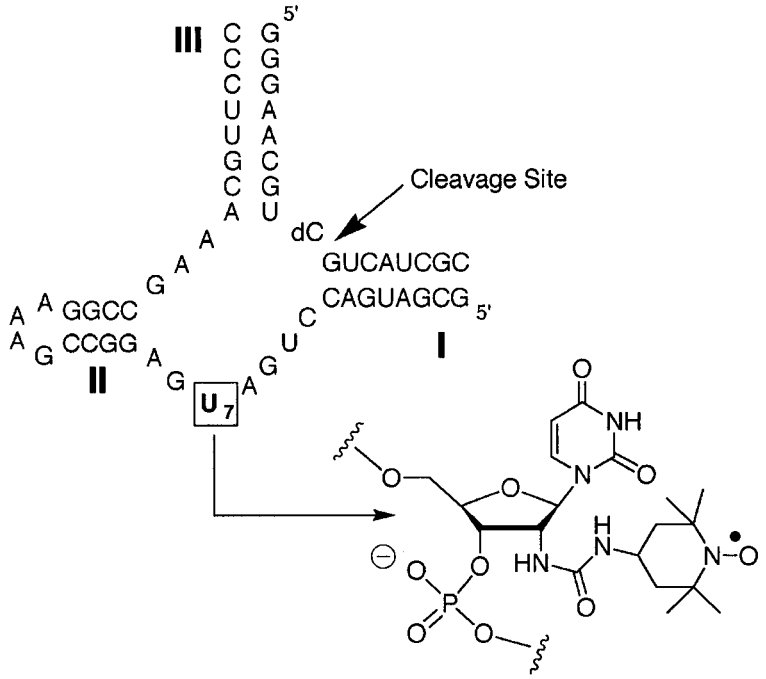

Figure 6.2. The primary and secondary structure of the hammerhead ribozyme. The 5' end of the substrate strand is located in stem III, while the 5' end of the ribozyme strand is located in stem I. The cleavage site is shown with an arrow, and U7, the site of spin-labeling in this study, is shown in bold, with an insert of the spin-label modified nucleotide. A 2'-deoxyribonucleoside (dC) was incorporated into the catalytic site to inhibit cleavage, allowing for the study of metal ion-dependent hammerhead ribozyme folding.

Metal ions in folding and catalysis of the hammerhead ribozyme

Biochemical experiments have shown that under physiological metal ion concentrations, divalent metal ions are required for hammerhead ribozyme folding and catalysis (Hammann and Lilley 2002; DeRose 2003). Therefore, divalent metal ions are either involved directly in catalysis or are important for tertiary structure formation prior to catalysis or both. The catalytic rate depends on the identity of the divalent metal ion present, and Mg^{2+} affords the highest catalytic rate (e.g. $K_{cat} \sim 2.2\ min^{-1}$ at 10 mM Mg^{2+}). Several biochemical and biophysical experiments have shown that metal ions affect the global conformation of the ribozyme. The X-ray crystal structures of the hammerhead ribozyme contained several bound divalent metal ions, although no high occupancy sites were located in close proximity to the scissile phosphate (Figure 6.3) (Pley, Flaherty et al.

1994; Scott, Finch et al. 1995). Comparative non-denaturing gel electrophoresis experiments in the presence of Mg^{2+} at concentrations near optimal for catalytic efficiency demonstrated a similar global fold of the hammerhead ribozyme as that found in the crystal structure (Bassi, Mollegaard et al. 1995). A three dimensional model of the hammerhead ribozyme based on FRET measurements in the presence of Mg^{2+} showed a similar global shape of the ribozyme, although the orientation of helices II and III were different than that obtained by X-ray crystallography (Tuschl, Gohlke et al. 1994). Disulfide cross-linking studies addressed this discrepancy and demonstrated that the orientation observed in the crystal structure was the likely orientation observed in solution (Sigurdsson and Eckstein 1995; Sigurdsson, Tuschl et al. 1995; Sigurdsson 1996).

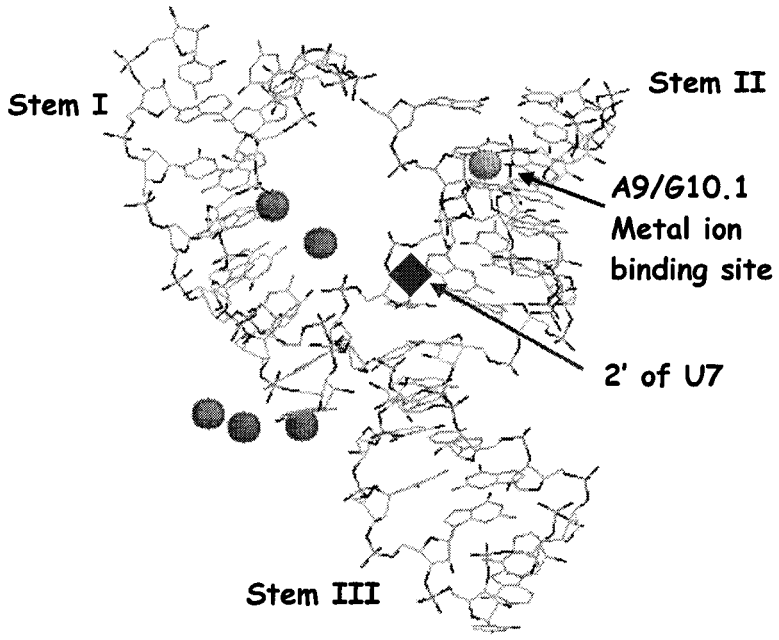

Figure 6.3. The X-ray crystal structure of the hammerhead ribozyme solved in the presence of Mg^{2+} is shown using the CPK color scheme (Murray, Szoke et al. 2000). The high affinity A9/G10.1 metal ion binding site is shown in magenta, while the lower affinity metal ion binding sites are shown in gray, and the 2'-spin-labeling site of U7 is shown in blue.

In addition to affecting the global shape of the hammerhead ribozyme, metal ions appear to affect the local structure. The crystal structures are believed to be low energy, inactive conformations of the hammerhead ribozyme because the atomic structure of the cleavage site is not assembled for an in-line attack necessary for catalysis (McKay 1996). Therefore, it is likely that the RNA must undergo a structural rearrangement in order to perform the observed chemistry. This analysis is consistent with numerous biochemical kinetic interference modifications which cannot be explained by the crystal structure (McKay 1996). Nevertheless, the hammerhead ribozyme was active in the crystal (Murray, Terwey et al. 1998), demonstrating that only a local conformational change was required to produce activity rather than a large global change in conformation. A modified RNA containing a 5'-methyl group at the leaving group resulted in the kinetic trapping of an 8.7 Å local conformational change at the cleavage site, positioning the nucleophile and the leaving group close to the required in line attack formation (Murray, Terwey et al. 1998). While the normal ribozyme was completely cleaved in the crystal after 4 min of soaking with 50 mM $CoCl_2$, this "kinetic bottleneck" 5'-methyl modified ribozyme was not cleaved even after 2.5 hours, demonstrating that this ribozyme forms the correct structural alignment in the presence of metal ions, but cleaves at a slower rate, allowing for the observation of the late transition state. This conformational change was further investigated and determined to be pH-dependent and the mechanistic rate-limiting step (Murray, Dunham et al. 2002), rather than a rate-limiting chemical step, such as 2'-OH deprotonation, in agreement with kinetic isotope experiments (Sawata, Komiyama et al. 1995). A detailed theoretical analysis of Mg^{2+}-mediated catalysis has been reported (Torres, Himo et al. 2003).

Site-specifically bound metal ions are thought to be important to the folding and activity of the hammerhead ribozyme. The crystal structures confirmed the presence of several low affinity metal ion binding sites as well as the presence of a high affinity metal ion binding site at A9/G10.1. While the low affinity sites' occupancy changed depending on the divalent metal ion present, the high affinity A9/G10.1 metal ion binding site was occupied in all of the structures. This site is believed to be important for the structural

assembly of domain 1 during hammerhead folding as described below. While no high occupancy metal ion binding sites were located near the scissile phosphate, flash-freezing experiments captured a Mg^{2+} ion bound to the pro-R oxygen of the scissile phosphate (Scott, Murray et al. 1996). This metal ion is thought to stabilize the developing negative charge that accumulates on the phosphate during the transition state. The binding of this metal ion directly involved in catalysis appears to be of moderate affinity (100 M^{-1}) which is significantly lower than the A9/G10.1 site (7600 M^{-1} (Menger, Tuschl et al. 1996) or 10 μM (Horton, Clardy et al. 1998)).

A two-step model for the divalent metal ion-dependent folding pathway of the hammerhead ribozyme has been developed using data acquired from non-denaturing comparative gel mobility assays (Bassi, Mollegaard et al. 1995), FRET measurements (Bassi, Murchie et al. 1997), EPR spectroscopy (Horton, Clardy et al. 1998), and ^{19}F NMR spectroscopy (Hammann, Norman et al. 2001). In this model, the absence of divalent metal ions resulted in a near co-axial orientation of stems I and II, whereas stem III is roughly perpendicular to the other stems (Figure 6.4). This structure has since been confirmed in solution by residual dipolar coupling NMR (Bondensgaard, Mollova et al. 2002). In the presence of 0.5 mM divalent metal ions, stems II and III stack, with stem I remaining in proximity to stem III. This step constitutes the folding of domain 2. In the presence of higher concentrations of divalent metal ions (e.g. 10 mM Mg^{2+}), stem I folds down closer to stem II, forming the active ribozyme. This step constitutes the folding of domain 1. As discussed above, the 2-aminopurine fluorescence data indicated multiple metal ion binding sites that could be separated into two categories with affinities in the range of 7600 to 12 M^{-1} at pH 7.5 (Menger, Tuschl et al. 1996). New FRET measurements in 100 mM NaCl (higher than than that studied above) indicated a different two-step folding transition, with the second step co-inciding with re-orientation of helical stems I and II to promote catalytic efficiency (Rueda, Wick et al. 2003). This result is in agreement with another recent study, demonstrating intercellular efficiency of hammerhead ribozymes containing a loop-loop interaction between stems I and II at 100 μM $MgCl_2$ (Khvorova, Lescoute et al. 2003).

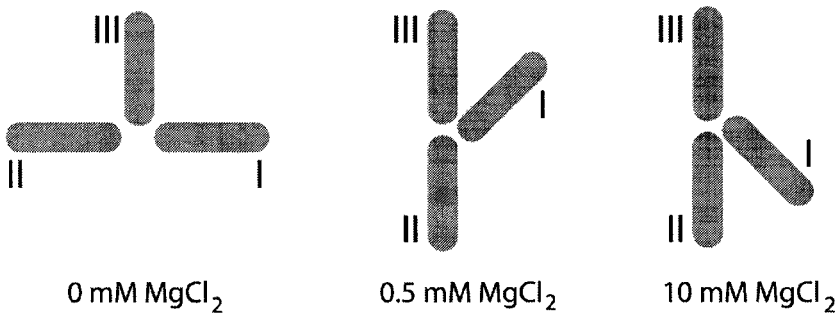

Figure 6.4. A simple model for the two-state divalent metal ion-dependent folding pathway of the hammerhead ribozyme

Interestingly, the hammerhead ribozyme was shown to be active in the absence of divalent metal ions and the presence of extremely high concentrations (4 M) of Li^+, Na^+, and NH_4^+, albeit at significantly lower catalytic rates ($K_{cat} \sim 0.29$ min^{-1}, $K_{cat} \sim 0.0075$ min^{-1}, and $K_{cat} \sim 0.014$ min^{-1}, respectively, as opposed to ~ 2.2 min^{-1} in the presence of 10 mM Mg^{2+}) (Murray, Seyhan et al. 1998; Curtis and Bartel 2001; O'Rear, Wang et al. 2001). These results argue against the requirement of divalent metal ions in hammerhead catalysis and support the notion that metal ions only perform structural roles in hammerhead ribozyme biochemistry. The presence of high concentrations of monovalent metal ions is thought to not perturb the global structure of the RNA, because the X-ray structures of the hammerhead were solved in the presence of high concentrations of monovalent metal ions (e.g. 1.8-2.4 M Li_2SO_4) and were shown to have a similar global fold as that found in solution (discussed above). Since this discovery, a hypothesis has been reported in which divalent metal ions promote cleavage through an efficient pathway, whereas monovalent metal ions promote cleavage through a different, inefficient pathway (Zhou, Zhou et al. 2002). Evidence for the divergent monovalent and divalent metal ion pathways include a kinetic solvent isotope effect of 2 for high concentrations of NH_4^+ (Takagi and Taira 2002) as opposed to an isotope effect of 1 for Mg^{2+} (Sawata, Komiyama et al. 1995), demonstrating that proton transfer is the rate-limiting chemical step in the presence of high concentrations of NH_4^+, but not in the presence of 10 mM Mg^{2+}. Furthermore, in the presence of low concentrations of Mg^{2+} or

Mn^{2+}, low concentrations of Na^{+} inhibited catalysis, whereas higher Na^{+} concentrations promoted catalytic rescue (Takagi and Taira 2002). These results imply that two types of metal ion binding sites are being filled at different concentrations, in agreement the two-state folding pathway.

Two additional catalytic sites have been discovered in the hammerhead ribozyme, one at A9 (Markley, Godde et al. 2001) and the other at U4 (Borda, Markley et al. 2003). The A9 site was dependent on divalent metal ion for catalysis, preferential for Zn^{2+}, and displayed a log-linear pH dependence that appeared to follow the pK_a trend of the Zn^{2+}-aqua complex with a pK_a ~ 8.5. In contrast to A9 cleavage, U4 cleavage was observed only after A9 cleavage, only in the presence of Zn^{2+}, and was highly pH sensitive, displaying activity only in a short pH window of 7.9-8.6. These results imply that the hammerhead ribozyme undergoes a pH-dependent conformational change in this range and are in rough agreement with crystallographic data (Murray, Dunham et al. 2002).

In the current report we used EPR spectroscopy to investigate metal ion-dependent folding of the hammerhead ribozyme. With the exception of the ^{19}F NMR study (Hammann, Norman et al. 2001) and 2-aminopurine fluorescence studies (Menger, Tuschl et al. 1996; Menger, Eckstein et al. 2000; Kirk, Luedtke et al. 2001), all other biophysical hammerhead ribozyme investigations have monitored changes in RNA global structure or stability upon metal ion binding. The current report describes the investigation of changes in RNA internal structure and dynamics during RNA folding by EPR spectroscopy and provides a new tool for characterizing ribozyme molecular structure assembly. A nitroxide spin-label was incorporated into the ribozyme strand of the HH16 construct at the 2'-position of U7. EPR spectroscopy was used to monitor the mobility of U7 under a variety of metal ion and inhibitor concentrations, as well as over a wide range in pH. Temperature dependent studies were performed for all samples. Although only small changes in U7 dynamics were observed upon incubation with Mg^{2+}, these changes were consistent with the proposed two-state folding model. At constant viscosity U7 was observed to be more mobile in the presence of 4 M monovalent metal ions rather than divalent metal ions, providing evidence that the microenvironment of U7

is different in the presence of 4 M monovalent metal ions than in the presence of 10 mM Mg^{2+}. In conclusion, these preliminary investigations into the metal ion-dependent folding pathway of the hammerhead ribozyme demonstrate the utility of EPR spectroscopy for monitoring RNA internal dynamics during complex molecular folding.

Selection of a spin-labeled hammerhead ribozyme and experimental conditions

Selection of a site for 2' spin-label modification within the catalytic core of the hammerhead ribozyme is challenging due to the fact that the catalytic core is highly sensitive to modification (Bratty, Chartrand et al. 1993; Blount, Grover et al. 2002). Two possible spin-labeling sites are those chosen for 5-fluoro uridine modification in a ^{19}F NMR hammerhead folding study, U4 and U7. In that study U7 modification was sensitive to the folding of both domain 1 and 2, whereas U4 was only sensitive to domain 1 folding. U7 was modified with a 2-aminopurine nucleoside in the fluorescence study without drastic reduction in catalytic activity (Menger, Tuschl et al. 1996). Steric interference modification at U7 with a 2'-(3-metcapto)-propionamido group resulted in a catalytic rate similar to that of the unmodified ribozyme ($K_{rel} \sim 0.89$); in contrast, 2'-acetamido and 2'-ethylureido modification at U4 severely decreased the catalytic rate ($K_{rel} \sim 0.02$ and 0.09, respectively) (Blount, Grover et al. 2002). Therefore, U7 was chosen as the site for spin-label modification for preliminary EPR experiments, and a U7 2'-spin-labeled sample was prepared using the HH16 ribozyme construct (Figure 6.2). In keeping with the literature, the following experimental conditions were selected: 50 μM RNA, 10 mM NaCl, 10 mM Tris·HCl (pH 7.5), and a non-cleavable substrate containing a 2'-deoxy nucleotide at the cleavage site (Hammann, Norman et al. 2001). Under non-frozen reduced temperature conditions (-10 °C), the EPR spectrum of U7 spin-labeled hammerhead ribozyme-non-cleavable substrate complex displayed slow motion regime dynamics with separated outer and inner hyperfine couplings (Figure 6.5). Consequently, sucrose was not necessary to slow the global tumbling of the molecule as was the case for

the TAR RNA samples. In contrast to the EPR spectrum at -10 °C, the same sample at 40 °C produced a typical fast motion dynamics (Figure 6.5).

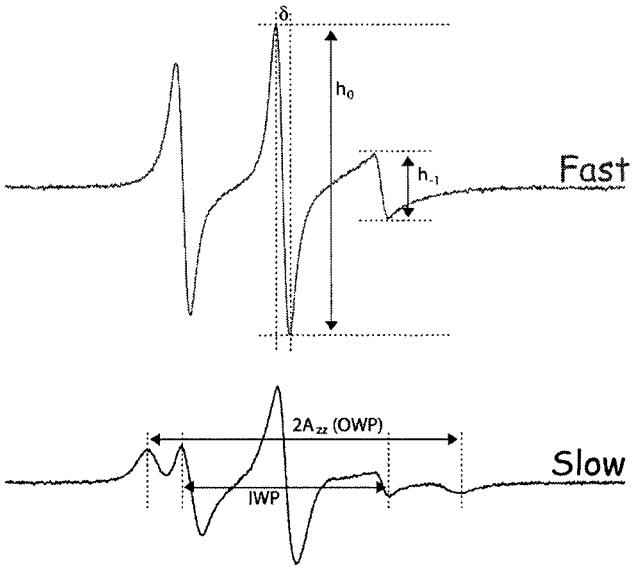

Figure 6.5. EPR spectra of U7 2'-spin-labeled hammerhead ribozyme-non-cleavable substrate complex in the absence of divalent metal ions at 40 °C (top spectrum) and -10 °C (bottom spectrum), showing a typical fast and slow motion regime EPR spectrum, respectively. EPR samples of spin-labeled RNA (50 μM) were prepared in 10 mM NaCl and 10 mM Tris·HCl, pH 7.5. The following spectral features are shown: center line width, δ; center line amplitude, h_0; high field line, h_{-1}; spectral width or outer wide hyperfine coupling peaks, OWP or $2A_{zz}$; and the inner wide hyperfine coupling peaks, IWP.

Due to the natural differences in the EPR spectral features under fast and slow motion regimes, the rotational correlation times (τ_R) of each spectrum are calculated using different equations. The equation for calculating τ_R of a spin-label in the fast motion regime is: $\tau_R = (6.5\text{x}10^{-10})(\delta)((h_0/h_{-1})^{0.5}-1)$ (Qin, Butcher et al. 2001). δ is the centerline width, h_0 is the centerline peak amplitude, and h_{-1} is the high field peak amplitude. The equation for calculating τ_R in the slow motion regime is: $\tau_R = (5.4\text{x}10^{-10})(1-(2A_{zz}/2A_{zz}^{max}))^{-1.36}$ (Freed 1976). $2A_{zz}$ is the spectral width and $2A_{zz}^{max}$ is the maximum spectral width (75.8 G). While these two methods for calculating τ_R are not directly comparable because they are biased toward different spectral features, the extremes at -10 and 40 °C are qualitatively comparable.

In the absence of Mg^{2+} at -10 °C, U7 of the hammerhead ribozyme had a τ_R of 2.59 ns, whereas in the hammerhead ribozyme-non-cleavable substrate complex U7 had a τ_R of 2.89 ns (slow motion regime). At 40 °C in the absence of Mg^{2+}, U7 of the hammerhead ribozyme had a τ_R of 1.11 ns, whereas U7 of the hammerhead ribozyme-non-cleavable substrate complex had a τ_R of 1.79 ns (fast motion regime). These differences in τ_R at a given temperature are consistent with the formation of a larger molecule tumbling more slowly and demonstrate ribozyme-substrate complex formation. The EPR spectra of these samples under several different temperatures are shown in Figure 6.6.

The scaled relative mobility factor, M_s, developed by Wayne Hubbell and co-workers as a semi-quantitative measure of nitroxide motion, reflects both changes in the nitroxide order parameter (S) and effective correlation time (τ_e) (Columbus and Hubbell 2002). M_s is defined as $(\delta^{-1} - \delta_i^{-1})/(\delta_m^{-1} - \delta_i^{-1})$, where δ is the centerline width of the sample being investigated, δ_i is the centerline width of the most immobile spin-probe, and δ_m is the centerline width of the most mobile spin-probe. δ_i and δ_m values of 8.4 and 2.1 G, respectively, were chosen by Hubbell and co-workers after the accumulation of a large body of literature using SDSL to study protein structure and dynamics. Due to the significantly smaller body of literature for RNA, the same values were used. Because M_s is a relative factor, the exact choice of δ_i and δ_m does not affect the conclusions. Values of M_s close to 1 are indicative of a high degree of mobility, whereas values close to 0 are indicative of a low degree of mobility. Changes in M_s are consistent with the changes in τ_R described above. For example, M_s values of 0.54 and 0.97 were observed for the ribozyme strand at -10 and 40 °C, respectively, whereas and M_s values of 0.53 and 0.86 were observed for the larger ribozyme-non-cleavable substrate complex at -10 °C and 40 °C, respectively.

Monitoring hammerhead ribozyme folding using EPR spectroscopy

To monitor the two-state divalent metal ion-dependent folding pathway of the hammerhead ribozyme, U7 spin-labeled ribozyme samples were incubated over a range of Mg^{2+} concentration (0, 0.25, 0.5, 2, 5, 10, 50 mM) and temperatures (-10 to 40 °C) (Figure 6.6). At low temperature (-10 and 0 °C), the EPR spectral width ($2A_{zz}$) of U7 decreased slightly (-0.2 G) in the presence of 0.25 mM Mg^{2+}, before increasing (+1.3 G at -10 °C or +1.8 G at 0 °C) in the presence of higher Mg^{2+} concentrations. The rotational correlation times (τ_R), which are calculated based on the spectral width, followed a similar pattern at low temperature. For example, at -10 °C τ_R decreased from 2.89 ns to 2.85 ns at 0.25 mM Mg^{2+}, increased to 2.92 ns at 0.5 mM Mg^{2+}, increased to 3.09 ns at 5 mM Mg^{2+}, and increased to 3.13 ns at 50 mM Mg^{2+} (Figure 6.7). The EPR results indicate that the first folding event occurs around 0.25 mM Mg^{2+}, while the second folding event happens at ca. 10 mM Mg^{2+}, in qualitative agreement with data obtained by FRET measurements, non-denaturing gel electrophoresis, and ^{19}F NMR which also show a two transition folding pathway. While the actual Mg^{2+} concentration value obtained for the first folding event is slightly lower than that reported from non-denaturing PAGE (Bassi, Mollegaard et al. 1995) and ^{19}F NMR data (Hammann, Norman et al. 2001) (0.5 mM Mg^{2+}), it is reasonably close. Furthermore, in the FRET study (Bassi, Murchie et al. 1997) the first folding event appeared to be complete at ~ 0.3 mM Mg^{2+}. In addition, the ^{19}F NMR data showed the largest change in chemical shift at 0.5 mM Mg^{2+}, but the largest change in linewidth at 0.25 mM Mg^{2+}, implying that depending on the technique and probe, the actual value may vary.

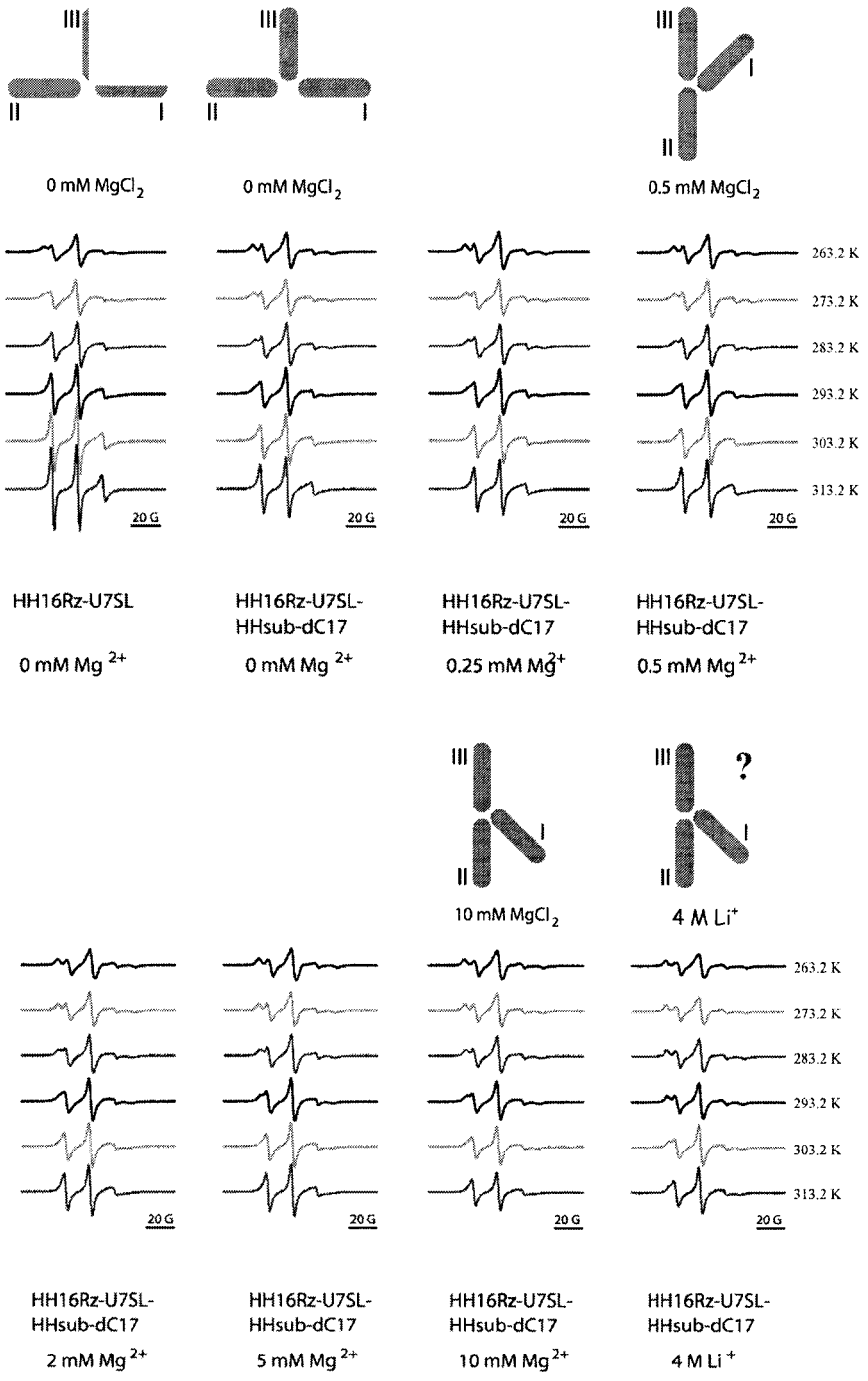

Figure 6.6. EPR spectra of U7 spin-labeled hammerhead ribozyme in the absence and presence of non-cleavable substrate under variable Mg^{2+} concentrations (0, 0.25, 0.5, 2, 5, and 10 mM), 4 M Li^{+} and variable temperatures (-10 to 40 °C). A schematic representation of the proposed folded state is depicted above and the metal ion conditions are shown below each temperature set of spectra. All spectra are normalized in spin-count to the first spectrum in the upper left hand corner.

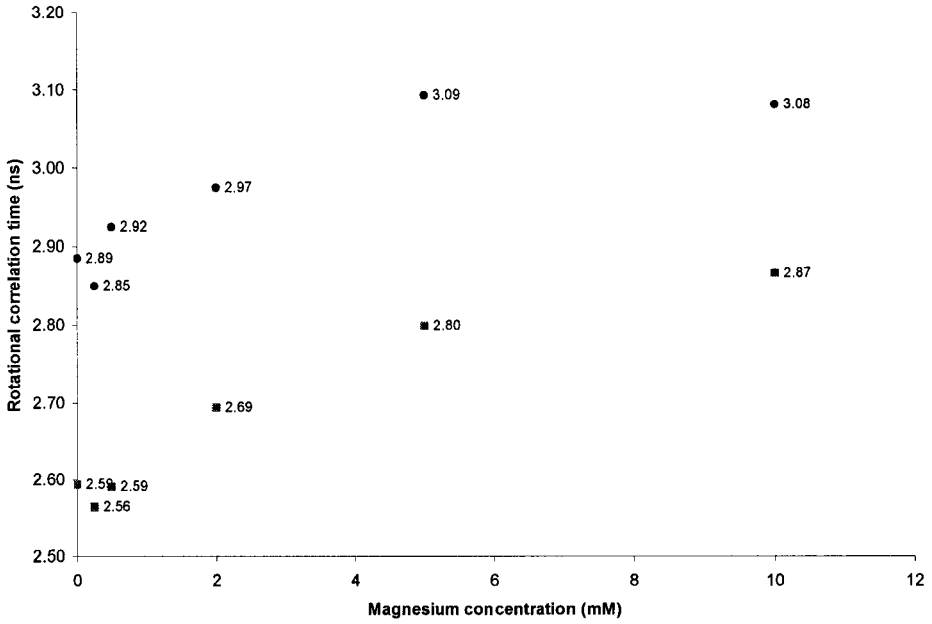

Figure 6.7. Monitoring the change in τ_R of the U7 spin-labeled hammerhead ribozyme-non-cleavable substrate complex in the presence of Mg^{2+} at -10 °C (circles) and 0 °C (squares) by EPR spectroscopy

In contrast to the low temperature data, at high temperature (30 and 40 °C) the folding events are not as well resolved (Figure 6.8). At 40 °C, the relative mobility (M_s) increases at 0.25 mM Mg^{2+} (0.87 from 0.86), then rapidly decreases up to 2 mM Mg^{2+} (0.75) and remains fairly constant through 50 mM (0.74). However, no corresponding increase in M_s at 0.25 mM Mg^{2+} is observed at 30 °C. In contrast to the ^{19}F NMR data reported at 300 K (Hammann, Norman et al. 2001) and the non-denaturing gel electrophoresis obtained at room temperature (Bassi, Mollegaard et al. 1995), the two-state folding transition is not well resolved in the higher temperature EPR experiments. This is an expected result, since the activation energies for transitions are likely lowered at elevated temperatures, effectively blending intermediate states. Nevertheless, the combined high and low temperature data demonstrate that EPR spectroscopy can be used to measure changes in RNA internal dynamics during metal ion-dependent folding.

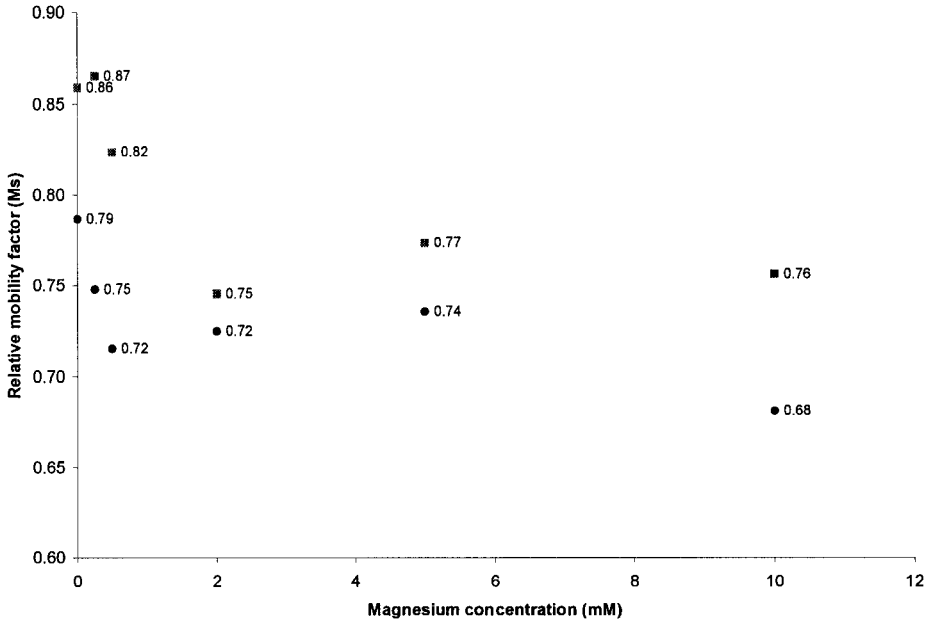

Figure 6.8. Monitoring relative mobility (M_s) of the U7 spin-labeled hammerhead ribozyme-non-cleavable substrate complex in the presence of Mg^{2+} at 30 °C (circles) and 40 °C (squares)

Hammerhead riboyzme dynamics in 4 M Li^+ and 4 M Na^+

The hammerhead ribozyme was shown to be active in the absence of divalent metal ions and the presence of high concentrations of monovalent metal ions, prompting the hypothesis that the metal ions are not directly involved in catalysis, but rather, are simple structural supports (Murray, Seyhan et al. 1998). To investigate this further, we acquired EPR spectra of the U7 ribozyme-non-cleavable substrate complex in the presence of 4 M Li^+ or 4 M Na^+ over a range of temperatures (-10 to 40 °C; Figure 6.6). Li^+ has the highest reported monovalent metal ion catalytic rate, while Na^+ is substantially lower (Curtis and Bartel 2001). In each case, U7 had a wider spectral width, implying it was more rigid, in the presence of monovalent metal ions than in the presence of Mg^{2+} (Figure 6.9). The rate of temperature-dependent change in the EPR spectral width was much faster in the presence of 10 mM Mg^{2+} than 4 M Li^+ or 4 M Na^+, implying that these conditions produce different microenvironments of U7 in the hammerhead ribozyme at a given temperature.

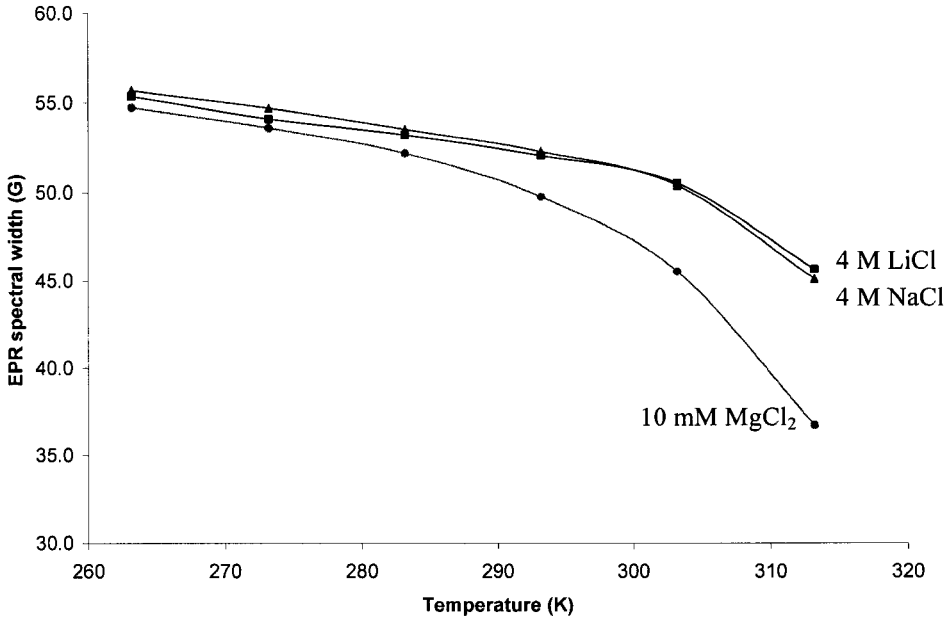

Figure 6.9. The temperature-dependence of the EPR spectral width ($2A_{zz}$) of U7 spin-labeled hammerhead ribozyme in the presence of 10 mM Mg^{2+} (circles), 4 M Li^{+} (squares), or 4 M Na^{+} (triangles)

The presence of high concentrations of monovalent metal ions alters the natural viscosity of the EPR sample, and therefore, direct comparison of monovalent and divalent metal ion data at a given temperature may not reflect comparative mobilities. To address this issue, we corrected for the natural viscosity of these solutions. The viscosity of water under various temperatures has been reported (Sober 1968) as has viscosity of aqueous NaCl solutions at 20 °C (Lide 1994). The percent mass composition of salts in the standard buffer (10 mM NaCl, 10 mM Tris·HCl, pH 7.5) including 10 mM $MgCl_2$ is <0.3% and likely has a negligible effect on the viscosity. Therefore, the reported viscosity of water was used for these solutions. The viscosity of 4 M NaCl is ca. 1.53 cP at 20 °C as opposed to the viscosity of water (1.002 cP) at 20 °C. Due to the unavailability of sodium or lithium viscosity data at other temperatures, a correction factor of 1.53 was applied to the reported viscosity of water over the temperatures studied (0 to 40 °C) to obtain a viscosity measurement for each of the monovalent metal ions. The viscosity of 4 M LiCl was assumed to be close to that of 4 M NaCl, although in actuality it is likely less

due to the smaller size of lithium. Comparison of the EPR spectral width data under similar viscosities demonstrates that U7 of the ribozyme is more rigid in the presence of divalent metal ions than in the presence of monovalent metal ions (Figure 6.10).

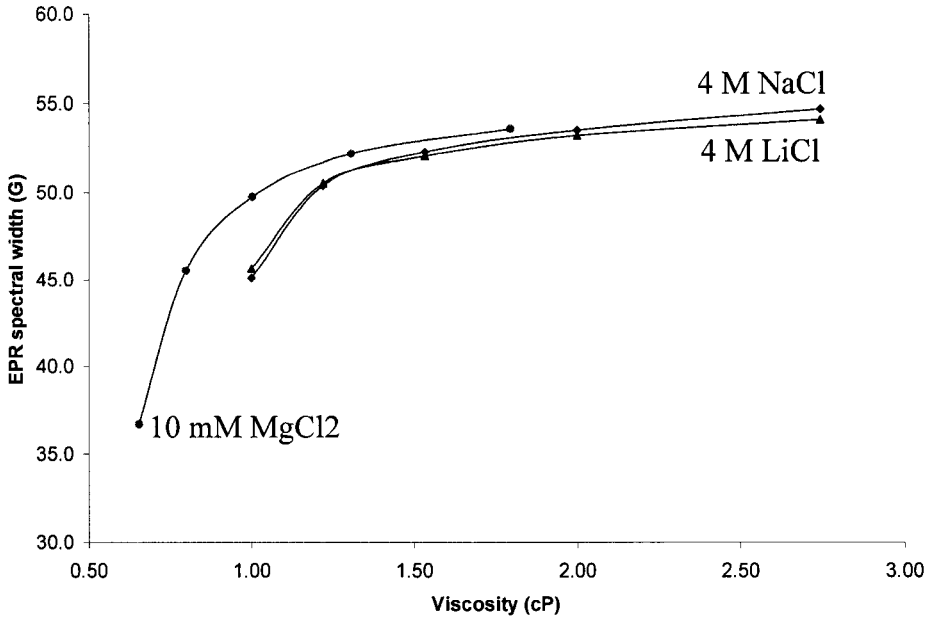

Figure 6.10. EPR spectral width ($2A_{zz}$) data that has been corrected for viscosity effects for the U7 spin-labeled hammerhead ribozyme-non-cleavable substrate complex in the presence of 10 mM $MgCl_2$ (circles), 4 M LiCl (diamonds), or 4 M NaCl (triangles)

Analysis of relative mobility (M_s) data, which is biased toward the center line width rather than the spectral width ($2A_{zz}$), revealed a similar trend (Figure 6.11). It is important to obtain both types of analysis because $2A_{zz}$ accurately reflects comparative mobility in the slow motion regime (i.e. higher viscosity), while M_s accurately reflects comparative mobility in the fast motion regime (i.e. lower viscosity).

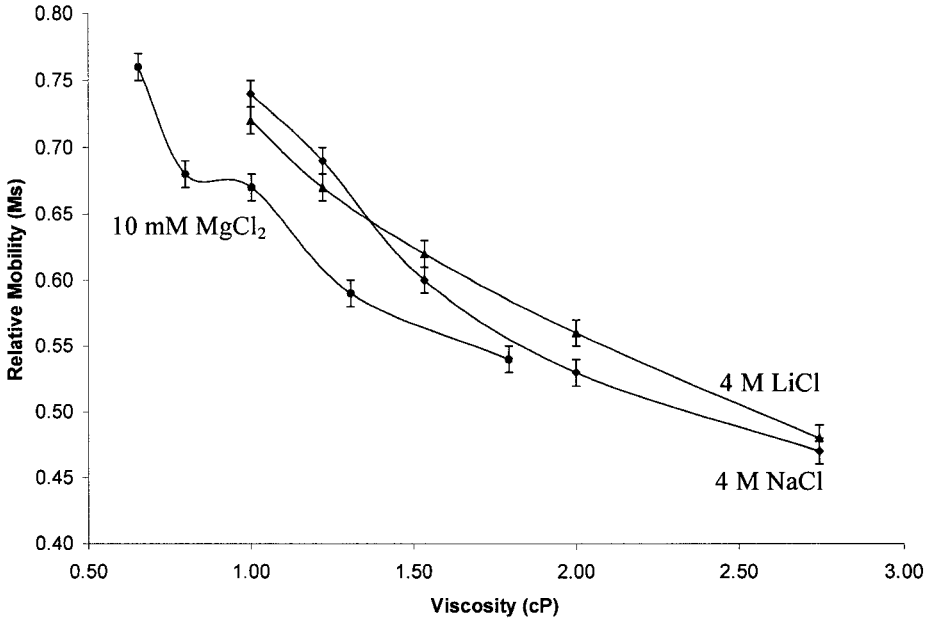

Figure 6.11. EPR relative mobility (M_s) data that has been corrected for viscosity effects for U7 spin-labeled hammerhead ribozyme-non-cleavable substrate complex in the presence of 10 mM $MgCl_2$ (circles), 4 M LiCl (diamonds), or 4 M NaCl (triangles)

Figures 6.10 and 6.11 show that after correcting for viscosity effects caused by high monovalent metal ion concentrations, U7 in the catalytic core of the hammerhead ribozyme is more rigid in the presence of Mg^{2+} than in the presence of the monovalent metal ions. The increased mobility in the presence of the monovalent metal ions at a given viscosity likely is associated with the reduced catalytic efficiency of the ribozyme in the absence of divalent metal ions. While it may be tempting to assert that the global structure of the ribozyme in the presence of monovalent metal ions is more dynamic than in the presence of divalent metal ions, a difference in dynamics at one internal site within the catalytic core may not necessarily reflect the global dynamics of the ribozyme. These results, which demonstrate a different microenvironment for U7 in the presence of monovalent or divalent metal ions, support the hypothesis of divergent high efficiency divalent metal ion and low efficiency monovalent metal ion catalytic pathways. Alternatively, one could add sucrose to change the viscosity of the 10 mM $MgCl_2$ sample, allowing one to keep viscosity and temperature constant (see further studies).

Possible structure and dynamics rescue with 1 equivalent of Mg^{2+}?

DeRose and co-workers have shown that the number of divalent metal ions bound depends on the concentration of monovalent metal ions (Horton, Clardy et al. 1998). For example, in the absence of NaCl, 16 Mn^{2+} were bound, as observed by the decrease in EPR signal of Mn^{2+} upon binding at X-band frequencies, whereas in the presence of 100 mM NaCl 5 were bound, or in the presence of 1.0 M NaCl at low Mn^{2+} concentration, 1 could be site specifically bound. Further experiments demonstrated that the data was consistent with site-specific binding to the A9/G10.1 metal ion binding site (Morrissey, Horton et al. 1999; Morrissey, Horton et al. 2000). Therefore, we decided to observe the dynamics of U7 in the presence of 1.0 M NaCl and 1 equivalent of Mg^{2+} (Figure 6.12) to determine whether or not 10 mM $MgCl_2$-like dynamics could be observed, demonstrating structural and dynamic rescue in the presence of a metal ion site-specifically bound at A9/G10.1. These results demonstrate dynamic recovery above 1.0 cP (i.e. below 20 °C, conditions previously observed (Horton, Clardy et al. 1998)), but dynamic separation below 1.0 cP.

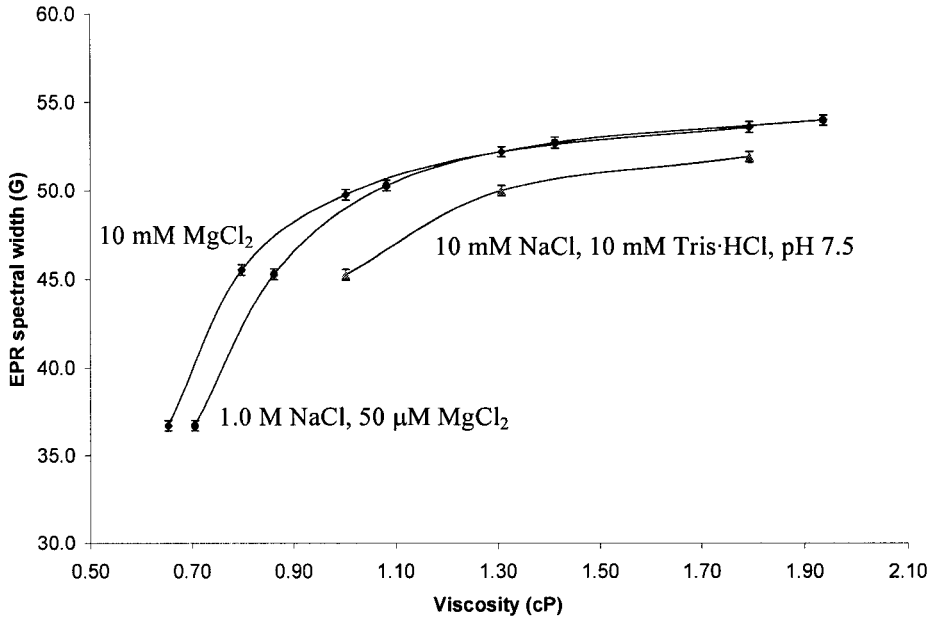

Figure 6.12. Monitoring the change in EPR spectral width ($2A_{zz}$) over a range of temperatures for U7 of the hammerhead ribozyme in the presence of 1.0 M NaCl and 50 μM $MgCl_2$ (1 equivalent) with comparison to the dynamics in the presence of the background buffer (10 mM NaCl, 10 mM Tris·HCl, pH 7.5). The data has been corrected for the viscosity effect as discussed above.

The difference in mobility between the samples show in Figure 6.12 at higher temperature may be due to dissociation of the bound Mg^{2+} ion. This was further investigated by substitution of the Mg^{2+} ion with the EPR active Mn^{2+} (d^5). In the bound state the zero-field splitting increases, effectively eliminating the EPR signal of Mn^{2+} at X-band frequencies (Horton, Clardy et al. 1998). Monitoring the EPR spectrum of U7 under these conditions reveals the presence of increasing amounts of free Mn^{2+} signal in the EPR spectrum as the temperature is increased (Figure 6.13), indicating dissociation of the metal ion from the ribozyme.

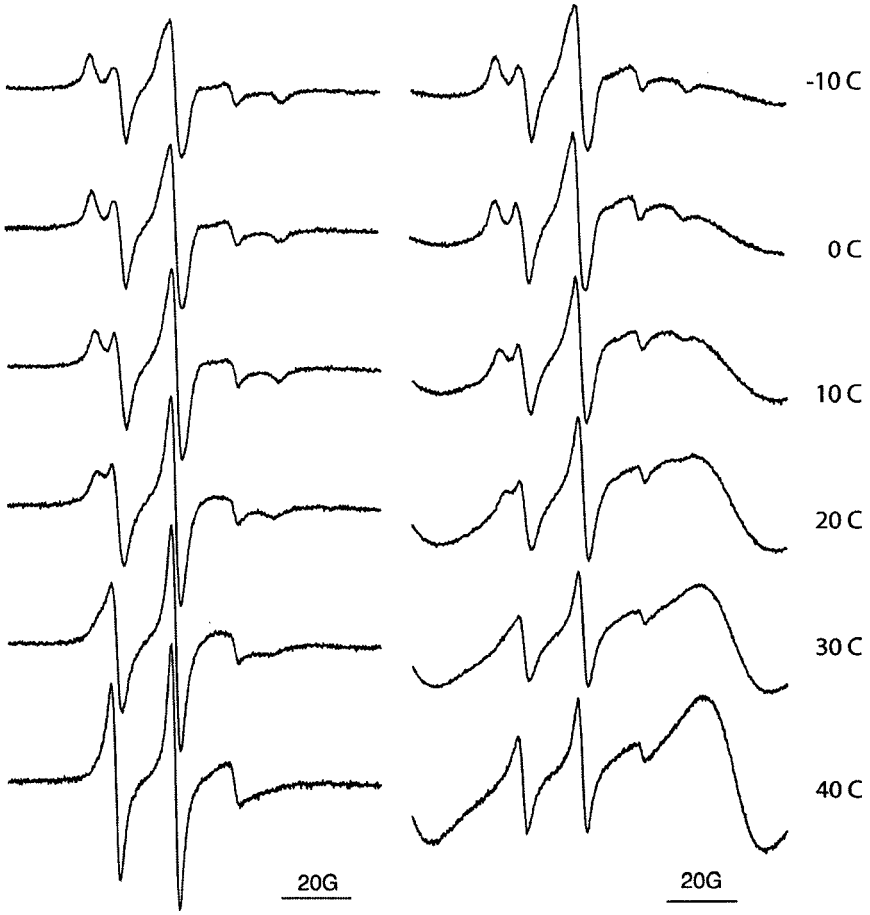

Figure 6.13. EPR spectra of U7 spin-labeled hammerhead ribozyme-non-cleavable substrate complex in the presence of 1.0 M NaCl and either 50 μM $MgCl_2$ (left column) or 50 μM $MnCl_2$ (right column) (50 μM RNA, 10 mM TrisHCl, pH 7.5).

Inhibition of the hammerhead ribozyme

Tb^{3+} (Feig, Scott et al. 1998; Feig, Panek et al. 1999; Feig and Uhlenbeck 1999) and neomycin (Clouet-d'Orval, Stage et al. 1995; Stage, Hertel et al. 1995; Kirk, Luedtke et al. 2001) are known to bind to the hammerhead ribozyme and inhibit phosphodiester cleavage. Tb^{3+} binds with strong affinity to N3 on the base-pairing face of G8 through outer sphere coordination with a $K_d \sim 5$ μM and to other sites on the hammerhead ribozyme with considerably lower affinity (Feig, Panek et al. 1999). We studied the dynamics of U7 in the presence of 50 and 100 μM Tb^{3+}, but observed only subtle changes in RNA internal dynamics. This result is in agreement with the crystal structure obtained

in the presence of Tb^{3+}, which displayed virtually no change in RNA global or local conformation upon Tb^{3+} binding (Feig, Scott et al. 1998). Neomycin inhibits hammerhead ribozyme cleavage with a K_I of 13.5 μM (Stage, Hertel et al. 1995), and therefore, should be specifically bound at 50 μM neomycin (50 μM RNA; 1 equivalent). Essentially no changes in U7 dynamics were observed in the presence of 50 μM neomycin. At higher neomycin concentrations (550 μM) a decrease in U7 dynamics was observed (Figure 6.14). As evident by the broadening of spectral features, numerous bound states likely exist in solution, implying that non-specific neomycin-ribozyme interactions are being observed.

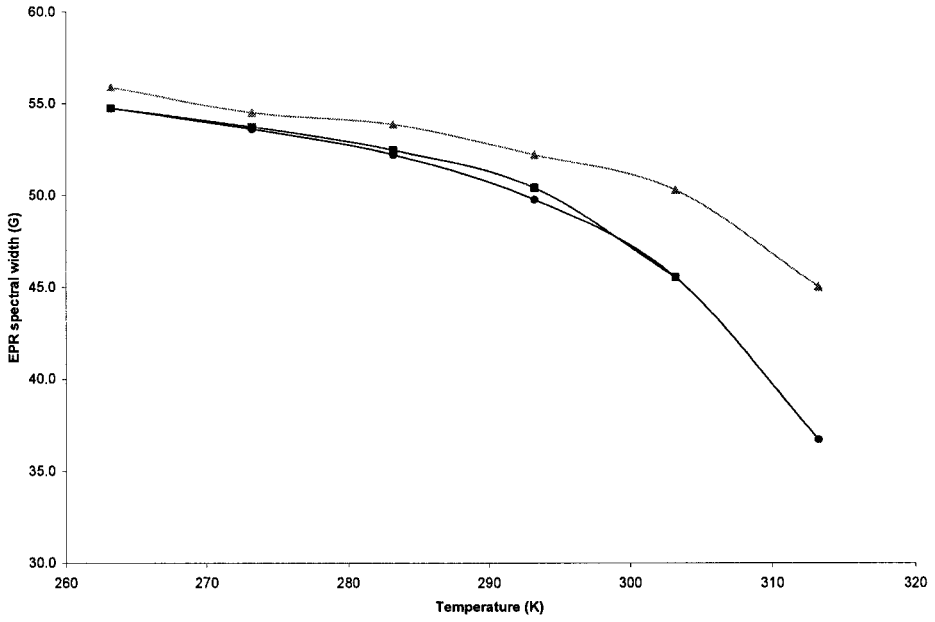

Figure 6.14. Monitoring the change in EPR spectral width ($2A_{zz}$) over a range of temperatures for U7 of the hammerhead ribozyme in the presence of 10 mM $MgCl_2$ and absence (circles) or presence of 50 μM neomycin (squares) or 550 μM neomycin (triangles)

Conclusion and suggestions for further studies

The preliminary results presented here demonstrate the utility of EPR spectroscopy for monitoring RNA internal dynamics during molecular structure

assembly. A nitroxide spin-label incorporated into U7 of the catalytic core was sensitive to the local and global RNA folding and was used to demonstrate evidence for a two-state divalent metal ion-dependent folding pathway of the hammerhead ribozyme. Furthermore, EPR data provided evidence that the microenvironment of U7 of the catalytic core is different in the presence of 10 mM Mg^{2+} than in the presence of monovalent metal ions. The changes in EPR spectral width, which are correlated with changes in RNA internal dynamics, were surprisingly small (e.g. at 0 °C, -0.2 G in the presence of 0.25 mM Mg^{2+}, 1.7 G in the presence of 10 mM Mg^{2+}; 2.8 G in the presence of 4 M Li^{+}) in comparison with TAR RNA-metal ion data (changes up to 10 G). However, the magnitude of change at individual positions may not entirely reflect the overall magnitude of change in the ribozyme. In conclusion the results presented here provide a sound foundation for future studies on hammerhead ribozyme dynamics using EPR spectroscopy.

Other experiments still need to be performed on this system to gain a more complete understanding of the role of dynamics in RNA folding and catalysis. First, the effect of the spin-label on the catalytic rate of the hammerhead ribozyme must be determined. Interference of the spin-label modification with catalysis may also result in interference with RNA folding. Second, the dynamics of the cleaved state in comparison with the non-cleaved state (presented here) should be investigated. Third, the dynamics of U7 during the proposed pH-dependent conformational change should be investigated by EPR. Fourth, the dynamics of U7 should be investigated in the A9 cleaved product. Lastly, investigation of RNA internal dynamics at other spin-labeled sites in the hammerhead ribozyme should give a more complete picture of the two-state folding pathway. U1.2, C1.3, and U1.5 of stem I are possible candidates. C3 is also particularly interesting because the 2'-amino group is only 11.4 Å away from the scissile phosphate, and 2'-modifications only decrease the cleavage ability of the ribozyme by 2-10-fold (Blount, Grover et al. 2002).

Chapter 7

Conclusions

The interaction of specific RNA molecules with metal ions, peptides, and small molecules has been of great interest to the scientific community for many years. Due to the difficulty of investigating RNA structure and dynamics in these interactions, techniques sensitive to the study of RNA structure and dynamics are necessary. Electron paramagnetic resonance (EPR) spectroscopy has been a valuable tool for the elucidation of protein structure and dynamics for over twenty years, and this thesis described the use of EPR to investigate molecular structure assembly of RNA macromolecules in complexes with metal ions, peptides, and small molecules. The first goal of the project was to develop a method for site-specific incorporation of nitroxide spin-labels into internal sites of a model RNA. After demonstration of structure-dependent dynamics of RNA by EPR spectroscopy, spin-labeled RNAs were used to study TAR RNA-metal ion, TAR RNA-Tat peptide, and TAR RNA-small molecule interactions as well as the metal ion-dependent folding pathway of the hammerhead ribozyme. These studies should provide a sound basis for the future study of RNA by EPR spectroscopy and have provided valuable insights into the important dynamic properties of RNA.

Chapter 8

Materials and Methods

General. All water and air sensitive reactions were carried out under a positive-pressure argon atmosphere. Trichloromethyl chloroformate (diphosgene) and 4-amino-2,2,6,6-tetramethylpiperidyl-*N*-oxyl (4-amino TEMPO) were obtained from Acros, Aldrich, and Avocado research throughout the project; these compounds were determined to be of sufficient purity by NMR spectroscopy and were not further purified. 2'-amino-2'-deoxyuridine, **4**, was prepared as previously described (Verheyden, Wagner et al. 1971; Kirschenheuter, Zhai et al. 1994) (see Appendix 1). LiCl, KCl, $SrCl_2$ and $BaCl_2$ were obtained from Aldrich, $NiCl_2 \cdot 6H_2O$ and $CdCl_2 \cdot 2\ 1/2\ H_2O$ from Alfa, $MgCl_2$ and $ZnCl_2$ from Baker, NaCl, $CaCl_2$ and $MnCl_2 \cdot 4H_2O$ from Fisher and $CoCl_2 \cdot 6H_2O$ from Mallinckrodt. Argininamide, Hoechst 33258 [2'-(4-hydroxyphenyl)-5-(4-methyl-1-piperazinyl)-2,5'-bis(1*H*-benzimidazole)], berenil [1,3-bis(4-phenylamidinium)triazene], and DAPI (4',6-diamidino-2-phenylindole) were purchased from Sigma. Neomycin sulfate was obtained from ICN Biomedicals (Aurora, OH). Guanidinoneomycin and CGP 40336A were generously donated by Profs. M. Goodman and Y. Tor (University of California, San Diego) and Novartis Pharma (Basel, Switzerland), respectively. Phosphodiesterase I (*Crotalus adamanteus* Venom) was obtained from USB and calf intestinal alkaline phosphatase from Promega. Methylene chloride was freshly distilled over CaH_2. Anhydrous DMF was obtained from Aldrich and used without further drying. TLC was performed on Merck silica gel 60 F_{254} 250 μm glass plates; column chromatography was performed using Merck 60 40-63 μm, 230-400 mesh silica gel.

Analytical RP-HPLC samples were run on a Varian ProStar HPLC system using a Varian Microsorb-MV^{TM} 300 Å 4x250 mm analytical C18 column and monitoring at 260 nm. Solvent gradients for analytical RP-HPLC (both enzymatic digestion analysis and NCO reaction monitoring) were run at 1.5 mL/min as follows. Solvent A, 50 mM Et_3NHOAc (pH 7.0); solvent B, 70% CH_3CN/30% 50 mM Et_3NHOAc; 15-min linear

gradient from 0% B to 23% B, 5-min linear gradient to 100% B, isocratic for 10 min, then a 3-min linear gradient to initial conditions. Analytical IE-HPLC samples were run at 90 °C on a Dionex DNAPac PA-100 4x250 mm analytical column heated by a Timberline Instruments column warmer. Solvent gradients for analytical IE-HPLC were run at 1.0 mL/min as follows. Solvent A, 25 mM Tris·HCl; Solvent B, 1.0 M NaCl, 25 mM Tris·HCl, pH 8.0; 35-min linear gradient from 10% B to 80% B, 5-min linear gradient to 10% B. For RP-HPLC peptide purification, samples were purified on a Beckman 421 HPLC monitoring at 275 nm using a Dynamax Raining 300 Å 25x250 mm preparatory C18 column. Solvent gradients were run at 10 mL/min as follows. Solvent A, 0.1% TFA in H_2O; solvent B, CH_3CN; 40-min linear gradient from 0% B to 50% B, 5-min linear gradient to 0% B.

^{1}H-NMR spectra were recorded on either a Bruker DRX or AMX 500 MHz spectrometer. Chemical shifts are reported in ppm relative to tetramethylsilane at δ 0.0 ppm. Coupling constants (J) were measured in Hertz. UV-monitored thermal denaturing experiments were performed on a Beckman DU 650 spectrophotometer. Infrared (IR) spectra were obtained on a Perkin-Elmer 1600 Series FTIR spectrophotometer. Mass spectra were obtained on a Bruker Esquire ion trap mass spectrometer using 50% MeOH/H_2O as the mobile phase for small molecules and 10 mM piperidine, 10 mM imidazole in 10% MeOH/H_2O for oligoribonucleotides. X-band (9.34 GHz) CW-EPR spectra were digitally recorded at on a Bruker EMX spectrometer with a TE_{102} cavity. Unless otherwise noted, all samples were obtained at 0 °C. Experimental parameters include 3355 G center field, 100 kHz modulation frequency, 1.0 G modulation amplitude, 10 mW power for the structure-dependent RNA dynamics study and 8 mW power for all other studies, 20.48 ms time constant, 40.96 ms conversion, 1024 points, sweep time 42 seconds, 110 G sweep width, typically 100-200 scans, and temperature regulated to ± 0.2 °C. Line samples of RNA for TAR RNA studies were obtained in a 0.8 x 1.0 mm quartz capillary (VitroCom, Inc.). Line samples of RNA for hammerhead ribozyme studies were obtained in 75 mL VWR Scientific glass micropipets. Although these glass tubes absorb some microwaves in the EPR spectrometer cavity and result in decreased signal to noise

(S/N) and increased difficulty in tuning, use of these tubes allowed for larger sample volumnes and consequently, lower RNA concentrations. Samples were stored at 4 °C between EPR experiments. EPR spectra in the presence of Mn^{2+} were acquired as above and the nitroxide component was solved by spectral subtraction of the excess, unbound Mn^{2+} spectrum from the spectrum of nitroxide spin-labeled RNA in the presence of Mn^{2+}. Changes in EPR spectral width, which spans the crest of the low field peak to the trough of the high field peak, were measured in Gauss. The error in measuring the spectral width is ± 0.3 G. EPR spectra were subsequently analyzed using WIN-EPR and Matlab.

Preparation of oligonucleotides. Oligoribonucleotides were either purchased from Dharmacon Research, Inc. or synthesized on an Applied Biosystems 394 DNA/RNA synthesizer using 2'-O-TOM protected- and 2'-amino-phosphoramidites obtained from Glen Research. 2'-Amino-phosphoramidites were incorporated into the growing chain via two sequential hand-couplings (7.5 equivalents of phosphoramidite for each coupling). Oligoribonucleotides were deprotected as directed by the manufacturer (60 °C for 30 min on hot block) and purified by 20% DPAGE. DNA oligonucleotides were synthesized on an Applied Biosystems 394 DNA/RNA synthesizer using standard phosphoramidite chemistry and subsequently purified trityl-on as previously described (Harwood, Sigurdsson et al. 1999).

Determination of RNA molar extinction coefficients. Extinction coefficients at 260 nm were determined after digestion of oligoribonucleotides (ca. 0.15 ODs in 1.0 mL of 50 mM Tris, pH 8.9, 1 mM $MgCl_2$, 0.1 mM $ZnCl_2$, 1 mM spermidine) with snake venom phosphodiesterase (0.5 units) and calf intestinal alkaline phosphatase (8 units) at 37 °C, for 3 h. Molar absorptivities for the ribonucleosides were obtained from the Handbook of Biochemistry and Molecular Biology Volume 1, 3rd Edition. The contribution from the 2'-spin-label modification was determined to be negligible. 5'-GCUCUCUGGCCC ε = 81,200 ± 1300 L/mol•cm; 5'-GGGCCAGAGAGC ε = 108,700 ± 900 L/mol•cm; 5'-GGCCAGAUCUGAGCG ε = 125,300 ± 8200 L/mol•cm. The molar extinction

coefficients used for the hammerhead ribozyme strand and non-cleavable substrate strand were those previously reported in the literature (Markley, Godde et al. 2001).

UV-Monitored thermal denaturation. For the thermal stability study (Chapter 2), unmodified and spin-labeled TAR RNA samples were prepared by dissolving RNA (ca. 0.8 OD_{260}) in buffer (350 μL, 5 mM sodium phosphate, 50 mM NaCl, 0.05 mM Na_2EDTA, pH 7.0). For determination of background metal ion concentrations for the TAR RNA-metal ion study (Chapter 3), three buffers were used: a) 50 mM NaCl, 5 mM sodium phosphate, 50 μM Na_2EDTA, pH 7.0 (58 mM sodium total) b) 10 mM potassium phosphate, pH 6.5 (15 mM potassium total) and c) 1.0 mM potassium phosphate, pH 6.5 (1.5 mM potassium total). For both studies, the TAR RNA samples were annealed using a fast cooling process: 90 °C for 2 min, 37 °C for 2 min, room temperature for 15 min. A_{260} was monitored ramping from 20 °C to 90 °C at 0.5 °C/min. Melting temperatures (T_m) and thermodynamic values were determined as described using a two state model (Breslauer 1994).

Enzymatic digestion of oligoribonucleotides. A solution of oligoribonucleotides (6.0 nmol) in Tris buffer (5 mM, 60 μL, pH 7.4) was treated with 0.5 units of snake venom phosphodiesterase and 8 units of calf intestinal alkaline phosphatase and incubated at 37 °C over 5 h. Samples were analyzed by analytical RP-HPLC as described above.

Spin-labeling of 2'-NH_2-containing oligoribonucleotides. Spin-labeling reactions were carried out at -8 °C in a NaCl ice water bath (-8 °C) in a cold room (~5 °C). For analytical reactions, a solution of 2'-amino-containing oligoribonucleotides (2 mM in 2.5 μL 70 mM boric acid, pH 8.6) was treated sequentially with pre-cooled solutions of formamide (1.5 μL) and **1** in DMF (1.0 μL, 75 mM). After 1 h, an aliquot (1.5 μL) was withdrawn, diluted with water (18.5 μL), washed with chloroform (2 x 75 μL) to remove most of the excess isocyanate and its hydrolysis products, and analyzed by RP-HPLC. The oligoribonucleotide solution was treated with a second aliquot of a fresh solution of **1**

(1.0 μL, 75 mM in DMF) and analyzed by RP-HPLC. For preparatory scale reactions, a solution of crude, deprotected 2'-amino-containing oligonucleotides (1/4 of a 1 μmol synthesis in 100 μL 70 mM boric acid buffer, pH 8.6) was treated sequentially with pre-cooled solutions of formamide (60 μL) and **1** in DMF (75 mM, 40 μL). After 1 h a second, freshly prepared, aliquot of **1** (60 μL, 75 mM in DMF) was added. After an additional hour, the solution was washed with $CHCl_3$ (2 x 75 μL), then diluted with sodium acetate (3.0 M, 50 μL, pH 5.3) and ethanol (-20 °C, 1.3 mL). The RNA was precipitated at –20 °C over 4 h, the sample was centrifuged (11,500 rpm, 15 min, 5 °C), and the supernatant was removed. The pellet was washed with cold ethanol (2 x 50 μL), dried, dissolved into aqueous urea (8 M, 150 μL), and purified by 20% denaturing PAGE. Samples were quantified with the experimentally determined molar extinction described above. Yields ranged from 100-170 nmols for ¼ of a 1.0 μmol synthesis, depending on the quality of the RNA synthesis. Electrospray ionization mass spectrometry verified the incorporation of the spin-label, for example 5'-GCUC(2'-NH_2U)CUGGCCC (3723.20 obs., 3723.29 calc.) had the mass of 3920.50 (calc. 3920.55) after reaction with **1**.

Peptide purification. The wild-type Tat-derived peptide (YGRKKRRQRRR) purchased (>95% purity) from United Biochemical Research, Inc. (Seattle, WA) contained a free radical contaminant and were purified by G10 Sephadex filtration. A Sephadex G10 column (2.0 g Sephadex) was washed with water (5 mL), and the peptide (306 nmol, 0.43 ODs in 1 mL water; ε = 1405, A_{275} single tyrosine) was loaded onto the column and eluted with water. The second 1.0 mL fraction contained most of the peptide (242 nmol, 0.34 ODs) and was shown to be free of the free-spin contaminant by EPR spectroscopy. The Tat(m1) peptide was a gift from Gary Drobny. The other Tat-derived peptides were purchased from United Biochemical Research, Inc. (Seattle, WA) in a crude form (>70%) and were shown to contain the appropriate peptide by MALDI-TOF MS. These peptides purified by RP-HPLC, dried *in vacuo*, and dissolved into 2 mL of H_2O. Samples were soft frozen and lyophilized to dryness.

Native gel shift assays. RNA samples were 5'-^{32}P radiolabeled as described (Gibco BRL) and purified by NAP 25 size exclusion chromatography (Pharmacia). TAR RNA samples (2.0 μM RNA in 50 mM sodium cacodylate, pH 6.0) were annealed on a thermocycler using the following step-wise cooling protocol: 90 °C for 2 min, 60 °C for 5 min, 50 °C for 5 min, 40 °C for 5 min, and 22 °C for 15 min. The samples were treated with an aqueous solution of the peptide, followed by water up to a final volume of 20 μL (final concentrations: peptide 0.1-20.0 μM, RNA 200 nM, buffer 5.0 mM). Samples were incubated in an ice water bath in a cold room (5 °C) for 5 min, diluted with 40% aqueous sucrose (5 μL), and loaded onto a 10% native polyacrylamide gel. The gel was run at 25 mA for 1 h, dried, and visualized by phosphorimaging.

Equilibrium dissociation constants were determined from between three and eight independent native gels, each of which contained 4-6 protein concentration data points for each RNA. The percentage of bound TAR-Tat complex was determined by densitometry analysis. The percent of bound complex was plotted as a function of Tat concentration using Mac Curve Fit 1.3.3 and the point at which 50% bound complex was estimated to be the K_d. The method of Black et al. (Black, Chan et al. 1998), which plots [RP]/[R] versus protein concentration, yielded essentially the same result.

EPR sample preparation. For the structure-dependent RNA dynamics study (Chapter 2), EPR samples were prepared in 50% sucrose/buffer (10 mM sodium phosphate, 100 mM NaCl, 0.1 mM Na_2EDTA, pH 7.0) w/v. The RNAs were dissolved directly into the sucrose solution (final conc. 200 μM), and the solution was heated for 1 min at 90 °C, incubated at 37 °C for 2 min and cooled to room temperature over 15 min. For the metal ion studies, EPR samples (2.0 nmols spin-labeled RNA in10 μL of 20% aqueous sucrose/1.0 mM potassium phosphate buffer pH 6.5, including metal chloride salts of appropriate concentration) were annealed as described for native gel shift assays. For the peptide and small molecule studies TAR RNA and TAR duplex samples (2.0 nmol in 7.0 μL of 20% aqueous sucrose/100 mM NaCl, 10 mM sodium phosphate, 0.1 mM Na_2EDTA, pH 7.0) were added to the peptide or small molecule (3.0 μL in above

aqueous sucrose buffer, additive concentration as appropriate) to produce 200 μM RNA samples. For the hammerhead ribozyme study, the RNA (50 μM RNA in 6-20 μL of 10 mM NaCl, 10 mM Tris·HCl, pH 7.5, including appropriate $MgCl_2$, LiCl, NaCl, $TbCl_3$, $NiCl_2$, $MnCl_2$, or neomycin concentrations; only 0.3-1.0 nmol spin-labeled RNA were needed per sample) was annealed as described above. For the pH study, the pH of the original buffer (10 mM NaCl, 10 mM Tris·HCl, pH 7.5) was adjusted prior to annealing of the sample (pH 7.0, 7.5, 8.0, 8.5).

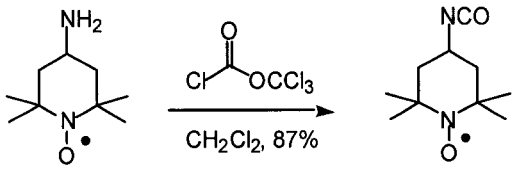

1

4-Isocyanato-tetramethylpiperidyl-N-oxy (4-isocyanato-TEMPO, 1). A solution of 4-amino-TEMPO (198 mg, 1.15 mmol) in CH_2Cl_2 (1.5 mL) was added rapidly (ca. 8 sec) via cannulae to a stirred solution of trichloromethyl chloroformate (25 μL, 0.21 mmol) in CH_2Cl_2 (1.5 mL) at –8 °C. The cooling bath was removed and the reaction was stirred for 2 min. The crude reaction mixture was diluted to 20 mL with CH_2Cl_2 and washed successively with 1 M HCl (6 x 20 mL) and NaOH (20 mL). The organic layer was dried (Na_2SO_4) and the solvent was removed *in vacuo* to yield a peach colored solid (66 mg, 0.33 mmol, 29% based on starting amine or 87% maximum theoretical yield). Isocyanate **1** was stored desiccated at –20 °C in CH_2Cl_2 (1 mg/100 μL). ^{1}H-NMR ($CDCl_3$, 500 MHz) δ 3.74 (br m, 1H), 1.98 (br d, 2H, J = 12.0), 1.81 (br t, 2H, J = 12.5), 1.24 (s, 6H), 1.22 (s, 6H); IR (CH_2Cl_2) 3001, 2255 (NCO), 1679, 1529, 1461, 1380, 1243, 1179, 1095 cm^{-1}; TLC (5% MeOH/CH_2Cl_2) 0.84 (SM 0.2).

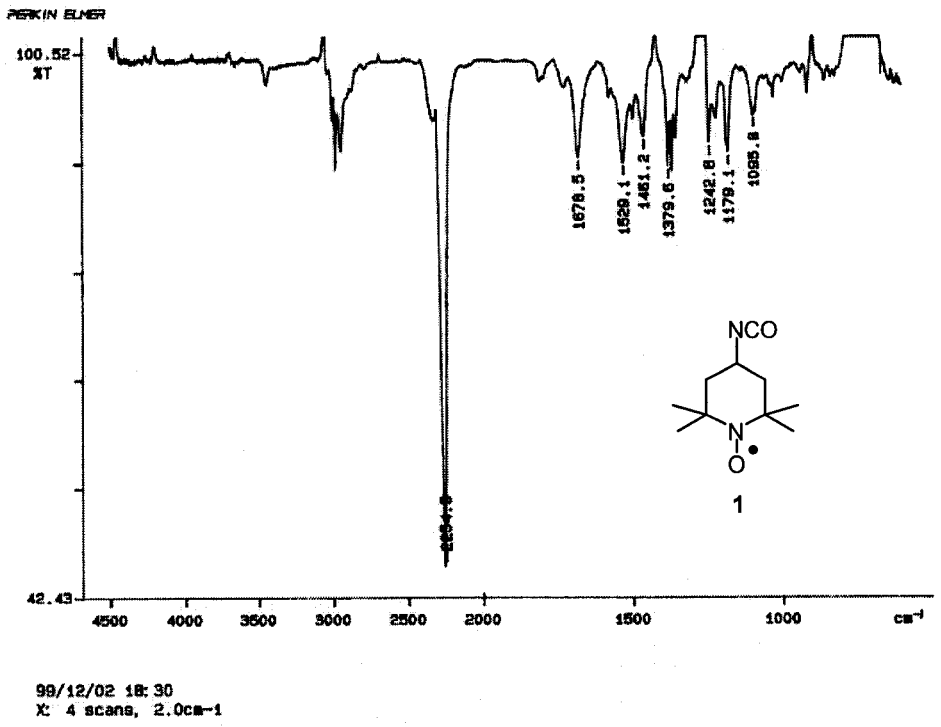

Figure 8.1. IR Spectra of spin-labeled isocyanate **1**.

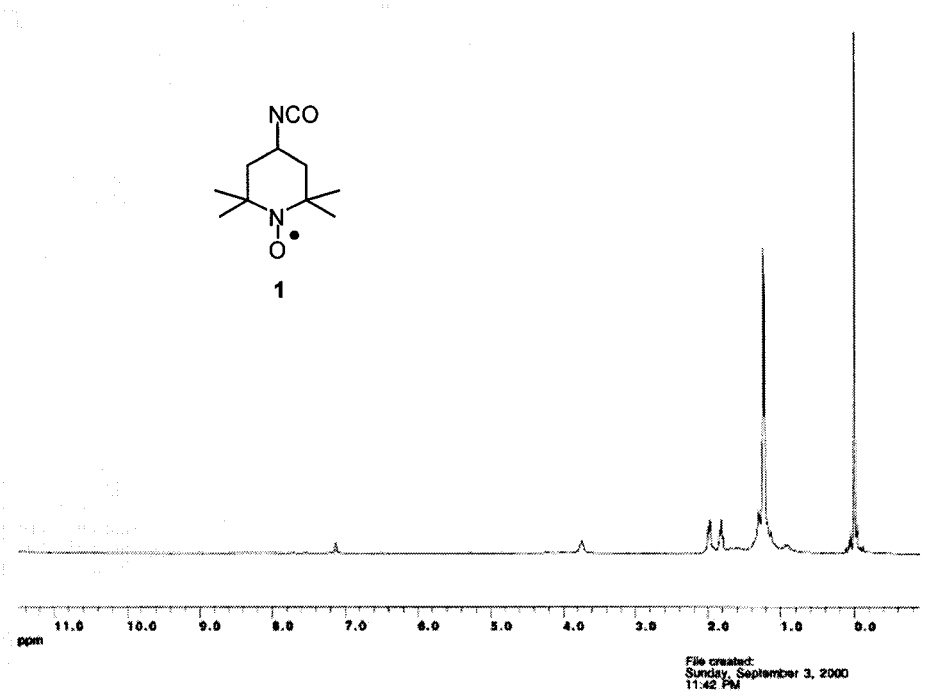

Figure 8.2. ^{1}H-NMR of spin-labeled isocyanate **1**.

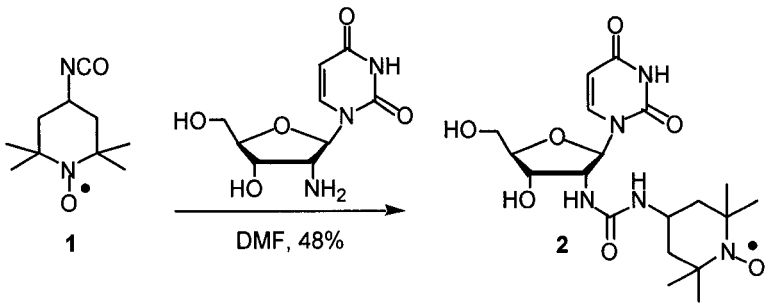

2'-(Uryl-N'-4-tetramethylpiperidyl-N-oxy) uridine (2'-Uryl-(4-TEMPO)-2'-amino-2'-deoxyuridine, 2). A solution of **1** (160 mg, 0.811 mmol) in DMF (4 mL) was treated with a solution of 2'-amino-2'-deoxyuridine (199 mg, 0.811 mmol) in DMF (4 mL) and stirred for 1 h at room temperature. The DMF was removed *in vacuo*, and the crude solid was purified by column chromatography (12% CH_3OH/CH_2Cl_2) to yield a peach-colored oil (173 mg, 0.393 mmol, 48%). ^{1}H-NMR (DMSO-d_6, 500 MHz) δ 11.27 (br s, 1H, NH), 7.89 (br s, 1H, H6), 6.11 (br s, 1H, H1'), 5.84 (br s, 1H, H5), 5.16 (br s, 1H, 5'-OH), 4.33 (br s, 1H, H2'), 4.05 (br s, 1H, H3'), 3.92 (br s, 1H, H4'), 3.58 (br s, 3H, H5', H4"), 1.64 (br t, 2H, H3"eq), 1.10 (br d, 2H, H3"ax), 1.02 (br s, 12 H, CH_3); ESMS *m/z* 441.3, 329.2, 244.0, 199.1; TLC (12% CH_3OH/CH_2Cl_2) Rf 0.23; UV_{max} = 261 nm, 417 nm (0.1%); UV_{min} 231 nm. To confirm the structure and existence of the free radical, 2 was reduced with dithiothreotol in DMSO-d_6 and analyzed by ^{1}H NMR (Figure 8.4). All peaks became sharp after reduction of the free radical, and in particular, the full intensity of the 12 methyl protons was rescued.

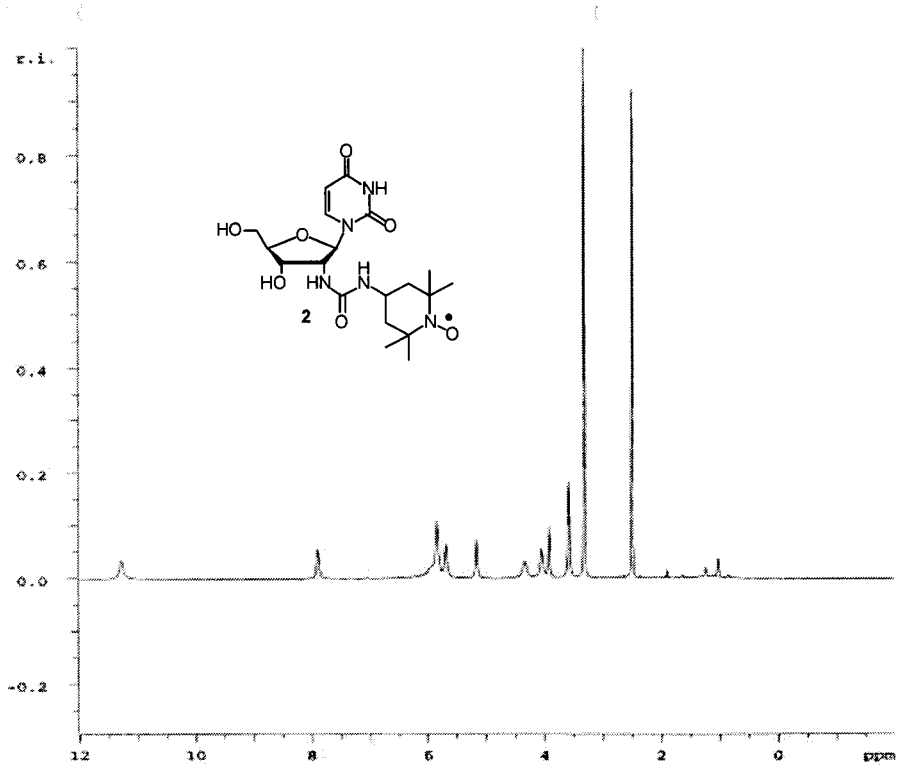

Figure 8.3. ^{1}H-NMR of spin-labeled nucleoside **2**.

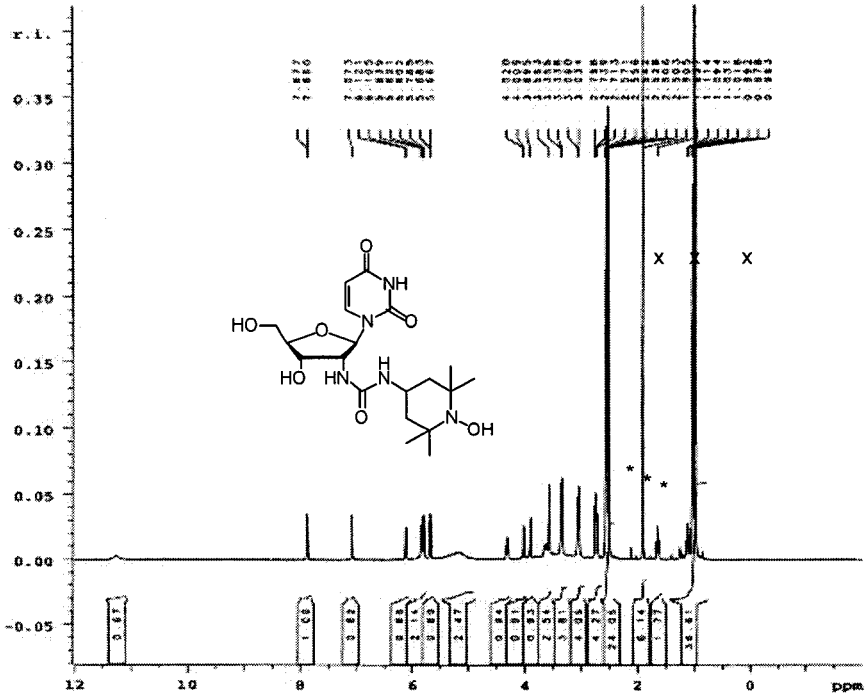

Figure 8.4. ^{1}H-NMR of the crude reaction mixture of the reduction of spin-labeled nucleoside **2**. The peaks marked with an asterisk denote dithiothreitol and the peaks marked with an x denote Et_3NHOAc.

EPR spectra of spin-labeled TAR RNAs in the absence of ligands

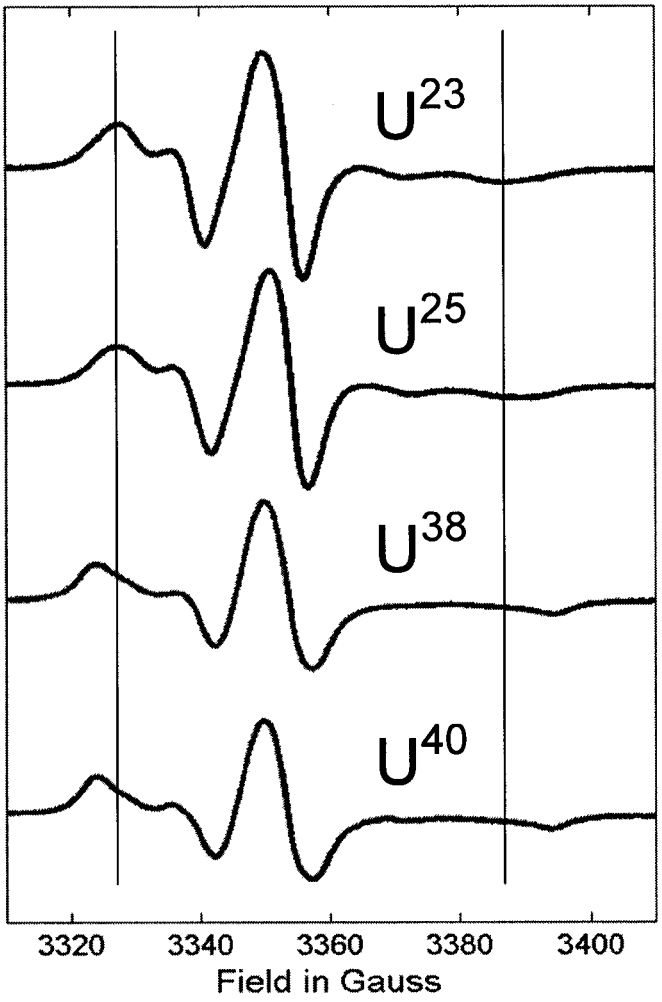

Figure 8.5. EPR spectra of spin-labeled HIV-1 TAR RNAs in the absence of ligands in 50% sucrose/PNE (100 mM NaCl, 10 mM sodium phosphate, 0.1 mM Na_2EDTA, pH 7.0) (Edwards, Okonogi et al. 2001).

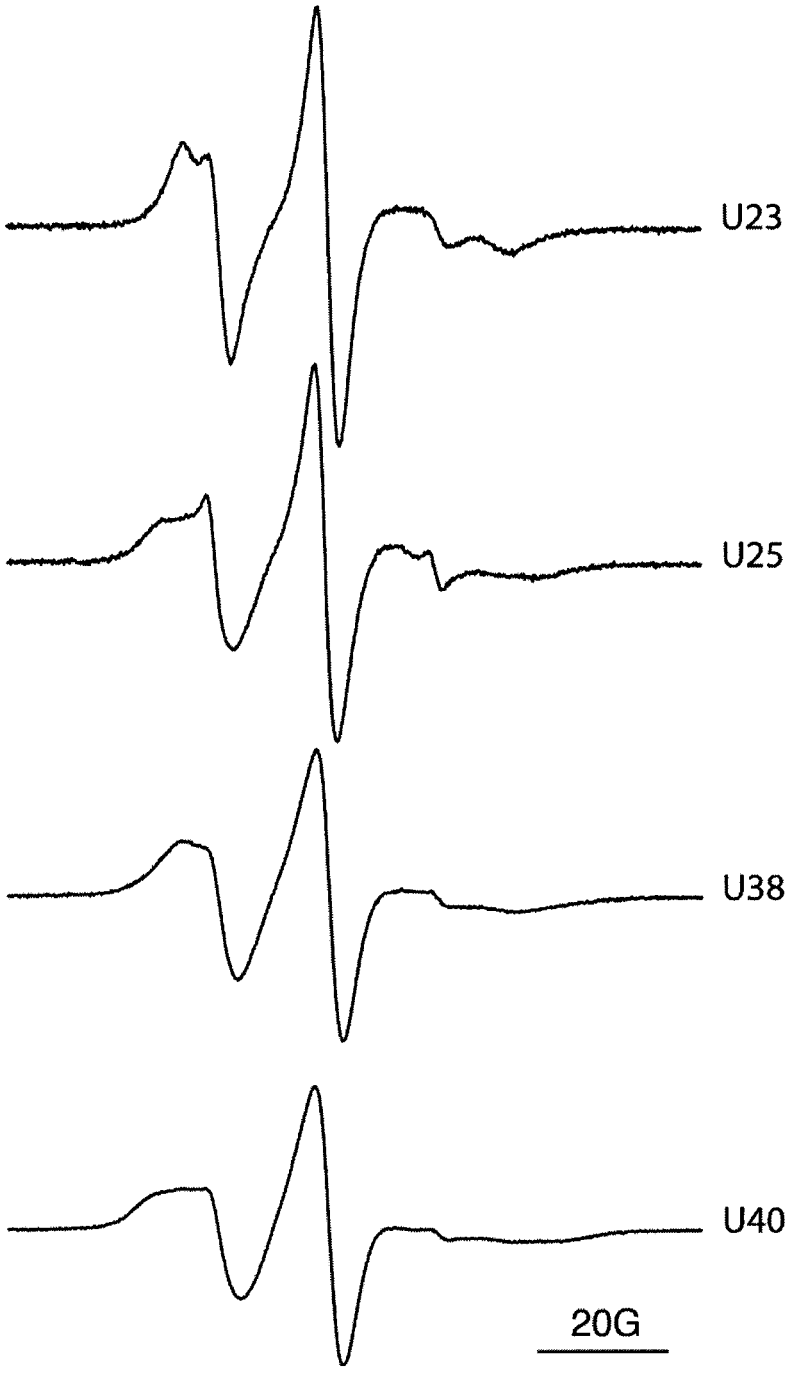

Figure 8.6. EPR spectra of spin-labeled HIV-1 TAR RNAs in the absence of ligands in 20% sucrose/PNE (100 mM NaCl, 10 mM sodium phosphate, 0.1 mM Na_2EDTA, pH 7.0) (Edwards and Sigurdsson 2002).

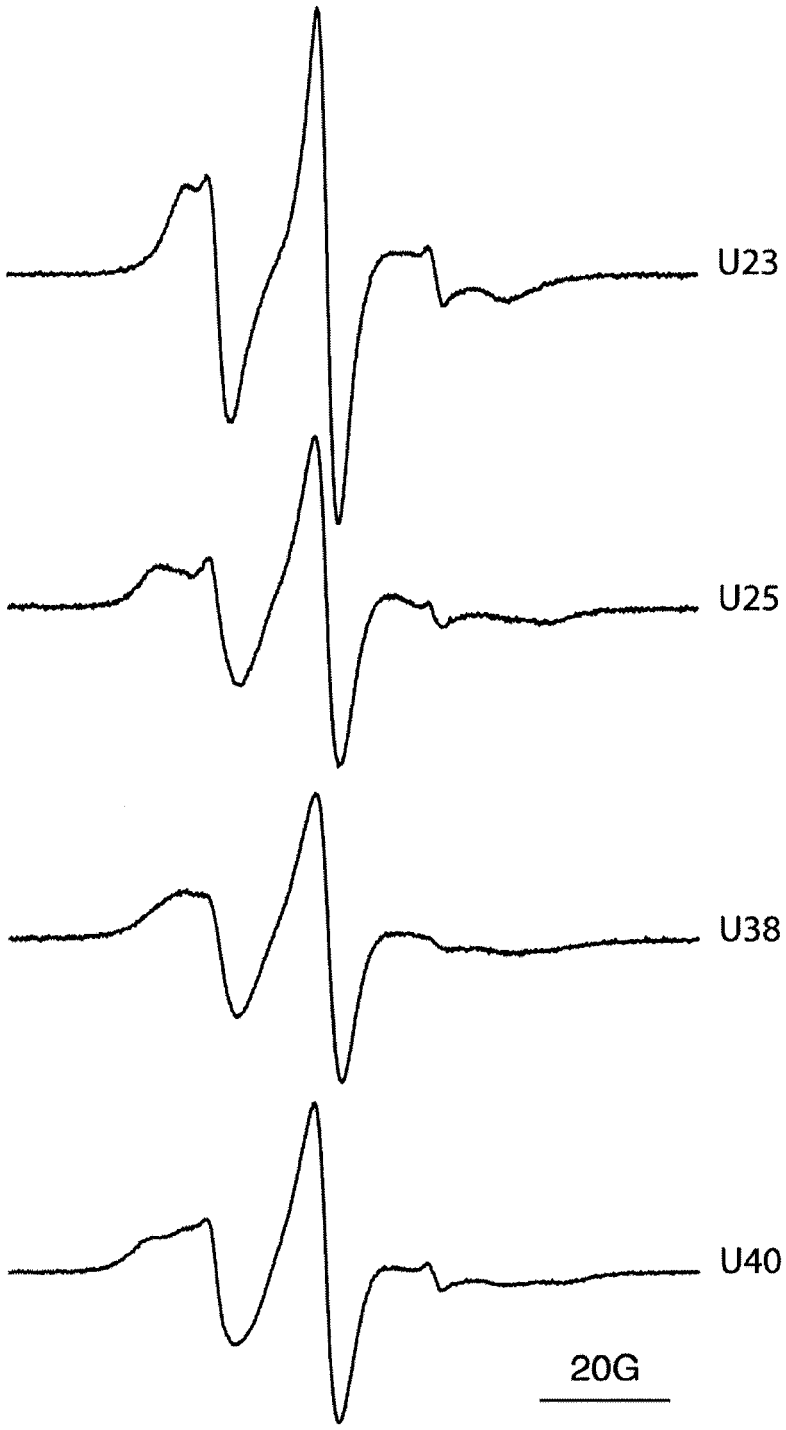

Figure 8.7. EPR spectra of spin-labeled HIV-1 TAR RNAs in the absence of ligands in 20% sucrose/KP (1.0 mM potassium phosphate, pH 6.5) (Edwards and Sigurdsson 2003).

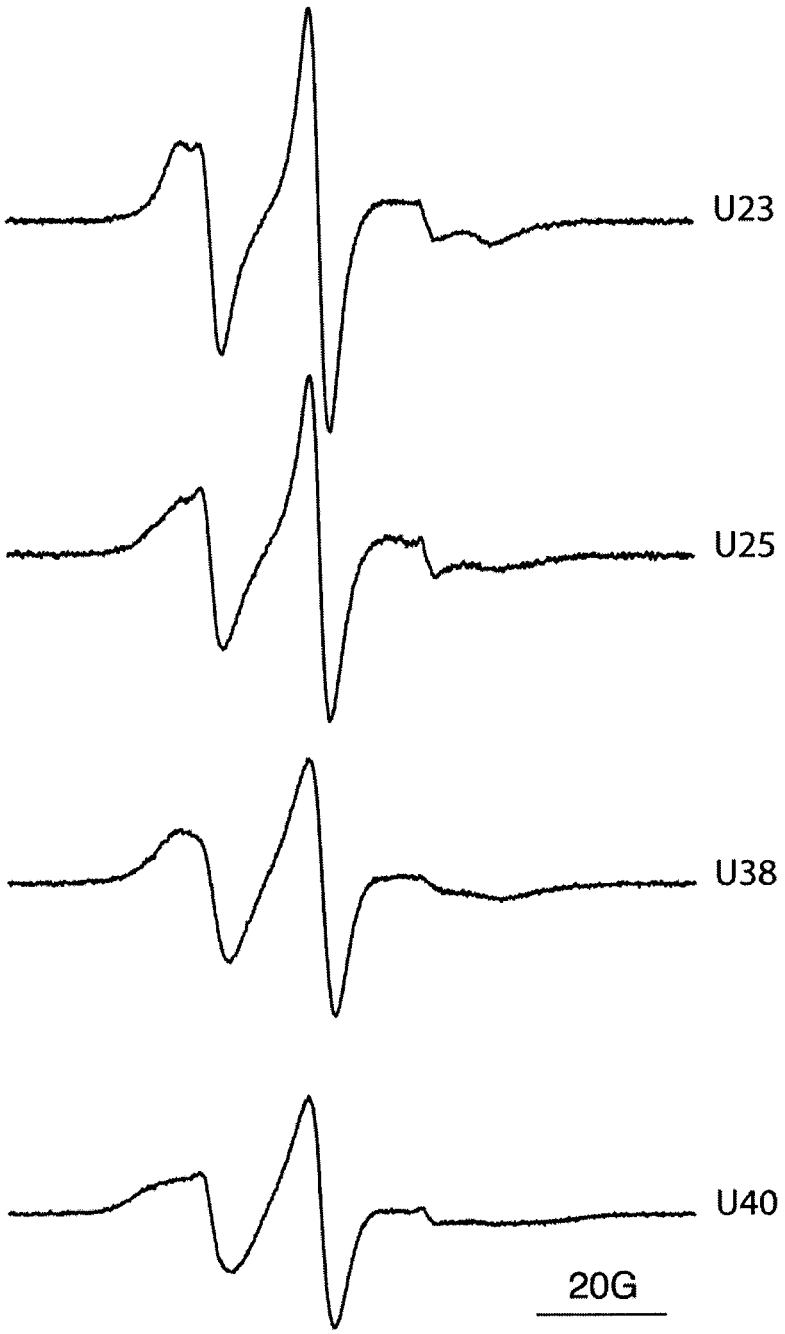

Figure 8.8. EPR spectra of spin-labeled HIV-1 TAR RNAs in the absence of ligands in 33.8% sucrose/500 mM NaCl, 50 mM MOPS, pH 6.6 (conditions used by Qin et al. (Qin, Hideg et al. 2003)).

EPR spectra of spin-labeled TAR RNAs in the presence of metal ions

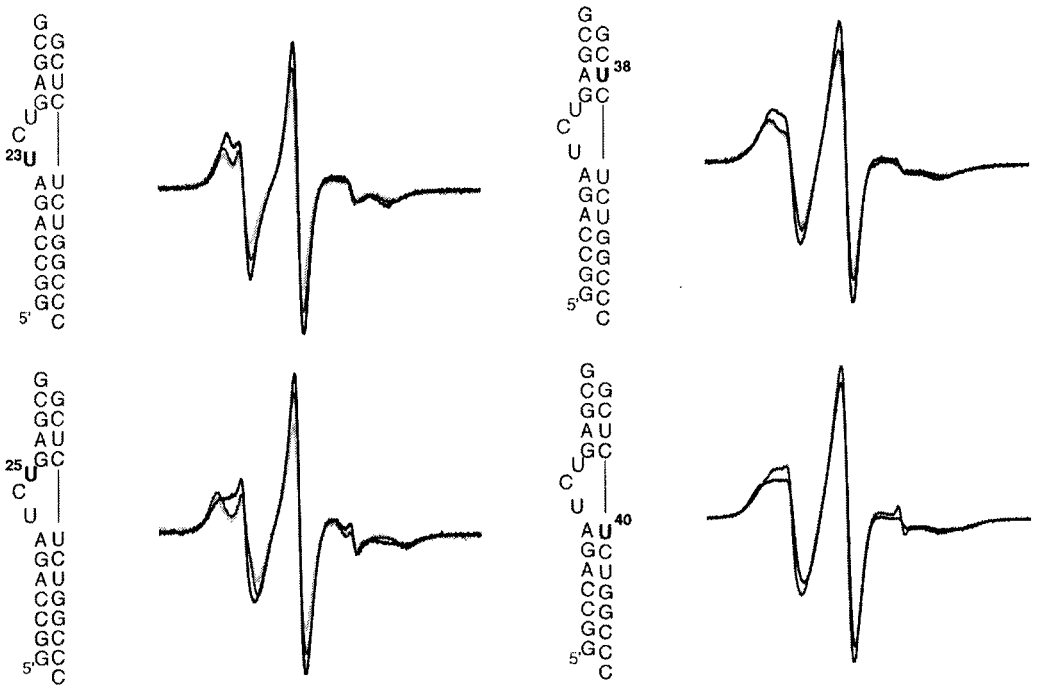

Figure 8.9. EPR spectra of spin-labeled TAR RNAs in the absence (black) and presence of 50 mM $CaCl_2$ (magenta) or 150 mM NaCl (cyan) in 20% sucrose/100 mM NaCl, 10 mM sodium phosphate, 0.1 mM Na_2EDTA, pH 7.0.

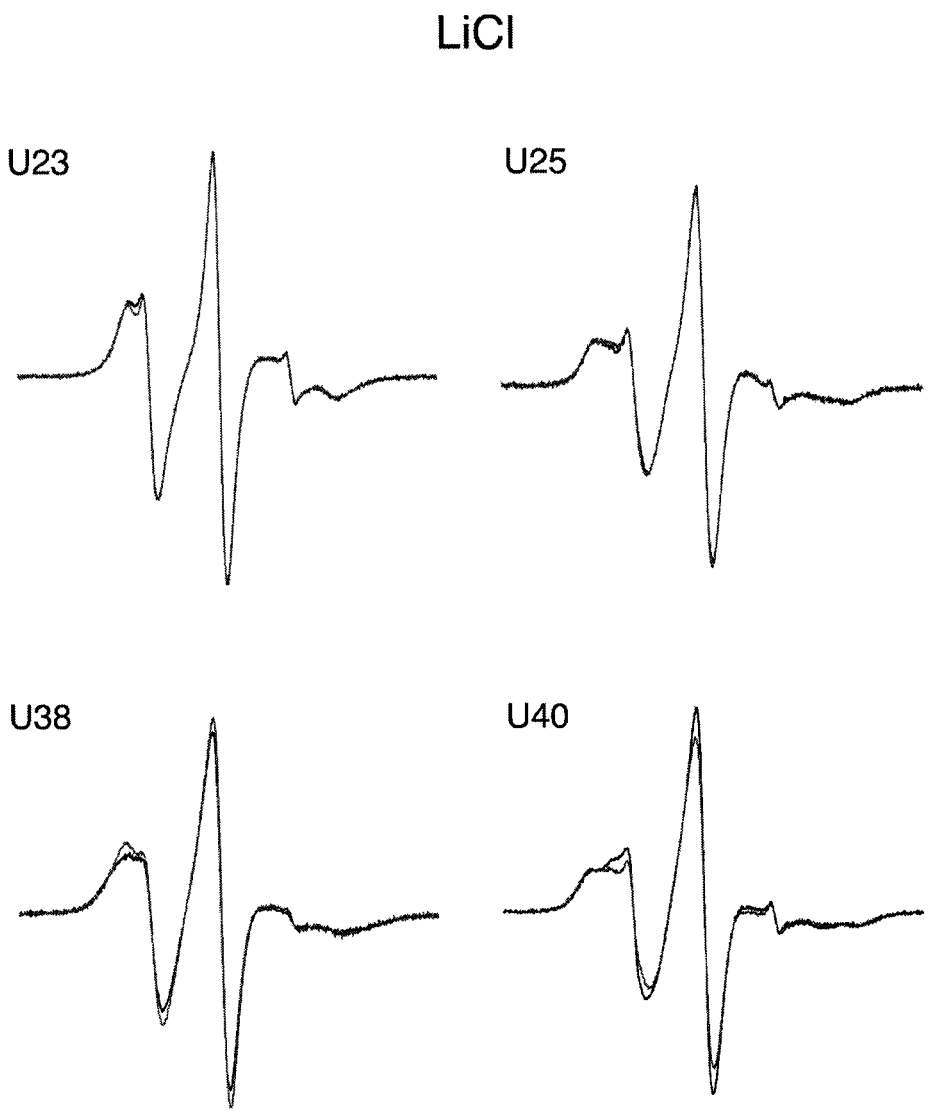

Figure 8.10. EPR spectra of spin-labeled TAR RNAs in the absence (black) and presence (gray) of 30 mM LiCl in 20%sucrose/1.0 mM potassium phosphate, pH 6.5.

Figure 8.11. EPR spectra of spin-labeled TAR RNAs in the absence (black) and presence (gray) of 30 mM KCl in 20%sucrose/1.0 mM potassium phosphate, pH 6.5.

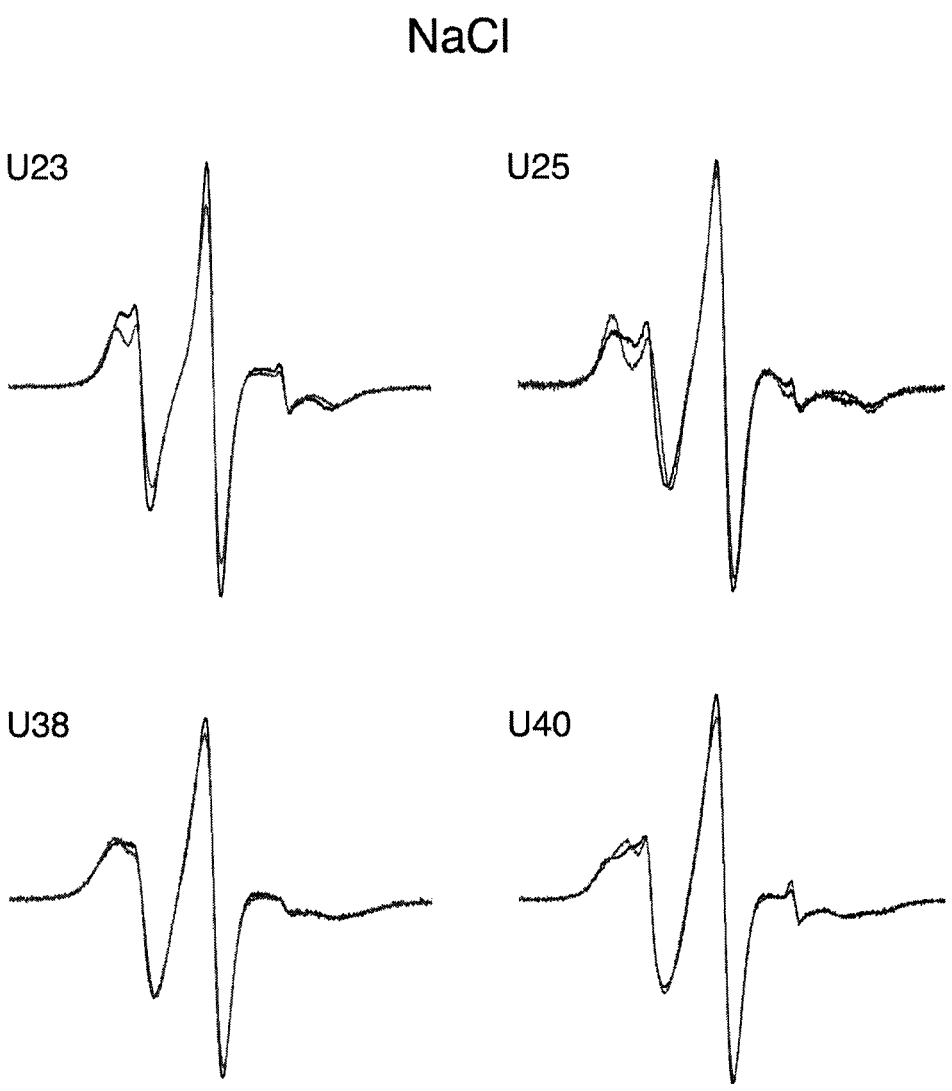

Figure 8.12. EPR spectra of spin-labeled TAR RNAs in the absence (black) and presence (gray) of 30 mM NaCl in 20%sucrose/1.0 mM potassium phosphate, pH 6.5.

Figure 8.13. EPR spectra of spin-labeled TAR RNAs in the absence (black) and presence (gray) of 30 mM $CaCl_2$ in 20%sucrose/1.0 mM potassium phosphate, pH 6.5.

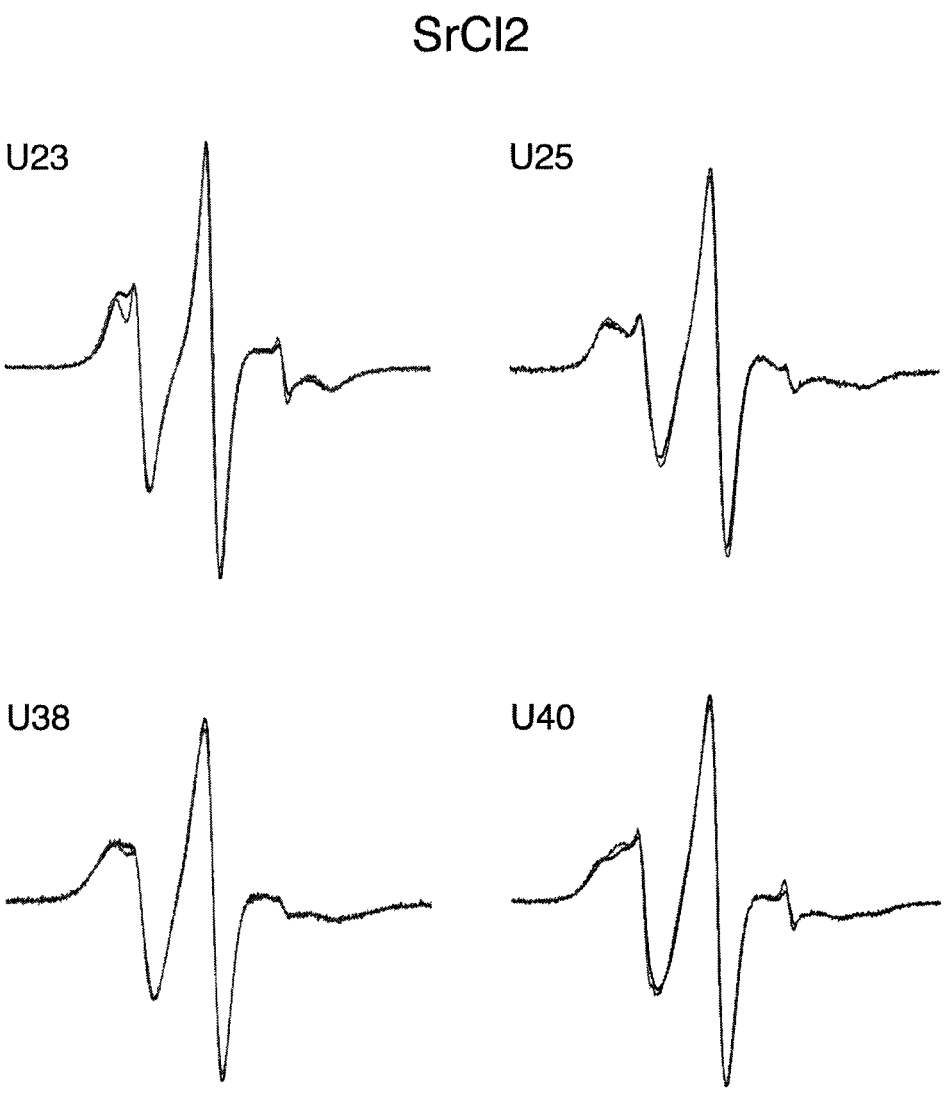

Figure 8.14. EPR spectra of spin-labeled TAR RNAs in the absence (black) and presence (gray) of 30 mM $SrCl_2$ in 20%sucrose/1.0 mM potassium phosphate, pH 6.5.

Figure 8.15. EPR spectra of spin-labeled TAR RNAs in the absence (black) and presence (gray) of 30 mM $MgCl_2$ in 20%sucrose/1.0 mM potassium phosphate, pH 6.5.

Figure 8.16. EPR spectra of spin-labeled TAR RNAs in the absence (black) and presence (gray) of 30 mM $CoCl_2$ in 20%sucrose/1.0 mM potassium phosphate, pH 6.5.

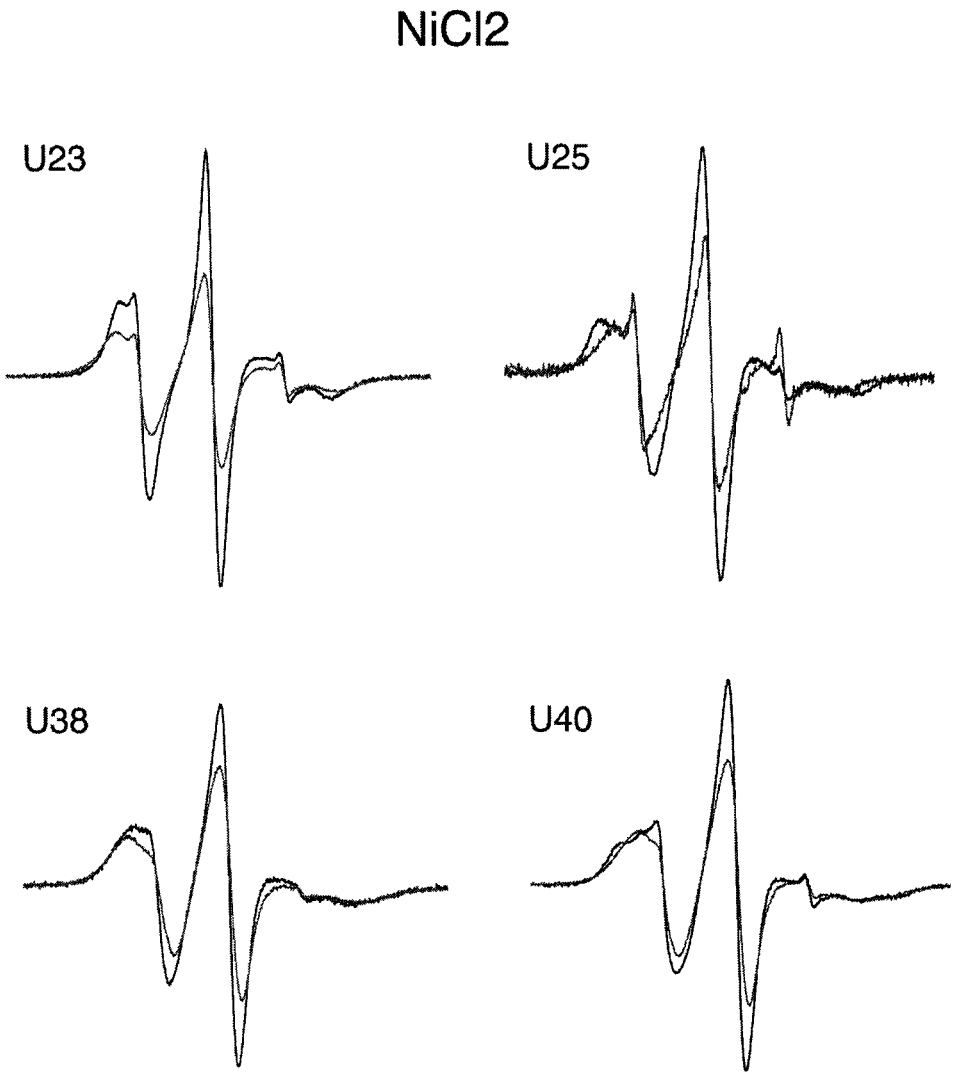

Figure 8.17. EPR spectra of spin-labeled TAR RNAs in the absence (black) and presence (gray) of 30 mM $NiCl_2$ in 20%sucrose/1.0 mM potassium phosphate, pH 6.5.

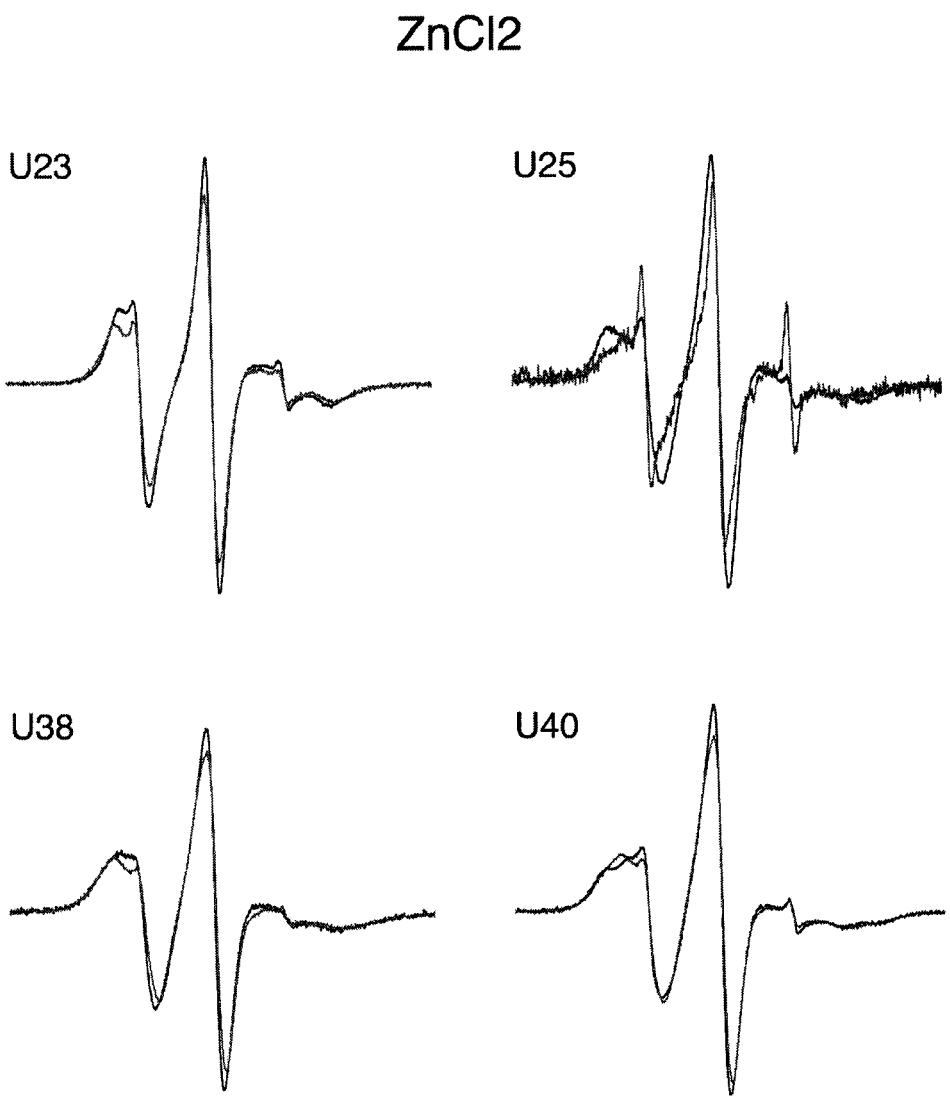

Figure 8.18. EPR spectra of spin-labeled TAR RNAs in the absence (black) and presence (gray) of 30 mM $ZnCl_2$ in 20%sucrose/1.0 mM potassium phosphate, pH 6.5.

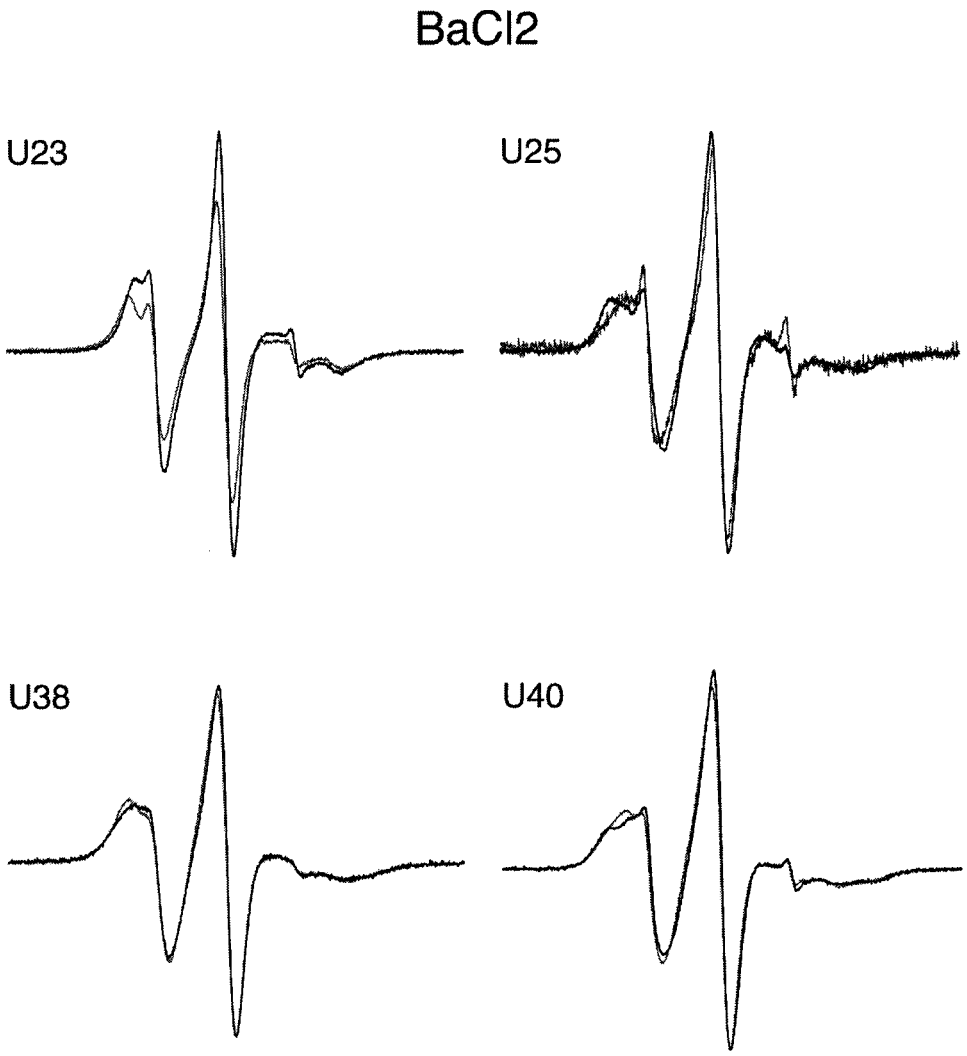

Figure 8.19. EPR spectra of spin-labeled TAR RNAs in the absence (black) and presence (gray) of 30 mM $BaCl_2$ in 20%sucrose/1.0 mM potassium phosphate, pH 6.5.

EPR spectra of spin-labeled TAR RNAs in the presence of Tat derivatives

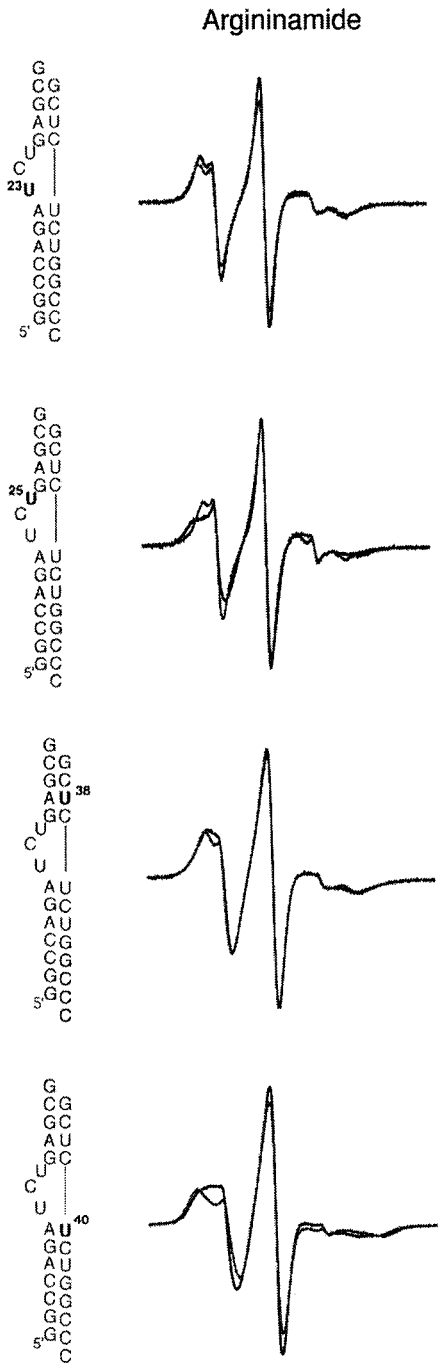

Figure 8.20. EPR spectra of spin-labeled TAR RNAs in the absence (black) and presence (gray) of 5 mM argininamide in 20%sucrose/100 mM NaCl, 10 mM sodium phosphate, 0.1 mM Na_2EDTA, pH 7.0.

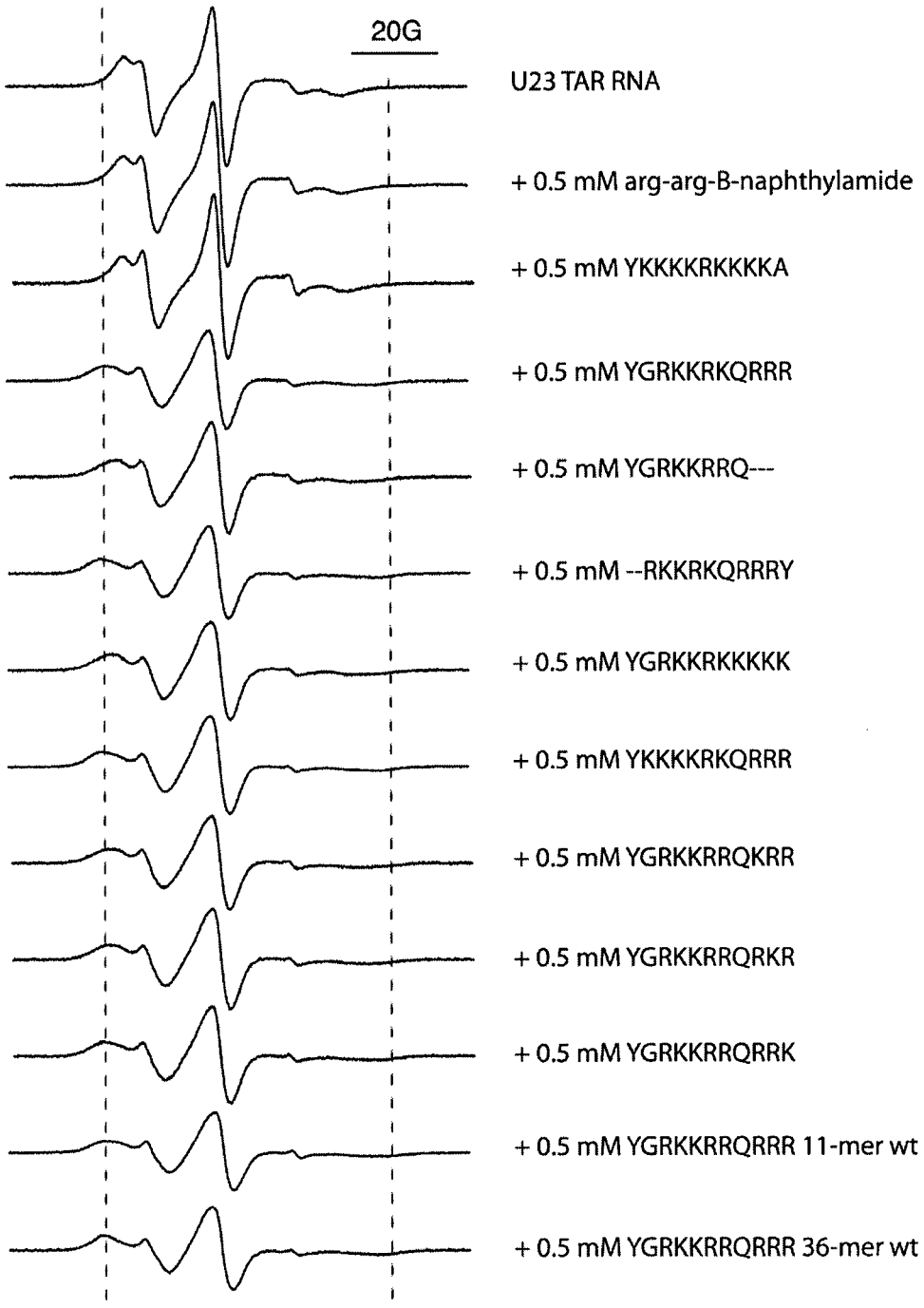

Figure 8.21. EPR spectra of U23 spin-labeled TAR RNA in the presence of derivatives of the Tat protein in 20% sucrose/100 mM NaCl, 10 mM sodium phosphate, 0.1 mM Na_2EDTA, pH 7.0. Vertical lines are for visual reference in comparison with the spectral width of U23 in the presence of the wild-type Tat 11-mer peptide (YGRKKRRQRRR).

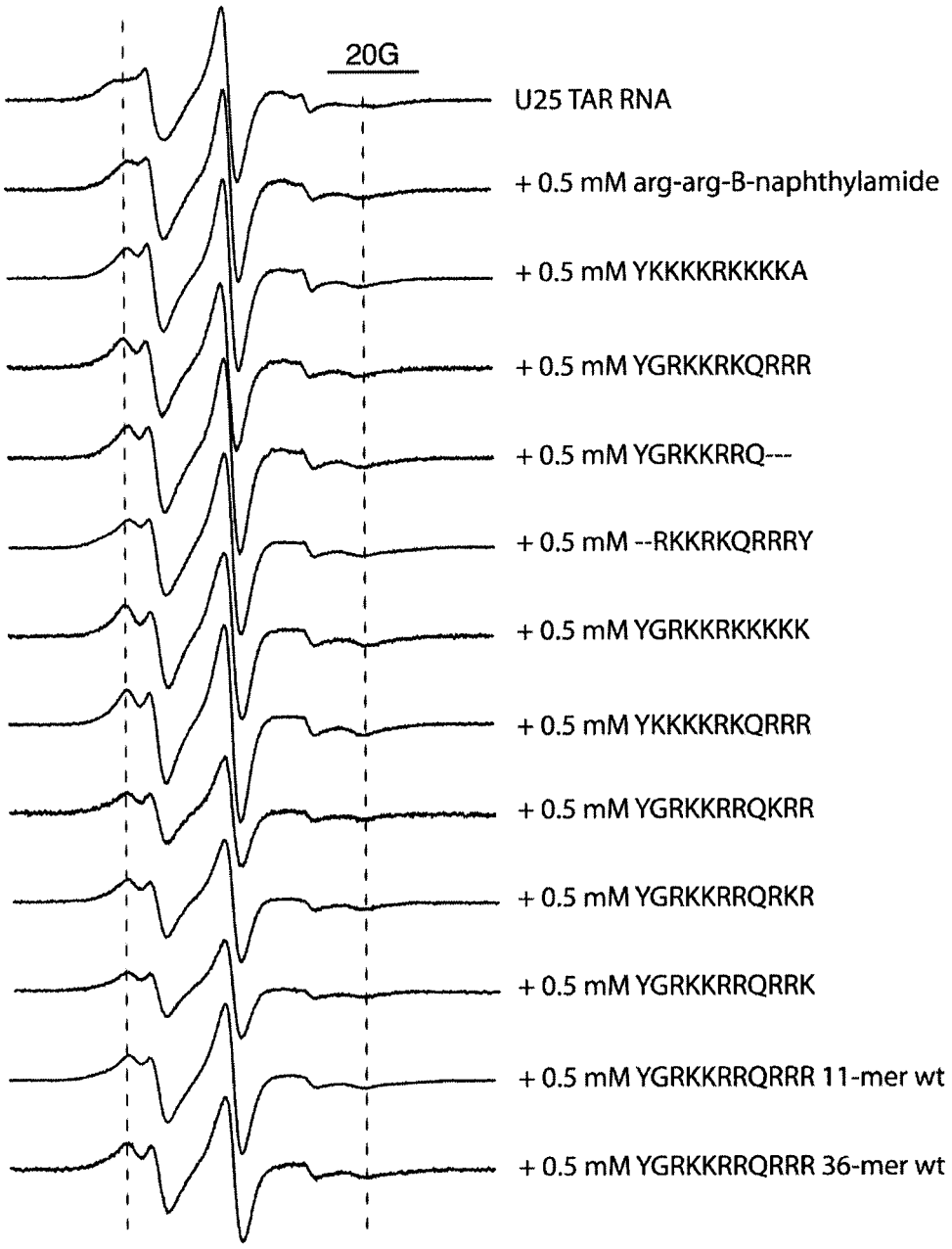

Figure 8.22. EPR spectra of U25 spin-labeled TAR RNA in the presence of derivatives of the Tat protein in 20% sucrose/100 mM NaCl, 10 mM sodium phosphate, 0.1 mM Na_2EDTA, pH 7.0. Vertical lines are for visual reference in comparison with the spectral width of U25 in the presence of the wild-type Tat 11-mer peptide (YGRKKRRQRRR).

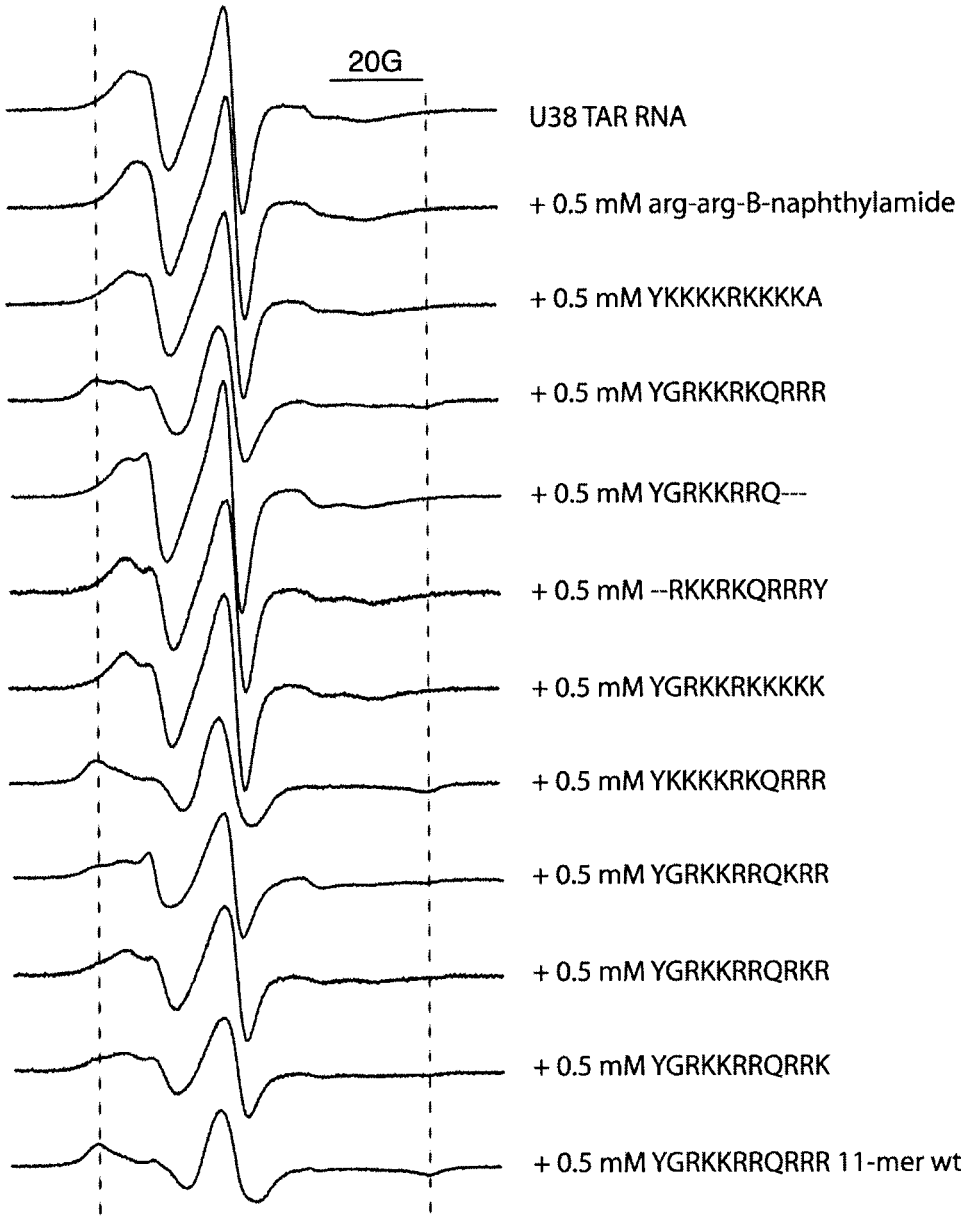

Figure 8.23. EPR spectra of U38 spin-labeled TAR RNA in the presence of derivatives of the Tat protein in 20% sucrose/100 mM NaCl, 10 mM sodium phosphate, 0.1 mM Na_2EDTA, pH 7.0. Vertical lines are for visual reference in comparison with the spectral width of U38 in the presence of the wild-type Tat 11-mer peptide (YGRKKRRQRRR).

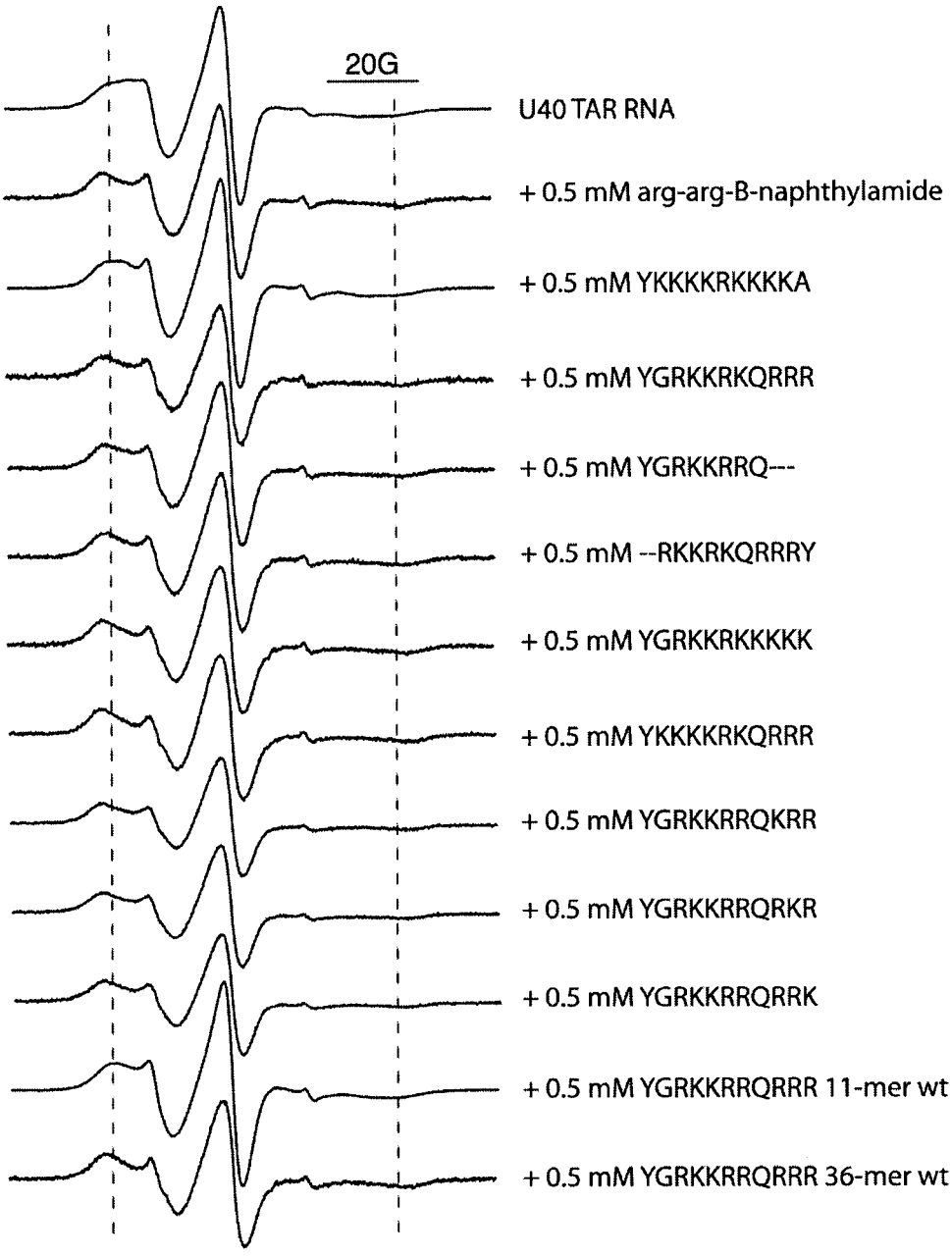

Figure 8.24. EPR spectra of U40 spin-labeled TAR RNA in the presence of derivatives of the Tat protein in 20% sucrose/100 mM NaCl, 10 mM sodium phosphate, 0.1 mM Na_2EDTA, pH 7.0. Vertical lines are for visual reference in comparison with the spectral width of U40 in the presence of the wild-type Tat 11-mer peptide (YGRKKRRQRRR).

EPR spectra of spin-labeled TAR RNAs in the presence of small molecules

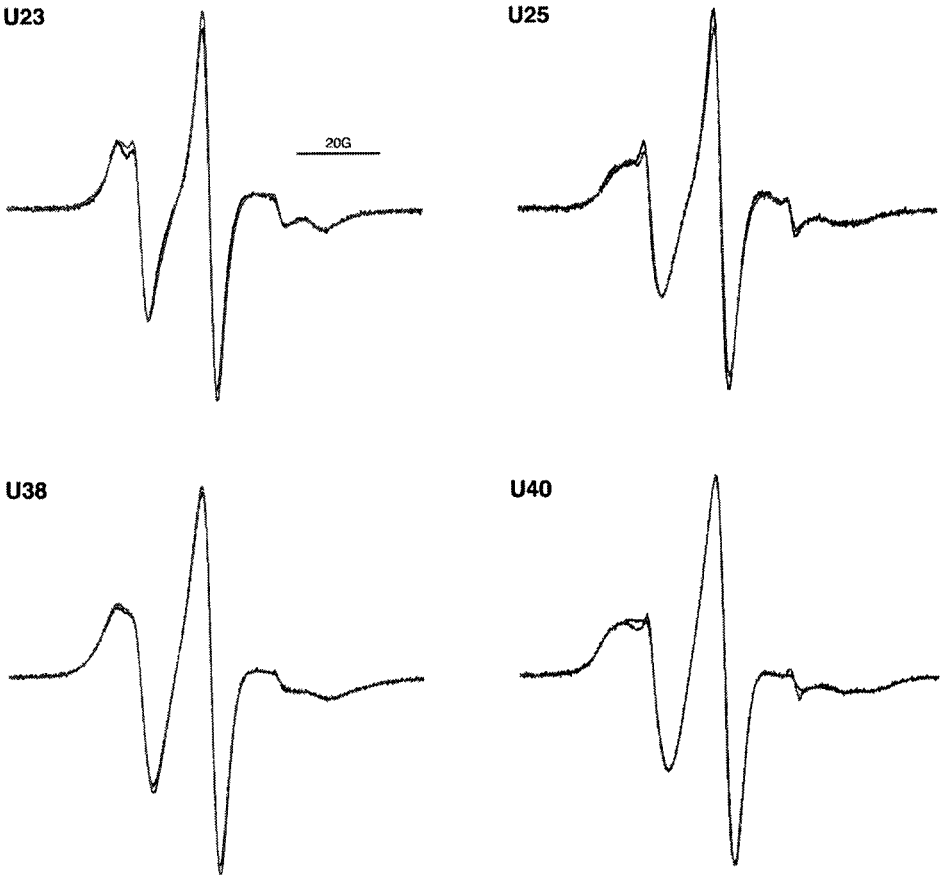

Figure 8.25. EPR spectra of spin-labeled TAR RNA in the presence (magenta) and absence of 0.5 mM Hoechst 33258. The position of the spin-label is marked on each set of normalized spectra.

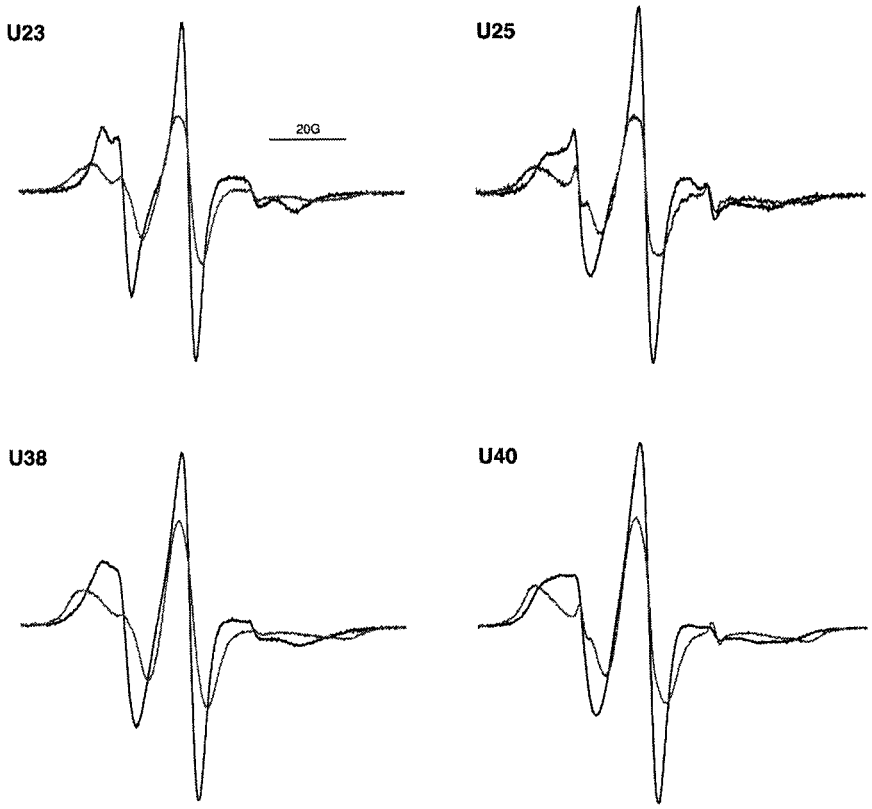

Figure 8.26. EPR spectra of spin-labeled TAR RNA in the presence (magenta) and absence of 5 mM Hoechst 33258.

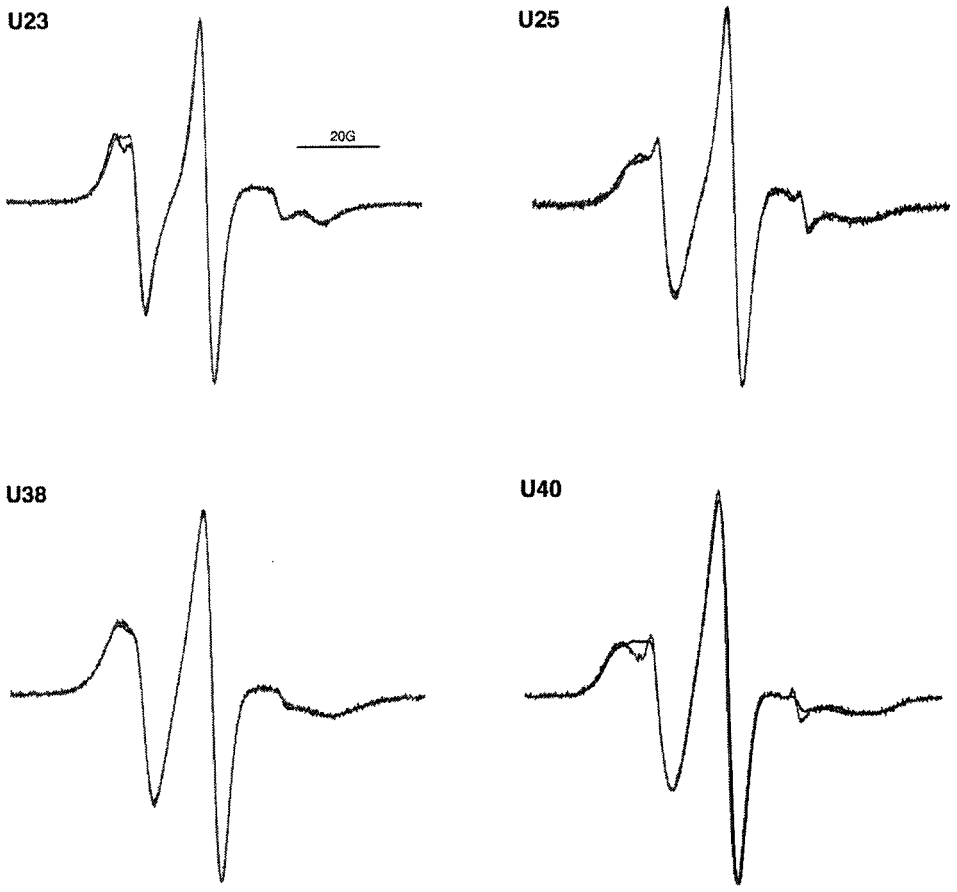

Figure 8.27. EPR spectra of spin-labeled TAR RNA in the presence (magenta) and absence of 0.5 mM DAPI.

Figure 8.28. EPR spectra of spin-labeled TAR RNA in the presence (magenta) and absence of 0.5 mM berenil.

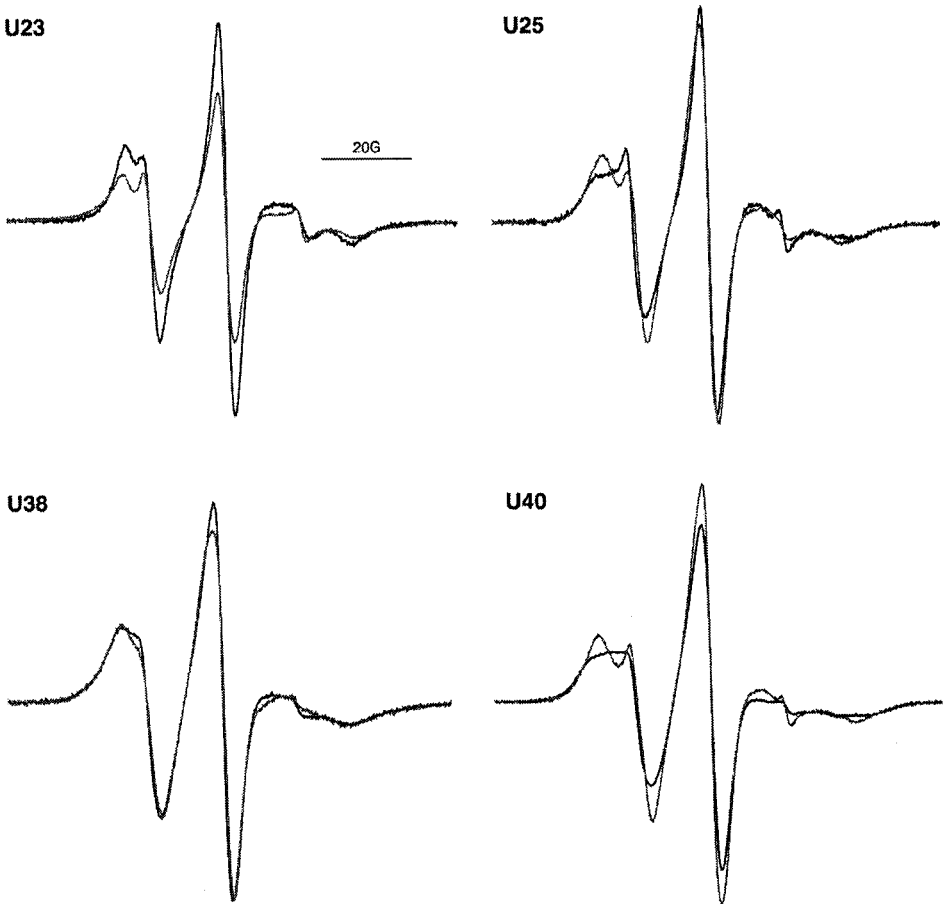

Figure 8.29. EPR spectra of spin-labeled TAR RNA in the presence (magenta) and absence of 0.5 mM CGP 40336a.

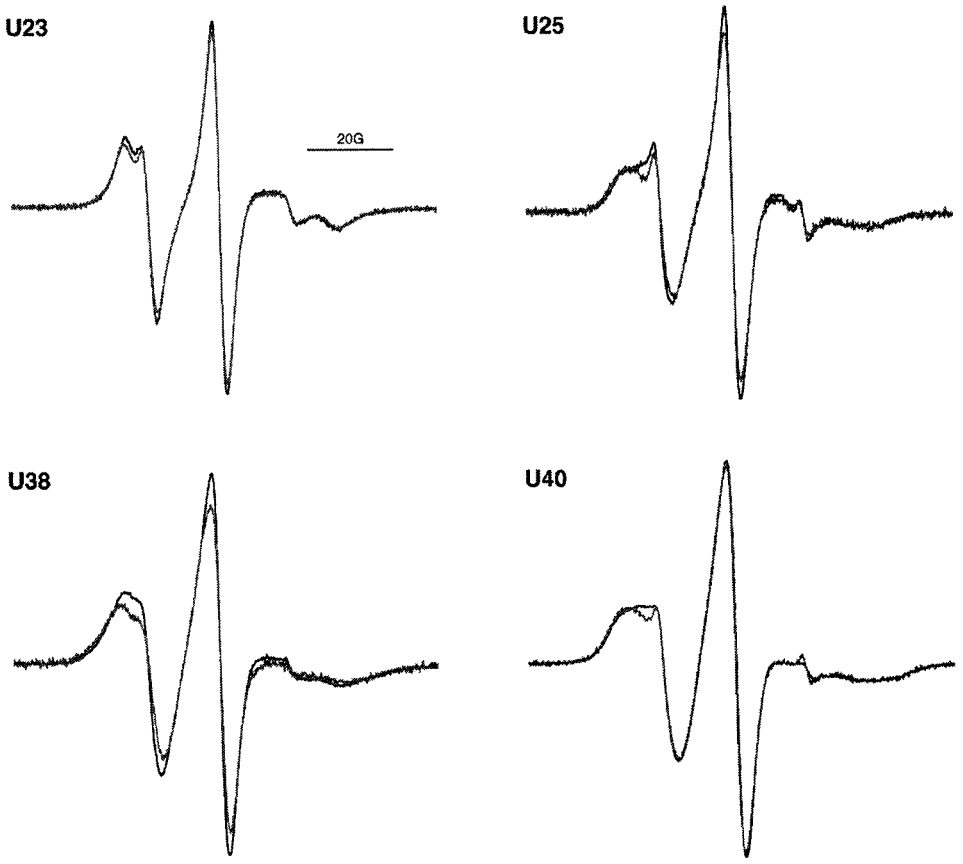

Figure 8.30. EPR spectra of spin-labeled TAR RNA in the presence (magenta) and absence of 0.4 mM neomycin.

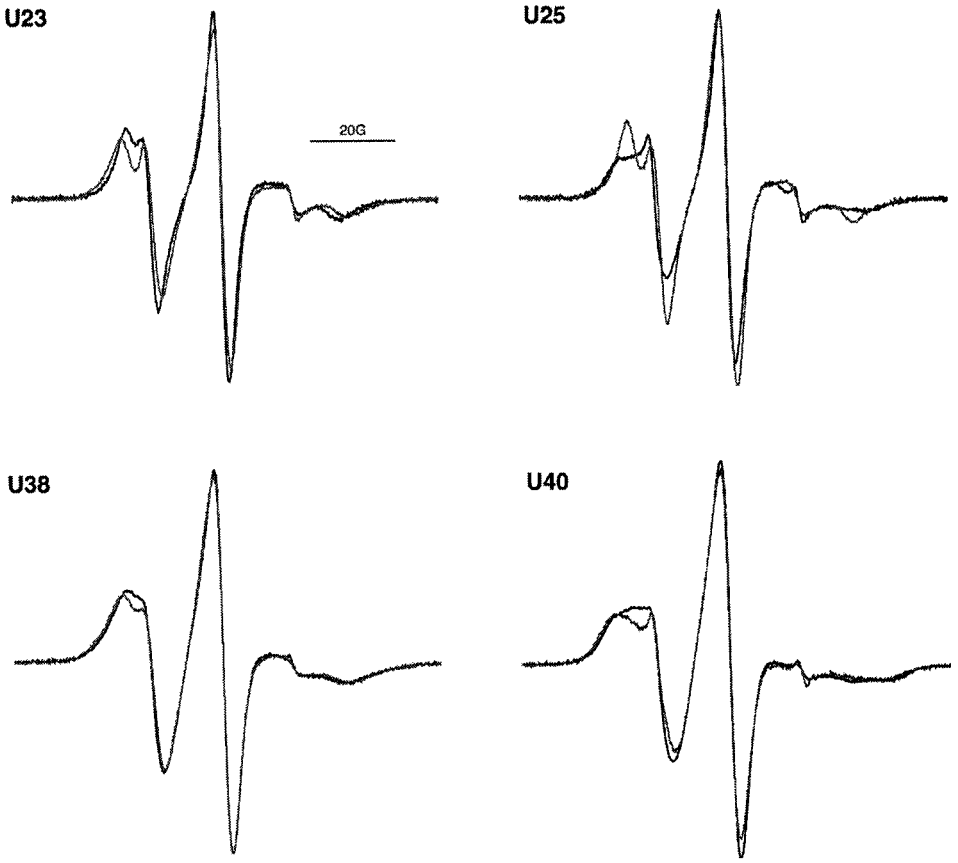

Figure 8.31. EPR spectra of spin-labeled TAR RNA in the presence (magenta) and absence of 0.4 mM guanidino neomycin.

Bibliography

Aboul-ela, F., J. Karn, et al. (1995). "The structure of the human immunodeficiency virus type-1 TAR RNA reveals principles of RNA recognition by Tat protein." J. Mol. Biol. **253**: 313-332.

Aboul-ela, F., J. Karn, et al. (1996). "Structure of HIV-1 TAR RNA in the absence of ligands reveals a novel conformation of the trinucleotide bulge." Nuc. Acids Res. **24**(20): 3974-981.

Al-Hashimi, H. M., Y. Gosser, et al. (2002). "Concerted motions in HIV-1 TAR RNA may allow access to bound state conformations: RNA dynamics from NMR residual dipolar couplings." J. Mol. Biol. **315**(2): 95-102.

Al-Hashimi, H. M., S. W. Pitt, et al. (2003). "Mg^{2+}-induced variations in the conformation and dynamcis of HIV-1 TAR RNA probed using NMR residual dipolar couplings." J. Mol. Biol. **329**(5): 867-73.

Altenbach, C., T. Marti, et al. (1990). "Transmembrane protein structure: Spin labeling of bacteriorhodopsin mutants." Science **248**: 1088.

Arzumanov, A., F. Godde, et al. (2000). "Use of the fluorescent nucleoside analogue benzo[*g*]quinazoline 2'-*O*-methyl-beta-D-ribofuranoside to monitor the binding of the HIV Tat protein or of antisense oligonucleotides to the TAR RNA step-loop." Helv. Chim. Acta **83**: 1424-36.

Bailly, C., P. Colson, et al. (1996). "The binding mode of drugs to the TAR RNA of HIV-1 studied by electric linear dichroism." Nuc. Acids Res. **24**(8): 1460-1464.

Bailly, C., V. Guerniou, et al. (2003). "Site-specific cleavage of the HIV-1 TAR RNA by a hydroxysalen-copper(III) complex." ChemBioChem **4**(1): 112-14.

Baker, T. J., N. W. Luedtke, et al. (2000). "Synthesis and anti-HIV activity of guanidinoglycosides." J. Org. Chem. **65**: 9054-9058.

Ban, N., P. Nissen, et al. (2000). "The complete atomic structure of the large ribosomal subunit at 2.4 Å resolution." Science **289**(5481): 905-920.

Bannwarth, W. and D. Schmidt (1994). "Oligonucleotides containing spin-labeled 2'-deoxycytidine and 5-methyl-2'-deoxycytidine as probes for structural motifs of DNA." Bioorg. Med. Chem. Lett. **4**(8): 977-80.

Bartlet, J. G. and R. D. Moore (1998) "Improving HIV therapy." Sci. Am. **279**(1): 84-87.

Bassi, G. S., N. E. Mollegaard, et al. (1995). "Ionic interactions and the global conformations of the hammerhead ribozyme." Struct. Biol. **2**(1): 45-55.

Bassi, G. S., A. I. H. Murchie, et al. (1997). "Ion-induced folding of the hammerhead ribozyme: A fluorescence resonance energy transfer study." EMBO J. **16**: 7481-89.

Batey, R. T., R. P. Rambo, et al. (1999). "Tertiary motifs in RNA structure and function." Angew. Chem. Intl. Ed. **38**: 2326-43.

Beigelman, L., A. Karpeisky, et al. (1995). "Synthesis of 2'-modified nucleotides and their incorporation into hammerhead ribozymes." Nucleic Acids Res. **23**: 4434-42.

Berengian, A. R., M. Parfenova, et al. (1999). "Site-directed spin labeling study of subunit interactions in the alpha-crystallin domain of small heat-shock proteins. Comparison of the oligomer symmetry in alphaA-crystallin, HSP 27, and HSP 16.3." J. Biol. Chem. **274**: 6305.

Berliner, L. J. (1976). Spin labeling: Theory and application. New York, Academic Press.

Berusui, R., F. Schlaenzen, et al. (2003). "Structural insight into the role of the ribosomal tunnel in cellular regulation." Nat. Struct. Biol. **10**(5): 366-70.

Bingman, C., X. Li, et al. (1992). "Crystal and molecular structure of d(GTGCGAC): Investigation of the effects of base sequence on the conformation of octamer duplexes." Biochemistry **31**: 12803-12.

Biswas, R., H. Kuhne, et al. (2001). "Use of EPR spectroscopy to study macromolecular structure and function." Science Progress **84**(1): 45-68.

Bittker, J. A., K. J. Phillips, et al. (2002). "Recent advances in the in vitro evolution of nucleic acids." Curr. Op. Chem. Biol. **6**(3): 367-74.

Black, D. L., R. Chan, et al. (1998). RNA:protein interactions. Oxford, UK, Oxford University Press: 109-136.

Blount, K. F., N. L. Grover, et al. (2002). "Steric interference modification of the hammerhead ribozyme." Chem. Biol. **9**(9): 1009-16.

Bondensgaard, K., E. T. Mollova, et al. (2002). "The global conformation of the hammerhead ribozyme determined using residual dipolar coupling." Biochemistry **41**: 11532-42.

Borda, E. J., J. C. Markley, et al. (2003). "Zinc-dependent cleavage in the catalytic core of the hammerhead ribozyme: evidence for a pH-dependent conformational change." Nucleic Acids Res. **31**(10): 2596-2600.

Botto, R. E. and B. Coxon (1984). "Two-dimensional proton J-resolved NMR spectroscopy of neomycin B." J. Carb. Chem. **3**(4): 545-563.

Brannvall, M., N. E. Mikkelsen, et al. (2001). "Monitoring the structure of *Escherichia coli* RNase P RNA in the presence of various divalent metal ions." Nucleic Acids Res. **29**(7): 1426-32.

Bratty, J., P. Chartrand, et al. (1993). "The hammerhead RNA domain, a model ribozyme." Biochim. Biophys. Acta **1216**: 345-59.

Breslauer, K. J. (1994). "Extracting thermodynamic data from equilibrium melting curves for oligonucleotide order-disorder transitions." Methods Mol. Biol. **26**: 347-372.

Brodsky, A. S. and J. R. Williamson (1997). "Solution structure of the HIV-2 TAR-argininamide complex." J. Mol. Biol. **267**(3): 624-39.

Budil, D. E., S. V. Kolaczkowski, et al. (2000). "Dynamics and ordering in a spin-labeled oligonucleotide observed by 220 GHz electron paramagnetic resonance." Biophys. J. **78**: 430-38.

Cabrera, C., A. Gutierrez, et al. (2002). "Anti-HIV activity of a novel aminoglycoside-arginine conjugate." Antiviral Res. **53**(1): 1-8.

Calnan, B. J., S. Biancalana, et al. (1991). "Analysis of arginine-rich peptides from the HIV Tat protein reveals unusual features of RNA-protein recognition." Genes Devel. **5**: 201-10.

Calnan, B. J., B. Tidor, et al. (1991). "Arginine-mediated RNA recognition: The arginine fork." Science **252**: 1167-1171.

Caron, M. and H. Dugas (1976). "Specific spin-labeling of transfer ribonucleic acid molecules." Nucleic Acids Res. **3**(1): 19-34.

Catani, M. V., M. T. Corasaniti, et al. (2003). "The Tat antagonist neomycin B hexa-arginine conjugate inhiits gp-120-induced death of human neuroblastoma cells." J. Neurochem. **84**: 1237-45.

Cate, J. H., A. R. Gooding, et al. (1996). "Crystal structure of a group I ribozyme domain: Principles of RNA packing." Science **273**: 1696-99.

Chow, C. S. and F. M. Bogdan (1997). "A structural basis for RNA-ligand interactions." Chem. Rev. **97**: 1489-1513.

Churcher, M. J., C. Lamont, et al. (1993). "High affinity binding of TAR RNA by the human immunodeficiency virus type-1 Tat protein requires base-pairs in the RNA stem and amino acid residues flanking the basic region." J. Mol. Biol. **230**: 90-111.

Clemons, W. M. J., D. E. Brodersen, et al. (2001). "Crystal structure of the 30 S ribosomal subunit from Thermus thermophilus: purification, crystallization and structure determination." J. Mol. Biol. **310**(4): 827-43.

Clouet-d'Orval, B., T. K. Stage, et al. (1995). "Neomycin inhbition of the hammerhead ribozyme involves ionic interactions." Biochemistry **34**: 11186-90.

Columbus, L. and W. L. Hubbell (2002). "A new spin on protein dynamics." Trends Biochem. Sci. **27**(6): 288-295.

Cordingley, M. G., R. L. LaFemina, et al. (1990). "Sequence-specific interaction of Tat protein and Tat peptides with the transactivation-responsive seqenece element of human immunodeficiency virus type 1 *in vitro*." Proc. Natl. Acad. Sci. U.S.A. **87**: 8985-8989.

Curtis, E. A. and D. P. Bartel (2001). "The hammerhead cleave reaction in monovalent cations." RNA **7**(4): 546-552.

Dassonneville, L., F. Hamy, et al. (1997). "Binding of Hoechst 33258 to the TAR RNA of HIV-1. Recognition of a pyrimidine bulge-dependent structure." Nuc. Acids Res. **25**(22): 4487-4492.

Davis, T. M. and W. D. Wilson (2001). "Surface plasmon resonance biosensor analysis of RNA-small molecule interactions." Methods Enzymol. **340**: 22-51.

Dayie, K. T., A. S. Brodsky, et al. (2002). "Base flexibility in HIV-2 TAR RNA mapped by solution ^{15}N, ^{13}C NMR relaxation." J. Mol. Biol. **317**: 263-78.

DeRose, V. J. (2002). "Two decades of RNA catalysis." Chem. Biol. **9**(9): 961-969.

DeRose, V. J. (2003). "Metal ion binding to catalytic RNA molecules." Curr. Op. Struc. Biol. **13**: 317-24.

Doherty, E. A. and J. A. Doudna (2000). "Ribozyme structures and mechanisms." Annu. Rev. Biochem. **69**: 597-615.

Du, Z., K. E. Lind, et al. (2002). "Structure of TAR RNA complexed with a Tat-TAR interaction nanomolar inhibitor that was identified by computer screening." Chem. Biol. **9**(6): 707-712.

Dugas, H. (1977). "Spin-labeled nucleic acids." Acc. Chem. Res. **10**: 47-54.

Dulog, L. and S. Lutz (1991). "Darstellung und Untersuchung eines neuen diacetylens mit nitroxylradikal-endgruppen." Liebigs Ann. Chem. **9**(9): 971-72.

Dunham, S. U., S. U. Dunham, et al. (1998). "Solution Structure of a DNA Duplex Containing a Nitroxide Spin-Labeled Platinum d(GpG) Intrastrand Cross-Link Refined with NMR-Derived Long-Range Electron-Proton Distance Restraints." J. Am. Chem. Soc. **120**(22): 5395 -5406.

Eckstein, F. (2002). "Developments in RNA chemistry, a personal view." Biochemie **84**(9): 841-48.

Edwards, T. E., T. M. Okonogi, et al. (2001). "Site-specific incorporation of nitroxide spin labels into internal sites of the TAR RNA; structure-dependent dynamics of RNA by EPR spectroscopy." J. Am. Chem. Soc. **123**: 1527-28.

Edwards, T. E., T. M. Okonogi, et al. (2002). "Investigation of RNA-protein and RNA-metal ion interactions by electron paramagnetic resonance spectroscopy: The HIV TAR-Tat motif." Chem. Biol. **9**(6): 699-706.

Edwards, T. E. and S. T. Sigurdsson (2002). "Electron paramagnetic resonance dynamic signatures of TAR RNA-small molecule complexes provide insight into RNA structure and recognition." Biochemistry **41**(50): 14843-47.

Edwards, T. E. and S. T. Sigurdsson (2003). "EPR spectroscopic analysis of TAR RNA-metal ion interactions." Biochem. Biophys. Res. Comm. **303**(2): 721-25.

Egli, M., G. Minasov, et al. (2002). "Metal ions and flexibility in a viral RNA pseudoknot at atomic resolution." Proc. Natl. Acad. Sci. U.S.A. **99**(7): 4302-07.

Ennifar, E., P. Walter, et al. (2003). "A crystallographic study of the binding of 13 metal ions to two related RNA duplexes." Nucleic Acids Res. **31**(10): 2671-82.

Eriksson, M. and B. Norden (2001). "Linear and circular dichroism of drug-nucleic acid complexes." Methods Enzymol. **340**: 68-98.

Eubank, T. D., R. Biswas, et al. (2002). "Inhibition of bacterial RNase P by aminoglycoside-arginine conjugates." FEBS Lett. **511**: 107-12.

Faber, C., H. Sticht, et al. (2000). "Structural rearrangement of HIV-1 Tat-responsive RNA upon binding of neomycin B." J. Biol. chem. **275**(27): 20660-20666.

Farrow, M. A., F. Aboul-ela, et al. (1998). "Site-specific cross-linking of amino acids in the basic region of human immunodeficiency virus type 1 Tat peptide to chemically modified TAR RNA duplexes." Biochemistry **37**(9): 3096-108.

Fedor, M. J. (2002). "The role of metal ions in RNA catalysis." Curr. Opin. Struct. Biol. **12**: 289-295.

Feig, A. L., M. Panek, et al. (1999). "Probing the binding of Tb(III) and Eu(III) to the hamemrhead ribozyme using luminescence spectroscopy." Chem. Biol. **6**(11): 801-10.

Feig, A. L., W. G. Scott, et al. (1998). "Inhibition of the hammerhead ribozyme cleavage reaction by site-specific binding of Tb(III)." Science **279**: 81-84.

Feig, A. L. and O. C. Uhlenbeck (1999). The role of metal ions in RNA biochemistry. The RNA World. R. F. Gesteland, T. R. Cech and J. F. Atkins, Ed. Cold Springs Harbor.

Feng, S. and E. C. Holland (1988). "HIV-1 Tat trans-activation requires the loop sequence within Tar." Nature **334**: 165-67.

Ferré-D'Amaré, A. R., K. Zhou, et al. (1998). "Crystal structure of a hepatitis delta virus ribozyme." Nature **395**: 567-574.

Fidanza, J. A. and L. W. McLaughlin (1992). "Use of a thiol tether for the site-specific attachment of reporter groups to DNA." J. Org. Chem. **57**: 2340-46.

Filikov, A. V., V. Mohan, et al. (2000). "Identification of ligands for RNA targets via structure-based virtual screening: HIV-1 TAR." J. Compter-Aided Mol. Design **14**: 593-610.

Fraldi, A., P. Licciardo, et al. (2001). "Distinct regions of CyclinT1 are required for binding to CDK9 and for recruitment of the HIV-1 Tat/TAR complex." J. Cell. Biochem. **S36**: 247/253.

Frankel, A. D. (1992). "Activation of HIV transcription by Tat." Curr. Opin. Genet. Dev. **2**: 293-298.

Frankel, A. D. (2000). "Fitting peptides into the RNA world." Curr. Op. Struct. Biol. **10**: 332-340.

Frankel, A. D. and J. A. Young (1998). "HIV-1: Fifteen proteins and an RNA." Annu. Rev. Biochem. **67**: 1-25.

Freed, J. H. (1976). Theory of slow tumbling ESR spectra for nitroxides. Spin labeling: Theory and application. L. J. Berliner. New York, Academic Press: 53-132.

Friedler, A., D. Friedler, et al. (2000). "Development of a functional backbone cyclic mimetic of the HIV-1 Tat arginine-rich motif." J. Biol. Chem. **275**(31): 23783-23789.

Fritz, J. J., A. Lewin, et al. (2002). "Development of hammerhead ribozymes to modulate endogenous gene expression for functional studies." Methods **28**(2): 276-85.

Froeyen, M. and P. Herdewijn (2002). "RNA as a target for drug design, the example of Tat-TAR interaction." Curr. Op. Med. Chem. **2**(10): 1123-45.

Gallego, J. and G. Varani (2001). "Targeting RNA with small-molecule drugs: Theraputic promise and chemical challenges." Acc. Chem. Res. **34**(10): 836-843.

Gannett, P. M., E. Darian, et al. (2002). "Probing triplex formation by EPR spectropscopy using a newly synthesized spin label for oligonucleotides." Nuc. Acids Res. **30**(23): 5328-37.

Gannett, P. M., E. Darian, et al. (2001). "A short procedure for synthesis of 4-ethynyl-2,2,6,6-tetramethyl-3,4-dehydro-piperidine-1-oxyl nitroxide." Syn. Comm. **31**(14): 2137-2141.

Gannett, P. M., J. H. Powell, et al. (2002). "Solid-phase DNA binding detection by EPR spectroscopy." Tet. Lett. **43**: 1931-33.

Garber, M. E. and K. A. Jones (1999). "HIV-1 Tat: coping with negative elongation factors." Curr. Opin. Immunol. **11**: 460-465.

Garber, M. E., T. P. Mayall, et al. (2000). "CDK9 autophorphorylation regulates high-affinity binding of the human immunodeficiency virus type 1 Tat-P-TEFb complex to TAR RNA." Mol. Cell. Biol. **20**(18): 6958-6969.

Garbesi, A., F. Hamy, et al. (1998). "TAR-RNA binding by HIV-1 Tat protein is selectively inhibited by its L-enantiomer." Nucleic Acids Res **26**(12): 2886-90.

Gayle, A. Y. and A. M. Baranger (2002). "Inhibition of the U1A-RNA complex by an aminoacridine derivative." Bioorg. Med. Chem. Lett. **12**: 2839-42.

Gelus, N., C. Bailly, et al. (1999). "Inhibition of HIV-1 Tat-TAR interaction by diphenylfuran derivatives: Effects of the terminal basic side chains." Bioorg. Med. Chem. **7**: 1089-1096.

Gelus, N., F. Hamy, et al. (1999). "Molecular basis of HIV-1 TAR RNA specific recognition by an acridine Tat-antagonist." Bioorg. Med. Chem. **7**: 1075-1079.

Gesteland, R. F., T. R. Cech, et al. (1999). The RNA world. Cold Springs Harbor.

Giordano, C., F. Fratini, et al. (2001). "Preparation of spin-labeled 2-amino-dA, dA, dC and 5-methyl-dC phosphoramidites for the automated synthesis of EPR active oligonucleotides." Synthesis **4**: 565-72.

Giordano, C., F. Pedone, et al. (2000). "Oligonucleotide labaleing: Synthesis of a new spin-labeled 2'-deoxyguanosine analogue." Nucleosides, Nucleotides, Nucl. Acids **19**(8): 1301-10.

Glasgow, B. J., O. K. Gasymov, et al. (1999). "Side chain mobility and ligand interactions of the G strand of Tear Lipocalins by site-directed spin labeling." Biochemistry **38**: 13707-13716.

Gold, L., B. Polisky, et al. (1995). "Diversity of oligonucleotide functions." Annu. Rev. Biochem. **64**: 763-97.

Gopalan, V., H. Kuhne, et al. (1999). "Mapping RNA-protein interactions in ribonuclease P from Escherichia coli using electron paramagnetic resonance spectroscopy." Biochemistry **38**(6): 1705-14.

Griffey, R. H., S. A. Hofstadler, et al. (1996). "Determinants of aminoglycoside-binding specificity for rRNA by using mass spectrometry." Proc. Natl. Acad. Sci. U.S.A. **96**: 10129-10133.

Griffith, O. H. and P. Jost (1976). Liquid spin labels in biological membranes. In spin labeling theory and applications. New York, Academic press.

Guerrier-Takada, C., K. Gardiner, et al. (1983). "The RNA moiety of ribonuclease P is the catalytic subunit of the enzyme." Cell **35**: 849-57.

Hamaski, K., W. M. C., et al. (2000). "An aminoglycoside antibiotic, neamine, and its aromatic ring-substituted derivatives as potential inhibitors for HIV-1 RRE-Rev." Tet. Let.. **41**: 8327-8332.

Hamaski, K. and A. Ueno (2001). "Aminoglycoside antibiotics, neamine, and its derivatives as potent inhibitors for the RNA-protein interactions derived from HIV-1 activators." Bioorg. Med. Chem. Lett. **11**: 591-594.

Hamma, T., A. Saleh, et al. (2003). "Inhibition of HIV tat-TAR interactions by an antisense oligo-2'-O-methylribonucleoside methylphosphonate." Bioorg. Med. Chem. Lett. **13**(11): 1845-48.

Hammann, C. and D. M. J. Lilley (2002). "Folding and activity of the hammerhead ribozyme." ChemBioChem **3**: 690-700.

Hammann, C., D. G. Norman, et al. (2001). "Dissection of the ion-induced folding of the hammerhead ribozyme using 19F-NMR." Proc. Natl. Acad. Sci. U.S.A. **98**(10): 5503-5508.

Hamy, F., U. Asseline, et al. (1993). "Hydrogen-bonding contacts in the major groove are required for human immunodeficiency virus type-1 Tat protein recognition of TAR RNA." J. Mol. Biol. **230**: 111-123.

Hamy, F., V. Brondani, et al. (1998). "A new class of HIV-1 Tat antagonist acting through Tat-TAR inhibition." Biochemistry **37**: 5086-8095.

Hamy, F., E. R. Felder, et al. (1997). "An inhbitor of the Tat/TAR RNA interaction that effectively suppresses HIV-1 replication." Proc. Natl. Acad. Sci. U.S.A. **94**: 3548-3553.

Hara, H., T. Horiuchi, et al. (1970). "4-Thiouridine-specific spin-labeling of E. coli transfer RNA." Biochem. Biophys. Res. Comm. **38**(2): 305-311.

Harborth, J., S. M. Elbashir, et al. (2003). "Sequence, chemical, and structural variation of small interfering RNAs and short hairpin RNAs and the effect on mammalian gene silencing." Antisense Nucleic Acid Drug Dev. **13**(2): 83-105.

Harwood, E. A., S. T. Sigurdsson, et al. (1999). J. Am. Chem. Soc. **121**: 5081-82.

Hennig, M. and J. R. Williamson (2000). "Detection of N-H...H hydrogen bonding in RNA via scalar couplings in the absence of observable imino proton resonances." Nuc. Acids Res. **28**(7): 1585-1593.

Hermann, T. and D. J. Patel (2000). "Adaptive recognition by nucleic acid aptamers." Science **287**: 820-25.

Hermann, T. and E. Westhof (1999). "Docking of cationic antibiotics to negatively charged pockets in RNA folds." J. Med. Chem. **42**(7): 1250-1261.

Hofstadler, S. A. and R. H. Griffey (2001). "Analysis of noncovalent complexes of DNA and RNA by mass spectrometry." Chem. Rev. **101**(2): 377-90.

Holmes, S. C., A. A. Arzumanov, et al. (2003). "Steric inhibition of human immunodeficiency virus type-1 Tat-dependent trans-activation in vitro and in cells by oligonucleotides containing 2'-O-methyl G-clamp ribonucleoside analogues." Nucleic Acids Res. **31**(11): 2759-68.

Hoogstraten, C. G. and R. D. Britt (2002). "Water counting: Quantitating the hydration level of paramagnetic metal ions bound to nucleotides and nucleic acids." RNA **8**(2): 252-260.

Hoogstraten, C. G., C. V. Grant, et al. (2002). "Structural analysis of metal ion ligation to nucleotides and nucleic acids using pulsed EPR spectroscopy." J. Am. Chem. Soc. **124**(5): 834-842.

Horton, T. E., D. R. Clardy, et al. (1998). "Electron paramagnetic resonance spectroscopic measurement of Mn^{2+} binding affinities to the hammerhead ribozyme and correlation with cleavage activity." Biochemistry **37**: 18094-18101.

Hubbell, W. L. and C. Altenbach (1994). "Investgation of structure and dynamics in membrane proteins using site-directed spin labeling." Curr. Opin. Struct. Biol. **4**: 566-573.

Hubbell, W. L., D. S. Cafiso, et al. (2000). "Identifying conformational changes with site-directed spin labeling." Nat. Struct. Biol. **7**(9): 735-739.

Hubbell, W. L., A. Gross, et al. (1998). "Recent advances in site-directed spin labeling of proteins." Curr. Op. Struct. Biol. **8**: 649-656.

Hunt, J. P. (1963). Metal ions in aqueous solution. New York, W. A. Benjamin, Inc.

Huppler, A., L. J. Nikstad, et al. (2002). "Metal binding and base ionization in the U6 RNA intramolecular stem-loop structure." Nat. Struct. Biol. **9**(6): 431 - 435.

Huq, I., N. Tamilarasu, et al. (1999). "Visualizing tertiary folding of RNA and RNA-protein interactions by a tethered iron chelate: Analysis of HIV-1 Tat-TAR complex." Nucleic Acids Res **27**(4): 1084-93.

Hustedt, E. J. and A. H. Beth (1999). "Nitroxide spin-spin interactions: Applications to protein structure and dynamics." Annu. Rev. Biophys. Biomol. Struct. **28**: 129-53.

Hustedt, E. J., J. J. Kirchner, et al. (1995). "Monitoring DNA dynamics using spin-labels with different independent mobilities." Biochemistry **34**: 4369-4375.

Hustedt, E. J., A. Spaltenstein, et al. (1993). "Motions of short DNA duplexes: An analysis of DNA dynamics using an EPR-active probe." Biochemistry **32**: 1774-87.

Hwang, S., N. Tamilarasu, et al. (1999). "Inhibition of gene expression in human cells through small molecule-RNA interactions." Proc. Natl. Acad. Sci. **96**(23): 12997-13002.

Imazawa, M. and F. Eckstein (1979). "Facile synthesis of 2'-amino-2'-deoxyribofuranosyl purine." J. Org. Chem. **44**: 2039-41.

Ippolito, J. A. and T. A. Steitz (1998). "A 1.3-A resolution crystal structure of the HIV-1 trans-activation response region RNA stem reveals a metal ion-dependent bulge conformation." Proc. Natl. Acad. Sci. U.S.A. **95**(17): 9819-24.

Jahnke, W. (2002). "Spin labels as a tool to identify and characterize protein-ligand interactions by NMR spectroscopy." ChemBioChem **3**: 167-73.

Jahnke, W., L. B. Perez, et al. (2000). "Second-site NMR screening with a spin-labeled first ligand." J. Am. Chem. Soc. **122**: 7394-7395.

Jeschke, G. (2002). "Determination of the nanostructure of polymer materials by electron paramagnetic resonance spectroscopy." Macromol. Rapid Commun. **23**: 227-246.

Jeschke, G. (2002). "Distance measurements in the nanometer range by pulse NMR." ChemPhysChem **3**: 927-32.

Jones, F. D. and S. A. Strobel (2003). "Ionization of a critical adenosine residue in the Neurospora Varkud Satellite ribozyme active site." Biochemistry **42**(14): 4265-76.

Jones, K. A. and B. M. Peterlin (1994). "Control of RNA initiation and elongation at the HIV-1 promoter." Annu. Rev. Biochem. **63**: 717-743.

Jones, S., D. D. T. A., et al. (2001). "Protein-RNA interactions: A structural analysis." Nucleic Acids Res. **29**(4): 943-54.

Kao, S. C. and A. M. Bobst (1985). "Local base dynamics and local structural features in RNA and DNA duplexes." Biochemistry **24**: 5465-5469.

Kaplan, R. S., J. A. Mayor, et al. (2000). "The yeast mitochondrial citrate transport protein: Determination of secondary structure and solvent accessibility of transmembrane domain IV using site-directed spin-labeling." Biochemistry **39**: 9157-9163.

Katritzky, A. R., B. Yang, et al. (1997). "(Trifluoroacetyl)benzotriazole: A convenient trifluoroacetylating reagent." J. Org. Chem. **62**: 726-28.

Keyes, R. S. and A. M. Bobst (1998). Spin-labeled nucleotides. Biological magnetic resonance. L. J. Berliner. New York, Plenum Press. **14:** 283-338.

Khvorova, A., A. Lescoute, et al. (2003). "Sequence elements outside the hammerhead ribozyme catalytic core enable intracellular activity." Nat. Struct. Biol. **10**(9): ASAP article.

Kikuta, E., S. Aoki, et al. (2001). "A new type of potent inhibitors of HIV-1 TAR RNA-Tat peptide binding by zinc(II)-macrocyclic tetraamine complexes." J. Am. Chem. Soc. **123**: 7911-7912.

Kim, H. D., G. U. Nienhaus, et al. (2002). "Mg^{2+}-dependent conformational change of RNA studied by fluorescence orrelation and FRET on immobilized single molecules." Proc. Natl. Acad. Sci **99**(7): 4284-89.

Kim, J. B. and P. A. Sharp (2001). "Positive transcription elongation factor b phosphroylates hSPT5 and RNA polymerase II carbozy-terminal domain independently of cyclin-dependent kinase-activating kinase." J. Biol. Chem. **276**(15): 12317-12323.

King, G. C., J. W. Harper, et al. (1995). "Isotope labeling for ^{13}C relaxation measurements on RNA." Methods Enzymol. **261**: 436-50.

Kirchner, J. J., E. J. Hustedt, et al. (1990). "DNA dynamics from a spin probe: Dependence of probe motion of tether length." Tet. Lett. **31**(5): 593-96.

Kirk, S. R., N. W. Luedtke, et al. (2001). "2-aminopurine as a real-time probe of enzymatic cleavage and inhibition of hammerhead ribozymes." Bioorg. Med. Chem. **9**: 2295-2301.

Kirschenheuter, G. P., Y. Zhai, et al. (1994). "An improved synthesis of 2'-azido-2'-deoxyuridine." Tet. Let.. **35**: 8517-20.

Kjems, J. and J. Egenbjerg (1998). "Modern methods for probing RNA structure." Curr. Op. Biotechnology **9**: 59-65.

Klug, C. S., S. W., et al. (1997). "Mapping of the residues involved in a proposed b-strand located in the ferric enterobactin receptor FepA using site-directed spin-labeling." Biochemistry **36**: 13027-13033.

Kolaczkowski, S. V., A. Perry, et al. (2001). "A spin-labeled abasic DNA substrate for AP endonuclease." Biochem. Biophys. Res. Comm. **288**: 722-726.

Kruger, K., P. J. Grabowski, et al. (1982). "Self-splicing: Autoexcision and autocyclization of the ribosomal RNA intervening sequence of *tetrahymena*." Cell **31**: 147-57.

Kusaba, M., K. Miyahara, et al. (2003). "Low glutelin content1: A dominant mutation that suppresses the glutelin multigene family via RNA silencing in rice." Plant Cell **15**: 1455-1467.

Lafontaine, D. A., D. G. Norman, et al. (2001). "Structure, folding and activity of the VS ribozyme: imporantce of the 2-3-6 helical junction." EMBO J. **20**(6): 1415-1424.

Lai, E. C. (2003). "RNA sensors and riboswitches: Self-regulating messages." Curr. Biol. **13**: R285-91.

Lakshmi, K. V. and G. W. Brudvig (2001). "Pulsed electron paramagnetic resonance methods for macromolecular structural determination." Curr. Opin. Struct. Biol. **11**: 523-531.

Langen, R., K. J. Oh, et al. (2000). "Crystal structures of spin labeled T4 lysozyme mutants: Implications for the interpretation of EPR spectra in terms of structure." Biochemistry **39**: 8396-8405.

Lapidot, A. and A. Litovchick (2000). "Novel HIV Tat Antagonists." Drug Dev. Res. **50**: 502-515.

Leulliot, N. and G. Varani (2001). "Current topics in RNA-protein recognition: Control of specificity and biological function throguh induced fit and conformational capture." Biochemistry **40**(27): 7947-7956.

Liang, Z., J. H. Freed, et al. (2000). "An electron spin resonance study of DNA dynamics using the slowly relaxing local structure model." J. Phys. Chem. B **104**(22): 5372-81.

Liao, X., P. S. R. Anjaneyulu, et al. (2001). "The Tetrahymena ribozyme cleaves a 5'-methylene phosphonate monoester ~10^2-fold faster than a normal phosphate diester: Implications for enzyme catalysis of phosphoryl transfer reactions." Biochemistry **40**(37): 10911-10926.

Lide, D. R. (1994). CRC Handbook of Chemistry and Physics. Boca Raton, CRC Press.

Lin, Y., R. Nielsen, et al. (1998). "Docking phospholipase A2 on membranes using electrostatic potential-modulated spin relaxation magnetic resonance." Science **279**: 1925-1929.

Lind, K. E., Z. Du, et al. (2002). "Structure-based computational database screening, in vitro assay, and NMR assessment of compounds that target TAR RNA." Chem. Biol. **9**(2): 185-93.

Litovchick, A., A. G. Evdokimov, et al. (1999). "Arginine-aminoglycoside conjugates that bind to HIV transactivation responsive element RNA in vitro." FEBS Lett. **445**: 73-79.

Litovchick, A., A. G. Evdokimov, et al. (2000). "Aminoglycoside-arginine conjugates that bind TAR RNA: Synthesis, characterization, and antiviral activity." Biochemistry **39**: 2838-2852.

Litovchick, A., A. Lapidot, et al. (2001). "Neomycin B-arginine conjugate, a novel HIV-1 Tat antagonist: Synthesis and anti-HIV activities." Biochemistry **40**(51): 15612-15623.

Liu, Y., Z. Wang, et al. (1996). "Visualizing a specific contact in the HIV-1 Tat protein fragment and *trans*-activation responsive region RNA complex by photocross-linking." J. Biol. Chem. **271**(17): 10391-10396.

Long, K. S. and D. M. Crothers (1995). "Interaction of Human Immunodeficiency Virus type 1 Tat-derived peptides with TAR RNA." Biochemistry **34**: 8885-95.

Long, K. S. and D. M. Crothers (1999). "Characterization of the solution conformations of unbound and Tat peptide-bound forms of HIV-1 TAR RNA." Biochemistry **38**: 10059-10069.

Luedtke, N. W., T. J. Baker, et al. (2000). "Guanidinoglycosides: A novel family of RNA ligands." J. Am. Chem. Soc. **122**: 12035-12036.

Lund, L. H., B. Wahren, et al. (2003). "A functional genetic approach suggests a novel interaction between the human immunodeficiency virus type 1 (HIV-1) Tat protein and HIV-1 TAR RNA in vivo." J. Gen. Virol. **84**(3): 603-06.

Macosko, J. C., M. S. Pio, et al. (1999). "A novel 5' displacement spin-labeling technique for electron paramagnetic resonance spectroscopy of RNA." RNA **5**: 1158-1166.

Mandal, M., B. Boese, et al. (2003). "Riboswitches control fundamental biochemical pathways in *Bacillus subtilis* and other bacteria." Cell **113**: 577-86.

Markley, J. C., F. Godde, et al. (2001). "Identification and characterization of a divalent metal ion-dependent cleavage site in the hammerhead ribozyme." Biochemistry **40**(46): 13849-56.

Matsugami, A., S.-I. Kobayashi, et al. (2003). "Structural basis of the highly efficient trapping of the HIV Tat protein by an RNA aptamer." Structure **11**(5): 533-45.

McKay, D. B. (1996). "Structure and function of the hammerhead ribozyme: An unfinished story." RNA **2**: 395-403.

McNulty, J. C., J. L. Silapie, et al. (2000). "Electron spin resonance of TOAC labeled peptides: Folding transitions and high frequency spectroscopy." Biopolymers **55**: 479-85.

McPike, M. P., J. Goodisman, et al. (2001). "Drug-RNA footprinting." Methods Enzymol. **340**: 431-449.

Mehl, R. A., J. C. Anderson, et al. (2003). "Generation of a bacterium with a 21 amino acid genetic code." J. Am. Chem. Soc. **125**(4): 935-9.

Mei, H. Y., M. Cui, et al. (1998). "Inhibitors of protein-RNA complexation that target the RNA: Specific recognition of human immunodeficiency virus type I TAR RNA by small organic molecules." Biochemistry **37**: 14204-14212.

Mei, H. Y., A. A. Galan, et al. (1995). "Inhibition of an HIV-1 Tat-derived peptide binding to TAR RNA by aminoglycoside antibiotics." Bioorg. Med. Chem. Lett. **5**(22): 2755-2760.

Mei, H. Y., D. P. Mack, et al. (1997). "Discovery of selective, small-molecule inhibitors of RNA complexes-I. The Tat protein/TAR RNA complexes required for HIV-1 transcription." Bioorg. Med. Chem. **5**(6): 1173-1184.

Menger, M., F. Eckstein, et al. (2000). "Multiple conformational states of the hammerhead ribozyme, broad time range of relaxation and topology of dynamics." Nucleic Acids Res. **29**(22): 4428-34.

Menger, M., T. Tuschl, et al. (1996). "Mg^{2+}-dependent conformational changes in the hammerhead ribozyme." Biochemistry **35**: 14710-16.

Merritt, M. E., S. T. Sigurdsson, et al. (1999). "Long-range distance measurements to the phosphodiester backbone of solid nucleic acids using ^{31}P-^{19}F REDOR NMR." J. Am. Chem. Soc. **121**(25): 6070-6071.

Mestre, B., A. Arzumanov, et al. (1999). "Oligonucleotide inhibiton of the interaction of HIV-1 Tat protein with the trans-activation responsive region (TAR) of HIV RNA." Biochemica et Biophysica Acta **1445**: 86-98.

Michienzi, A., S. Li, et al. (2002). "A nucleolar TAR decoy inhibitor of HIV-1 replication." Proc. Natl. Acad. Sci **99**(22): 14047-52.

Miller, T. R., S. C. Alley, et al. (1995). "A probe for sequence-dependent nucleic acid dynamics." J. Am. Chem. Soc. **117**: 9377-78.

Miller, T. R. and P. B. Hopkins (1994). "Toward the synthesis of a second-generation nitroxide spin probe for DNA dynamics studies." Bioorg. Med. Chem. Lett. **4**(8): 981-86.

Misra, V. K. and D. E. Draper (1998). "On the role of magnesium ions in RNA stability." Biopolymers **48**: 113-35.

Monaco, V., F. Formaggio, et al. (1999). "Orientation and immersion depth of a helical lipoprotein in membranes using TOAC as an ESR probe." Biopolymers **50**: 239-53.

Morrissey, S. R., T. E. Horton, et al. (2000). "Mn^{2+} sites in the hammerhead ribozyme investigated by EPR and continuous-wave q-band ENDOR spectroscopies." J. Am. Chem. Soc. **122**: 3473-3481.

Morrissey, S. R., T. E. Horton, et al. (1999). "Mn^{2+}-nitrogen interactions in RNA probed by electron spin-echo envelope modulation spectroscopy: application to the hammerhead ribozyme." J. Am. Chem. Soc. **121**: 9215-9218.

Mucha, P., A. Szyk, et al. (2002). "Structural requirements for conserved Arg52 residue for interaction of the human immunodeficiency virus type 1 trans-activation responsive element with trans-activator of transcription protein (49-57) cappillary electrophoresis mobility shift assay." J. Chromatography A **968**: 211-20.

Mundoma, C. and N. L. Greenbaum (2002). "Sequestering of Eu(III) by a GAAA RNA tetraloop." J. Am. Chem. Soc. **124**: 3525-3532.

Mundoma, C. and N. L. Greenbaum (2003). "Binding of Europium(III) ions to RNA stem loops: Role of the primary hydration sphere in complex formation." Biopolymers **69**(1): 100-09.

Murray, J. B., C. M. Dunham, et al. (2002). "A pH-dependent conformational change, rather than the chemical step, appears to be rate-limiting in the hamerhead ribozyme cleavage reaction." J. Mol. Biol. **315**: 121-30.

Murray, J. B., A. A. Seyhan, et al. (1998). "The hammerhead, hairpin, and VS ribozymes are catalytically proficient in monovalent metal cations alone." Chem. Biol. **5**: 587-95.

Murray, J. B., H. Szoke, et al. (2000). "Capture and visualization of a catalytic RNA enzyme-product complex using crystal lattice trapping and X-ray holographic reconstruction." Mol. Cell **5**(2): 279-287.

Murray, J. B., D. P. Terwey, et al. (1998). "The structural basis of hammerhead ribozyme self-cleavage." Cell **92**: 665-73.

Muth, G. w., L. Ortoleva-Donnelly, et al. (2000). "A single adenosine with a neutral pKa in the ribosomal peptidyl transferase center." Science: 947-950.

Nagel, R. and M. Ares (2000). "Substrate recognition by a eukaryotic RNase III: The double-stranded RNA-binding domain of Rnt1p selectively binds RNA containing a 5'-AGNN-3' tetraloop." RNA **6**: 1142-1156.

Naryshkin, N. A., M. A. Farrow, et al. (1997). "Chemical cross-linking of the human immunodeficiency virus type 1 Tat protein to synthetic models of the RNA recognition sequence TAR containing site-specific trisubstituted pyrophosphate analogues." Biochemistry **1997**(36): 3496-505.

Nifosi, R., C. M. Reyes, et al. (2000). "Molecular dynamics studies of the HIV-1 TAR and its complex with argininamide." Nucleic Acids Res. **28**(24): 4944-55.

Nissen, P., J. Hansen, et al. (2000). "The structural basis of ribosome activity in peptide bond synthesis." Science **289**: 920-930.

Okonogi, T. M., S. C. Alley, et al. (2002). "Phosphate backbone neutralization increases duplex DNA flexibility: A model for protein binding." Proc. Natl. Acad. Sci. USA **99**(7): 4156-60.

Okonogi, T. M., S. C. Alley, et al. (2000). "Sequence-dependent dynamics in duplex DNA." Biophys. J. **78**: 2560-71.

Okonogi, T. M., S. C. Alley, et al. (2002). "Sequence-dependent dynamics of duplex DNA: The applicability of a dinucleotide model." Biophys. J. **83**: 3446-59.

Okonogi, T. M., A. W. Reese, et al. (1999). "Flexibility of duplex DNA on the submicrosecond timescale." Biophysical Journal **77**: 3256-3276.

Olejniczak, M., Z. Gdaniec, et al. (2002). "The bulge region of HIV-1 TAR RNA binds metal ions in solution." Nuc. Acids Res. **30**(19): 4241-4249.

O'Rear, J. L., S. Wang, et al. (2001). "Comparison of the hammerhead cleavage reactions stimulated by monovalent and divalent cations." RNA **7**(4): 537-545.

Patel, D. J. and A. K. Suri (2000). "Structure, recognition and discrimination in RNA aptamer complexes with cofactors, amino acids, drugs, and aminoglycoside antibiotics." Rev. Mol. Biotech. **74**: 39-60.

Pauling, L. (1946). "Molecular architecture and biological reactions." Chem. Eng. News **24**(16): 1375-77.

Peytou, V., R. Condom, et al. (1999). "Synthesis and antiviral activity of ethidium-arginine conjugates directed against the TAR RNA of HIV-1." J. Med. Chem. **42**: 4042-4053.

Piccirilli, J. A., J. S. Vyle, et al. (1993). "Metal ion catalysis in the *Tetrahymena* ribozyme reaction." Nature **361**: 85-88.

Pilch, D. S., M. A. Kirolos, et al. (1995). "Berenil [1,3-bis(4'-amidinophenyl)triazene] binding to DNA duplexes and to a RNA duplex: Evidence for both intercalative and minor groove binding properties." Biochemistry **34**: 9962-9976.

Pley, H. W., K. M. Flaherty, et al. (1994). "Three-dimensional structure of a hammerhead ribozyme." Nature **372**: 68-74.

Plonka, P. M. and M. Elas (2002). "Application of the electron paramagnetic resonance spectroscopy to modern biotechnology." Curr. Topics Biophys. **26**(1): 175-89.

Pritchard, C. E., J. A. Grasby, et al. (1994). "Methylphosphonate mapping of phosphate contacts critical for RNA recognition by the human immunodeficiency virus Tat and Rev proteins." Nucleic Acids Res. **22**(13): 2592-2600.

Pscheidt, R. H. and B. D. Wells (1986). "Different conformations of the 3' termini of initiator and elongator transfer ribonucleic acids. An EPR study." J. Biol. Chem. **261**(16): 7253-7256.

Puglisi, J. D., L. Chen, et al. (1995). "Solution structure of a bovine immunodeficiency virus Tat-TAR peptide-RNA complex." Science **270**(November 17, 1995): 1200-1203.

Puglisi, J. D., C. L., et al. (1993). "Role of RNA structure in arginine recognition of TAR RNA." Proc. Natl. Acad. Sci. U.S.A. **90**: 3680-3684.

Puglisi, J. D., R. Tan, et al. (1992). "Conformation of the TAR RNA-arginine complex by NMR spectroscopy." Science **257**: 76-80.

Pyle, A. M. (1993). "Ribozymes: A distinct class of metalloenzymes." Science **261**: 709-714.

Pyle, A. M. and J. B. Green (1995). "RNA folding." Curr. Opin. Struct. Biol. **5**: 303-310.

Qin, P. Z., S. E. Butcher, et al. (2001). "Quantitative analysis of the isolated GAAA tetraloop/receptor interaction in solution: A site-directed spin labeling study." Biochemistry **40**(23): 6929-6936.

Qin, P. Z., K. Hideg, et al. (2003). "Monitoring RNA base structure and dynamics using site-directed spin labeling." Biochemistry **42**(22): 6772-83.

Rabenstein, M. D. and Y. K. Shin (1995). "Determination of the distance between two spin labels attached to a macromolecule." Proc. Natl. Acad. Sci. **92**: 8239-8243.

Ramos, A. and G. Varani (1998). "A new method to detect long-range protein-RNA contacts: NMR detection of electron-proton relaxation induced by nitroxide spin-labeled RNA." J. Am. Chem. Soc. **120**: 10992-10993.

Recht, M. I., D. Fourmy, et al. (1996). "RNA sequence determinants for aminoglycoside binding to an A-site rRNA model oligonucleotide." J. Mol. Biol. **262**(4): 421-36.

Reid, D. G. and K. Gajjar (1987). "A proton and carbon 13 nuclear magnetic resonance study of neomycin B and its interactions with phosphatidylinositol phosphate." J. Biol. Chem. **262**(17): 7967-7972.

Rigl, C. T., D. H. Lloyd, et al. (1997). "Structural RNA mimetics: N3'-->P5' phosphoramidate DNA analogs of HIV-1 RRE and TAR RNA form A-type helices that bind specifically to Rev and Tat-related peptides." Biochemistry **36**(3): 650-9.

Robinson, B. H., C. Mailer, et al. (1997). "Site-specific dynamics in DNA: Experiments." Annu. Rev. Biophys. Biomol. Struct. **26**: 629-58.

Rosendahl, G. and S. Douthwaite (1994). "The antibiotics micrococcin and thiostrepton interact directly with 23S rRNA nucleotides 1067A and 1095A." Nucleic Acids Res. **22**(3): 357-63.

Roy, S., U. Delling, et al. (1990). "A bulge structure in HIV-1 TAR RNA is required for Tat binding and Tat-mediated *trans*-activation." Genes Devel. **4**: 1365-1373.

Rueda, R., K. Wick, et al. (2003). "Diffusely bound Mg^{2+} ions slightly reorient stems I and II of the hammerhead ribozyme to increase the probability of formation of the catalytic core." Biochemistry **43**(33): 9924-36.

Rupert, P. B. and A. R. Ferré-D'Amaré (2001). "Crystal structure of a hairpin ribozyme-inhibitor complex with implications for catalysis." Nature **410**: 780-786.

Rupert, P. B., A. P. Massey, et al. (2002). "Transition State Stabilization by a Catalytic RNA." Science **298**: 1421-24.

Sannes-Lowry, K. A., P. Hu, et al. (1997). "HIV-1 Tat peptide binding to TAR RNA by electrospray ionization mass spectrometry." Anal. Chem. **69**(5130-5135).

Sawata, S., M. Komiyama, et al. (1995). "Kinetic evidence based on solvent isotped effects for the nonexistence of a proton-transfer process in reactions catalyzed by a hammerhead ribozyme: Implications to the double-metal-ion mechanism of catalysis." J. Am. Chem. Soc. **117**: 2357-58.

Schiemann, O., J. Fritscher, et al. (2003). "Structure of the high affinity Mn^{2+}-binding site in the hammerhead ribozyme and the influence of neomycine-B. An approach by EPR-spectroscopy and DFT-calculations." ChemBioChem **submitted**.

Schiemann, O., A. Weber, et al. (2003). "Nanometer distance measurements on RNA using PELDOR." J. Am. Chem. Soc. **125**(12): 3434-35.

Schmitz, M. and I. J. Tinoco (2000). "Solution structure and metal-ion binding of the P4 element from bacterial RNase P RNA." RNA **6**: 1212-1225.

Scott, W. G., J. T. Finch, et al. (1995). "The crystal structure of an all RNA hammerhead ribozyme: A proposed mechanism for RNA catalytic cleavage." Cell **81**: 991-1002.

Scott, W. G., J. B. Murray, et al. (1996). "Capturing the structure of a catalytic RNA intermediate: The hammerhead ribozyme." Science **274**: 2065-2069.

Seewald, M. J., A. U. Metzger, et al. (1998). "Structural model of the HIV-1 Tat(46-58)-TAR complex." J. Biomol. Struct. Dyn. **16**(3): 683-692.

Shan, S., A. V. Kravchuck, et al. (2001). "Defining the catalytic metal ion interactions in the Tetrahymena ribozyme reaction." Biochemistry **40**(17): 5161-5171.

Sharma, R. M., Bobek, et al. (1974). "Synthesis and biological activity of 2'-amino-2'-deoxy-5-fluorouridine." J. Med. Chem. **17**: 466-68.

Sigurdsson, S. T. (1996). "Isolation of oligonucleotides containing intramolecular cross-links." Analytical Biochemistry **235**: 241-42.

Sigurdsson, S. T. and F. Eckstein (1995). "Structure-function relationships of hammehead ribozymes: From understanding to applications." Trends Biotech. **13**(8): 286-89.

Sigurdsson, S. T. and F. Eckstein (1996). "Site specific labelling of sugar residues in oligoribonucleotides: Reactions of aliphatic isocyanates with 2' amino groups." Nucleic Acids Research **24**(16): 3129-3133.

Sigurdsson, S. T., B. Seeger, et al. (1996). "A mild and simple method for the preparation of isocyanates from aliphatic amines using trichloromethyl chloroformate. Synthesis of an isocyanate containing an activated disulfide." J. Org. Chem. **61**: 3883-84.

Sigurdsson, S. T., J. B. Thomson, et al. (1998). Small ribozymes. RNA Structure and Function, Cold Spring Harbor Laboratory Press. **35**.

Sigurdsson, S. T., T. Tuschl, et al. (1995). "Probing RNA teriary structure: Interhelical crosslinking of the hammerhead ribozyme." RNA **1**: 575-83.

Silverman, S. K. (2003). "Rube Goldberg goes (ribo)nuclear? Molecular switches and sensors made from RNA." RNA **9**(4): 377-83.

Sines, C. C., L. McFail-Isom, et al. (2000). "Cations mediate B-DNA conformational heterogeneity." J. Am. Chem. Soc. **122**: 11048-56.

Sober, H. A. (1968). CRC Handbook of Biochemistry: Selected Data for Molecular Biology. Cleveland, The Chemical Rubber Co.

Sontheimer, E. J., S. Sun, et al. (1997). "Metal ion catalysis during splicing of premessenger RNA." Nature **388**: 801-805.

Spaltenstein, A., B. H. Robinson, et al. (1988). "A rigid and nonperturbing probe for duplex DNA motion." J. Am. Chem. Soc. **110**: 1299-1301.

Spaltenstein, A., B. H. Robinson, et al. (1989). "DNA structural data from a dynamics probe. The dynamic signatures of single-stranded, hairpin-looped, and duplex forms of DNA are distinguishable." J. Am. Chem. Soc. **111**: 2303-05.

Spaltenstein, A., B. H. Robinson, et al. (1989). "Sequence- and structure-dependent DNA base dynamics: Synthesis, structure, and dynamics of site and sequence specifically spin-labeled DNA." Biochemistry **28**(24): 9484-9495.

Stage, T. K., K. J. Hertel, et al. (1995). "Inhibition of the hamemrhead ribozyme by neomycin." RNA **1**: 95-101.

Steinhoff, H. J., N. Radzwill, et al. (1997). "Determination of interspin distances between spin labels attached to insulin: comparison of electron paramagnetic resonance data with the X- ray structure." Biophys. J. **73**: 3287-3298.

Strube, T., O. Schiemann, et al. (2001). "A new facile method for spin-labeling of oligonucleotides." Nucleosides, Nucleotides, Nucl. Acids **20**(4-7): 1271-74.

Summers, J. S., J. Shimko, et al. (2002). "Displacement of Mn^{2+} from RNA by K^{+}, Mg^{2+}, neomycin B, and an arginine-rich peptide: Indirect detection of nucleic acid/ligand interactions using phosphorous relaxation enhancement." J. Am. Chem. Soc. **124**(50): 14934-14939.

Sumner-Smith, M., S. Roy, et al. (1991). "Critical chemical features in *trans*-acting-responsive RNA are required for interaction with human immunodeficiency virus type 1 Tat protein." J. Virol. **65**(10): 5196-5202.

Surridge, C. (2003). "RNA interference: Cereal adultery." Nature **423**(6938): 390.

Sussman, D., J. C. Nix, et al. (2000). "The structural basis for molecular recognition by the vitamin B_{12} RNA aptamer." Nat. Struct. Biol. **7**(1): 53-57.

Takagi, Y. and K. Taira (2002). "Detection of a proton-transfer process by kinetic solvent isotope effect in NH_4^{+}-mediated reactions catalyzed by a hammerhead ribozyme." J. Am. Chem. Soc. **124**: 3850-52.

Takagi, Y., M. Warashina, et al. (2001). "Recent advances in the elucidation of the mechanism of action of ribozymes." Nucleic Acids Res. **29**(9): 1815-34.

Tamilarasu, N., I. Huq, et al. (1999). "High affinity and specific binding of HIV-1 TAR RNA by a Tat-derived oligourea." J. Am. Chem. Soc. **121**: 1597-1598.

Tanious, F. A., J. M. Veal, et al. (1992). "DAPI (4',6-diamidino-2-phenylindole) binds directly to RNA and RNA: Minor-groove binding at AT sites and intercalation at AU sites." Biochemistry **31**: 3103-3112.

Tao, J., L. Chen, et al. (1997). "Dissection of the proposed base triple in human immunodeficiency virus TAR RNA indicates the importance of the Hoogsteen interaction." Biochemistry **36**: 3491-3495.

Tao, J. and A. D. Frankel (1992). "Specific binding of arginine to TAR RNA." Proc. Natl. Acad. Sci. U.S.A. **89**: 2723-2726.

Tao, J. and A. D. Frankel (1993). "Electrostatic interactions modulate the RNA-binding and transactivation specificities of the human immunodeficiency virus and simian immunodeficiency virus Tat proteins." Proc. Natl. Acad. Sci. U.S.A. **90**: 1571-1575.

Tirado, M. M. and J. Garcia de la Torre (1980). "Rotational dynamics of a rigid symmetric top macromolecule application to circular cylinders." J. Chem. Phys. **73**: 1986-93.

Torres, R. A., F. Himo, et al. (2003). "Theoretical examination of Mg^{2+}-mediated hydrolysis of a phosphodiester linkage as proposed for the hammerhead ribozyme." J. Am. Chem. Soc. **125**: 9861-67.

Turner, B. G. and M. F. Summers (1999). "Structural biology of HIV." J. Mol. Biol. **285**: 1-32.

Tuschl, T., C. Gohlke, et al. (1994). "A three-dimensional model for the hammerhead ribozyme based on fluorescence measurements." Science **266**: 785-88.

Tutter, A. and K. A. Jones (1998). "Chemicals that footprint DNA: Hitting HIV-1 in the minor groove." Proc. Natl. Acad. Sci **95**(22): 12739-41.

Valadkhan, S. and J. L. Manley (2002). "Splicing-related catalysis by protein-free snRNAs." Nature **413**: 701-07.

Varani, G. (1997). "RNA-protein intermolecular recognition." Acc. Chem. Res. **30**(5): 189-95.

Verheyden, J. P. H., D. Wagner, et al. (1971). "Synthesis of some pyrimidine 2'-amino-2'-deoxynucleosides." J. Org. Chem. **36**: 250-54.

Wada, T., T. Takagi, et al. (1998). "Evidence that P-TEFb alleviates the negative effect of DSIF on RNA polymerase II-dependent transcription in vitro." EMBO J. **17**: 7395-7403.

Walter, F., Q. Vicens, et al. (1999). "Aminoglycoside-RNA interactions." Curr. Opin. Chem. Biol. **3**: 694-704.

Wang, D. Y., B. H. Lai, et al. (2002). "A general strategy for effector-mediated control of RNA-cleaving ribozymes and DNA enzymes." J. Mol. Biol. **318**(1): 33-43.

Wang, S., P. W. Huber, et al. (1998). "Binding of neomycin to the TAR element of HIV-1 RNA induces dissociation of Tat protein by an allosteric mechanism." Biochemistry **37**: 5549-5557.

Wang, Z., I. Huq, et al. (1999). "Proximity of a Tat peptide to the HIV-1 TAR RNA loop region determined by site-specific photo-cross-linking." Bioconjug Chem **10**(3): 512-9.

Weeks, K. M. and D. M. Crothers (1991). "RNA recognition by Tat-derived peptides: Interactions in the major groove?" Cell **66**: 577-588.

Williamson, J. R. (2000). "Induced fit in RNA-protein recognition." Nat. Struct. Biol. **7**: 834-37.

Wilson, T. J. and D. M. J. Lilley (2002). "Metal ion binding and the folding of the hairpin ribozyme." RNA **8**: 587-600.

Wilson, W. D., L. Ratmeyer, et al. (1993). "The search for structure-specific nucleic acid-interactive drugs: Effects of compound structure on RNA versus DNA interaction strength." Biochemistry **32**: 4098-4104.

Woo, N. H., B. A. Roe, et al. (1980). "Three-dimensional structure of *Escheriachia coil* initiator $tRNA_f^{met}$." Nature **286**: 346-51.

Wu, H., P. K. Yang, et al. (2001). "A novel family of RNA tetraloop stucture forms the recognition site for *Saccharomyces cerevisiae* RNase III." EMBO J. **20**(24): 7240-7249.

Wyszko, E., M. Z. Barciszewska, et al. (2001). "The specific hydrolysis of HIV-1 TAR RNA elemet with the anti-TAR hammerhead ribozyme: Structural and functional implications." Intl. J. Biol. Macromol. **28**: 373-80.

Yamaguchi, Y. T., T. Wada, et al. (1998). "Interplay between positive and negative elongation factors: drawing a new view of DRB." Genes Cells **3**: 9-15.

Yoshizawa, S., D. Fourmy, et al. (2002). "Sequence-specific recognition of the major groove of RNA by deoxystreptamine." Biochemistry **41**: 6262-70.

Yu, Y. G., T. E. Thorgeirsson, et al. (1994). "Topology of an amphiphilic mitochondrial signal sequence in the membrane-inserted state: A spin labeling study." Biochemistry **33**: 14221-14226.

Zacharias, M. and P. J. Hagerman (1995). "The bend in RNA created by the trans-activation response element bulge of human immunodeficiency virus is straightened by arginine and by Tat-derived peptide." Proc. Natl. Acad. Sci **92**: 6052-6056.

Zhang, Q., R. Throolin, et al. (2003). "Probing motions between equivalent RNA domains using magnetic field induced residual dipolar couplings: Accounting for correlation between motion and alignment." J. Am. Chem. Soc. **125**: ACS ASAP.

Zhou, J. M., D. M. Zhou, et al. (2002). "Existance of efficient divalent metal ion-catalyzed and inefficient divalent metal ion-independent channels in reactions catalyzed by a hammerhead ribozyme." Nucleic Acids Res. **30**(11): 2374-82.

Zhuang, X., H. Kim, et al. (2002). "Correlating structural dynamics and function in single ribozyme molecules." Science **296**: 1473-1476.

Appendix 1

Synthesis of the 2'-amino uridine phosphoramidite

Synthetic procedure

The 2'-amino uridine phosphoramidite, 5'-*O*-(4,4'-Dimethoxytrityl)-2'-trifluoro-acetamido-2'-deoxyuridine, 3'-[β-cyanoethyl *N,N*-diisopropylphosphoramidite], **7**, is now commercially available. However, it was not commercially available in the summer of 1998 when this project was started. Therefore, **7** was synthesized in five steps with a 45% overall yield (Scheme A1.1). This method uses some synthetic steps published previously as well as some new steps. Briefly, using 2,2'-anhydrouridine was converted to 2'-azido-2'deoxyuridine, **3**, in a 84% yield, by *in situ* generation of LiN_3 from $TMSN_3$ and LiF (Kirschenheuter, Zhai et al. 1994). This step required a challenging silica gel column. Structural assignments for **1** were done using 2D $^1H,^1H$ COSY NMR spectroscopy and coupling constants from the 1D ^1H spectrum. The azide group was reduced to the amine, **4**, by Pd-catalyzed hydrogenation in near quantitative yield (Verheyden, Wagner et al. 1971). Compound **4** was sufficiently pure after reaction and filtration, and no further purification was necessary. Trifluoroacetylation was accomplished in near quantitative yield using trifluoroacetylimidazole. The last two steps, dimethyloxy tritylation and phosphitylation followed standard nucleic acid phosphoramidite procedures in 75% and 73% yields, respectively.

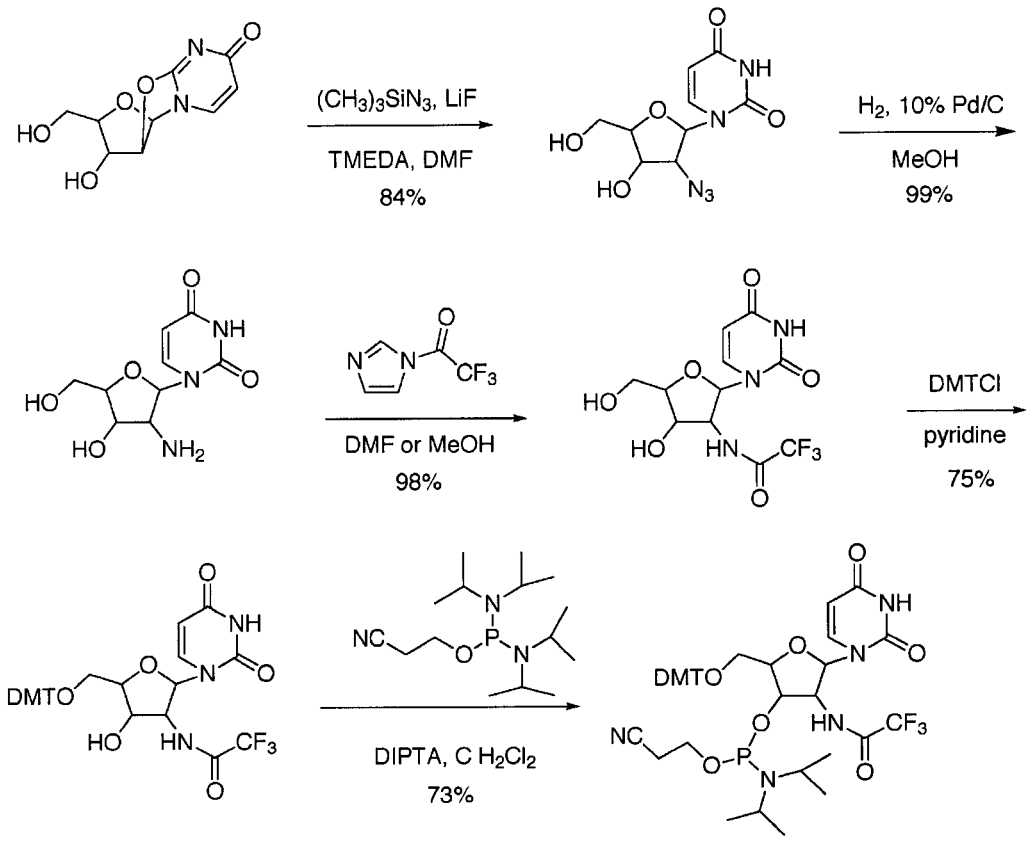

Scheme A1.1. Synthesis of 2'-amino uridine phosphoramidite in five steps with an overall yield of 39%

Trifluoroacetylation was the most challenging step of the synthesis. Trifluoroacetylation with (trifluoroacetyl)benzotriazole (Katritzky, Yang et al. 1997) was unsuccessful due to the inability to find a sufficient non-reactive solvent. Another reagent, trifluoroacetic anhydride, was not selective enough to only react with the amine. Other research groups have used this procedure, although they have had to remove the trifluoroacetyl group from the hydroxyl groups with some type of base, followed by a difficult purification (Sharma, Bobek et al. 1974). A third reagent, ethyl trifluoroacetate was also attempted, but after heating at reflux for 2 d with 20 equivalents of reagent, only a 58% yield was obtained. The fourth reagent, S-ethyl trifluorothioacetate, worked quite well (78%) using a procedure developed by Eckstein (Imazawa and Eckstein 1979). This reaction was complete in 24 h with an additional 2-3 h to remove the foul smelling ethanethiol by-product. While this reaction works quite nicely, a quicker, better smelling

alternative was sought. The more reactive trifluoroacetylimidazole was found to be a quick (30 min) and effective method of trifluoroacetylation. This product of this reaction was of sufficient purity to not require silica gel chromatography, providing another an improvement over the S-ethyl trifluorothioactate procedure which required silica gel chromatography.

Materials and Methods

General. Thin layer chromatography and preperatory TLC were done using Merck 60 F_{254} silica gel plates and Aldrich 1000 micron 20 x 20 cm plate with fluorescent indicator. Spots were visualized by ultraviolet light and ninhydrin (in *i*PrOH/3% AcOH) for free amines or *p*-anisaldehyde for compounds containing 4,4'-dimethoxytrityl groups. All ^{31}P and ^{1}H NMR spectra were obtained on a Bruker 200 MHz or a Varian 499 MHz NMR spectrometer. Electrospray mass spectrometry was performed on a Kratos Profile HV-4 electrospray mass spectrometer with a 1% AcOH/49.5% H_2O/49.5% MeOH v/v/v mobile phase. Electron impact mass spectrometry was performed on a Hewlett-Packard 5971/5890A gas chromatograph-mass spectrometer. After an initial column temperature of 60° C for the solvent delay, the temperature was ramped linearly to 300° C over 12 min and then maintained for 15 min before ramping down to the initial conditions. 2,2'-anhydouridine was obtained from Reliable Biopharmaceuticals and 4,4'-dimethoxytrityl chloride was obtained from Avocado Research Chemicals, Inc, while all other reagents were obtained from Aldrich Chemical Company. Diisopropyltetrazolite, DIPTA, was synthesized as described. Solvents were obtained from Fischer Scientific unless noted as freshly distilled.

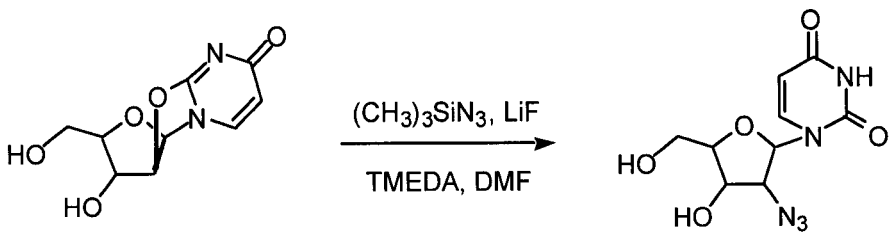

2'-azido-2'-deoxyuridine (3). A 250 mL oven dried RB flask equipped with a magnetic stir follower was charged with lithium fluoride (1.33 g, 51.3 mmol) dissolved in DMF (50 mL) and heated to 110° C under N_2. Tetramethylethylenediamine (50 mL) was added in one portion. After temperature stabilization azidotrimethylsilane (6.0 mL, 45.2 mmol) was added slowly over 10 min and allowed to stir for an additional 10 min. The mixture was charged with 2,2'-anhydrouridine (5.66 g, 25.0 mmol), and the setup was equipped with a reflux condenser. The mixture was then heated to 120° C for 3 d. The solvent was then removed under rotary evaporation with the residual being removed *in vacuo* at 60° C overnight. Flash chromatography (12% MeOH/EtOAc) and subsequent collection of fractions containing a product with R_f 0.5 yielded 6.55 g of a yellow oil (24.3 mmol, 97% by weight). By ^{1}H-NMR it was determined that the mixture contained 13% (by weight) contamination of DMF resulting in an overall yield of 84% (21.0 mmol). ^{1}H-NMR (DMSO-d_6, 499 MHz) δ 7.87 (d, 1H, J = 8.5 Hz, C_6H), 5.96 (br s, 1H, C_3'OH), 5.89 (d, 1H, J = 5.5 Hz, C_1'H), 5.70 (d, 1H, J = 8.0 Hz, C_5H), 5.25 (br s,1H, C_5'OH), 4.30 (dd, 1H, J = 5.0 Hz, J = 4.5 Hz, C_3'H), 4.05 (dd, 1H, J = 5.5 Hz, J = 5.5 Hz, C_2'H), 3.93-3.84 (m, 1H, C_4'H), 3.66 (dd, 1H, J = 3.0 Hz, J = 12.0 Hz, C_5'H_α), 3.57 (dd, 1H, J = 2.5 Hz, J = 12.0 Hz, C_5'H_β). 2D ^{1}H,^{1}H COSY (DMSO-d_6, 499 MHz) crosspeaks δ 7.87 to 5.70 (C_6H to C_5H), 5.89 to 4.05 (C_1'H to C_2'H); 4.05 to 4.30 (C_2'H to C_3'H), 4.30 to 3.90 (C_3'H to C_4'H), 3.90 to 3.66 (C_4'H to C_5'H_α), 3.90 to 3.57 (C_4'H to C_5'H_β), 3.66 to 3.57 (C_5'H_α to C_5'H_β). 2D ^{1}H,^{1}H ROESY (DMSO-d_6, 499 MHz) crosspeaks δ 7.87 to 5.89 (C_6H to C_1'H), 7.87 to 5.70 (C_6H to C_5H), 7.87 to 4.30 (C_6H to C_3'H), 7.87 to 4.05 (C_6H to C_2'H), 5.89 to 4.05 (C_1'H to C_2'H), 5.89 to C_4'H), 4.30 to 4.05 (C_3'H to C_2'H), 4.30 to 3.88 (C_3'H

to $C_{4'}H$), 4.30 to 3.66 ($C_{3'}H$ to $C_{5'}H_{\alpha}$), 4.30 to 3.57 ($C_{3'}H$ to $C_{5'}H_{\beta}$), 3.88 to 3.66 ($C_{4'}H$ to $C_{5'}H_{\alpha}$), 3.88 to 3.57 ($C_{4'}H$ to $C_{5'}H_{\beta}$).

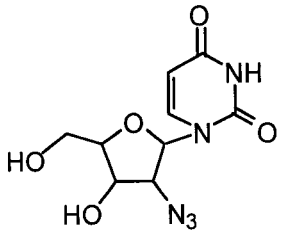

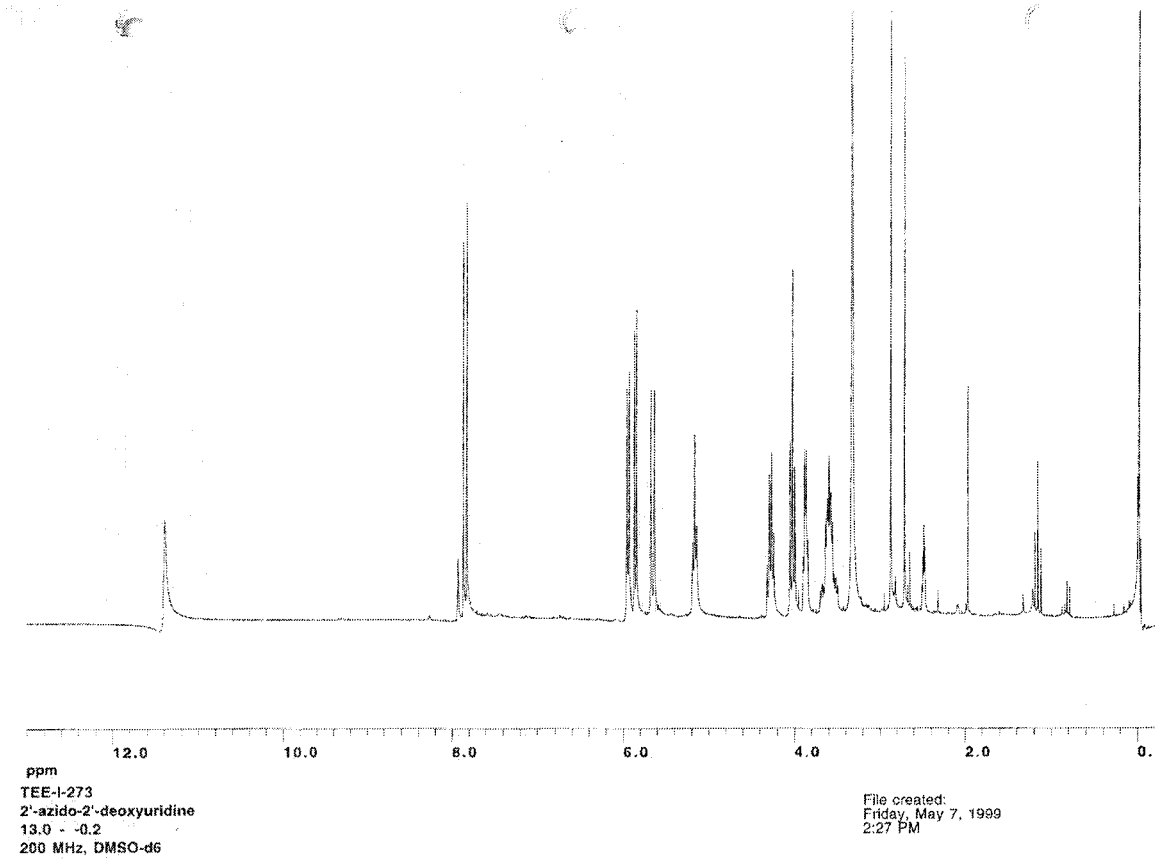

Figure A 1.2. ^{1}H NMR spectrum of compound **3**.

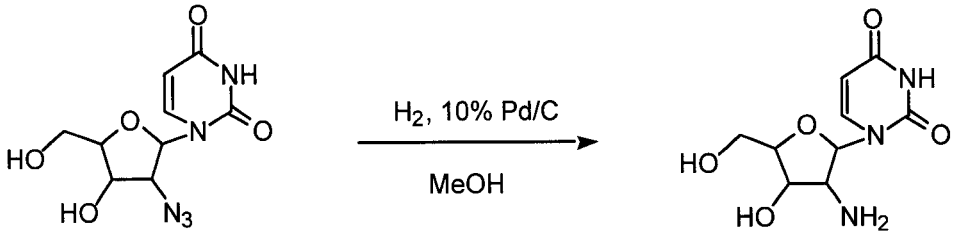

2'-amino-2'-deoxyurdine (4). Compound **3** (6.55 g, 24.3 mmol) was dissolved in methanol (40 mL). Activated palladium on carbon (10%, 350 mg) was added as a catalyst. The mixture was placed into a pressure bottle and the bottle was sparged. The bottle was then filled with hydrogen gas at 30 psi and agitated for 2 h. The pressure was removed and the solution was filtered over frit. TLC (2:1 CH_2Cl_2/MeOH) showed a single spot. The solvent was removed by rotary evaporation yielding a light yellow solid (5.84 g, 24.1 mmol, 99%). ^{1}H-NMR (DMSO-d_6, 200 MHz) δ 7.83 (d, 1H, J = 8.0 Hz, C_6H), 5.66 (2d, 2H, J = 8.2 Hz, C_1'H and C_5H), 3.90-3.80 (2m, 2H, J = 5.2 Hz, J = 4.4 Hz, C_2'H, C_3'H), 3.56-3.49 (d, 1H, J = 3.2 Hz, C_4'H), 3.47-3.14 (m, 2H, J = 5.0 Hz, J = 2.6 Hz, C_5'$\underline{H}_2$).

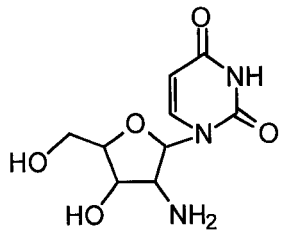

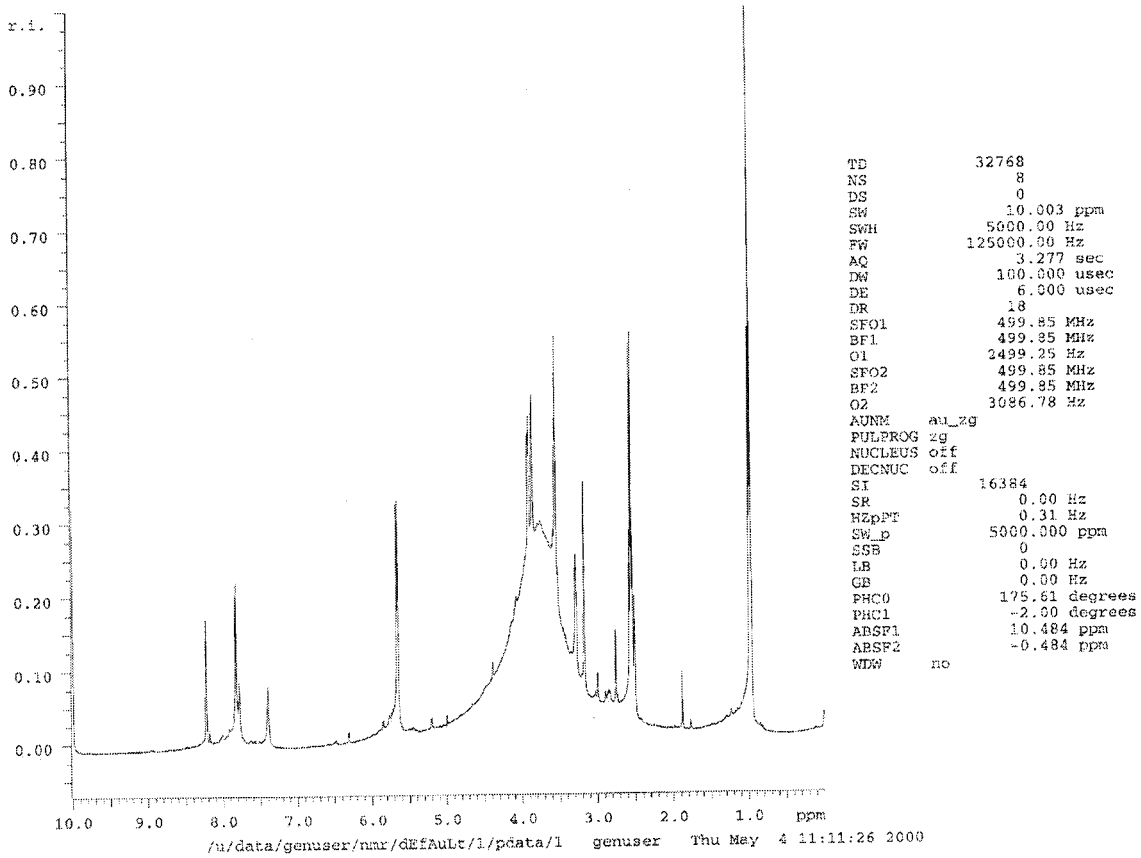

Figure A1.3. ^{1}H NMR spectrum of compound **4**.

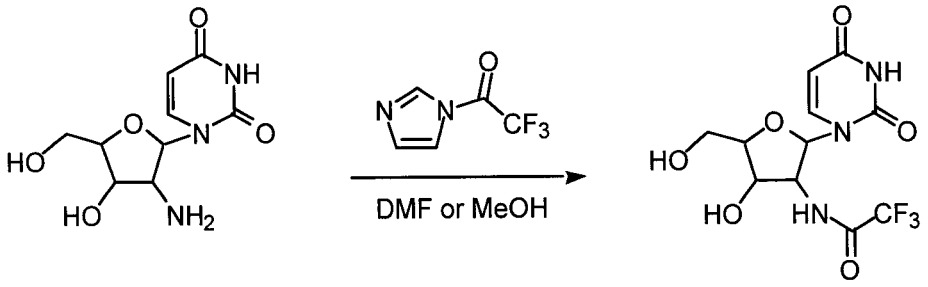

2'-trifluoroacetamido-2'-deoxyuridine (5). A 10 mL oven dried recovery flask equipped with a magnetic stir follower was charged with **4** (264 mg, 1.09 mmol) in 7 mL of MeOH. The system was placed under argon and (trifluoroacetyl)imidazole (0.15 mL, 1.31 mmol) was added dropwise by syringe followed by 2 mL additional MeOH. The solution was stirred for 90 min. TLC (20% MeOH/CH_2Cl_2) showed near quantitative conversion to a higher spot (R_f 0.76). The solvent was removed *in vacuo* and the residue was purified by flash chromatography (20% MeOH/CH_2Cl_2; R_f 0.55) yielding a dark yellow solid (362 mg, 1.07 mmol, 98%). ^{1}H-NMR (DMSO-d_6, 200 MHz) δ 11.38 (s, 1H, NH), 9.42 (s, 1H, NH), 7.91 (d, 1H, J = 8.0 Hz, C_6H), 6.07 (d, 1H, J = 7.8 Hz, $C_{1'}$H), 5.86 (br s, 1H, $C_{5'}$OH), 5.71 (d, 1H, J = 8.2 Hz, C_5H), 5.28 (br s, 1H, $C_{3'}$OH), 4.58-4.44 (m, 1H, $C_{2'}$H), 4.25-4.16 (m, 1H, $C_{3'}$H), 3.99-3.92 (d, 1H, J = 3.0 Hz, $C_{4'}$H), 3.67-3.53 (m, 2H, J = 3.6 Hz, $C_{5'}\underline{H_2}$).

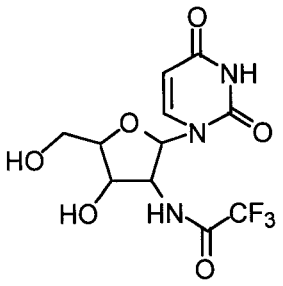

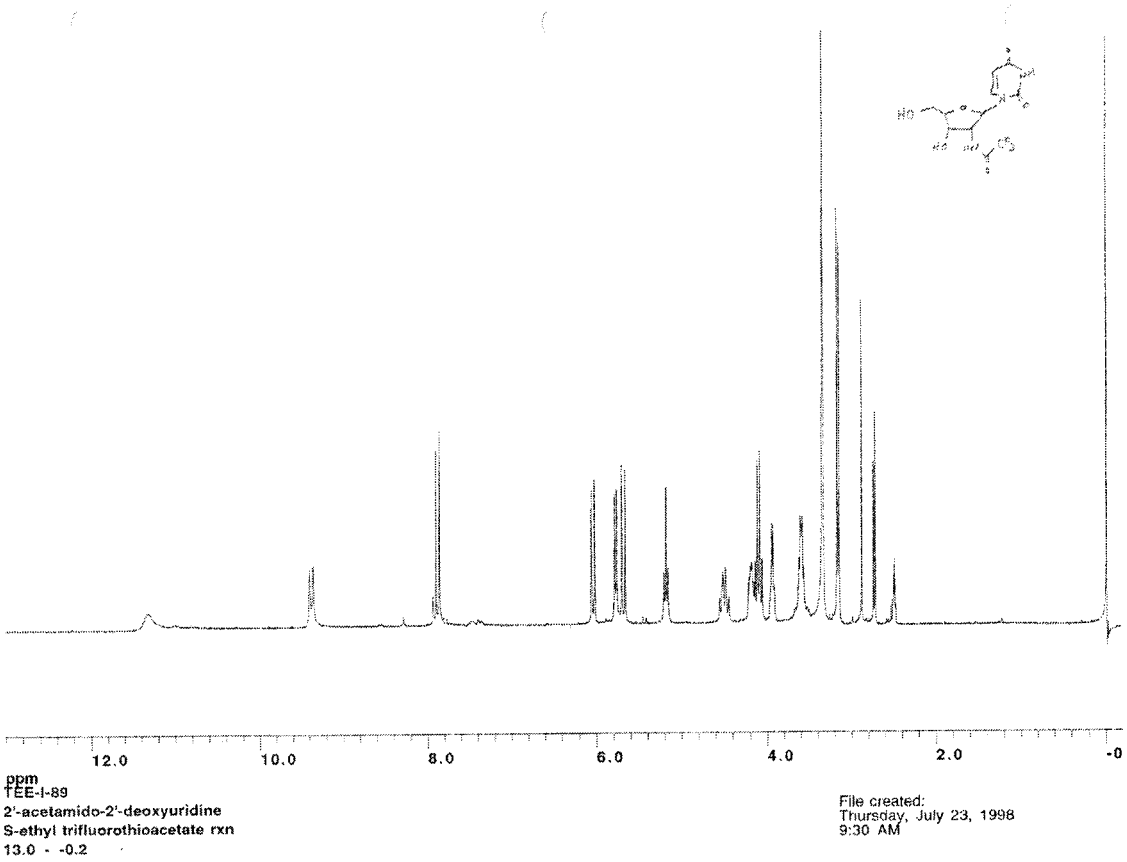

Figure A1.4. ^{1}H NMR spectrum of compound **5**.

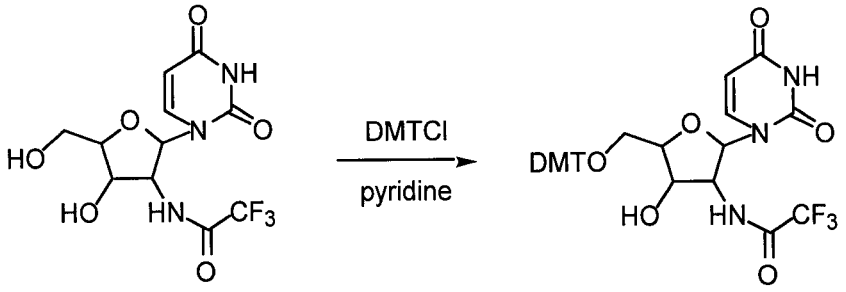

5'-*O*-(4,4'-dimethoxytrityl)-2'-trifluoroacetamido-2'-deoxyuridine (6). An oven dried 200 mL recovery flask equipped with a magnetic stir follower was charged with **5** (2.30 g, 6.78 mmol) and azeotroped twice (rotary evaporation) with freshly distilled pyridine to remove any water. The protected amine was then dissolved in freshly distilled pyridine (100 mL) under N_2. 4,4'-Dimethoxytrityl chloride (2.79 g, 8.23 mmol) was added in one portion and the mixture was allowed to stir for 16 h. TLC (5% MeOH/CH_2Cl_2) showed >90% conversion to a higher moving spot (R_f 0.3). Methanol was added and the solution was stirred for another 10 min. The solvent was then removed under rotary evaporation in a warm water bath (45° C) and the residual solvent was removed *in vacuo*. The crude solid was dissolved in methylene chloride (50 mL) and washed with sat $NaHCO_3$ (35 mL). The aqueous layer was back extracted with methylene chloride (30 mL). The combined extracts were washed with brine (35 mL), again back extracting the aqueous layer with methylene chloride (30 mL). The solvent from the combined extracts was dried ($MgSO_4$), filtered and then removed under rotary evaporation yielding a dark yellow oil. The oil was then purified by flash chromatography using a solvent ramp. First the mixture was eluted with methylene chloride which afforded unreacted 4,4'-dimethoxytrityl chloride. Then, eluting with 10% MeOH/CH_2Cl_2 afforded an off-white solid after removal of the solvent (3.27, 5.1 mmol, 75%). ^{1}H-NMR ($CDCl_3$, 200 MHz) δ 7.71 (d, 1H, J = 8.0 Hz, C_6H), 7.46-7.08 (m, 9H, H_B), 6.87 (d, 4H, H_A ArH next to methoxyl substituent), 6.27 (d, 1H, J = 8.0 Hz, C_1'H), 5.47 (d, 1H, J = 8.0 Hz, C_5H), 4.82-

4.67 (m, 1H, $C_{2'}H$), 4.53-4.42 (m, 1H, $C_{3'}H$), 4.25-4.16 (d, 1H, $C_{4'}H$), 3.78 (s, 6H, OCH_3) 3.49-3.36 (m, 2H, $C_{5'}\underline{H_2}$).

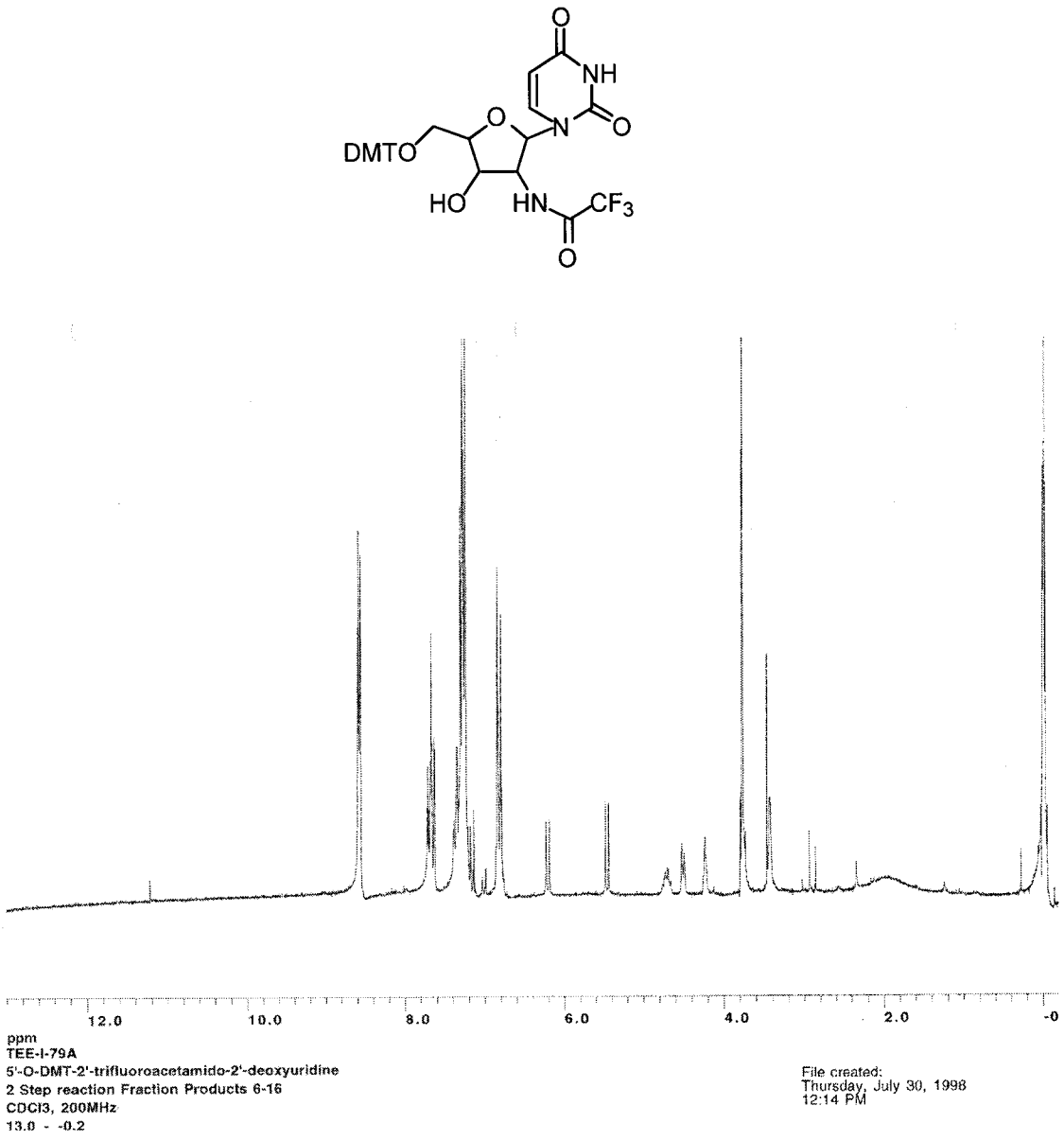

Figure A1.5. ^{1}H NMR of compound **6**.

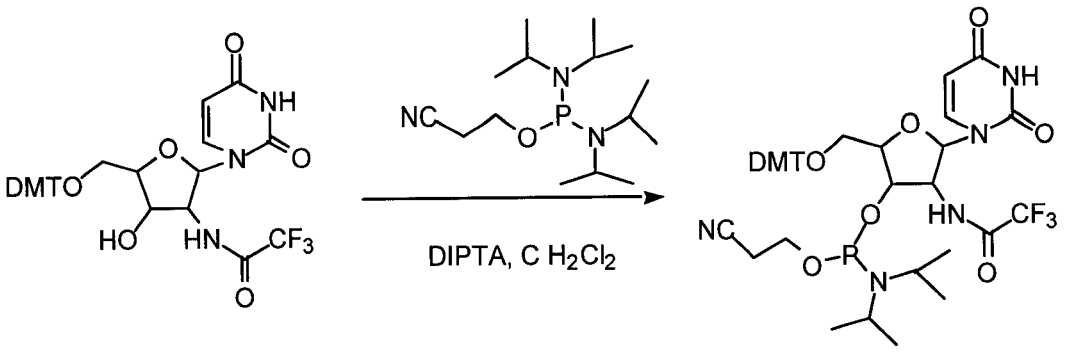

5'-*O*-(4,4'-Dimethoxytrityl)-2'-trifluoroacetamido-2'-deoxyuridine, 3'-[β-cyanoethyl *N,N*-diisopropylphosphoramidite] (7). An oven dried 50 mL RB flask was charged with **6** (457 mg, 0.712 mmol) and diisopropyltetrazolite (DIPTA, 73 mg, 0.43 mmol) and azeotroped twice with freshly distilled methylene chloride. The solids were then dissolved in freshly distilled methylene chloride and the flask was equipped with a magnetic stir follower under N_2. β-Cyanoethyl tetraisopropylphosphoramidite (0.20 mL, 0.87 mmol) was added by syringe to the rapidly stirring solution. The solution was stirred for 22 h and TLC (4% MeOH/CH_2Cl_2 with 2% Et_3N) showed about 25% conversion to a higher moving product (Rf 0.3). Another portion of β-cyanoethyl tetraisopropylphosphoramidite (40 μL, 0.17 mmol) was added by syringe, as was 0.1 mL Et_3N. Then, the solution was allowed to stir for another 24 h. TLC (4% MeOH/CH_2Cl_2 with 2% Et_3N) showed complete disappearance of starting material (R_f 0.2). The solvent was then removed by rotary evaporation and the crude residual was purified by flash chromatography. First methylene chloride was used to remove any of the higher moving materials (unreacted phosphoramidite and hydrolyzed phosphoramidite), then 10% MeOH/CH_2Cl_2 with 2% Et_3N was used to elute the title compound as an off-white solid (440 mg, 0.523 mmol, 73%).

Vita

Thomas Eugene Edwards was born in Albany, Oregon in 1975 to Michael M. Edwards and Judy A. C. Edwards. He lived in Madison, CT until high school where he attended Choate Rosemary Hall in Wallingford, CT. In 1998 he earned a Bachelor of Science degree in Chemistry from the University of Puget Sound in Tacoma, WA. In 2003 he earned his Doctorate in Philosophy from the Department of Chemistry at the University of Washington in Seattle, WA.